Performance Evaluation of a Vaporizing Liquid Microthruster using nitrogen and water as propellants

A. Pappadimitriou

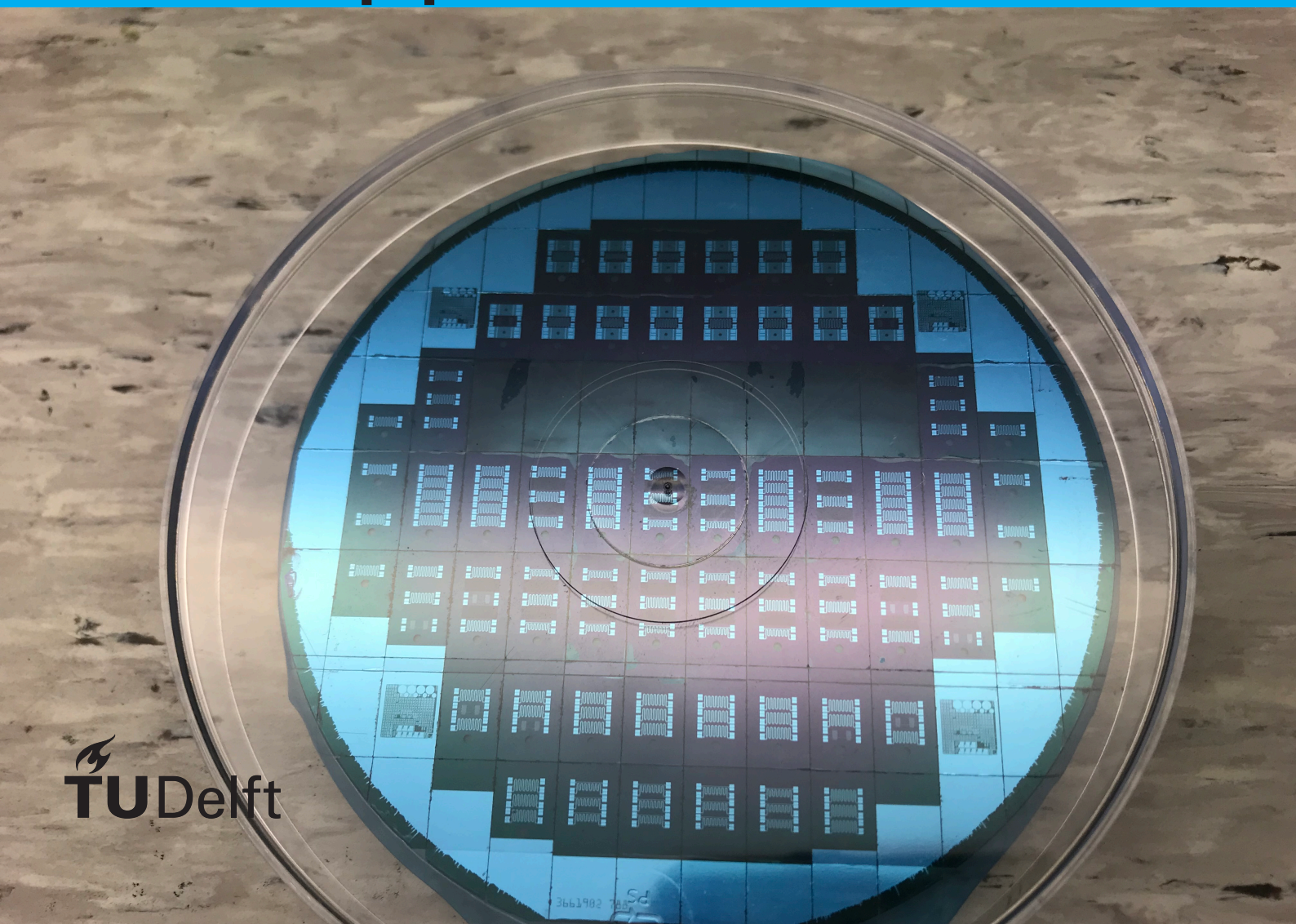

TU Delft

Performance Evaluation of a Vaporizing Liquid Microthruster using nitrogen and water as propellants

by

A. Pappadimitriou

to obtain the degree of Master of Science
at the Delft University of Technology,
to be defended publicly on Wednesday March 23, 2021 at 9:30 AM.

Student number: 4340884

Thesis committee:	Prof. dr. E. K. A. Gill,	TU Delft, Chair
	Ir. B. T. C. Zandbergen,	TU Delft, Supervisor
	Dr. ing. H. W. van Zeijl,	TU Delft
	Ir. M. C. Naeije,	TU Delft

TU Delft

Preface

This final thesis report will conclude a very exciting and challenging project that I have undertaken for my master of science degree. Since finishing my bachelor study in aerospace engineering at the same faculty, I have also undertaken a half year internship for ArianeGroup in Munich, Germany. My experiences both there and here at the Delft University of Technology have been memorable and something I look back to, as I continue to learn.

For my final research of my MSc-degree, under the supervision of Barry Zandbergen, I worked on developing and improving a new thruster interface, to carry out thrust tests at higher chamber temperatures. This way the thrust data could be used to validate an improved thrust performance model. I have learnt much on how to carry out experimentation, analyze data and perform various design tasks, which I am sure will benefit me in my future endeavours.

First off, I want to thank my supervisor, Barry Zandbergen, for his insightful support and encouragement throughout the duration of the thesis. Additionally, I want to thank Henk van Zeijl for his help in manufacturing the new thruster interfaces and Durga Manila for helping me in using the microscopes in the lab. More thanks goes to Angelo Cervone, for willingly contributing some of his budget, to obtain a set of propellant feed adapters, that were used in this thesis. This project was also made possible with the help of Şevket Uludağ and Vidhya Pallichadath, who helped with their expertise involving the cleanroom and obtaining components to be used in the thesis. Lastly, I want to thank all my friends from the master thesis room for the many coffee breaks, game nights and fun times we have had together.

A. Pappadimitriou
Delft, March 2021

Abstract

A current trend, in recent decades, in spacecraft engineering is the miniaturization of satellites and their subsystems. One of these subsystems is for propulsion, which is important for orienting satellites and performing orbital manoeuvres.

Currently one such micropropulsion system, being developed at the Space Engineering department at the Delft University of Technology, is called the “Vaporizing Liquid Microthruster”. These thrusters are manufactured using Deep Reactive Ion Etching on silicon wafers. They operate by resistively heating the propellant, vaporizing and expanding it throughout the nozzle to create thrust.

Currently, several experimental investigations have been conducted to formulate models that can predict the performance of these microthrusters, on a wide range of operating conditions, without the use of expensive testing. These models can then be validated comparing them to experimental data.

Thrust tests were performed with nitrogen, for three different thrusters in ambient, cold conditions, for operating pressures of 2-5bars. From these tests, the discharge coefficient was predicted within 10% of the experimental values. So the model’s prediction of the discharge coefficient was valid. It was also immediately clear that the thruster was not designed for ambient conditions due its low specific impulse values of 7.6-22.7s, resulting in incomplete flow expansion in the nozzle.

The current 1st generation thruster interface used at the department is limited to 150^{o}C due to its teflon material. Therefore, an alternate design using a printable circuit board was investigated to reach at least 600K, where the thruster would be glued to it using a thermally resistant, ceramic based glue (Thermeez 7020). Unfortunately, the design was limited to 150^{o}C due to the low adhesive quality of the glue, which meant that the thruster inlet could not be sealed off and a less suitable replacement glue had to be used.

Heated thrust tests were performed for two thrusters up to around 150^{o}C in ambient conditions. For this increase in temperature , throat Reynolds numbers decreased from 2915 to 779, while the discharge coefficient increased from 0.71 to near 1. However, a less suitable mass flow sensor had to be used, so the validation of the model based on the hot thrust tests was inconclusive for discharge coefficient and the Isp efficiency.

Overall, the goals for this experimental research study were partially reached. Thrust tests were conducted, using nitrogen as propellant, for cold conditions and up to 150^{o}C. The experiments could not substantially validate the prediction of the Isp efficiency, however the model is accurate to within 10% of the experimental values for the discharge coefficient. Experimental data from literature also could not validate the Isp efficiencies of the model, unless the fitting constant of the thrust coefficient relation was altered. It is recommended to focus on experimenting with the use of water as a propellant and make minor improvements to the thruster design, to obtain accurate performance data at higher temperatures.

Contents

List of Figures

List of Tables

Nomenclature

Latin Symbols

$\dot{m}$	Mass flow	mg s^{-1}
$\dot{Q}$	Power	W
A	Area	µm
AR	Area ratio	–
$c*$	Characteristic velocity	meter/s
C_D	Discharge coefficient	–
C_f	Thrust coefficient	–
D_H	Hydraulic diameter	µm
dp	Pressure loss	Pa
f	Friction factor	–
F_t	Thrust	N
g	Gravitational acceleration	m^2 s^{-1}
h	Enthalpy	J kg^{-1} K^{-1}
h	Height or depth	µm
I	Current	A
Isp	Specific Impulse	s
Kn	Knudsen number	
l	length	µm
l_{eq}	Equivalent length	meter
M	Mach number	–
M_w	Molecular weight	g mol^{-1}
R	Resistance	Ω
r	Radius	µm
R_A	Universal gas constant	J mol^{-1} K^{-1}
$r_{t,c}$	Radius of curvature	µm
Re	Reynolds number	
T	Temperature	K
V	Voltage	V
v	Velocity	m s^{-1}

w	width	µm
S	Magnetic force per unit current	

Greek Symbols

Δd	Relative displacement of the pendulum	µm
ΔI	Actuator current difference	A
η_c	Combustion quality	–
η_d	Divergence loss factor	–
η_f	Isp efficiency	–
η_{heat}	Heater efficiency	–
η_n	Nozzle quality	–
Γ	Vandekerckhove value	
γ	Specific heat ratio	–
μ	Dynamic viscosity	Pa s
ρ	Density	$kg^3\ m^{-1}$
ρ_{wire}	Wire resistivity	
θ	Divergence half angle	°

Subscripts

a	ambient
c	chamber
e	exit
f	final
i	initial
L, c	Conductive loss
L, h	Convective loss
L, r	Radiative loss
L, w	Wire loss
mod	modified
n	nozzle
nc	Nozzle Convergent
nd	Nozzle Divergent
$PP - C2S$	pendulum pivot to C2S sensor
$prop$	Propellant
t	Throat
tbl	throat boundary layer

vap	Vaporisation
w	wall
0	Room temperature and pressure
act	actuator
C2S-M	C2S sensor to magnet
J	Refers to CD model by Johnson et al. [13]
KH	Refers to CD model by Kuluva and Hosack [14]
TF	Refers to CD model by Tang and Fenn [31]

Acronyms

1 Introduction

1.1. Background

The Space Systems Engineering faculty, at the Delft University of Technology, has been interested in implementing new technologies for micropropulsion systems. With the continued cooperation of the Else Kooi Laboratory, at the Faculty of Electrical Engineering, Mathematics and Computer Science, these thrusters can be manufactured and tested, to be used on future micro- and pico- satellites. Several examples from the past include the Delfi-n3Xt and Delfi-PQ satellites, which used cold gas propulsion systems, as explained by Speretta et al. [28], Bouwmeester et al. [4] and Guo, Bouwmeester, and Gill [11]. Cold gas thrusters have lower performances compared to when the propellant is heated using microresistojets. The use of a MEMS based Vaporizing Liquid microthrusters (VLM), can increase the Isp reached compared to cold gas thrusters. These VLM usually reach thrust levels and Isp values between 1-10mN and 50-200s, respectively Cervone et al. [7].

The Space system engineering department is currently investigating Low Pressure Microthrusters and Vaporizing Liquid Microthrusters as suitable options. The VLM is of interest in this report. The VLM operates by heating the propellant in the vaporizing chamber, using resistors as heaters, to supersonic speeds through the nozzle, to create thrust.

For Vaporizing Liquid microthrusters the majority of testing, at the Delft University of technology, has been performed at lower operating temperatures. The work of Silva et al. [27] managed to reach temperatures of 150^{o}C, which was limited by the material used to interface the thruster to the thrust measurement apparatus. Kurmanbay [15] was able to reach temperatures of 350^{o}C using a PCB as the interface where a thruster is glued to. However, he was unable to perform thrust measurements with it. An important aspect to investigate is design an interface that can handle high chamber temperatures, up to 600K, while also being able to measure the thrust. Obtaining measurable mass flow, thrust and efficiency data, at high operational temperatures,for the VLM's available at the Delft University of Technology (DUT) would be a valuable contribution of scientific data. The work of Versteeg [36] was able to reach temperatures up 400^{o}C, by using wire electric discharge machining to develop a thruster. This design has currently reached the highest operating temperature for thrust testing, for thrusters developed and manufactured at the Delft University of Technology.

Currently, different analytical and numerical models have been developed to predict and characterize the performance of microthrusters, with a given set of inputs. It would be useful to have a model that can characterize a thruster over its entire operating range, accurately. Based on the findings of a literature study Pappadimitriou [22], an analytical model based on the reader by Zandbergen [37] was adapted by the work of Makhan [18] and Versteeg [36] will be used. This model applies necessary corrections to the ideal thruster model, such as the divergence effects, viscous effects and boundary layer effects. In addition, the models for predicting the discharge coefficient by Tang and Fenn [31], Kuluva and Hosack [14] and Johnson et al. [13] will also be investigated.

1.2. Research Objective

The main objective of the thesis is as follows: " The objective is to verify and validate a model presented in the work of Zandbergen [37] and improved by Makhan [18], that can predict the thrust performance

of a Vaporizing Liquid microthruster across the entire operating range by comparing predicted data with experimental data."

Predicting the performance of the thruster with an 10% inaccuracy was considered sufficient for this thesis. The reason is that a 10% inaccuracy in the thrust and/or Isp can easily be compensated in the design by carrying 10% more propellant mass than is needed. Considering that satellites in question are small microsats, this would mean a few more grams of propellant would be added in practice, which should not be an issue for meeting the mass budget of most microsats.

The operating range refers to a chamber pressure range of around 2-5 bars and a chamber temperature from room temperature to at least 600K. It is expected to achieve thrust levels between 0.12-3mN, which is a defined requirement from the Delfi-PQ satellite Turmaine [34]. The sub-objectives to achieve the main goal of the thesis can be seen below. Additionally, each sub-objective is linked to a central research question, as can be seen in italics at the end of each objective.

1. Obtain experimental performance data, using both nitrogen and (if time permits) water through an operating range of 2-5 bars chamber pressure and to at least 600K in chamber temperature, that is reproducible and accurate. (*RQ 1a, 1d, 1e*)
2. Design and/or improve the thruster interface to allow thrust tests to take place at high temperatures, above 600 K, without damaging the set up, by investigating different insulative/protective solutions. (*RQ 2a-c*)
3. Determine the accuracy of the model at different operating conditions by comparing the predicted performance values and efficiencies with the real experimental values for each propellant. (*RQ 1b, 1c*)
4. Investigate the difference in performance between using nitrogen and Vaporizing water as a propellant, by comparing the acquired experimental data between them. (*RQ 3a-d*)
5. Provide recommendations to improve the chip design, chip interface, test-up and the models used, by providing solutions to any limitations and/or deficiencies in the work. (*RQ 4*)

The main research question to be answered is the following: "What are the effects of heating the 3rd gen. VLM microthruster on the thruster performance when thrust experiments are performed throughout the operating range and used to validate a performance predicting model?" The central questions below will be used to help answer the main research question above. Additionally, the central questions are also used to achieve the sub-objectives stated above.

1. What can be learned by investigating the mass flow, thrust, specific impulse, Isp quality, discharge coefficient, the thrust quality, heater power and heater efficiency of the VLM thruster, with respect to its operating conditions (chamber pressure and chamber temperature)?
   (a) To what extent do the relationships found match experimental data from literature?
   (b) To what extent can the performance and thermal model predict the experimental thruster performances stated in the central question?
   (c) Does the accuracy vary throughout the operating range?
   (d) What are the effects of the improvements made to the performance model compared to the previous version by Makhan [18]?
2. How well does the chosen thermal protection method allow VLM testing to occur at higher chamber temperatures?
   (a) What is the maximum achievable chamber temperature and pressure before failure or damage occurs?
   (b) Where on the thruster interface and test set-up does failure occur due to heating with and without the thermal protection?
   (c) Are there any alterations to the design and/or dimensions of the thruster interface and/or thruster test set-up that need to be considered to fit the thermal protection design?
   (d) How well does the design fair against previous designs a the faculty?

3. What is the influence between using nitrogen and Vaporizing water as well as propellant for the VLM?
    (a) What is the difference in performance parameters attained?
    (b) What is the influence of the required heater power for each propellant?
    (c) At what operating point can complete vaporization, for liquid water, be noticed in the experimental results?
    (d) What changes to the test set-up need to be incorporated to perform thrust tests using Vaporizing water compared to gaseous nitrogen?
4. What are the recommendations for improving the thruster chip design, thruster interface design, thruster performance model design, thruster thermal model, the test set-ups and procedures?

1.3. Methodology and Approach

The section will briefly cover the approach taken to obtain the research goals stated in the previous chapter. The approach is based on the project plan given in Appendix D.

First a literature study was made to investigate the different methods possible for the microthruster design and packaging, as well the performance model that will be used for predicting the performance of the thruster. After this, a basic design was made for the thruster interface, which was manufactured at the Else Kooi lab. Afterwards, the thrust tests were performed in cold and heated conditions, and the dimensions of the thrusters were measured.Once experimental data was collected. This was compared to the predicted performance values of the model and checked to see if the model was valid.

Overall, the selected propellants for this thesis are nitrogen and water. The reason is due to the fact that nitrogen and water are readily available at the faculty labs. In addition, according Silva et al. [27], water seems to be the best candidate as it outperformed other propellants in terms of Isp and is safe to handle. However, there was no time within the thesis to perform testing with water.

The chosen models for predicting the discharge coefficients is an analytical relation from Kuluva and Hosack [14], an analytical relation from Tang and Fenn [31] and a semi-empirical relation from the work of Johnson et al. [13]. These were found through performing a literature study [22]. The thrust and Isp are being predicted using the model of Spisz, Brinich, and Jack [29]. The models will predict the performances of the thruster over a pressure range of 2-5 bars and a temperature range from room temperature to at least 600K.

The test set-up will involve the use of the TB-5m thrust pendulum, which is available in the clean-room of the Space system engineering floor.

1.4. Key Design Requirements

The driving requirements for the thruster, testing and test set-up will be presented in this section. A list of requirements for the propulsion subsystem of the Delfi-PQ satellite is available and are listed in the work of Turmaine [34]. If the reader wishes to know the full list of requirements for the Delfi-PQ propulsion subsystem, then it is recommended to read Section 2.3 from the work of Turmaine [34]. Only the performance and functional requirements for the thruster chip, within the scope of this thesis, are listed below.

- **PROP-FUN-1:** “The thruster shall be able to operate on gaseous N_2, as well as on liquid H_2O.”
- **PROP-PERF-1:** “The thrust provided by the propulsion system shall be 3 mN as a maximum.”
- **PROP-PERF-2:** “The thrust provided by the propulsion system shall be at least 0.12 mN.”

Also, some additional requirements are mentioned which are considered essential for the testing and experimentation phase of the thesis.

- **PROP-FUN-2:**“The thruster and thruster interface shall be compatible with the thrust pendulum available in the clean room of the micropropulsion lab.”
- **PROP-INT-1:** “The interface and thruster shall be able to function properly to at least 600K.”

- **PROP-INT-2:** “There shall be no leakage caused to the thruster for pressures lower or equal to 5 bars.” This is based on previous studies, where experiments reached 5 bars before leakage Makhan [18] Kurmanbay [15].

1.5. Thesis Outline

To begin with, chapter 2 will characterize and describe the thruster chips and their packaging as completely as possible. The theoretical background behind the thruster performance will be discussed in in chapter 3, where the model used will be discussed, validated with literature and used to predict the expected performance of the chosen thrusters. Afterwards, the prepatory tests and test set up will be presented in chapter 5 and chapter 4 to ensure the test results are reliable and that thrust tests can be repeated. The results for the thrust tests and their analysis will be given in chapter 6 and chapter 7, for cold and hot testing respectively. Lastly, conclusions and recommendations for the thesis will be summarized in chapter 8.

2

Thruster Fabrication

To be able to reach higher chamber temperatures, the packaging of the VLM needs to be considered, to handle high temperature thrust testing. The purpose of this chapter is to

- provide background information on the VLMs used in this thesis.
- present the packaging design intended to be used for hot testing.
- compare the thrusters and packaging design to previous designs used.

The reader shall know, by the end of this chapter, what the thruster looks like and how the newly designed interface differs from the previous interfaces seen in Makhan [18] and Kurmanbay [15], with appropriate reasoning for the changes. section 2.1 provides some background on the VLM chips themselves and characterizes the thruster nozzles and thermal characteristics. section 2.2 describes and illustrates the previous interfaces used for the VLM. section 2.3 discusses the redesigned packaging method for the VLM, while section 2.5 summarizes the main findings of this chapter.

2.1. Thruster chip design

To begin with, the VLM used for the thesis, will described and characterized in this section.

2.1.1. Evolution of the thruster chip design

The thruster chips used at the department have gone through many iterations and are created through the use of Deep Reacive Ion etching. The first VLM design was produced by the work of Mathew [19], which can be seen in Figure 2.2. It has a single channel where propellant is heated through the use of thin film heaters.

Afterwards, several experimental studies attempted to improve the design. The work of Poyck [23] introduced thrusters with widened chambers, so more heating channels could be introduced, in the second iteration of the design. Additionally, the heating channels now contained meandering shapes to help maximize the transfer of heat to the propellant. Additionally, one side of the thruster chip was covered in glass to give visual access to the thruster. Van Wees [35] used this design as well.

The 3rd iteration used by Silva et al. [27] and Makhan [18] replaced the silicon carbide heaters of Van Wees [35] with molybdenum heaters, that were integrated onto the design of the thruster.

The current design used in this thesis is similar to the version used by Silva et al. [27] and Makhan [18] except the vaporization channels are sectioned off, as can be seen in Figure 2.1. An approach and fabrication method, for the current design, is described in the work of Kurmanbay [15].

The VLM chips used for this thesis are based off a modular fabrication approach using many manufacturing techniques such as DRIE, etching, lithography and different deposition techniques. A description and explanation of the fabrication method of the VLM thruster chips can be found in the work of Kurmanbay [15]. This will not be described in great detail in this thesis, since the fabrication of the VLM chips is not the main focus for this thesis. The thrusters are fabricated on a wafer, as seen on Figure 2.3. However, the main parts of the thruster and general background information will be given. These techniques

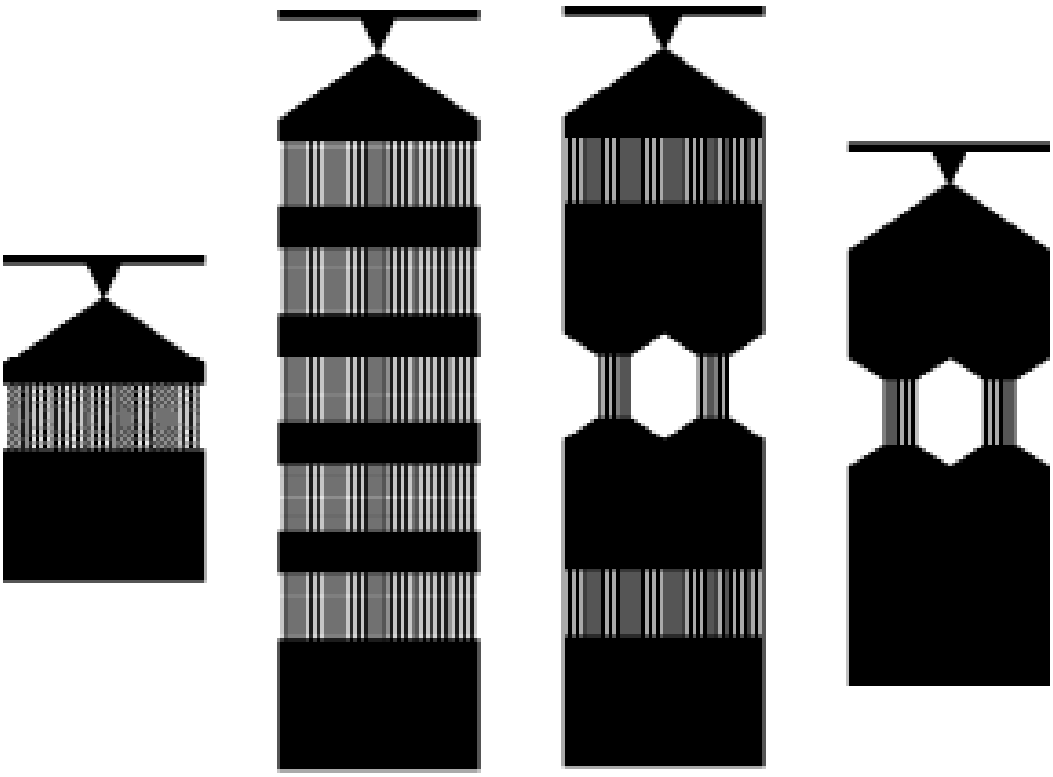

Figure 2.1: Current design by Kurmanbay [15].

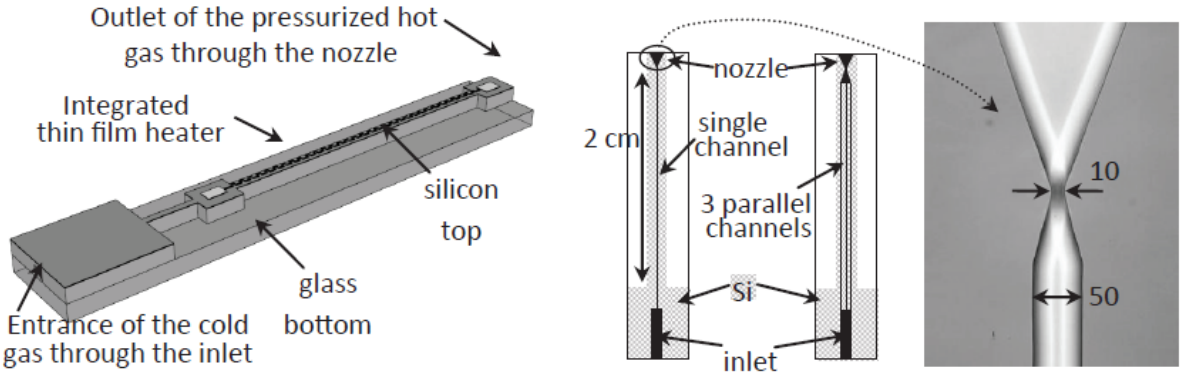

Figure 2.2: First iteration of the VLM design by Mathew [19].

Table 2.1: List of thrusters manufactured by TU-Delft/EWI for the present work.

Thruster	R5C1	R4C2 + R4C9	R4C4 + R4C7	R4C5	R4C6
# Heaters	3	5	5	3	3
Glue for inlet	ABLESTIK	ABLESTIK	ABLESTIK	BISON	BISON
Glue for chip	ABLESTIK	Thermeez 7020	Thermeez 7020	Thermeez 7020	BISON
Vaporizing channels	Serpentine	Serpentine	Diamond	Straight	Straight

have also been used in the work of Bayt [1]. The VLM thrusters that will be used are made up of three main components: a nozzle, a vaporizing chamber and one/multiple heater/s.

VLM nozzles can be designed in either a bell or conical shape. However, for the available mask only conical nozzles were available.

The vaporizing chamber is where the propellant is heated and vaporized. Three different channels were available from the mask: straight ducts, serpentine channels and diamond shapes. These options have varying dimensions. It should be noted that the effect different vaporizing channels have on performance was not a main focus here.

The external heaters are placed on the top of thruster chip surface. The number of heaters depends on the length of the chip, where the number varied between 1 and 5. The heaters are made out of Molybdenum, which have been used by Silva et al. [27], Makhan [18], Kurmanbay [15] and Mele et al. [21]. The heaters themselves are made of molybdenum, which can handle temperatures as high as 850^{o}C. Despite their high melting point, they are very susceptible to oxidation at around 300^{o}C as pointed out Mele et al. [21]. Therefore, a layer of silicon dioxide needs to be layered to protect these heaters. The heaters used in the design have Aluminum pads at each end, to allow wires to be bonded to them and allow a current to flow.

2.1.2. Thruster naming convention and selection

In total, 7 chips were chosen for the thesis. The chips were chosen from an available wafer, as can be seen in Figure 2.3. Figure 2.4 shows the rear of the wafer. The wafer is symmetrically fabricated so that everything on the left half of the wafer, matches the right. This is represented by the thick red line in Figure 2.3. These chips were then attached to their PCB and given a name: R#$_R$C#$_C$. The #$_R$ represents the row number from the wafer and #$_C$ the column. Table 2.1 summarizes all the available thrusters currently, while also giving details on their design.

These thrusters can be found in the workshop on the 8th floor of the aerospace faculty, in the thesis box under the name of Aris Pappadimitriou. The 7 thrusters are located in two petri dishes and have been labelled by a marker to classify which thruster is which.

2.1.3. Optical Characterization test

The purpose of the optical characterization test is to determine the dimensions and sizing of the thruster chip accurately. These thruster dimensions are needed to predict the thruster performances. The silicon MEMS VLM thruster has a glass plane which allows the user to view and measure relevant dimensions in the heating chamber and nozzle using a microscope.

The relevant parameters that will be measured or calculated are listed in Table 2.2, along with uncertainties. These values were found for the thruster chips: R5C1, R4C7 and R4C9. The dimensions for these thrusters were measured using the VHX-2000 digital microscope, with different lenses, since its high magnification abilities allows for accurate measurements of dimensions in the scale of micrometers. The lenses that were used are 500-5000x magnification lens and the 100-1000x magnification. The supervisor of the microscope room at Delft Aerospace and Structures Materials Laboratory (DASML) is Durga Mainali, who helped in accessing the lab and changing the lenses for the microscope.

When performing the measurements, it was important to ensure that the plane of the thruster remained completely flat with respect the microscope lens. If the thruster plane was set at an angle that was not completely perpendicular to the lens, inaccurate dimensions could be measured. R5C1 broke off from its PCB during a test set up procedure, with the metallic needle still attached to it. To ensure the thruster was flat it was taped to a flat 3D printed part as can be seen in Figure 2.5. Even though this is a very quick solution, it still provided a flat enough plane to observe the thruster. R4C7 failed during hot testing, where the glue holding the inlet needle melted, causing the needle to fall out. So the thruster

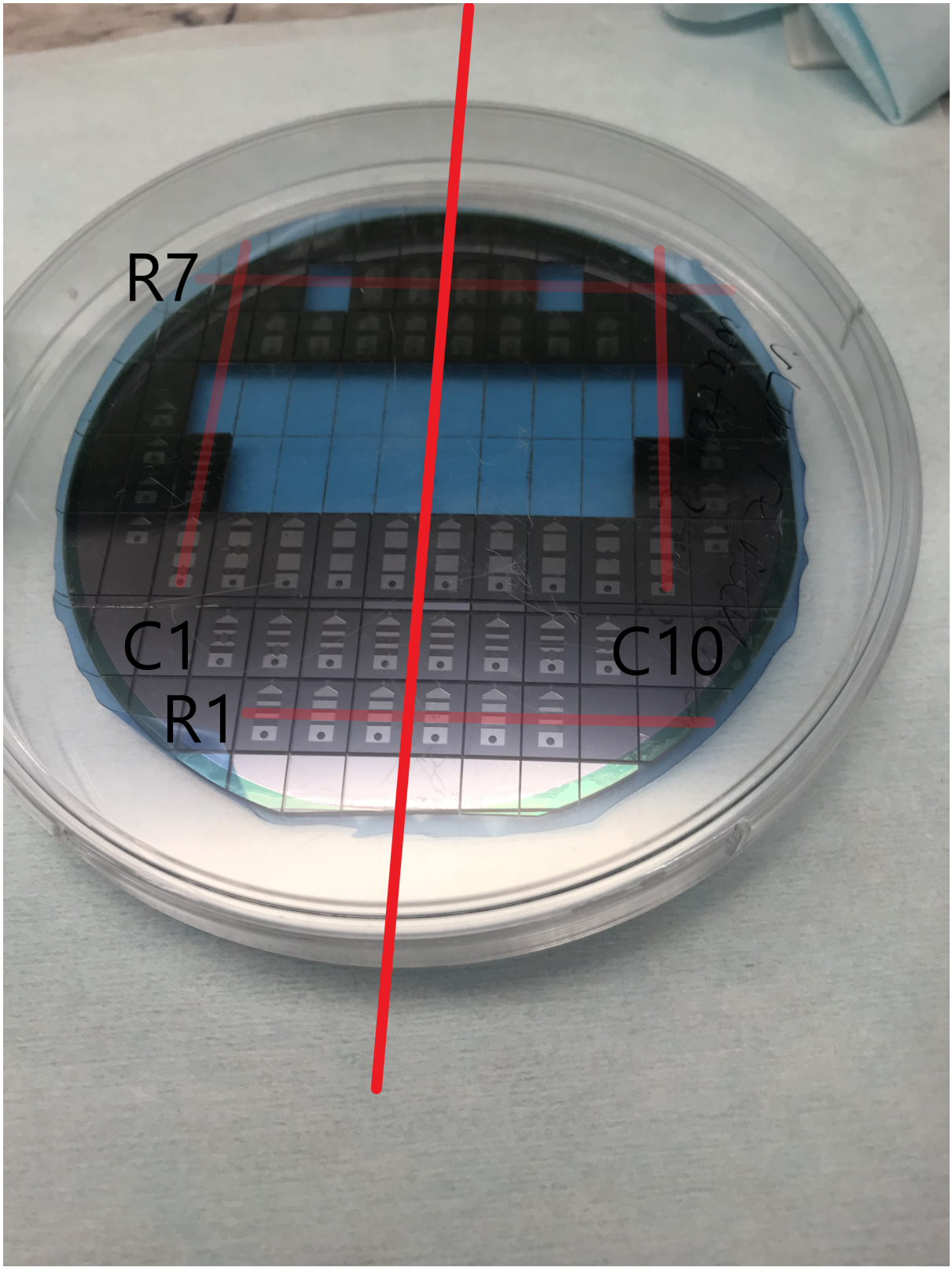

Figure 2.3: Picture showing wafer with various different thruster options. A few of the thrusters were already used. The thick red line represents the line of symmetry. The labels show where each row and column number starts.

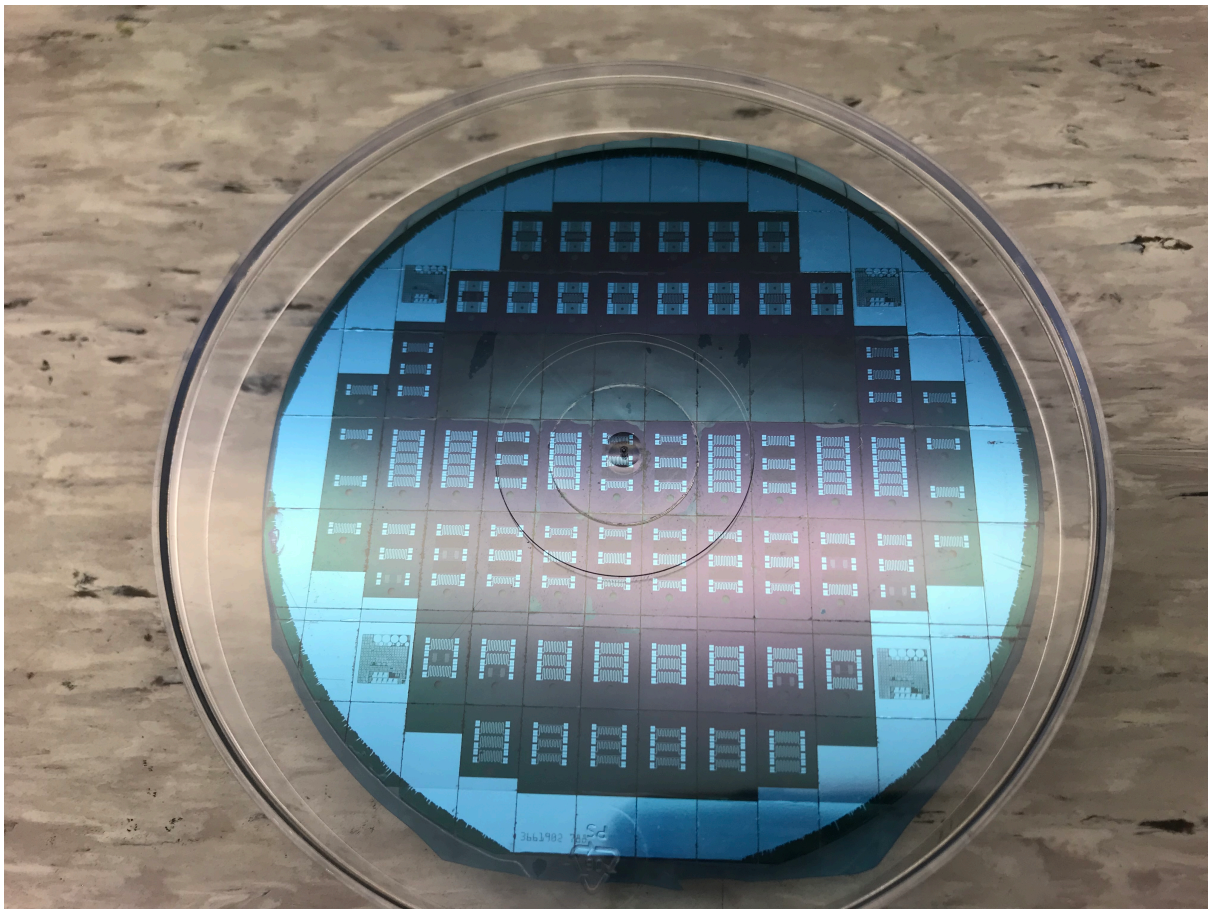

Figure 2.4: The rear of thrusters shown in Figure 2.3, where the external heaters are located.

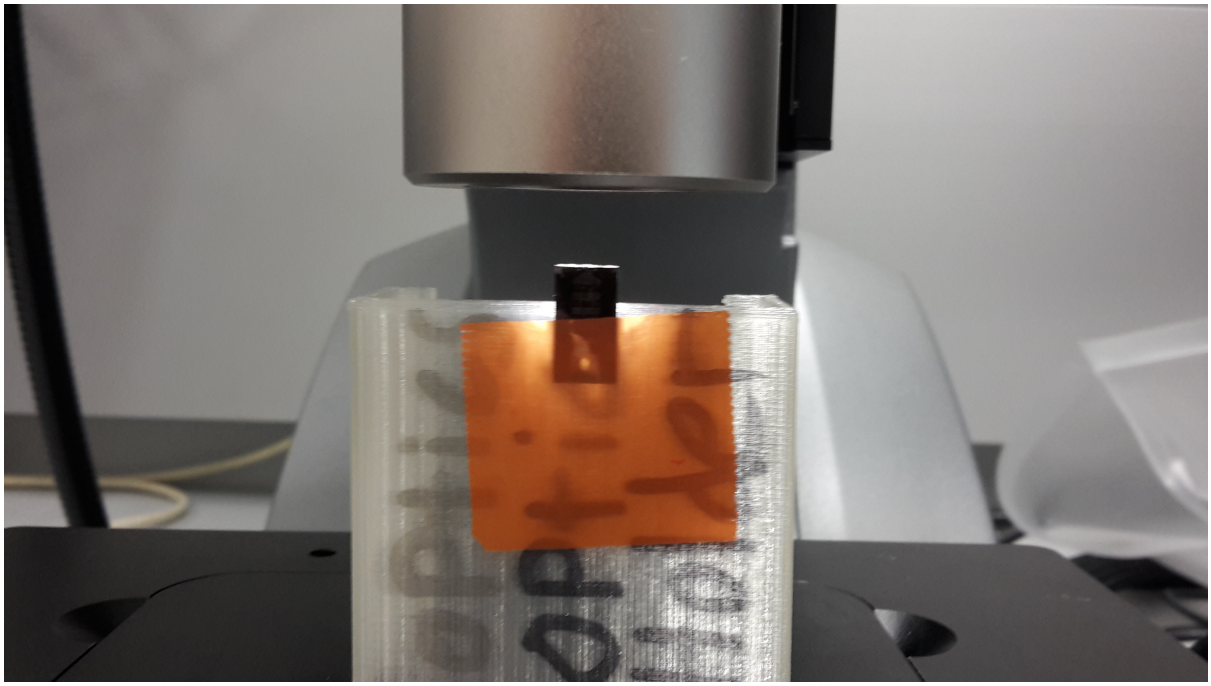

Figure 2.5: The thruster was taped to this flat surface to see and measure the exit width and exit height of the nozzle.

was removed from the PCB purposefully and placed under microscope normally. R4C9 was measured before performing any hot tests with it, so a component was 3D printed (see Figure 2.5) that would hold the thruster upside down under the microscope.

There was an issue in getting measurements for the R4C9 thruster using the 500-5000x lens, where the PCB the thruster was attached to, prevented the lens from being positioned close enough to the thruster to get a clear image. So for this thruster a 100x-1000x was used instead. For this reason, the uncertainties are slightly larger compared to the other thrusters. The 500-5000x lens was used for R5C1 and R4C7, since both of these thrusters were detached from their PCB. This meant the lens could be brought very close to the thruster chip to measure the necessary dimensions.

For future tests, it would be advisable to perform the optical measurements before the thruster chips are bonded to their PCB. Otherwise, the 500x-5000x lens will be obstructed by the PCB and the 100x-1000x lens will have to be used instead.

Additionally, the glue used to attach the thruster to the PCB accidentally obscured the area near the nozzle throat and exit during assembly, which meant these areas could not be viewed under microscope. This was the case for both thruster R4C7 and R4C9. However, this issue was quickly resolved by taking a small scalpel and slowly scraping away the fibrous, ceramic glue until the throat and exit could be viewed under the microscope clearly. Additionally, this glue also obscured the entirety of the chip before the nozzle, which meant that measurements could not be taken of the vaporizing channels. This unfortunately means that the entire thruster chips can not be fully characterized, as was the goal for this chapter. However, performance model predictions can still be made to predict the mass flow, thrust and quality factors of the thrusters. But no conclusions can be made to compare the effectiveness of using different vaporizing channels or heaters.

Measuring the h_t is not possible using the microscope stated, so it is assumed to be equal to the nozzle height at the nozzle exit h_e, which is straightforward to measure. The difference in height is expected to be negligible. Figure 2.7 shows the image captured by the microscope and the measurement made to determine h_e. The w_e and w_t were measured as can be seen in Figure 2.8 and Figure 2.9, respectively. The uncertainties for these values were determined by a pixel count. The thickness of the measurements lines was about 3 pixels each, so a total uncertainty of 6 pixels was used for the measurements. The length that corresponds to 6 pixels was found by comparing it to the scale at the bottom of each picture and how many pixels make up the stated length of that scale. The uncertainties in length for R4C9 are larger, since a less accurate 100x-1000x lens was used instead.

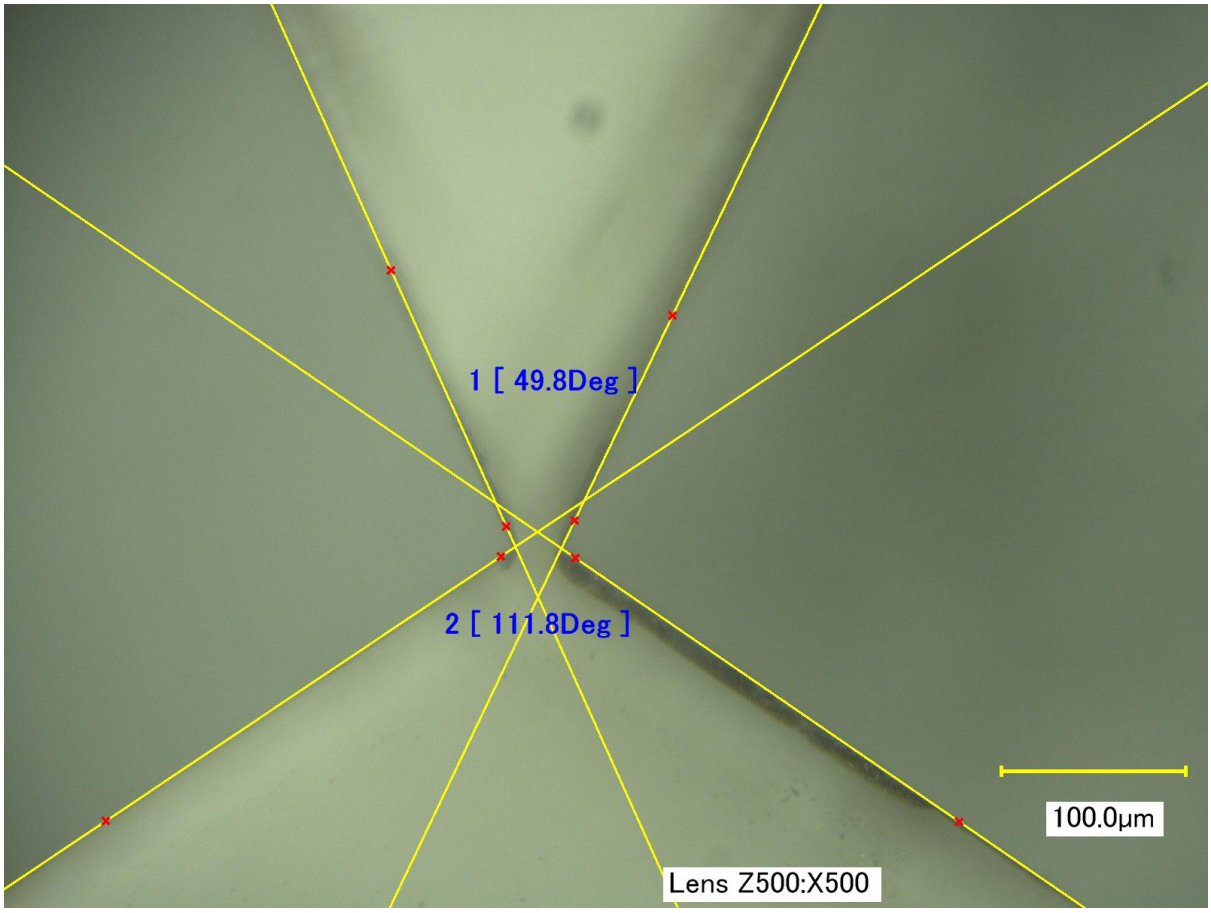

Figure 2.6: Convergent and divergent angles found at x500 magnification.

The $r_{t,c}$ measurement can be seen in Figure 2.10. An issue with this measurement is the fact that it was very difficult to align the circle to the location of the nozzle throat, by eye. For this reason a relatively large uncertainty of ± 0.25 μm was used.

The divergent and convergent half angle (θ_d and θ_c) were measured, as can be seen in Figure 2.6. An estimated uncertainty of $\pm 0.5^{o}$ was used.

Since these thrusters all come from the same wafer, they should have similar nozzle dimensions. Looking at Table 2.2, w_e and h_t some deviations can be noticed when comparing the thrusters to each other. The deviations can vary anywhere between 15μm for w_e and 6μm for h_t, which will give much larger deviations for A_e. This will result in expected performance variations in both the mass flow and the thrust predicted.

2.1.4. Electrical/Thermal Characterization

The purpose of the electrical/thermal characterization test is to form a relation between the input power to the heaters and the thruster chip temperature. Additionally, a description of the heaters and how they are powered will be given to provide as complete an overview as possible. This way the chip temperature could be estimated based on the power fed to the heater. Based on data from Silva et al. [27] and Kurmanbay [15] it was expected, before any testing was done, that the thruster temperature would increase linearly as the input power increases. However, the number of heaters attached to the thruster, the heater material and the thruster dimensions may affect the gradient of this relation.

A single test was done using thruster R4C7, without attaching it to the thruster pendulum.This test was performed in ambient conditions with no propellant flow. This was done by performing 4 point probe measurements on the thruster, which improves the accuracy of the measurements by reducing the effect of contact resistances. The results for that test can be seen in Table 2.5. R5C1 could not be characterized, since the thruster was severed after cold testing and could not be repaired on time.

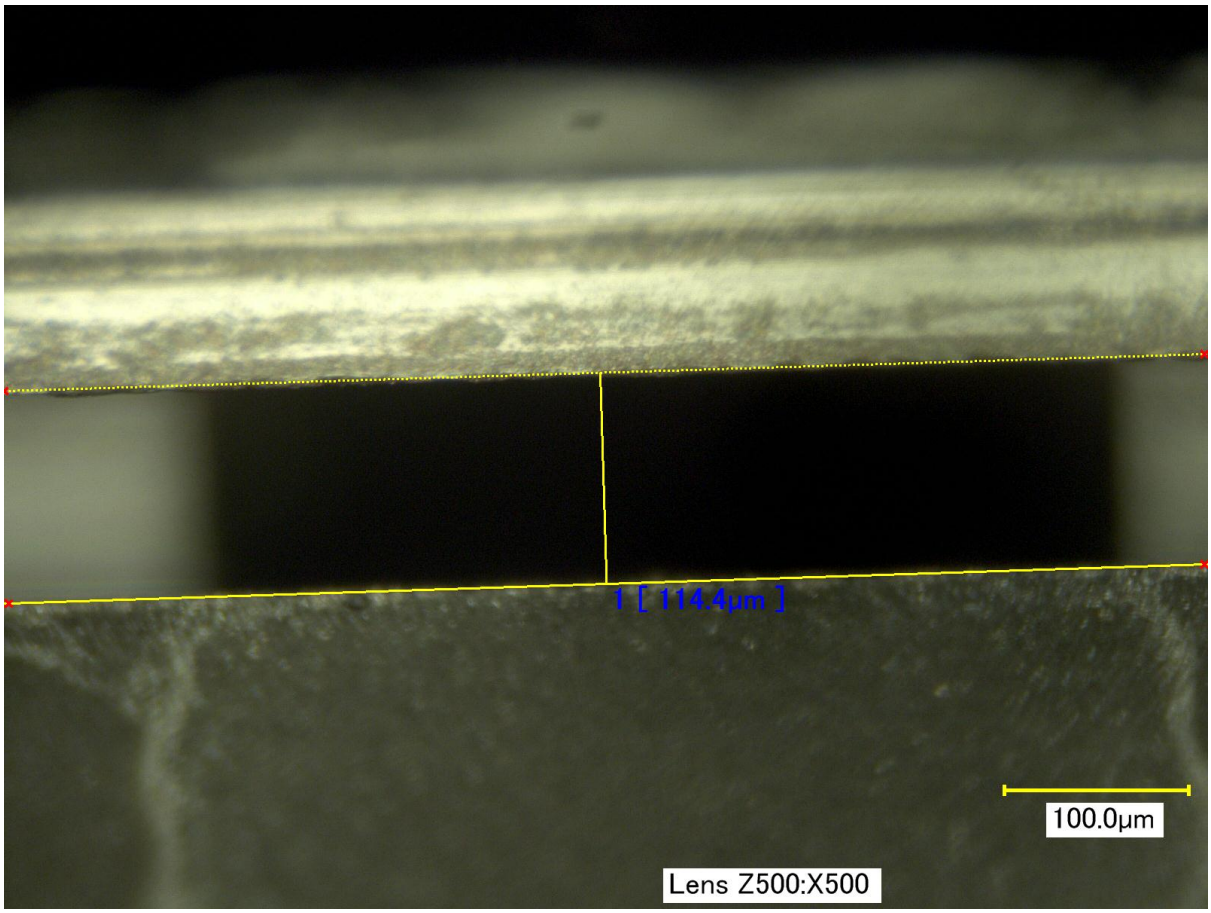

Figure 2.7: Exit height of the nozzle.

Table 2.2: Thruster dimensions measured, using a VHX 2000 digital microscope, for the three thrusters used during cold and hot testing.

Thruster	R5C1	R4C7	R4C9
θ_c (°)	24.9±0.5	25.4±0.5	25.5±0.5
θ_d (°)	55.8±0.5	56.1±0.5	56.1±0.5
w_e (μm)	484.2±2.44	484.4±2.44	499.6±2.51
w_t (μm)	25.36±0.26	25.84±0.26	25.90±1.27
$r_{t,c}$ (μm)	0.52±0.26	0.50±0.26	0.50±0.26
h_t (μm)	114.4±2.44	108.7±2.44	115.0±2.51
A_t (μm^2)	2901.18±91.62	2808.81±91.31	2978.50±211.06
A_e (μm^2)	55392.48±1460.58	52654.28±1447.16	57454.00±1542.65
AR (-)	19.09±1.11	18.75±1.12	19.29±1.05
$D_{H,t}$ (μm)	41.52±2.11	41.75±2.20	42.28±4.13

Table 2.3: The relevant thruster dimensions used by Makhan [18] during thruster testing.

w_t [μm]	17.2±1.2
h_t [μm]	81±5
θ_c [o]	20.5
A_t [μm^2]	1.4e+3±1.3e+2
A_e [μm^2]	4.2e+4±2.7e+3
$D_{H,t}$ [μm]	28.7±3.7

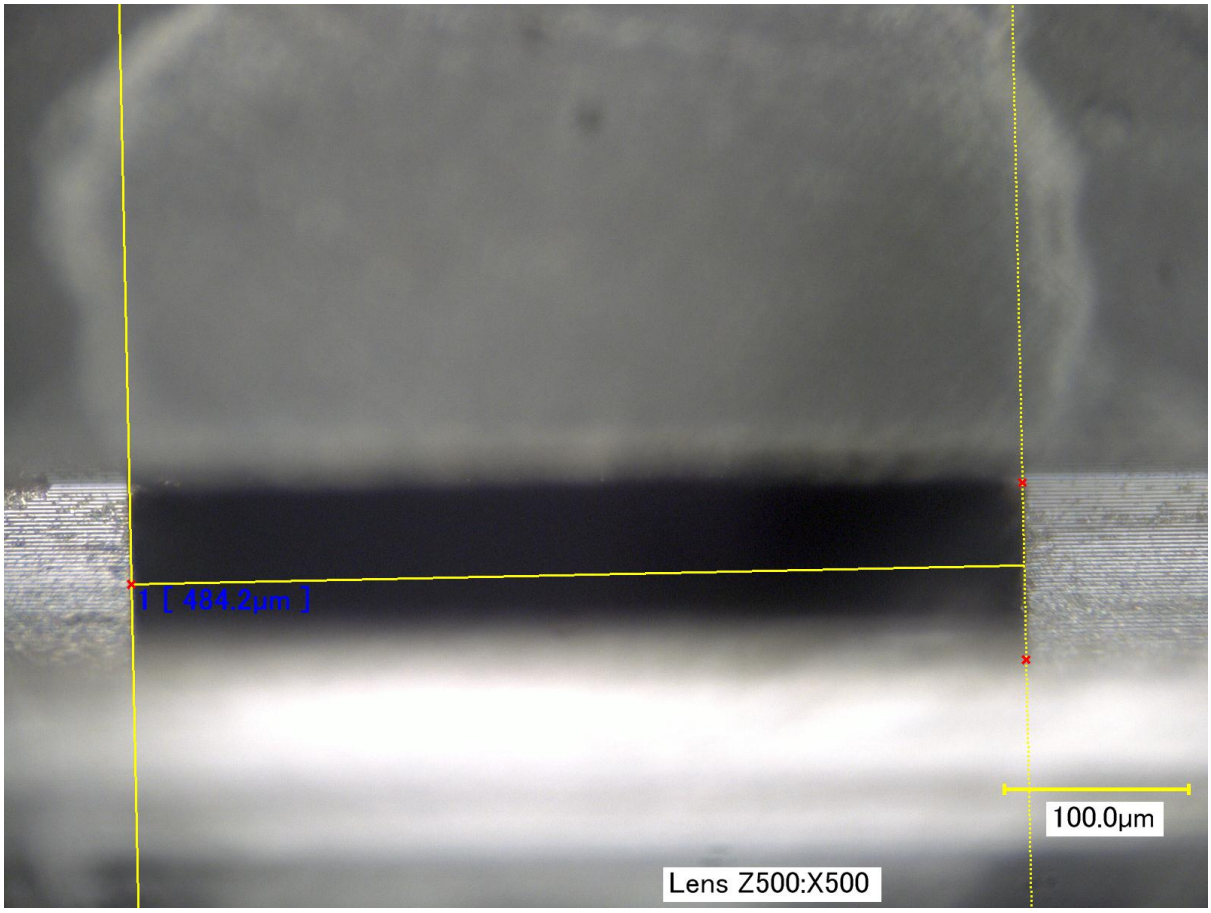

Figure 2.8: Exit width of the nozzle.

Table 2.4: The relevant thruster dimensions used by Bayt [1] during hot thruster testing.

w_t [μm]	65
h_t [μm]	491
θ_c [o]	20.5
A_t [m^2]	3.19E-08
A_e [m^2]	2.63E-07
$D_{H,t}$ [μm]	114.75

Table 2.5: Electrical/Thermal characterization test for thruster R4C7.

V_{input} (V)	V_{actual} (V)	P_{input} (W)	P_{actual} (W)	Temperature (^oC)
1.0±0.03	0.89±0.03	0.02±0.05	0.02±0.05	35.0±5
5.0±0.06	4.52±0.06	0.53±0.25	0.48±0.25	62.7±5
6.0±0.07	5.43±0.07	0.74±0.30	0.67±0.30	74.1±5
8.0±0.08	7.25±0.08	1.22±0.38	1.11±0.38	101.7±5
10.0±0.09	9.06±0.09	1.77±0.49	1.61±0.49	131.9±5
11.5±0.10	10.43±0.10	2.20±0.58	2.00±0.58	154.8±5

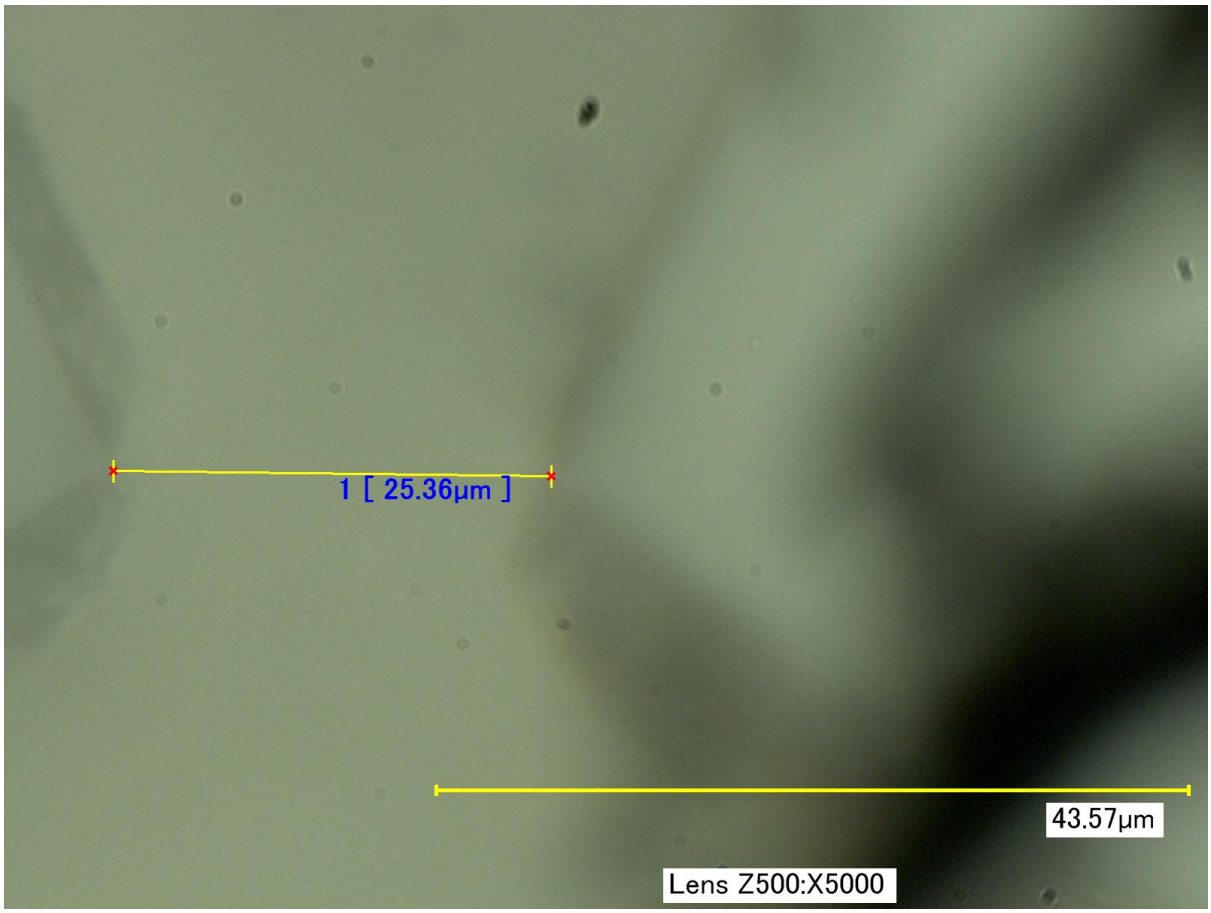

Figure 2.9: Throat width of the nozzle.

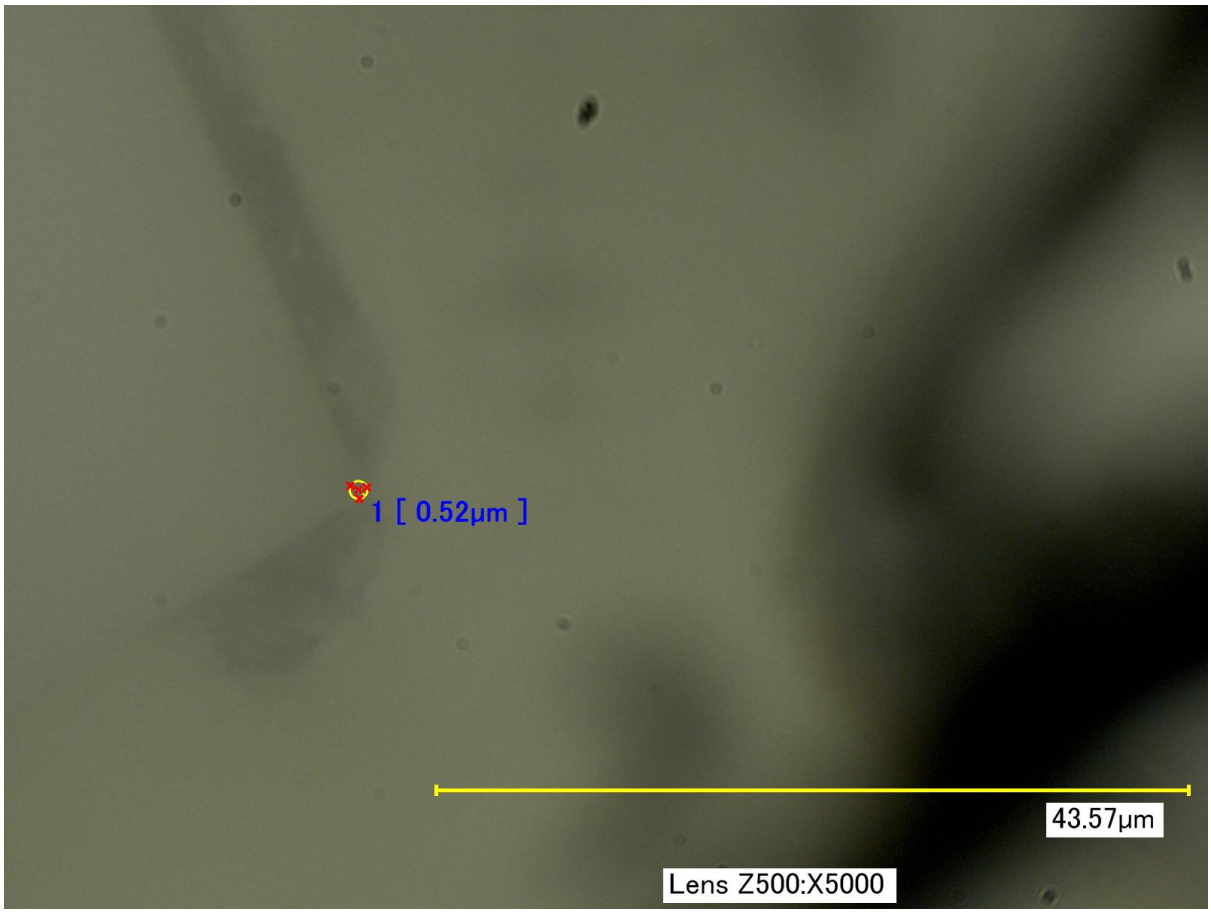

Figure 2.10: Radius of curvature for the throat of the nozzle.

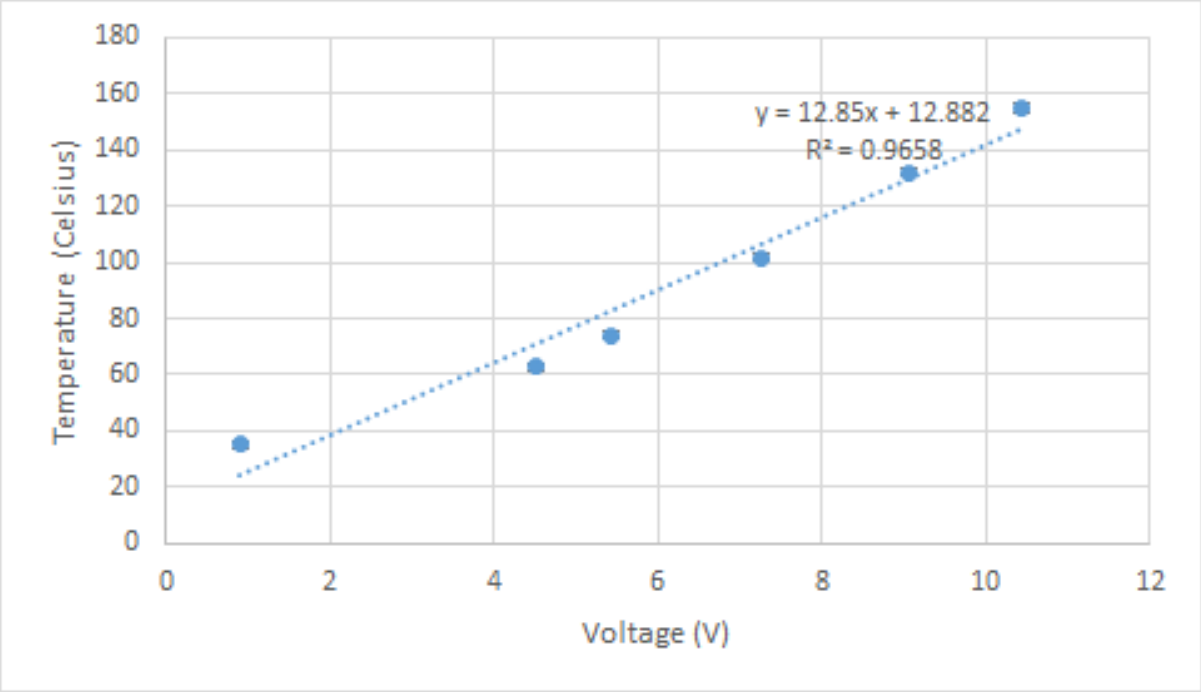

Figure 2.11: Relation between the expected chamber temperature and the actual input voltage to the thruster heaters.

The electrical characterization relations for R4C7 can be seen in Equation 2.1 and Figure 2.11 is where the relation is derived from. The relation between the power and the temperature of the chip is almost linear. This relation can be used to estimate the temperature for larger input powers. However, the relations for R4C9 and R5C1 are expected to be different and still need to be characterized.

$$T = 12.85^{o}C/V \cdot V_{actual} + 12.882 \tag{2.1}$$

2.2. Previous Thruster Interfaces

This section will cover the two previous interfaces used to hold the VLM thruster chips and interface with the pendulum. Initially, the PCB interface was used by Van Wees [35] and Kurmanbay [15], however use of a teflon block was used in later research by Silva et al. [27] and Makhan [18]. Despite the compact and more robust nature of the second interface, the low operating temperature of the design limited its use at higher operating temperatures. For this reason, it was decided to use the PCB interface instead with a more heat resistant glue.

2.2.1. Printable Circuit Board Interface

One design of the thruster interface, used by Van Wees [35] and Kurmanbay [15], involved attaching a thruster chip to a PCB, using ABLESTIK glue, to electrically interface the external heaters to a power source. Figure 2.12a shows the layout of the PCB used for the electrical interface of the thruster. The PCB is 45x25 mm and has gold plated pads which correspond to a pin number. Thin wires are bonded to the Au plates on the PCB and are connected to the Aluminum pads found on the thruster heaters. This is how the electrical current flows from the pins to the thruster heaters. Additionally, a 16.25x2 mm window is present, to view the VLM during testing. Kurmanbay [15] performed tests up to a around 350^{o}C, however this was for thrusters were one heater was operational. So the entire thruster chip was not uniform in temperature. A plastic dispensing tip was also glued to the inlet of the thruster. The dispensing tip has a female luer lock.

Van Wees [35] was then able to use a 3D printed platform that could hold and attach the PCB to the thrust pendulum. It was intended to use this platform during testing, however after searching it could not be found and smaller and a simpler platform, shown in subsection 4.1.6, was built instead.

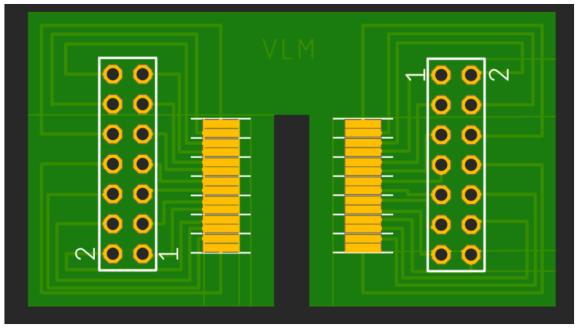

(a) PCB board.

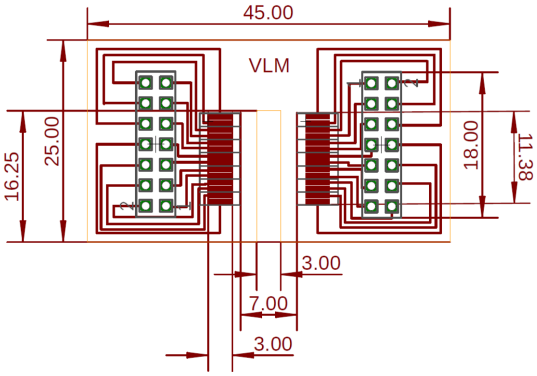

(b) PCB board with dimensions.

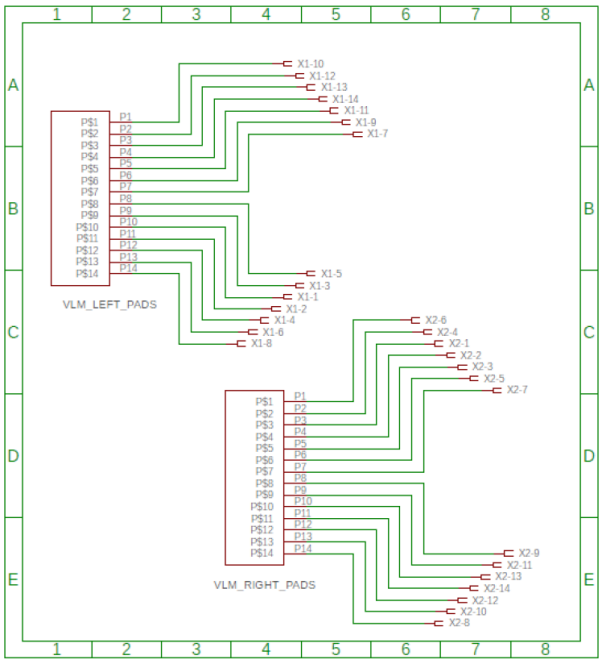

(c) Pin layout and electronics.

Figure 2.12: PCB board illustration and layout. Figures courtesy of Kurmanbay [15].

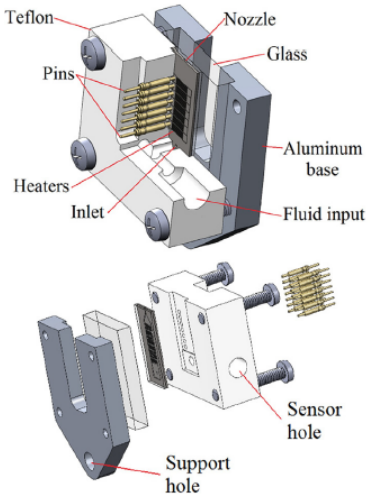

Figure 2.13: Top view and exploded view of the 1st generation teflon interface by Silva et al. [27].

2.2.2. Teflon Interface Design

The interface, used by Silva et al. [27] and Makhan [18], uses a teflon block with aluminium plates, for sealing the thruster and propellant. This interface can be seen in Figure 2.13. Makhan [18] noted that the thruster tended to warp and bend at high temperatures, which would cause leakages. Despite this, Silva et al. [27] was still able to perform hot tests up to 420K, before this became an issue. This is very much a limiting factor of this design, for performing hot thrust tests at higher temperatures.

The sensor hole, on the interface, allows for direct measurement of the temperature and pressure just outside the inlet. So it is not able to directly measure the chamber conditions.

Additionally, spring loaded pins are used for power delivery to the heaters and the glass window allows users to directly view what is occurring the vaporization chamber.

Overall, this design is a lot more compact compared to the PCB interface and is less fragile. However, the low operating temperature of the design, limited by the teflon material used for the interface, means the design is limited to around 420K.

2.3. Redesigned Thruster Interface

With the help of Henk van Zeijl[1], a thermal protection design will be tested and applied to the PCB interface to create a thruster interface with an extended maximum operating temperature, to allow high enough chamber temperatures to reach full vaporization throughout the entire thruster. To reach full vaporization throughout the nozzle, it needs to be understood that the vaporization temperature for water increases as the chamber pressure increases. So, to reach full vaporization in the thruster chamber with a chamber pressure of 5 bars, the vaporization temperature is expected to increase to 150^{o}C. This is explained in more depth in section 3.6, where the effects of condensation at the nozzle throat is also considered.

The PCB style interface used by Kurmanbay [15] and Van Wees [35] will be used as a base. The new interface is made up of four parts, which can all be found in the thesis box of Aris Pappadimitriou, in the cleanroom:

1. A PCB where the thruster is glued to and allows for electrical interfacing (see Figure 2.12a).
2. An optional 3d printed platform to hold the PCB (see Figure 2.14a).
3. A 3d printed cover that attaches the platform to the pendulum arm.
4. A metallic dispensing needle which is glued in place to the thruster inlet (see Figure 2.14b). Make sure to use the dispensing tips which have the gauge length of 19.

[1]Henk van Zeijl is a professor at the Laboratory of Electronic Components, Materials and Technology, at the Electrical Engineering faculty of the DUT.

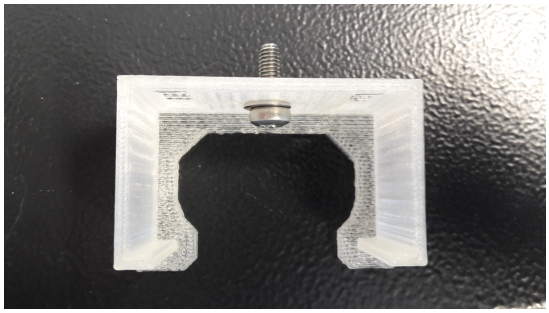

(a) Cover.

(b) Stainless steel dispensing tip. Picture courtesy of FISNAR.

Figure 2.14: The figures showing the stainless steel dispensing tip and the 3D printed cover.

Glue	Thermeez 7020	Bison	ABLESTIK
Max Temperature (^{o}C)	1260	300	150
Material	White fibrous putty	Black flexible silicon	Silverish die attach epoxy
Thermal Conductivity (W/mK)	1.12	not given	2.4

Table 2.6: Glue characteristics *Ceramic Adhesives and Putty* [6], *Technical Data Sheet LOCTITE ABLESTIK 84-1LMI* [33] and *Bison Siliconenkit High Temp Zwart Tube 60 ml NL /FR* [3].

Using PCB's as an electrical interface for the thruster is a method that has been used previously Kurmanbay [15] Van Wees [35]. The layout of the PCB can be seen in Figure 2.12a, where the pin layout is shown along with the dimensions of the PCB. There is a 3mm by 16.25mm window on the PCB, where the fluid motion can be observed through. The bottom wafer of the thruster is made of pyrex glass which allows the user to see the fluid motion through the wafer.

The cover is designed to hold a 45x25 mm PCB. The top of the cover has a hole in it to allow an M4 screw to be fitted in and attach to the pendulum arm. The cover comes with an optional platform which is placed under the PCB, but it is not really necessary for testing. The design of the cover was made using CATIA software. For a CATIA drawing see Figure B.1 from Appendix B.

A needle is then fitted to the inlet of the VLM and glued in place. The dispensing tips used by Kurmanbay [15] had some parts made of plastic. To avoid the likelihood of melting, these dispensing tips were replaced by stainless steel ones from FISNAR [2]. The diameter of the inlet hole is 1 mm, so the chosen dispensing tips had a gauge length of 19, which corresponds to an outer diameter of 0.9 mm. This will allow the dispensing tip to fit inside the inlet hole. The opposite side of the dispensing tip is a female luer lock.

Additionally, several glues were considered for connecting the inlet needle to the thruster chip and attaching the thruster chip to the PCB:

1. LOCTITE ABLESTIK 84-1LMI glue
2. Bison Siliconkit High Temp Black
3. Thermeez 7020 ceramic glue

These glues are currently in the possession of Henk van Zeijl. Some characteristic data for this glue can be seen in Table 2.6.

The thruster chip is attached to a PCB using glue. To minimize the transfer of heat from the thruster to the PCB a ceramic glue called Thermeez 7020 was considered for both the dispensing tip and attaching the VLM to the PCB. This glue has a higher operational temperature and lower thermal conductance compared to ABLESTIK glue. This means the transfer of heat from the thruster chip to the PCB will be less, therefore it should be able to handle higher temperatures before any damage to the PCB occurs. Data on the ceramic glue can be found in *Ceramic Adhesives and Putty* [6]. Additionally, a handbook

[2] https://www.fisnar.com/products/dispensing-accessories/dispensing-tips/stainless-steel-dispensing-tips/

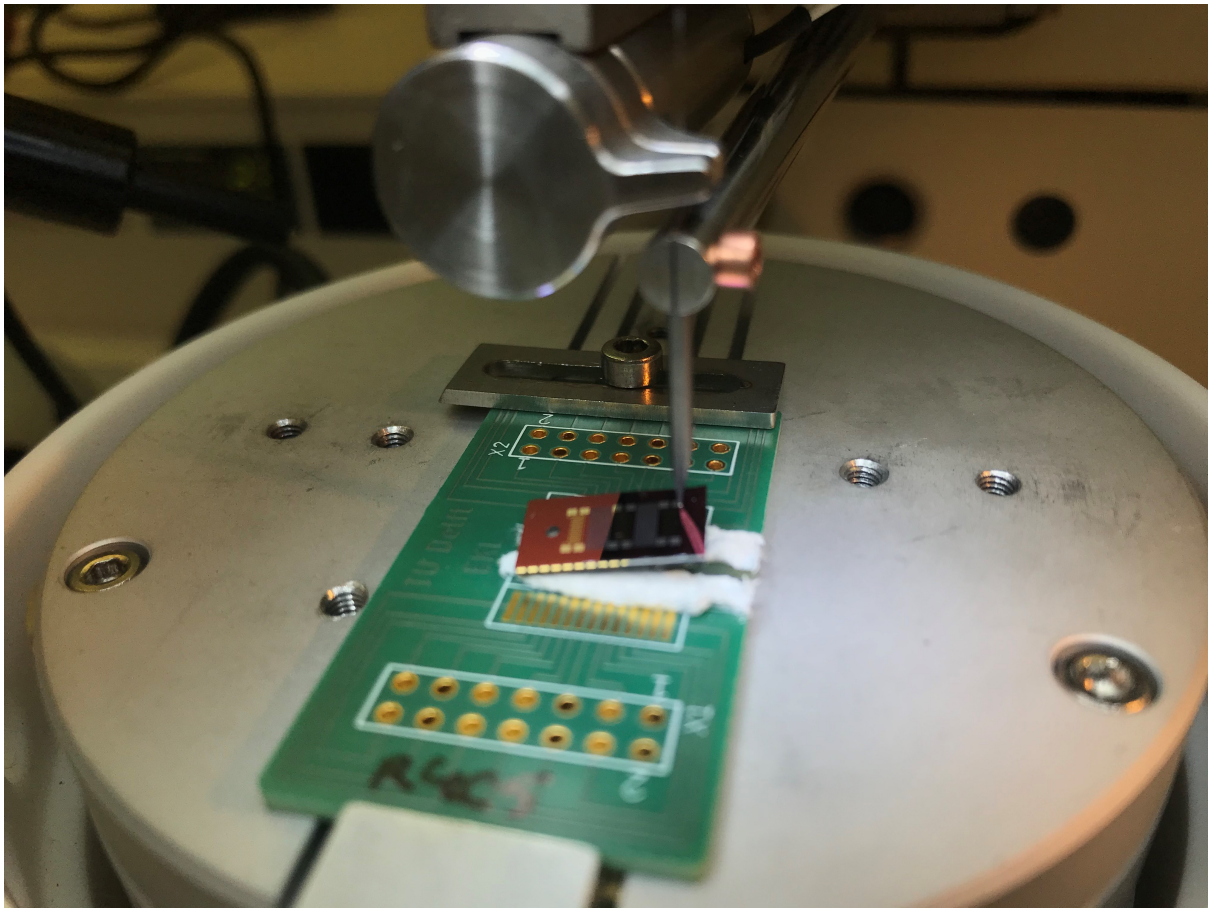

Figure 2.15: Thruster here was pulled from its PCB during the wirebonding process, when using the ceramic glue. Picture courtesy of Henk van Zeijl.

for the Thermeez glue, which includes its handling, implementation and information, will be given to the lab. During fabrication, however, Henk noticed several issues that resulted in slightly altering the design or using different glues.

The ceramic glue, on its own, has a very poor adhesive quality. During the wire-bonding process, the back-pull of the aluminium wires is enough to pull the thruster off of the PCB. To fix this issue, Henk used a locking method to attach the thruster to the PCB. This is done by placing a small layer of adhesive ABLESTIK glue on the thruster and curing it at 120^{o}C. Then the ceramic glue is layered on top of the ABLETICK glue and wrapped around the lengthwise edge of the thruster to hold it. This method provided a much better hold on the thruster and counteracted the pull of the aluminium bond wires.

Additionally, the poor adhesion also means that it can not be used to attach the microfluidic dispensing tip to the thruster inlet. The BISON glue was going to be used as a replacement due to its high operational temperature and better adhesivity. However, this glue was very soft and failed almost immediately during leak testing, for both the R4C5 and R4C6 thrusters, meaning that these thrusters are now inoperable. Therefore, the ABLESTIK glue, used in the previous design Kurmanbay [15], will have to be used. Due to this reason, it was expected that the thruster inlet would be the first part of the design to fail, due to the lower maximum operating temperature of the ABLESTIK glue. During hot testing for thruster R4C7, this prediction was proven correct at around 150^{o}C. For future work, it is recommended to try and find a low conductivity glue that has a better adhesive quality than Thermeez 7020. If this is not possible, then a thruster redesign will need to be done to isolate the thruster inlet from the heaters. An illustration of the final design, using the locking method, can be seen in Figure 2.16.

The second issue is that the glue, near the inlet, can sometimes cover the aluminium pads from which the wires are supposed to be bonded to. This was the case for thruster R5C1. This makes it impossible to bond wires and carry out heated thruster tests, since the glue can not be removed from the thruster without damaging the aluminium pads. The only way to mitigate this issue is to apply the

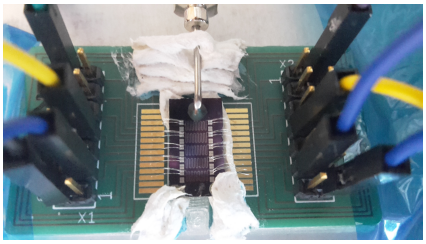

Figure 2.16: Final design iteration of the thruster, attached to a PCB, using Thermeez 7020 and ABLESTIK glue.

required glue carefully and and in small amounts.

The last issue was that the small window for observing the vaporisation chamber, was obscured by the glue. This would make optical characterization (see subsection 2.1.3) more difficult. However, this issue was solved by using a small, sharp scalpel to scrape away some of the excess ceramic glue, to view the nozzle throat and exit. This could not be done to view the vaporizing channels unfortunately, as it involved some risk of scratching the thruster and/or severing the thruster from its PCB.

2.4. Fragility of the Redesigned Thrusters

One important outcome of the design, which was discovered during the prepatory and thrust testing phases of the thesis, is overall fragility of the design. Of the 7 thrusters made, 4 are now inoperable.

To summarize:

- Thruster R4C5 and R4C6 failed during testing, due to the softness of the BISON glue used to attach the dispensing tip to the thruster inlet. The thrusters showed noticeable leakages at pressures as low as 2 bars. BISON glue is not a suitable glue to use for the thruster inlet.
- Thruster R5C1 broke when attaching the thruster to the thrust test bench, when trying to perform the first hot test. It is very easy to accidentally rip off the thruster from its PCB so special care is needed during the test set up.
- Thruster R4C7 failed at the end of the first hot test. The ABLESTIK glue used for the inlet melted at a chip temperature of 150^{o}C. Therefore, the current design could not reach the minimum temperature goal of 600K.

Therefore, it is recommended that future researchers who wish to use this design have two identical thrusters ready, for each thrust test they intend to do. For example, if 5 thrust tests will be performed with 5 different thrusters, manufacture 5 pairs of thrusters (10 in total), so there is always a backup thruster available.

2.5. Conclusions

Overall, the thruster chips that will be used have been partly described in and the rationale behind the design for the interface has been provided.

Of the 7 provided thrusters, three of them have had their nozzles characterized under a microscope, which will provide the necessary input values for predicting the thruster performance of the nozzles. Their vaporizing channels and heaters could not be measured in time unfortunately. The vaporizing channels could not be measured as the glue obscured the area beneath the PCB, where the vaporizing channels could be viewed. Additionally a linear power to temperature relation could be found for thruster R4C7, which was $T = 12.85W/^{o}C \cdot P + 12.882$. R4C9 and R5C1 did not have been thermally characterized yet.

It was chosen to use the PCB interface used by Kurmanbay [15] and Van Wees [35]. Despite its greater fragility and being less compact than the 3rd generation interface used by Silva et al. [27] and Makhan [18]. It was expected that it would be able to handle much higher operating temperatures, if a glue with a higher operating temperature was used to attach the thruster to the PCB and the metal dispensing tip to the thruster inlet. A ceramic glue (Thermeez 7020) was determined to be the most suitable glue at the time, due to its higher operating temperature of 1260^{o}C. However, its poor adhesion meant that it could not be used for the dispensing tip and after consultation, it was decided to continue with a glue which had a lower maximum temperature use.

Unfortunately, the new design will most likely not be able to withstand temperatures up to 600K, as it is expected that the glue at the thruster inlet will fail around its maximum operating temperature of 150^{o}C, before reaching that temperature. Due to lack of time and availability of thruster manufacturing at the Electrical engineering faculty, it was decided to continue on with testing the thruster.

For future work, it is recommended to:

- Perform the optical characterization of the thrusters before they are attached to their PCB. This will alleviate the following problems:
  - The PCB blocking the placement of the 500-5000x lens, meaning a smaller and less accurate 100-1000x lens had to be used for thruster R4C9 [3].
  - The ceramic glue obscuring the viewing window of the PCB, meaning that the vaporizing channels could not be measured for any of the thrusters.
- Remeasure the dimensions for thruster R4C9, with greater magnification. This should help reduce the dimension uncertainties and therefore lead to more confidence in the thruster test results.
- Determine a better glue that can be used to attach the dispensing tip to the thruster inlet. This glue should have better adhesive qualities than Thermeez 7020, but should also be able to withstand temperatures higher than 600K.
- Thermally characterize thruster R4C9 and R5C1 to investigate the effects of the different heaters on the relation between input power and chip temperature.
- Ensure that for future tests at least two identical thrusters are available for each thrust test that will be carried out. This is due to the fragility of the thruster design.

[3] Thruster R4C7 and R5C1 was measured using the 500-5000x lens, since the thruster chips were detached from their PCB accidentally.

3

Thruster Performance Model

The goal of the thesis is to be able to predict the performance of a microresistojet across the entire operational range by building a valid model. So it is important to discuss the model that will be used to predict the performance of the thruster. The goal of this chapter is to:

- Discuss the model that will be used to quantitatively determine the performance of the thruster.
- Validate the chosen models by comparing it to existing test data from literature.
- Predict the expected performances of the thrusters R5C1, R4C7 and R4C9.

The performance model was built using Excel and can be found by contacting Barry Zandbergen or looking in the data disk for Micropropulsion Contributors, under the name of Aris. The excel file with the performance model is named the ”Predictive Thruster Performance Model.xslx”.

The method of predicting the performance of the thruster is based off of the reader by Zandbergen [37]. Makhan [18] applied and extended this model. The model was adapted to be applied for 2D thrusters, instead of 3D thrusters. The model uses ideal rocket theory, explained in section 3.1, with corrections that take into account the effect of characteristic length, boundary layer losses, viscous losses and divergent nozzle losses. These corrections are presented in section 3.2, section 3.3 and section 3.4 and section 3.5. The predicted outcomes of the performance model and the validation of the model will be explained and presented in section 3.7. The expected thruster performances are presented in section 3.8. Lastly, conclusions will be summarized in section 3.9.

3.1. Ideal thruster performance

The approach to creating the thruster performance model are based off of the reader by Zandbergen Zandbergen [37], who took different methods and equations from a variety of sources. The equations to calculate $(\dot{m})_{ideal}$, $(F_t)_{ideal}$ and $(Isp)_{ideal}$ are Equation 3.1, Equation 3.2 and Equation 3.3, respectively.

$$\dot{m}_{ideal} = \frac{P_c \cdot A_t}{c^*} \tag{3.1}$$

$$F_{ideal} = \dot{m}_{ideal} \cdot C_{F,ideal} \cdot c^* \tag{3.2}$$

$$Isp_{ideal} = \frac{F_{ideal}}{g_0 \cdot \dot{m}_{ideal}} \tag{3.3}$$

Additionally, several more intermediate equations are shown in Equation 3.4 to Equation 3.10, which follow from ideal rocket theory as well.

$$\Gamma = \sqrt{\gamma \cdot (\frac{1+\gamma}{2})^{\frac{1+\gamma}{1-\gamma}}} \tag{3.4}$$

$$T_t = \frac{2}{\gamma + 1} \cdot T_c \tag{3.5}$$

$$P_t = (\frac{2}{\gamma + 1})^{\frac{\gamma}{\gamma - 1}} \cdot P_c \tag{3.6}$$

$$c^* = \frac{1}{\Gamma} \cdot \sqrt{\frac{R_A}{M_w} \cdot T_c} \tag{3.7}$$

$$(C_F)_{ideal} = C_F^0 + (\frac{P_e}{P_c} - \frac{P_a}{P_c}) \cdot AR \tag{3.8}$$

$$C_F^0 = \frac{v_e}{c^*} \tag{3.9}$$

$$v_e = \sqrt{\frac{2 \cdot \gamma}{\gamma - 1} \cdot \frac{R_A \cdot T_c}{M_w} \cdot [1 - (\frac{P_e}{P_c})^{(\frac{\gamma - 1}{\gamma})}]} \tag{3.10}$$

Additionally, the calculation of the Reynolds number (Re) is necessary to incorporate the correction factors in the following sections. The Re at the throat using ideal rocket theory can be calculated using Equation 3.11, where μ_t is the dynamic viscosity of the flow at the throat and d is the characteristic length of the nozzle, which in the case of round nozzles is the diameter. However, it is explained in section 3.2 how different dimensions can be used depending on the cross section of the thruster throat.

$$Re_t = \frac{\dot{m} \cdot d}{\mu_t \cdot A_t} \tag{3.11}$$

The following observations can be made on the previous equations, based on the literature study by Pappadimitriou [22]:

- T_t, $c*$, CF_{ideal}, CF^0 and v_e basically remain constant despite the pressure differences. The effect of chamber pressure is very small for these parameters, which makes sense since none of these parameters are directly affected by chamber pressure in their respective equations.
- P_t is much lower than its respective P_c, where the P_t is about 53% of its respective P_c, when $\gamma = 1.4$ is used for cold nitrogen. Additionally, as the P_c increases so does the P_t, which is in agreement with Equation 3.6.
- Lastly, the Re_t increases as the P_c increases. The reasoning is that as the chamber pressure increases the mass flow of the thruster is expected to increase according to Zandbergen Zandbergen [37]. This increase in mass flow causes an increase in Re_t, which means that as the P_c increases, the flow shifts from laminar flow at lower pressures to more turbulent flows at much higher pressures.

3.2. Hydraulic diameter correction

The hydraulic diameter is an important factor in the determination of the throat Reynolds number in Equation 3.12. d_t represents the characteristic length of the nozzle, where in the case of circular throats, would be equal to the diameter of the throat. However, rectangular planar nozzles will be used in this thesis, so a different characteristic length needs to be used. It directly affects the viscous losses and throat boundary layer losses experienced in the nozzle, which can alter the predicted mass flow and thrust. A discussion with Barry Zandbergen lead to the realization that the d_t used by Makhan [18] and Bayt [1] are defined differently. Additionally, the use of a different definition might be applicable and worth investigating. Through comparing the methodology of the work of Makhan [18] and Bayt [1], Makhan [18] used Equation 3.13 and Bayt [1] used Equation 3.14, to determine the hydraulic diameter at the throat.

$$Re_t = \frac{\dot{m} d_t}{\mu_t A_t} \tag{3.12}$$

$$d = D_{H,t} = \frac{4 \cdot A_t}{P_t} \tag{3.13}$$

$$d = w_t \tag{3.14}$$

Equation 3.13 is based of the actual definition of the hydraulic diameter while Equation 3.14 is an assumption made for nozzles with a very high aspect ratio, where the height of the nozzle throat is much larger than the width of the nozzle throat. The nozzle height (h_t) is defined in Figure 2.7 and the nozzle throat width (w_t) is defined in Figure 2.9. The nozzle throat height is assumed to be similar to the exit throat height, due to the difficulty in measuring the nozzle throat height directly, with the used microscope, and is not expected to be very different. Note that the dimension that should be used is the smallest value, which in this case is the width of the nozzle.

3.3. Discharge coefficient

The discharge coefficient is the value that compares the acquired experimental mass flow with the ideal mass flow from Equation 3.1. The mathematical equation for the discharge coefficient can be seen in Equation 3.15. Several different methods were found from literature that predicted the discharge coefficient for the thruster assuming a sonic condition at the throat.

$$C_D = \frac{\dot{m_{exp}}}{\dot{m_{ideal}}} \tag{3.15}$$

3.3.1. TF Model

The first method, is the analytical solution of Tang and Fenn [31], which has been used by previous students Makhan [18], represented by Equation 3.16. The analytical method takes into account the presence of the throat boundary wall in calculating $C_{d,TF}$, by using Equation 3.16. The valid range reported was $100 < Re_t < 10000$. The input parameters for the method involve γ and a modified Reynolds number $Re_{t,J}$, that can be calculated by using Equation 3.17 where $r_{t,c}$ is the radius of curvature of the nozzle throat [m], d is the characteristic length of the nozzle throat [m] and Re_t is the Reynolds number at the throat [-]. It is important to note that r_t refers to the radius of a circular throat, however the thrusters in thesis have rectangular profiles. So for the case of this thesis, r_t actually refers to $\frac{D_{H,t}}{2}$ or $\frac{w_t}{2}$, depending on which definition of the characteristic length is being used.

$$C_{D,TF} = 1 - (\frac{\gamma+1}{2})^{3/4}(\frac{72-32\sqrt{6}}{3(\gamma+1)} + \frac{4\sqrt{6}}{3})(\frac{1}{\sqrt{Re_{mod}}}) + (\frac{2\sqrt{2}(\gamma-1)(\gamma+2)}{3\sqrt{\gamma+1}})(\frac{1}{R_{mod}}) \tag{3.16}$$

$$Re_{mod} = Re_t \sqrt{\frac{d}{r_{t,c}}} \tag{3.17}$$

3.3.2. J Model

The second method is a empirical solution created by Johnson et al. [13], who was able to create relations to predict the C_d for Nitrogen, Argon, Carbon dioxide and and hydrogen fed nozzles for an Re between 2000-22000. It was assumed that the gas was a perfect gas and had a constant cp. Johnson et al. [13] determined a linear relation for the C_d for these gases with respect to the $1/\sqrt{R_t}$. This relation can be seen in Equation 3.18, where β represents the slope of the relation and α represents the y-intercept of the relation. Johnson et al. [13] has these values for 4 different gases in his work, but the experimental values for nitrogen will be used for this thesis. These values are $\alpha = 1$ and $\beta = 3.62$.

$$C_{D,J} = \alpha - \frac{\beta}{\sqrt{Re_t}} \tag{3.18}$$

3.3.3. KH Model

The third and final method, is based off of the work of Kuluva and Hosack [14], and involves the use of a semi-empirical equation to predict the discharge coefficient. The valid range of this relation is $0 \leq r_c/w_t \leq 20$ and $50 \leq Re_{t,ideal} \leq 100000$, as reported by the original work. This method was used by Giorgi and Fontanarosa [10] to model the performance of a rectangular outlet thruster, but was not compared to experimental data.

$$C_{D,KH} = \left(\frac{r_{t,c} + 0.05 \cdot 0.5d}{r_{t,c} + 0.75 \cdot 0.5d}\right)^{0.019} \cdot \left[1 - \left(\frac{r_{t,c} + 0.10 \cdot 0.5d}{0.5d}\right)^{0.21} \cdot \frac{1}{\sqrt{Re_{t,ideal}}}(0.97 + 0.86\gamma_c)\right] \tag{3.19}$$

3.4. Knudsen number

The knudsen number is a value that shows whether rarefaction in the nozzle is present or not. La Torre [16] showed that for values of $Kn \leq 0.01$ the effects of rarefaction could be ignored. All the experimental data points satisfied this relation, therefore the effects of rarefaction were ignored.

$$Kn = \frac{M}{Re} \cdot \sqrt{\frac{\gamma \cdot \pi}{2}} \tag{3.20}$$

3.5. Nozzle quality

The nozzle quality is a quantifiable number that shows the real Isp of the nozzle, compared to its ideal Isp, as can bee seen in Equation 3.21. The best method to determining the nozzle quality is to find out the amount of thrust that is lost, when the nozzle operates in real conditions compared to an ideal environment. These improvements were initially found in a detailed summary form by Zandbergen [37], however the original sources will be mentioned.

$$\epsilon_F = \frac{Isp_{exp}}{Isp_{ideal}} \tag{3.21}$$

The first loss to take into account are the divergence losses. Ideal rocket theory assumes that the flow is one dimensional, however in reality the flow is able to act tangentially and radially as well, which affects the performance of the thruster. Equation 3.22 from Farokhi [8] is a relation that calculates the effect of divergence losses for a 2D, thin microthruster. This factor is multiplied to the $C_{f,0}$, which alters Equation 3.8 to Equation 3.23.

$$\eta_{d,2D} = \frac{sin(\theta_{nd})}{\theta_{nd}} \tag{3.22}$$

$$C_f = \eta_{d,2D} \cdot C_F^0 + \left(\frac{P_e}{P_c} - \frac{P_a}{P_c}\right) \cdot AR \tag{3.23}$$

An empirical method by Spisz, Brinich, and Jack [29] is also used to approximate the $C_{f,loss}$ for the thruster. This method takes into account any viscous losses experienced within the nozzle. The empirical solution of Spisz, Brinich, and Jack [29] was determined by using asymmetrical nozzles, compared to linear slit nozzles, that will be used in this thesis. Therefore, the initial relation uses the hydraulic diameter ($D_{H,t}$) for the characteristic length (d), instead of the throat width (w_t). This will be corrected for in Equation 3.24, when w_t is used.

$C_{f,loss}$ is subtracted from the $C_{f,ideal}$, to reach an approximate final value of $C_{f,real}$. The empirical data involves a number of asymmetrical nozzles with a θ_d=20^o and expansion ratios from 25 to 150. The range for which the empirical data corresponds to are for $500 \leq Re_t \leq 180000$. The empirical relation uses an adjusted Reynolds number at the wall of the throat. In addition, Hydrogen was used as the propellant instead of Nitrogen, so the relation from Spisz, Brinich, and Jack [29] have been corrected for Nitrogen by using the value of 1.727 below. Additionally, $Re_{t,ideal}$ is based on the ideal case, therefore it is corrected by multiplying by the C_D. Also, Spisz, Brinich, and Jack [29] used a recovery factor of 0.84 to come to a value of $T_t/T_w = 0.857$. This was only used for cold data, since it was expected that the wall and propellant stagnation temperature to be the same for the larger thruster. Since the thruster used in this thesis is very small, the same value will be used, because it is expected that the wall and propellant temperature will be equivalent.

$$Re_{t,w} = (C_D \cdot Re_{t,ideal}) \cdot \frac{T_t}{T_{wall}}^{1.727} \tag{3.24}$$

The $C_{f,loss}$ is then calculated using Equation 3.25.

$$C_{f,loss} = 17.6\frac{exp(0.0032AR)}{\sqrt{Re_{t,w}}} \tag{3.25}$$

As a result, $C_{f,real}$ is calculated using Equation 3.26, using the method by Spisz, Brinich, and Jack [29] and taking into account divergence losses.

$$C_{f,real} = \eta_{d,2D}C_{f,0} + \frac{p_e - p_a}{p_c}AR - C_{f,loss} \tag{3.26}$$

3.6. Thermal Model

The purpose of this section is to present the thermal model that will be used to predict the heater efficiency. The heater efficiency is an important parameter, because it gives insight into how much of the total input power is used to raise the temperature of the propellant. A low heater efficiency would mean that more input power would be needed to raise the temperature the same amount compared to a thruster with a high heater efficiency. The increase in input power would drive up the mass and cost of the power subsystem of the microsatellites. The heater efficiency can be calculated using Equation 3.27 where P_{fluid} is the power used to heat the fluid propellant, P_{inp} is the total input power, P_{cond} is the power loss due to conduction, P_{rad} is the power loss due to radiation, P_{conv} is the power loss due to convection and P_{wire} is the power lost in the wires. The total input power is determined by using Equation 3.29 where V_{inp} is the input voltage and I_{inp} is the input current of the power source.

The experimental heater efficiency will be found using Equation 3.27. It will be assumed that the chip temperature measured by the infrared camera (details on the camera are found in chapter 4), will be equal to the propellant temperature. In reality the efficiency will be lower, because the propellant will not be the exact temperature of the chip. So Equation 3.27 will be transformed to Equation 3.28, to determine the experimental heater efficiency, where the enthalpies H are found using Lemmon et al. [17] for the measured chip temperatures.

$$\eta_{heater} = \frac{P_{fluid}}{P_{inp}} = \frac{P_{fluid}}{P_{fluid} + P_{cond} + P_{rad} + P_{conv} + P_{wire}} \tag{3.27}$$

$$\eta_{heater,exp} = \frac{\dot{m}(H_{N2,hot} - H_{N2,cold})}{P_{inp}} \tag{3.28}$$

$$P_{inp} = V \cdot I \tag{3.29}$$

$$P_{fluid} = \dot{m} \cdot (e_2 - e_1) \tag{3.30}$$

$$P_{cond} = \frac{k \cdot A}{L}(T_2 - T_1) \tag{3.31}$$

$$P_{rad} = \epsilon \cdot \sigma \cdot A \cdot (T_2^4 - T_{ambient}^4) \tag{3.32}$$

$$P_{conv} = h \cdot A \cdot (T_2 - T_{ambient}) \tag{3.33}$$

$$P_{wire} = I^2 R_{wire} \tag{3.34}$$

Another important aspect to consider, when using water as the nozzle propellant, is the increase in boiling temperature with pressure. The Clausius-Clapeyron relation, seen in Equation 3.35,can be used to determine the relationship between the vaporizing temperature (T_{vap}) and the vaporizing pressure (P_{vap}) of water. The result of the relation can be seen in Figure 3.1, which indicates the minimum

Table 3.1: Required chamber vaporization temperature and pressure needed for complete vaporization throughout the entire nozzle. These values correspond to the ”Chamber” and ”Throat” graph in Figure 3.1.

$P_{c,vap}$ (bar)	2	3	4	5
$T_{c,vap}$ (K)	435	451	463	473
$T_{c,vap}$ (C)	162	178	190	200
γ_c (-)	1.33	1.34	1.34	1.34
P_t (bar)	1.08	1.62	2.15	2.69
T_t (K)	373	386	396	404
T_t (C)	100	113	122	130

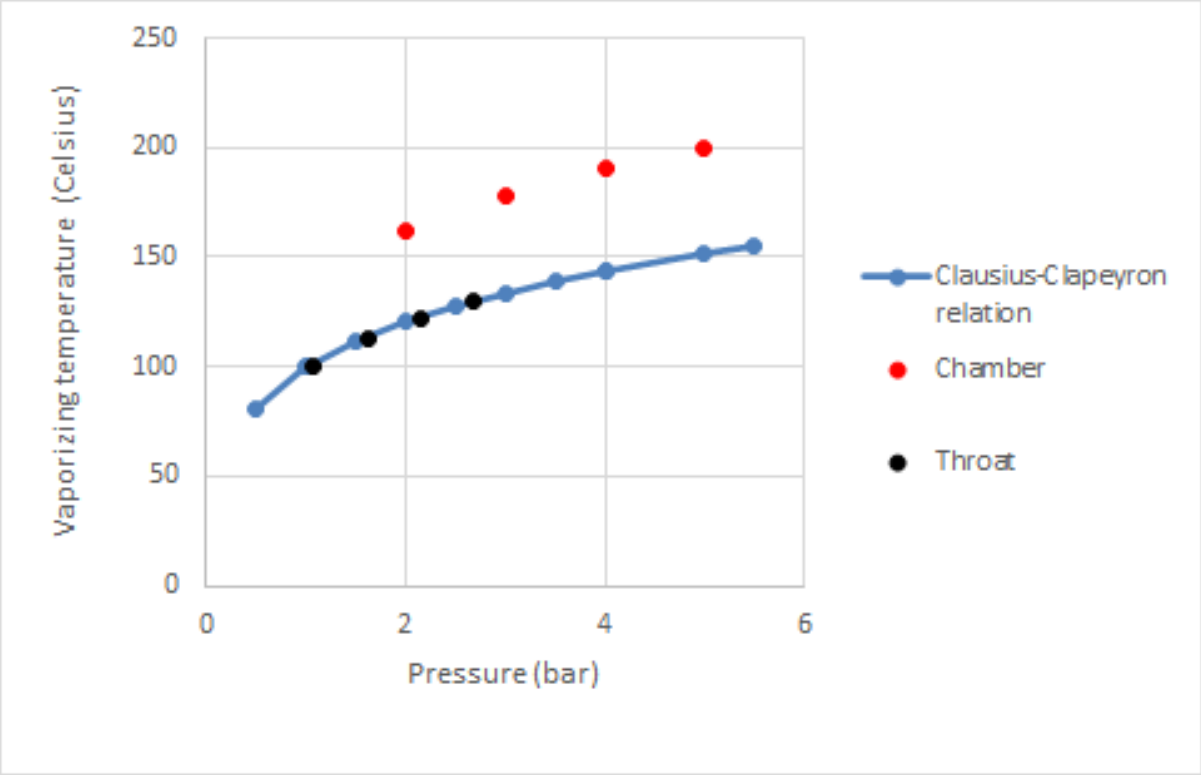

Figure 3.1: Vaporization temperature versus pressure using thruster R4C7.

temperature needed to vaporize the water, for a given pressure. Therefore, it can be seen that for vaporization to occur, in the nozzle chamber, at 5 bars of pressure, a chamber temperature of 152°C is needed.

Additionally, it should be noted that as the propellant flows towards the nozzle throat, the propellant expands. This can sometimes cause the formation of droplets due to condensation. To avoid this, a higher temperature is needed to ensure full vaporization throughout the nozzle. To check if the water condenses at the nozzle throat, Equation 3.6 and Equation 3.5, are calculated and compared to the Clausius-Clapeyron relation, seen in Equation 3.35. The chamber pressure, chamber temperature and specific heat ratios are needed as inputs. It can be seen in Figure 3.1 and Table 3.1, that the required temperature needed for full vaporization is much higher compared to vaporization in the nozzle chamber alone. For example, at a chamber pressure of 5 bars, a chamber temperature of 200°C is needed to vaporize the liquid in the nozzle chamber and throat, which is 48°C higher compared to the 152°C needed for vaporization in the nozzle chamber alone.

$$T_{vap} = \frac{T_1 \cdot \Delta h_{vap}}{T_1 \cdot R \cdot ln(\frac{p_1}{p}) + \Delta h_{vap}} \tag{3.35}$$

Table 3.2: Experimental data from the work of Makhan [18], including the corrected thrust values.

Test	P_a (Pa)	P_c (bar)	T_c (K)	$\dot{m}$ (mg/s)	$F_{T,exp}$ (mN)	$F_{T,corrected}$ (mN)
TT-04_p1	35±4	1.92±0.05	295.9±1.5	0.65±0.083	0.072±0.017	0.066±0.017
TT-04_p2	50±6	2.95±0.05	295.9±1.5	0.96±0.083	0.25±0.016	0.23±0.017
TT-04_p3	68±8	4.03±0.05	296.0±1.5	1.31±0.083	0.45±0.016	0.41±0.016
TT-04_p4	85±11	5.04±0.05	296.0±1.5	1.66±0.083	0.64±0.015	0.58±0.015
TT-05_p1	35±5	1.82±0.05	294.1±1.5	0.59±0.083	0.064±0.018	0.058±0.018
TT-05_p2	54±8	2.98±0.05	294.2±1.5	0.94±0.083	0.27±0.022	0.25±0.022
TT-05_p3	69±10	4.03±0.05	294.2±1.5	1.29±0.083	0.46±0.022	0.42±0.022
TT-05_p4	83±12	5.06±0.05	294.3±1.5	1.64±0.083	0.65±0.018	0.59±0.018

3.7. Validation of Model based on literature

Now that the different models have been introduced, the model will now be compared to literature to determine which of the models is best suited for predicting the performance of the thrusters.

The models will be compared to the corrected, cold thrust data of TT-04, from Makhan [18] (see section 5.4 for an explanation of the correction). From literature, the dimensions of the thruster used by Makhan [18] (see Table 2.3) most closely resemble the dimensions of the thruster used for the experiments (see Table 2.2). The experimental data, including corrected thrust values, can be seen in Table 3.2.

Since Makhan [18] did not perform hot thrust tests using nitrogen as a propellant, the hot, thrust data of Versteeg [36] will also be compared to the performance models for validation, even though the dimensions of the thruster used by Versteeg [36] are much larger than the thrusters used.

3.7.1. Discharge Coefficient

Figure 3.2 shows the graph of a cold thrust test done by Makhan [18] compared to the predicted discharge coefficients using the TF, KH and J model, with w_t and $D_{H,t}$ as the characteristic dimensions. Initial impressions show that, both the KH and J models provide more accurate predictions of the C_D, compared to the TF model used by Makhan [18]. Additionally, the use of w_t as the characteristic dimension also improves the prediction of C_D. Furthermore, the increase in Reynolds number results in an improvement in predicting the real experimental discharge coefficients for all three models used.

Looking at Figure 3.3, the J (d=Dh) and J (d=wt) models, both satisfy the 10% inaccuracy requirement throughout the entire operating range of TT-04 from Makhan [18]. The percentage varies between 4.6% to -2.2% for J (d=wt) and 9.1% to 0.2% for J(d=Dh). The use of w_t improves the percentage inaccuracy from 9.1% to 4.6%. However, at higher Reynolds numbers, the percentage inaccuracy worsens and starts to underpredict the values of the $C_{D,exp}$ of TT-04. Additionally, when looking at Figure 3.4 and Figure 3.5, the J model is still able to predict the hot experimental values of Versteeg [36] within 10%. As the Reynolds number increases, the percentage difference decreases from 5.69% to 2.37% and 7.23% to 4.67%, for the J (d=wt) and J (d=Dh) models, respectively.

The TF model overpredicts the experimental values of Makhan [18] and is the least accurate model, as can be seen in Figure 3.3. The percentage inaccuracy varies from 16.3% to % 4.2 and 19.1% to 5.6%, for the TF (d=wt) and TF (d=Dh) models, respectively. At Reynolds numbers greater than 910 and 1695, the percentage difference between the TF (d=wt) and TF (d=Dh) models are less than 10%, respectively.

The KH model performs a good job of predicting the discharge coefficient and almost performs similarly compared to the J model. The KH ($d = w_t$) model is within 12.8% to 1.0% of the experimental values, while the KH ($d = D_{H,t}$) model is within 14.4% to 1.6% of the experimental values. Looking at Figure 3.3,at a Reynolds number greater than 550 and 1110, the percentage difference is less than or equal to 10%, for the KH ($d = w_t$) and KH ($d = D_{H,t}$) models, respectively.

Versteeg [36] and Makhan [18] used the model of Tang and Fenn [31], to predict the discharge coefficient. As can be seen from Figure 3.4 and Figure 3.2, Versteeg [36] and Makhan [18] experimental data were within 10% of the predictions of all 3 models, when using $d = D_{H,t}$. This would satisfy the accuracy requirement of 10%, meaning all 3 models are valid. However, it can be noticed that the model of Johnson et al. [13] improves the prediction of to be within 0-7%, especially for lower Reynold numbers,

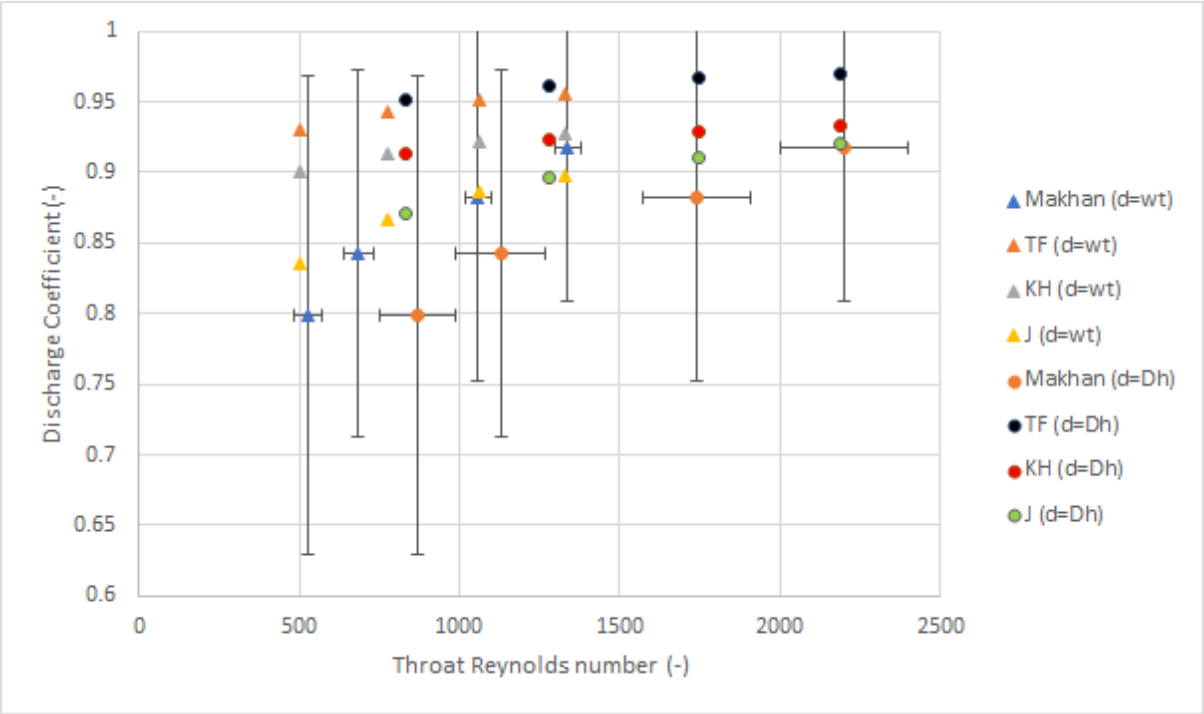

Figure 3.2: Experimental discharge coefficients of TT-04 from Makhan [18] and the modelled discharged coefficients TF, KH and J.

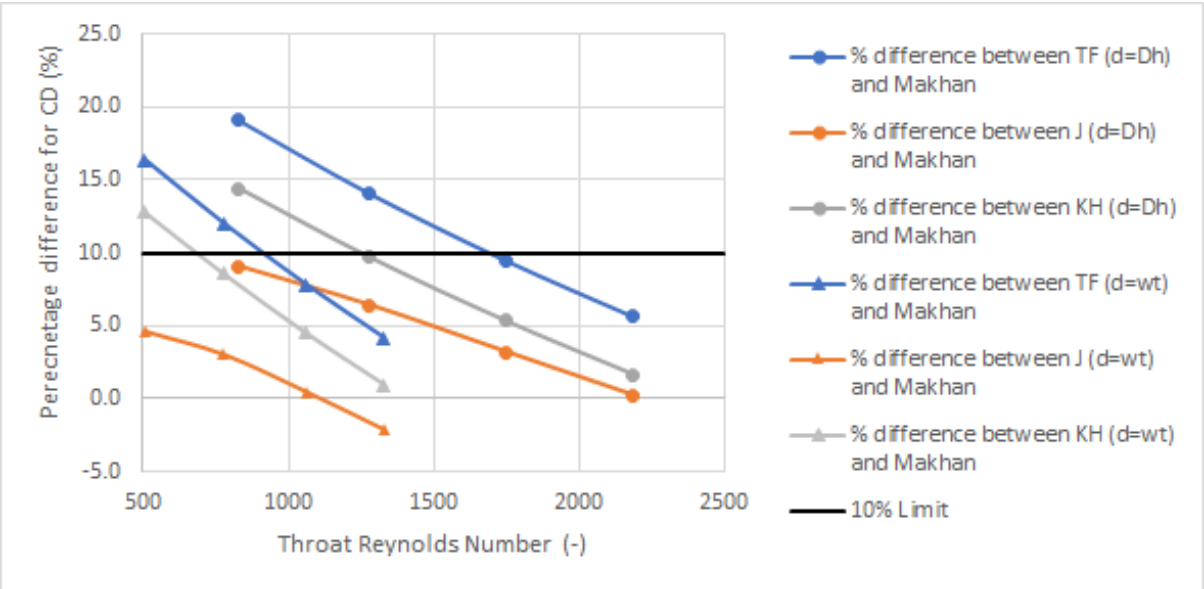

Figure 3.3: The percentage difference between the TF, J and KH models, and the experimental values of TT-04 from Makhan [18].

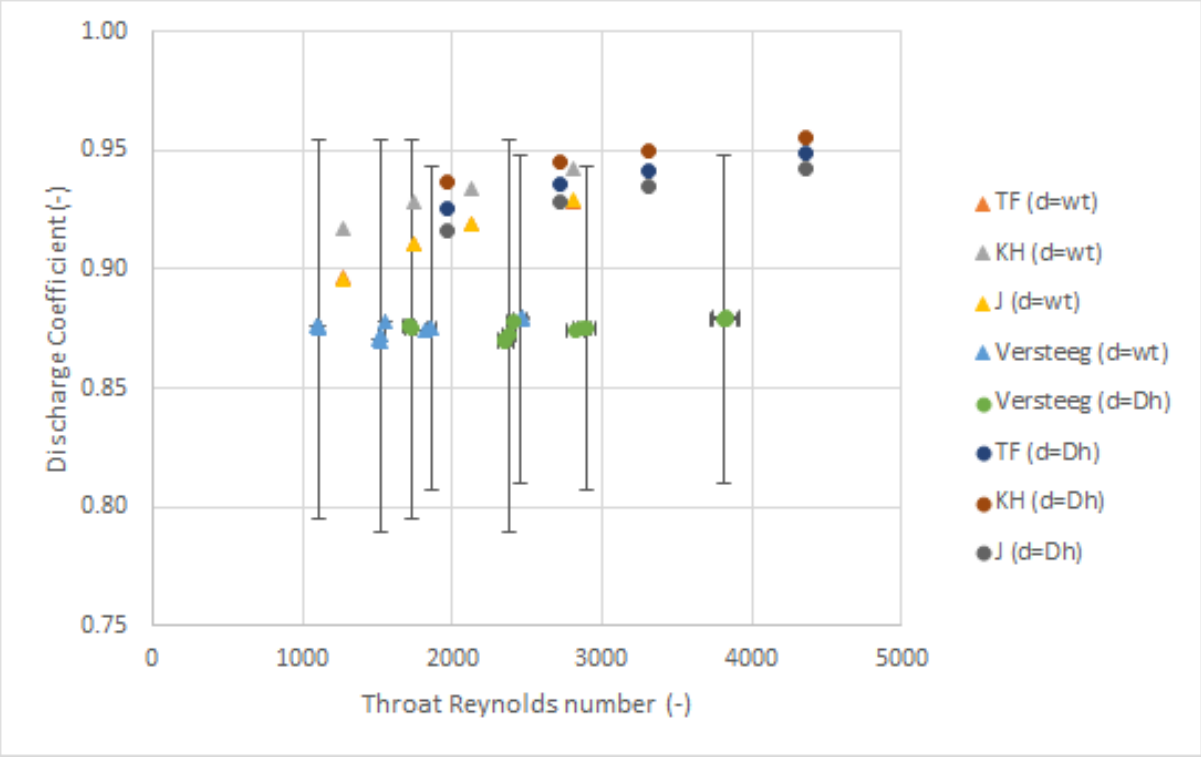

Figure 3.4: Experimental discharge coefficients of TTH-1.1 to TTH-4.3 from Versteeg [36] and the modelled discharged coefficients TF, KH and J.

compared to Tang and Fenn [31] and Kuluva and Hosack [14]. The model of Kuluva and Hosack [14] is able to predict the values of Makhan [18] with slightly less accuracy, compared to Johnson et al. [13].

Overall, the TF model seems to provide a minimal estimation of the C_D, as experimental literature shows that $C_{D,exp}$ is much lower. A case can be made that the models of Kuluva and Hosack [14] and Johnson et al. [13] could be used instead of Tang and Fenn [31], as they seem to predict the values more accurately. For this reason, the model of Kuluva and Hosack [14] and Johnson et al. [13] will be compared to the cold/hot tests, along with the model of Tang and Fenn [31]. Then, each model can be checked for their validity and accuracy. Additionally, the use of $d = w_t$ provides much better estimations for the data of Makhan [18]and Versteeg [36].

3.7.2. Isp Efficiency

Initial impressions show that the use of $d = w_t$ gives more accurate predictions when compared to the experimental values of Makhan [18] and less accurate values when compared to the experimental values of Versteeg [36]. The model overpredicts the experimental values of Makhan [18] and underpredicts the values of Versteeg [36], because the use of $d = w_t$ causes the predicted η_{isp} graph to shift downwards and vice versa for $d = D_{H,t}$. Additionally, the choice of C_D values from the three different models makes a small difference to the calculated η_{isp} compared to the $\eta_{isp,exp}$, at high Reynolds numbers. The selected C_D model seems to make a much more noticeable difference at lower Reynolds numbers, as can be seen for when the J (d=wt) model is used compared to the J ($d = D_{H,t}$).

Looking at Figure 3.6 and Table 3.3, the model overestimates the experimental values of Makhan [18] by 14-189%, depending on the characteristic length and C_D used, as the Reynolds number decreases. The model is not able to predict the values to within 10%, however as the Reynold number increases the percentage difference may decrease enough to reach 10%. Additionally, the use of $d = w_t$ also helps reduce the percentage difference, especially at low Reynolds numbers. Despite this, some values were within 20% of the model, which even though is not the target, can be considered decent enough.

When using $d = D_{H,t}$ the model is able to predict the Isp efficiencies for the hot tests of Versteeg [36] within -10% to -12% of the experimental values. For the case of $d = w_t$, the percentage difference is around -16% to -20%. This shows that, compared to the smaller thruster of Makhan [18], the model

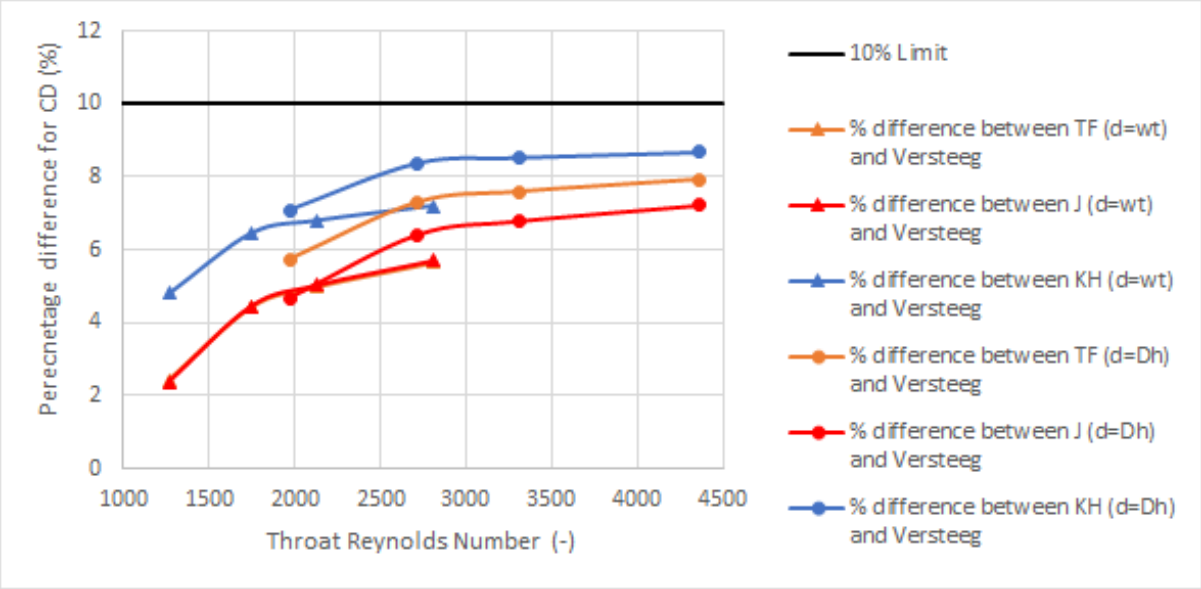

Figure 3.5: The percentage difference between the TF, J and KH models, and the experimental values of TTH-1.1 to 4.1 from Versteeg [36]. Note, the orange line with triangle markers, is hidden behind the red line with triangle markers.

used to predict the Isp efficiency does a better job for the larger thruster of Versteeg [36]. Despite that most values could not be estimated within 10% of the true experimental value, within 20% is still a good prediction.

In the work of Versteeg [36], he determined that the η_{isp} from the model underestimated the real experimental values by 12 to 14 % when using $D_{H,t}$ and 15 to 23 % using w_t. To rectify this, he changed the fitting constant in the empirical relation, Equation 3.25, from 17.6 to 12. This caused all of the predicted Isp efficiencies to fall within 10% of the experimental values.

When applying a fitting constant of 22.75, for the case of $d = w_t$, all the Isp efficiencies predicted using the three different C_D models, are within 20% of the experimental values of Makhan [18]. This can be seen in Figure 3.8 and Table 3.4. This was only done for $d = w_t$ since this length was more accurate in determining both the predicted C_D and η_{isp} from the models. The $\eta_{isp,KH}$, which uses $C_{D,KH}$, had Isp efficiencies within 10% of the model, when using the larger fitting constant of 22.75. It still needs to be determined if the fitting constant of 22.75 works well for hot thrust testing and for the thrusters used in this thesis.

3.8. Expected Thruster Performances

The expected results of the chosen thrusters that were tested, based on the presented model, will be provided in this section. By doing this, an estimated thrust and mass flow range for the thrusters can be determined. These ranges can then help support the choices made for measurement apparatus and thrust pendulum used to measure the operating conditions and the thruster outputs. The expected performances were found using $D_{H,t}$ for the characteristic length, instead of w_t since this gave larger expected mass flows and thrust values. Therefore, the maximum expected mass flow and thrust values could be determined, to choose a suitable mass flow sensor and thrust pendulum.

3.8.1. Cold Testing

The inputs, operating ranges and the performance outputs for the thrusters R5C1, R4C7 and R4C9, using nitrogen as a propellant, can be seen in Table 3.5, Table 3.6 and Table 3.7, respectively. Also, the hydraulic diameter is used for the characteristic length in calculating the performance parameters.

To begin with, the throat Reynolds numbers range from 1250 to 3250, for a pressure range of 2 to 5 bars, at 293.15K. This Reynolds number range is within the valid ranges for the three different relations used for determining the discharge coefficient, as well as the empirical method by Spisz, Brinich, and Jack [29] for determining the thrust coefficient. Despite this, it still needs to be determined how well the model predicts the performance of the chosen thrusters, which is explained in chapter 6, for cold tests.

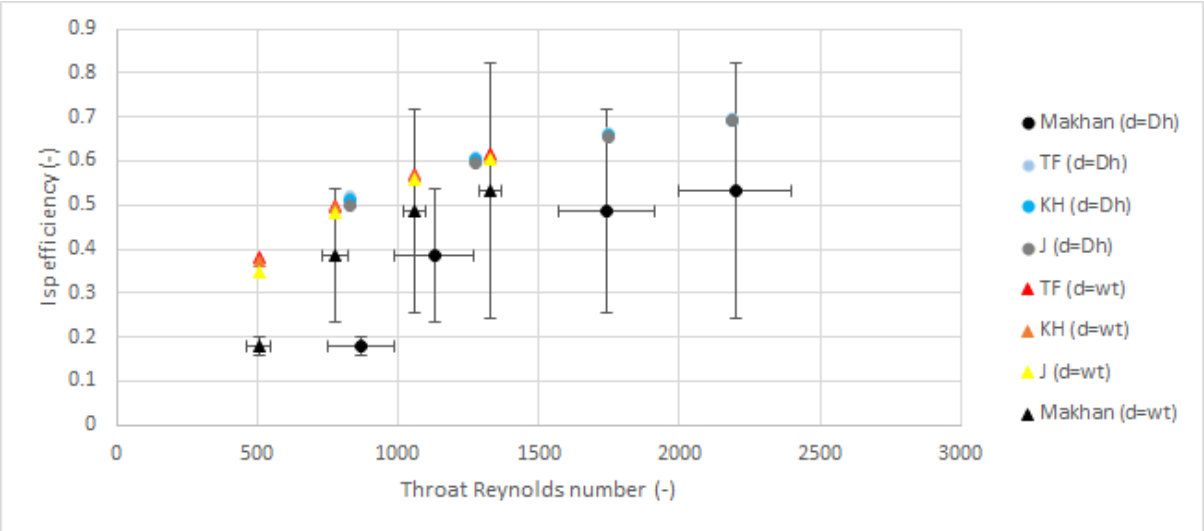

Figure 3.6: Isp efficiencies predicted by the model versus the experimental values of TT-04, from Makhan [18].

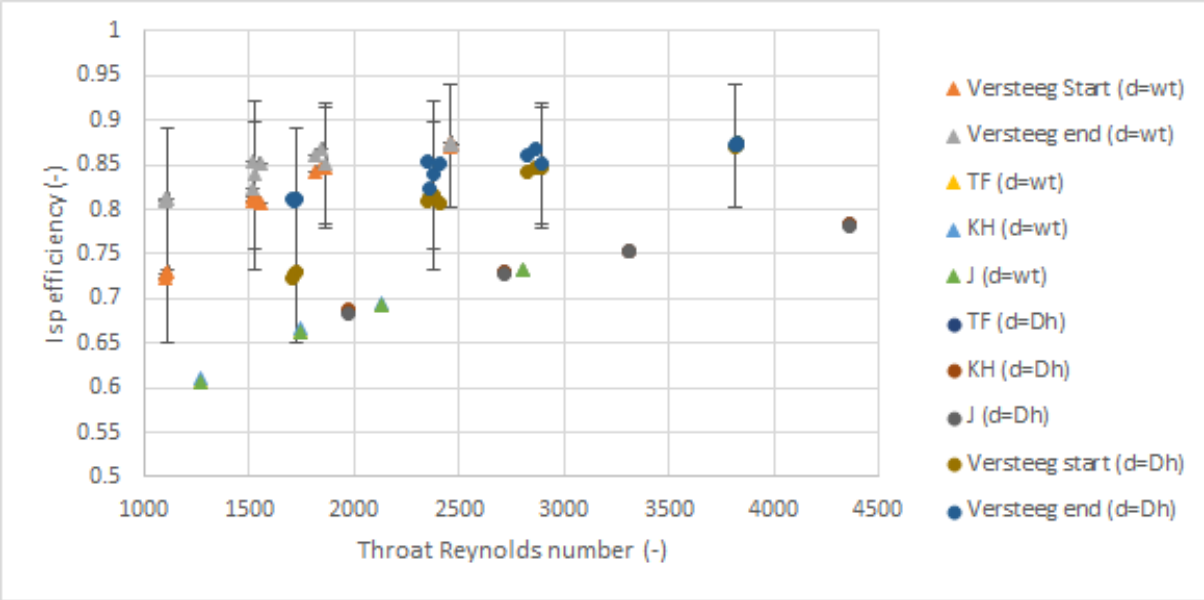

Figure 3.7: Isp efficiencies predicted by the model versus the experimental values of Versteeg [36].

Table 3.3: Percentage difference between the calculated Isp efficiency from the model ,to the experimental values of Makhan [18] (TT-04) and Versteeg [36] (HTT-1.1,2.1,3.1,4.1), using $d = w_t$ and $d = D_{H,t}$.

	Percentage difference to experimental values			
	Re_t	$\eta_{isp,TF}$	$\eta_{isp,KH}$	$\eta_{isp,J}$
Makhan (d=wt)	527	112	107	94
	685	30	28	24
	1057	18	16	15
	1336	16	15	14
Makhan (d=Dh)	868	189	184	177
	1128	58	56	55
	1740	37	36	35
	2200	31	30	30
Versteeg (d=wt)	2457	-16	-16	-16
	1862	-18	-18	-18
	1529	-20	-20	-20
	1109	-21	-21	-21
Versteeg (d=Dh)	3818	-10	-10	-10
	2894	-11	-11	-11
	2376	-12	-12	-12
	1723	-11	-11	-11

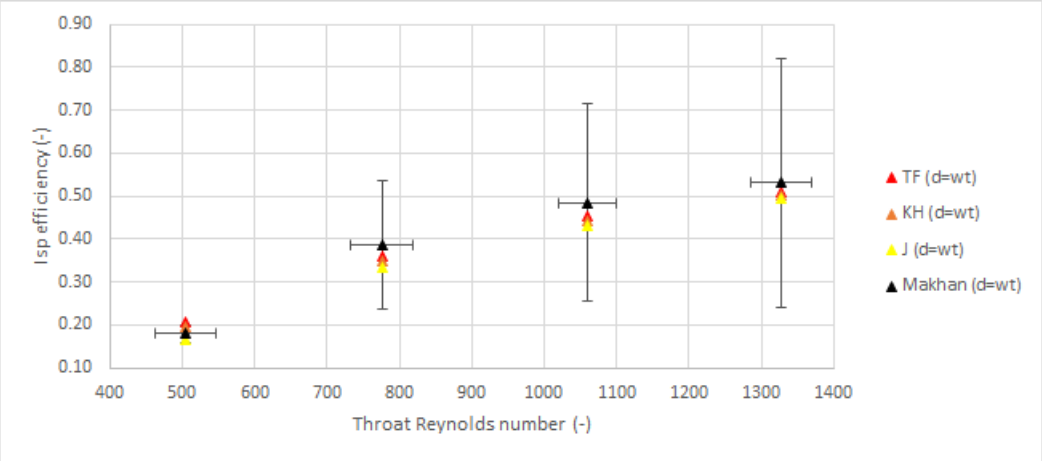

Figure 3.8: Isp efficiency of the models, using the corrected fitting constant of 22.5, compared to experimental data of Makhan [18], for $d = w_t$.

Table 3.4: Percentage difference between the corrected Isp efficiencies predicted by the model and the experimental values of TT-04 from Makhan [18].

	Percentage difference to experimental values			
	Re_t	$\eta_{isp,TF}$	$\eta_{isp,KH}$	$\eta_{isp,J}$
Makhan (d=wt)	527	14.9	8.1	-8.6
	685	-6.6	-9.1	-13.5
	1057	-6.9	-8.6	-10.8
	1336	-4.1	-5.5	-7.0

Table 3.5: Expected performance for thruster R4C7 under cold conditions.

Inputs and Operating Range				
P_c [bar]	2	3	4	5
T_c [K]	293.150	293.150	293.150	293.150
γ [-]	1.40	1.40	1.41	1.41
M_w [kg/kmol]	28.013	28.013	28.013	28.013
Specific gas constant	296.798	296.798	296.798	296.798
$D_{H,t}$	4.18E-05	4.18E-05	4.18E-05	4.18E-05
P_a [bar]	0	0	0	0
P_t [bar]	1.06	1.58	2.11	2.63
T_t [K]	244.0	243.8	243.6	243.4
μ_t [Pa-s]	1.52E-05	1.52E-05	1.52E-05	1.52E-05
Re_t [-]	1276	1914	2553	3193
Critical pressure ratio [-]	0.528	0.527	0.527	0.527
Performance Parameters				
Kn [-]	1.29E-03	8.62E-04	6.47E-04	5.17E-04
$\dot{m}_{ideal}$ [mg/s]	1.31	1.96	2.61	3.27
$F_{T,ideal}$ [mN]	0.95	1.42	1.89	2.36
Isp_{ideal} [s]	74.0	73.9	73.8	73.7
v_e [m/s]	133	133	132	132
$\dot{m}_{TF}$ [mg/s]	1.27	1.91	2.56	3.20
F_T [mN]	0.56	0.93	1.32	1.72
v_{eff} [m/s]	441	489	517	536
c* [m/s]	430	430	430	430
Isp [s]	45.0	49.9	52.8	54.7
$C_{D,TF}$ [-]	0.970	0.975	0.979	0.981
$C_{D,J}$ (-)	0.896	0.914	0.925	0.933
$C_{D,KH}$ (-)	0.919	0.926	0.930	0.933
Thrust efficiency	0.590	0.659	0.700	0.728
Isp efficiency	0.608	0.675	0.715	0.742
Combustion quality	1	1	1	1

The fact that Spisz, Brinich, and Jack [29] used asymmetrical nozzles instead of linear slit nozzles, could mean that the model may be less accurate. Additionally, the expected mass flow range for the thrusters lies between 1.17-3.40mg/s, when looking at all three C_D models, which will help in selecting a suitable mass flow sensor. The thrust range varies between 0.5-2.0mN and Isp ranges between 40-60s. Looking at the Isp, full flow expansion is expected when performing thrust tests in a vacuum.

The difference in expected performance between each thruster is quite small, considering that the thruster nozzle dimensions are relatively similar. The C_D and Isp efficiency have very small deviations between each other, as illustrated by Figure 3.9. The difference in Isp is at most 0.2s, between each thruster, at the same pressures. This would not have a significant difference on the performance difference of the thrusters.

3.8.2. Hot Testing

The inputs, operating ranges and the performance outputs for the thrusters R5C1, R4C7 and R4C9, using nitrogen as a propellant, can be seen in Table 3.8, Table 3.9 and Table 3.10, respectively. Also, the hydraulic diameter is used for the characteristic length in calculating the performance parameters.

To begin with, the throat Reynolds numbers range from 511 to 2018, for a pressure range of 2 to 5 bars and temperature range of 423-600K. This Reynolds number range is within the valid ranges for the Tang and Fenn [31] and Kuluva and Hosack [14] relations used for determining the discharge coefficient, as well as the empirical method by Spisz, Brinich, and Jack [29] for determining the thrust coefficient. It is below the range of $Re_{t,ideal}$ used by Johnson et al. [13]. Despite this, it still needs to be determined how well the model predicts the performance of the chosen thrusters, which is explained in chapter 7,

Table 3.6: Expected performance for thruster R4C9 for cold conditions.

Inputs and Operating Range				
P_c [bar]	2	3	4	5
T_c [K]	293.15	293.15	293.15	293.15
γ (-)	1.40	1.40	1.41	1.41
M_w[kg/kmol]	28.013	28.013	28.013	28.013
Specific gas constant	296.80	296.80	296.80	296.80
$D_{H,t}$	4.23E-05	4.23E-05	4.23E-05	4.23E-05
P_a [bar]	0	0	0	0
P_t [bar]	1.06	1.58	2.11	2.63
T_t [K]	243.97	243.79	243.60	243.42
μ_t [Pa-s]	1.52E-05	1.52E-05	1.52E-05	1.52E-05
Re_t [-]	1292	1938	2585	3233
Critical pressure ratio	0.528	0.527	0.527	0.527
Performance Parameters				
Kn [-]	1.29E-03	8.60E-04	6.45E-04	5.16E-04
$\dot{m}_{ideal}$ [mg/s]	1.38	2.08	2.77	3.46
$F_{T,ideal}$ [mN]	1.00	1.51	2.01	2.51
Isp_{ideal} [s]	74.0	74.0	73.9	73.8
v_e [m/s]	133	133	133	132
$\dot{m}_{TF}$ [mg/s]	1.34	2.03	2.71	3.40
F_T [mN]	0.59	0.99	1.41	1.83
v_{eff} [m/s]	443	491	519	538
c* [m/s]	430	430	430	430
Isp [s]	45.2	50.0	52.9	54.8
$C_{D,TF}$ [-]	0.970	0.976	0.979	0.981
$C_{D,J}$ (-)	0.896	0.915	0.926	0.933
$C_{D,KH}$ (-)	0.919	0.926	0.930	0.933
Thrust efficiency	0.592	0.660	0.701	0.729
Isp efficiency	0.610	0.677	0.716	0.743
combustion quality	1	1	1	1

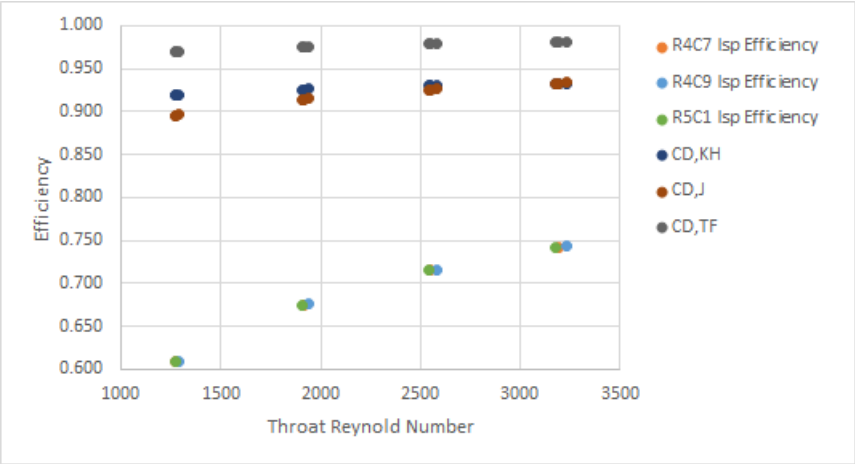

Figure 3.9: Expected CD and Isp efficiency for R4C7, R4C9 and R5C1.

Table 3.7: Expected performance for thruster R5C1 under cold conditions.

Inputs and Operating Range				
P_c [bar]	2	3	4	5
T_c [K]	293.15	293.15	293.15	293.15
γ (-)	1.40	1.40	1.41	1.41
M_w[kg/kmol]	28.013	28.013	28.013	28.013
Specific gas constant	296.80	296.80	296.80	296.80
$D_{H,t}$	4.15E-05	4.15E-05	4.15E-05	4.15E-05
P_a [bar]	0	0	0	0
P_t [bar]	1.06	1.58	2.11	2.63
T_t [K]	243.97	243.79	243.60	243.42
μ_t [Pa-s]	1.52E-05	1.52E-05	1.52E-05	1.52E-05
Re_t [-]	1268	1903	2539	3174
Critical pressure ratio	0.528	0.527	0.527	0.527
Performance Parameters				
Kn [-]	1.32E-03	8.79E-04	6.59E-04	5.27E-04
$\dot{m}_{ideal}$ [mg/s]	1.35	2.02	2.70	3.37
$F_{T,ideal}$ [mN]	0.98	1.47	1.95	2.44
Isp_{ideal} [s]	74.0	73.9	73.8	73.7
v_e [m/s]	133	133	132	132
$\dot{m}_{TF}$ [mg/s]	1.31	1.97	2.64	3.31
F_T [mN]	0.58	0.97	1.37	1.78
v_{eff} [m/s]	441	489	518	537
c* [m/s]	430	430	430	430
Isp [s]	45.0	49.9	52.8	54.7
$C_{D,TF}$ [-]	0.970	0.975	0.978	0.981
$C_{D,J}$ (-)	0.895	0.914	0.925	0.933
$C_{D,KH}$ (-)	0.919	0.926	0.930	0.933
Thrust efficiency	0.590	0.659	0.700	0.728
Isp efficiency	0.608	0.675	0.715	0.742
combustion quality	1	1	1	1

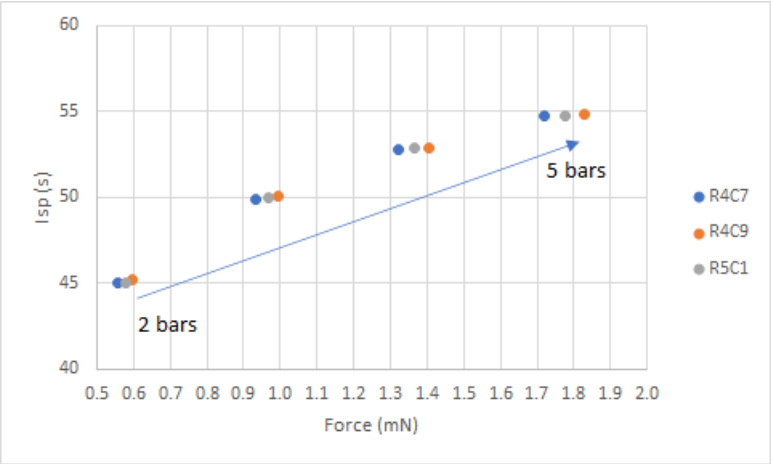

Figure 3.10: Expected thrust and Isp values for thruster R4C7, R4C9 and R5C1.

Table 3.8: Expected performance of R4C7 hot tests.

Inputs and Operating Range				
P_c [bar]	2	5	2	5
T_c [K]	423	423	600	600
γ (-)	1.41	1.43	1.39	1.40
M_w[kg/kmol]	28.013	28.013	28.013	28.013
Specific gas constant	296.798	296.798	296.798	296.798
$D_{H,t}$	4.18E-05	4.18E-05	4.18E-05	4.18E-05
P_a [bar]	0	0	0	0
P_t [bar]	1.05	2.62	1.06	2.65
T_t [K]	351.1	348.1	502.6	500.9
μ_t [Pa-s]	2.03E-05	2.04E-05	2.63E-05	2.64E-05
Re_t [-]	797.01	1992.90	514.29	1283.98
Critical pressure ratio	0.526	0.523	0.530	0.529
Performance Parameters				
Kn [-]	1.55E-03	6.22E-04	1.85E-03	7.40E-04
$\dot{m}_{ideal}$ [mg/s]	1.09	2.73	0.91	2.28
$F_{T,ideal}$ [mN]	0.94	2.35	0.95	2.37
Isp_{ideal} [s]	88.50	87.55	106.72	106.23
v_e [m/s]	158.89	157.48	191.16	190.45
$\dot{m}_{TF}$ [mg/s]	1.05	2.67	0.87	2.21
F_T [mN]	0.46	1.55	0.36	1.40
v_{eff} [m/s]	442.55	582.85	417.52	635.87
c* [m/s]	516	514	618	617
Isp [s]	45.1	59.4	42.6	64.8
$C_{D,TF}$ [-]	0.962	0.976	0.953	0.970
$C_{D,J}$ [-]	0.869	0.916	0.837	0.896
$C_{D,KH}$ [-]	0.909	0.926	0.898	0.919
Thrust efficiency	0.491	0.662	0.380	0.592
Isp efficiency	0.510	0.679	0.399	0.610

for hot tests.

Additionally, the expected mass flow range at 423K for the thrusters lies between 0.91-2.83mg/s and at 600K is 0.76-2.34mg/s, when looking at all three C_D models, which will help in selecting a suitable mass flow sensor. The thrust range varies between 0.36-1.65mN and Isp ranges between 42-65s. Similar to the expected cold results, full flow expansion is expected when performing thrust tests in a vacuum. Additionally, the Isp shows an increase as the temperature increases, which is expected according to literature Zandbergen [37].

Similar to expected cold results, the difference in expected performance between each thruster is quite small, considering that the thruster nozzle dimensions are relatively similar. The C_D and Isp efficiency have very small deviations between each other. The difference in Isp is at most 0.2-0.4s, between each thruster, at the same pressures. The deviations in Isp is slightly larger as the temperature increases, but still within acceptable bounds.

3.9. Conclusions

Overall, the performance models that will be used for determining the thruster performances were described and analyzed. Three models were discussed for determining the discharge coefficient: the analytical model of Tang and Fenn [31] (TF model), the semi-empirical model of Johnson et al. [13] (J model) and the analytical model of Kuluva and Hosack [14] (KH model). Comparing these models to the experimental data of Makhan [18] and Versteeg [36], showed that the model of Tang and Fenn [31] has a smaller effect on C_D, and overestimated the experimental data, compared to the other two models. The models of Johnson et al. [13] and Kuluva and Hosack [14] actually provided more accurate estimations

Table 3.9: Expected performance of R4C9 hot tests.

Inputs and operating range				
P_c [bar]	2	5	2	5
T_c [K]	423	423	600	600
γ (-)	1.41	1.43	1.39	1.40
M_w[kg/kmol]	28.013	28.013	28.013	28.013
Specific gas constant	296.798	296.798	296.798	296.798
$D_{H,t}$	4.18E-05	4.18E-05	4.18E-05	4.18E-05
P_a [bar]	0	0	0	0
P_t [bar]	1.05	2.62	1.06	2.65
T_t [K]	351.1	348.1	502.6	500.9
μ_t [Pa-s]	2.03E-05	2.04E-05	2.63E-05	2.64E-05
Re_t [-]	807.01	2017.91	520.74	1300.09
Critical pressure ratio	0.526	0.523	0.530	0.529
Performance Parameters				
Kn [-]	1.55E-03	6.20E-04	1.85E-03	7.38E-04
$\dot{m}_{ideal}$ [mg/s]	1.15	2.90	0.96	2.41
$F_{T,ideal}$ [mN]	1.00	2.49	1.01	2.52
Isp_{ideal} [s]	88.53	87.50	106.94	106.43
v_e [m/s]	158.98	157.34	191.76	190.98
$\dot{m}_{TF}$ [mg/s]	1.11	2.83	0.92	2.34
F_T [mN]	0.49	1.65	0.39	1.50
v_{eff} [m/s]	444.90	584.02	420.84	638.49
c* [m/s]	516	514	618	617
Isp [s]	45.4	59.6	42.9	65.1
$C_{D,TF}$ [-]	0.962	0.976	0.954	0.970
$C_{D,J}$ [-]	0.896	0.896	0.896	0.896
$C_{D,KH}$ [-]	0.919	0.919	0.919	0.919
Thrust efficiency	0.493	0.664	0.383	0.594
Isp efficiency	0.512	0.681	0.401	0.612

Table 3.10: Expected performance of R5C1 hot tests.

Inputs and operating range				
P_c [bar]	2	5	2	5
T_c [K]	423	423	600	600
γ (-)	1.41	1.43	1.39	1.40
M_w[kg/kmol]	28.013	28.013	28.013	28.013
Specific gas constant	296.798	296.798	296.798	296.798
$D_{H,t}$	4.18E-05	4.18E-05	4.18E-05	4.18E-05
P_a [bar]	0	0	0	0
P_t [bar]	1.05	2.62	1.06	2.65
T_t [K]	351.1	348.1	502.6	500.9
μ_t [Pa-s]	2.03E-05	2.04E-05	2.63E-05	2.64E-05
Re_t [-]	792.47	1981.56	511.36	1276.68
Critical pressure ratio	0.526	0.523	0.530	0.529
Performance Parameters				
Kn [-]	1.58E-03	6.33E-04	1.89E-03	7.54E-04
$\dot{m}_{ideal}$ [mg/s]	1.12	2.82	0.94	2.35
$F_{T,ideal}$ [mN]	0.98	2.42	0.98	2.45
Isp_{ideal} [s]	88.53	87.50	106.94	106.43
v_e [m/s]	158.98	157.34	191.76	190.98
$\dot{m}_{TF}$ [mg/s]	1.08	2.76	0.89	2.28
F_T [mN]	0.48	1.60	0.37	1.45
v_{eff} [m/s]	441.18	581.73	415.21	635.02
c* [m/s]	516	514	618	617
Isp [s]	45.0	59.3	42.3	64.8
$C_{D,TF}$ [-]	0.962	0.976	0.953	0.970
$C_{D,J}$ [-]	0.896	0.896	0.896	0.896
$C_{D,KH}$ [-]	0.919	0.919	0.919	0.919
Thrust efficiency	0.489	0.661	0.377	0.590
Isp efficiency	0.508	0.678	0.396	0.608

of the discharge coefficient. When comparing the the three models to the cold test data of Makhan [18], all three models were able to stay within 20% of the true value. With respect to the experimental data of Versteeg [36], all three models could predict the hot test values of Versteeg [36], within 10% of the true value. A case can be made that the models of Kuluva and Hosack [14] and Johnson et al. [13] are more suitable, since they provide more accurate predictions of data from Makhan [18] and Versteeg [36], as can be seen in Figure 3.2 and Figure 3.4.

The Isp efficiency values of the cold test of Makhan [18] had a predicted percentage difference between 30-189%, when using the hydraulic diameter ($D_{H,t}$) for the characteristic dimension (d). Using the throat width (w_t) improved the percentage difference to 14-112%, as using a smaller dimension causes the C_F to decrease, which makes a better fit for the data of Makhan [18]. From these percentage differences, it shows that the model can not predict the Isp efficiency within 10% of the true value, which technically means the model is not valid. Despite the large variation in percentage difference, at around $Re_t = 685$, the percentage difference is around 24-30% (depending on which C_D model is used). Although this is larger than the 10% difference, this may be considered good enough, because this uncertainty can be taken into consideration by adding an extra 24-30% of propellant mass. For a small microsat, this is not really a huge strain on the mass budget. The model prediction for the Isp efficiency, η_{isp}, was underestimated by 10% to 21% overestimated compared to the experimental data, as can be seen in Table 3.3. Even though this does not meet the inaccuracy limit of 10%, these values are still very good, as they can be compensated by taking around 20% more propellant than is needed. For cubesat designs, the propellant mass is very small compared to the overall mass of the satellite, so taking 20% more propellant does not put a large strain on the mass or cost budget. However, the large confidence bounds of the experimental values make it difficult to say for sure. Additionally, the chosen C_D from the TF, KH and J model, used for determining the C_F in Equation 3.25, may no difference in improving the prediction of the Isp efficiency. Using w_t for the characteristic dimension actually made the accuracy of the model worst for determining the experimental values of Versteeg [36]. Furthermore, if the fitting constant of 17.6, from Equation 3.25, is changed to 22.75, the percentage difference with the true experimental values shifts within 10%, when the C_D from the KH ($d = w_t$) model is used. It would be interesting, given that the thruster of Makhan [18] has a smaller w_t and aspect ratio, to see if this new fitting constant also gives accurate predictions for the thrusters used in this thesis.

The expected performance ranges for a pressure range of 2-5 bars for cold testing is a mass flow of 1.17-3.40mg/s, a thrust of 0.5-2.0mN and Isp range between 40-60s. When heated to 423K and 600K, a mass flow of 0.76-2.34mg/s, thrust of 0.36-1.65mN and Isp between 42-65s is expected, when in vacuum. With these values a suitable mass flow sensor and thrust stand could be selected in section 4.3, based on their measurement ranges. Furthermore, the thrusters showed minimal deviations in thruster efficiencies between each other, considering that the thrusters have similar thruster dimensions. The Isp deviations were 0-0.4s apart, throughout the entire temperature and pressure range. So the thrusters should give similar values during testing, for the same operating points. The thrust range fell into the required range of 0.12-3mN, satisfying both the **PROP-PERF-1** and **PROP-PERF-2** requirements.

4

Thrust Bench Test Set-Up

In this chapter, the thruster test bench will presented and discussed. The purpose of this chapter is to:

- present what the thrust bench looks like and how it works.
- present the hardware and software used for the testing.
- determine which input and performance parameters will be measured and how.

By the end of this chapter, the reader should have all the necessary details required, to repeat these tests. Additionally, the reader should be confident that the chosen thrust bench is satisfactory enough to perform the necessary thrust tests and be aware of any areas of improvement. section 4.1 will discuss the hardware used for the thrust test. section 4.2 will give brief introduction to programs used for the test. section 4.3 will describe the test set up used for performing the thruster testing. Lastly, section 4.4 will introduce the thrust measurement methods that will be investigated during the thesis: the displacement method and the force compensation method.

4.1. Thrust Stand Hardware

The thrust bench that was used for testing was the TB-5m thrust pendulum. The pendulum consists of a hanging thruster that rotates on smooth hinges, whenever thrust is produced, causing a displacement. A small rotary spring and mass at the top of the pendulum causes the thruster to return to its original position. The thruster pendulum is able to measure up to a maximum thrust of 5 mN. Previous studies for VLM thrusters were either unable to directly measure thrust during heated conditions Makhan [18] or estimated the thrust based on the measured mass flow Kurmanbay [15] Silva et al. [27].

This test set up was chosen, since it was readily available in the lab. It's maximum measurable thrust of 5mN is also large enough to cover the expected thrust range of 0.5-2.0mN, for the thrusters calculated in section 3.8.

An overview of the different hardware components can be found in Table 4.1. Most of the hardware used is similar to the testing done by Makhan [18], however several extra components are included to help interface the thruster design to the pendulum.

Additionally, testing was performed without a vacuum chamber and in ambient conditions. Removing the vacuum chamber made it easier to directly measure the temperature of the thruster during heating, using the infrared camera. The infrared camera had to be connected to the PC, which could only be done if the vacuum chamber door was opened.

4.1.1. Nitrogen feed system

The nitrogen feed system is made up of different components that feed nitrogen propellant to the thruster and is located in the cleanroom, behind the vacuum chamber. The nitrogen is stored in a 200 bar nitrogen tank, which has a valve that can be opened and closed to let gas flow. The gas then flows to a rotary valve, pressure regulator and main shut off valve. The pressure regulator can be opened and closed to the desired pressure needed to carry out the test. The main shut off valve, when opened, leads to

Table 4.1: General overview of the hardware.

Component	Function
Brooks 5850S MFC	Measure the N_2 mass flow rate from the storage tank to the thruster feed system. Mass flow controls were not used during experiments. Two different MFC's are available: 0-144sccm and 0-2000sccm.
Pressure block interface	Measures the pressure and temperature upstream from the inlet
$\mu\epsilon$ CS2 displacement sensor	Measure the displacement of the pendulum.
Variable-Turn Density Coil (VTDC)	Provide electromagnetic force to push the pendulum to a distance set point, determined by the user, during testing. The amount of electromagnetic force can be used to estimate the thrust force of the thruster.
Delta Elektronica SM-7020-D power supply	Provides a current to the electromagnetic coil which in turn creates an electromagnetic force.
Delta Elektronica SM-7020 power supply	Provides current for the heaters.
Delta Elektronica E-030-10 power supply	Provides input for spike and hold drivers
Delta Elektronica D-030-10 power supply	Provides input for spike and hold drivers
Arduino board	Controls a spike and hold driver and interfaces with the cleanroom computer.
Lee company solenoid valve	Allows and disallows flow to the thruster.
Clean room PC	Reads out data measured by sensors and actuators, runs Labview software and stores data.
NI-8451 I^2C-SPI DAQ	Reads pressure/temperature and interfaces with computer
NI-6008 USB DAQ	Provides 2.5V line for the pressure block interface
NI-PCI-6229 DAQ	Interfaces with 7020-D PSU and Brooks mass flow sensor.
$\mu\epsilon$ DT6220/DL6230 DAQ	Reads the displacement of the pendulum and converts it to digital data.
PEEK: 125/156 Female MINSTAC – Male Luer Lock Adapter	One of two parts that allows the gas tubes to interface with the inlet needle of the thruster.
PEEK: 062 MINSTAC Adapter – 125/156 MINSTAC	The second part that allows the gas tubes to interface with the inlet needle of the thruster.
3D printed PCB platform	Holds the PCB to which the thruster is glued to.
3D printed PCB to pendulum interface	Holds the PCB platform and connects it to the thrust pendulum, with an M4 screw.
Heating wires	Carries the current from the power supply to the external heaters on the thruster.
A35sc Thermal camera	Measures the temperature of the thruster.

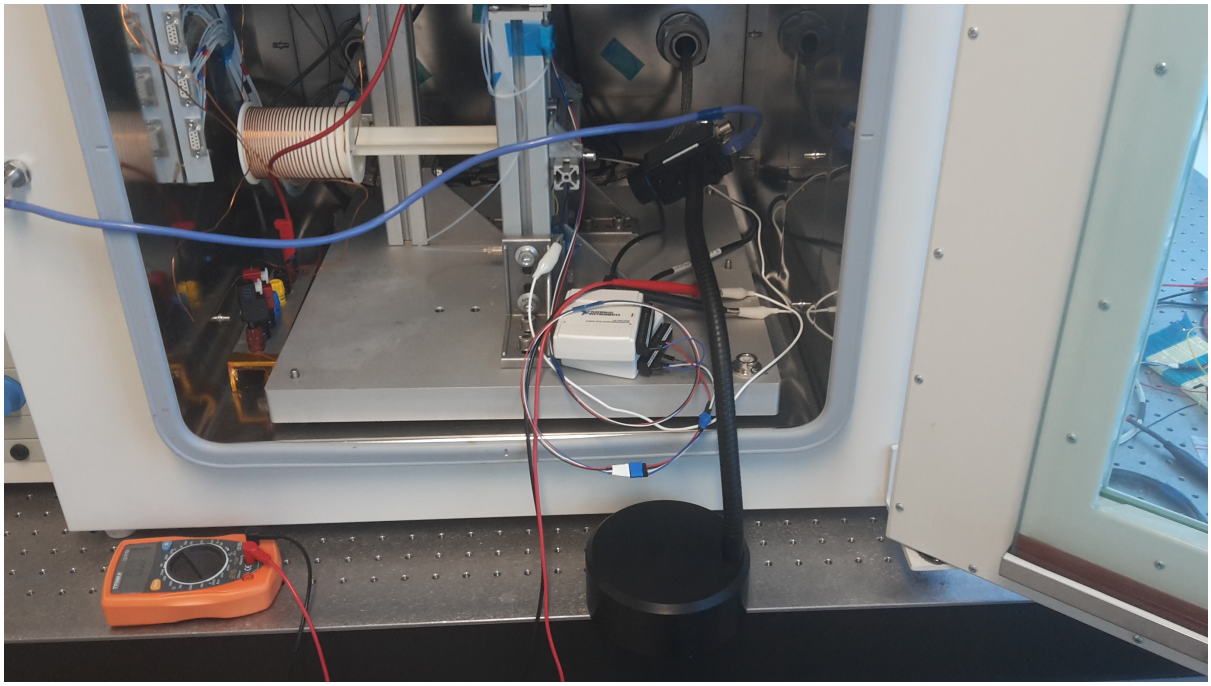

Figure 4.1: This is the set up from Figure 4.9, but now with the thermal camera installed

three section valves. The left most section valve leads to the 0-144 sccm Brooks MFC, the right one leads to the second 0-2000 sccm Brooks MFC and the middle section valve leads to no MFC. When the chosen valve section is opened, the gas flows to the nitrogen feedline and towards the vacuum chamber. Figure 4.2 shows the nitrogen feed system with labelling.

Jansen [12] discovered that there was a leak between the pressure regulator and rotary valve. An attempt was made by Bijster [2] to fix this leak, but with no success. Therefore, it is important to ensure that the valve on the nitrogen bottle and the in-line rotary valve are closed, when not in use.

4.1.2. Solenoid Valve

The solenoid valve is a component that can be used to allow and disallow the nitrogen flow without manually closing the rotary valve on the nitrogen feed system. It is located in the thesis box labelled ”Aris Pappadimitriou”, in the workshop. The solenoid valve is electrically interfaced to the computer and can be switched on and off in the Labview files available. The valve is powered by the Delta Elektronica E-030-10 and Delta Elektronica D-030-10, which is where it gets its spike voltages to open and close the valve. So the nitrogen can flow or be stopped at the click of a button on the Labview window. The solenoid valve is connected before the pressure sensor interface block.

4.1.3. Pressure/temperature sensor

For the thesis, a TE Connectivity MS5837-30BA pressure/temperature sensor is used which was attached to a sensor block created by Melaika [20]. This sensor block can be found in the thesis box labelled ”Aris Pappadimitriou”, in the workshop. The data sheet for the pressure senor can be found at *TE Connectivity Sensor Solutions. MS5837-30BA Ultra Small Gel Filled Pressure Sensor. Tech. Data Sheet* [32]. The pressure sensor block, shown in Figure 4.4, is between the thruster and the solenoid valve. This means that the propellant pressure and temperature measured, are not directly at the chamber, but upstream from the thruster inlet. It is assumed that the pressure drop from the sensor block to the thruster chamber is negligible. It was initially intended to use an EPCOS pressure sensor from *Pressure Sensors: Absolute pressure sensor die for wet media* [24], which was available at the EWI lab. This sensor is able to directly measure the chamber pressure/temperature of the VLM and has been used before by Kurmanbay [15]. However, it was determined that the maximum operational temperature of the sensor, which was 105^{o}C, was too low and therefore the use of the Infrared camera was considered instead.

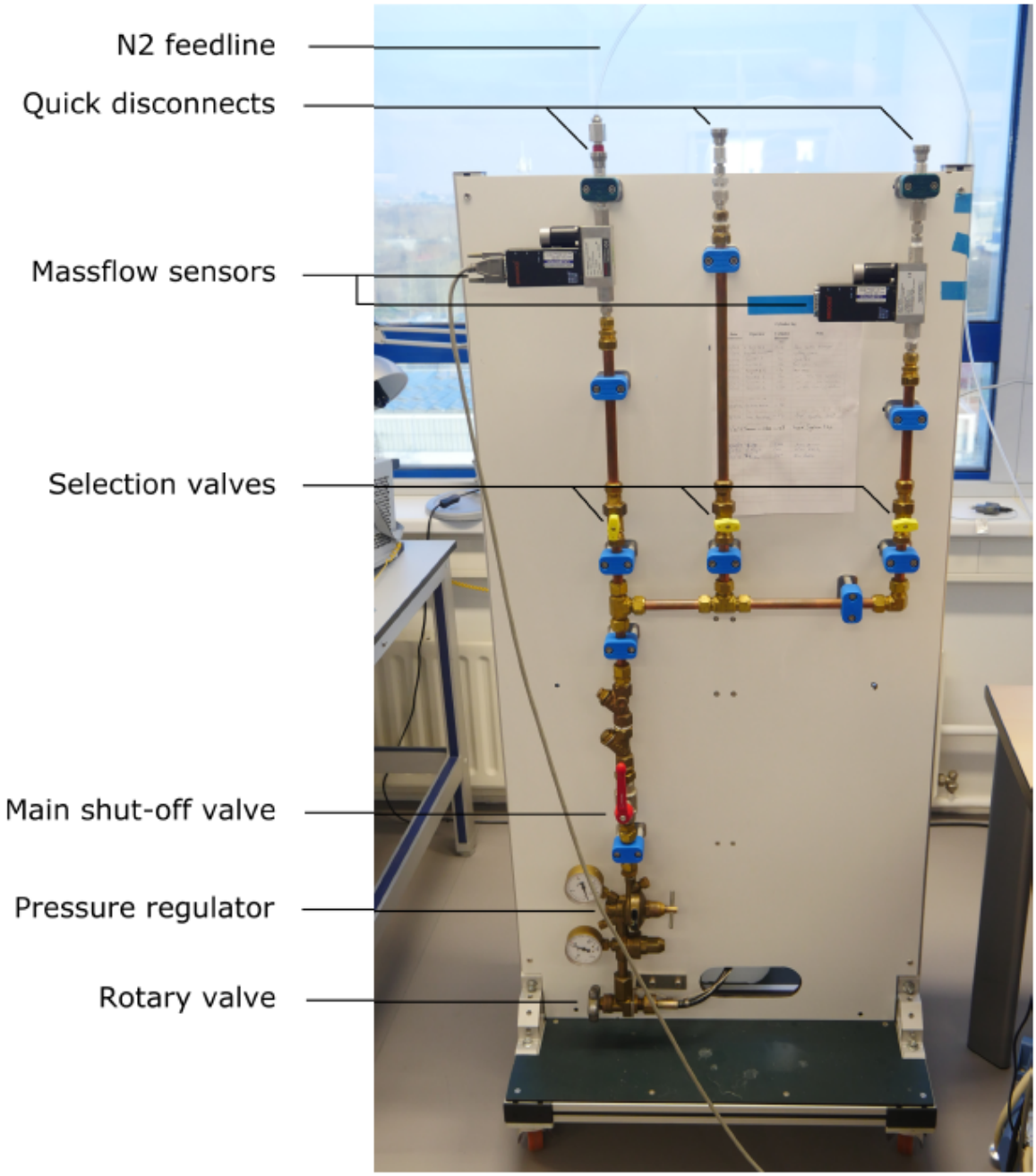

Figure 4.2: The nitrogen feed system can be seen here, with labels for the necessary valves and components.

Figure 4.3: The solenoid valve.

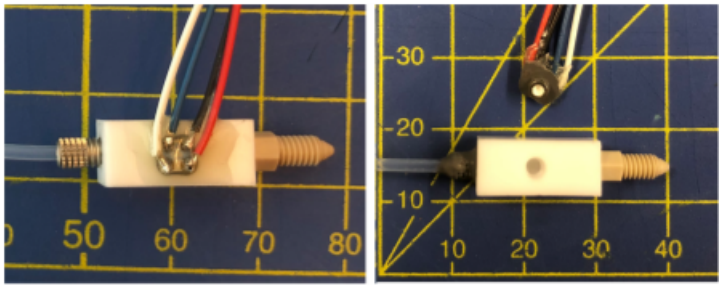

Figure 4.4: The glued (left) and delaminated (right) pressure block interface. Pictures courtesy of Melaika [20].

The ranges and accuracies of the Ms5837-30BA sensor, applicable for the testing ranges for the thesis, are: 0-6 bar $\pm$0.05 bar and 0-25^{o}C $\pm$1.5^{o}C. This data was found from *TE Connectivity Sensor Solutions. MS5837-30BA Ultra Small Gel Filled Pressure Sensor. Tech. Data Sheet* [32].

The necessary electrical interface and LabView code were already available from previous studies to extract the pressure and temperature data of the propellant. Four wires are connected to the sensor which in turn are wired to the DAQ, to record and transfer data.

4.1.4. A35sc Thermal Camera

The A35sc thermal camera has the ability to measure and record temperature data at specified points by the user. The camera is connected using USB cables to the back off the PC and he adapter which plugs in to the wall. To use the thermal camera, the software “Research IR” is needed to view the images of the camera, in real time, and select points on the image for recording the temperature. The manual for this program can be found here *ResearchIR 4 User’s Guide* [25]. The thermal camera is placed in vacuum oven facing the thruster nozzle exit. The temperatures during thrust testing were measured by placing a cursor point on the thruster,directly next to the heaters and not on them. It is also possible to make pictures and recordings with the thermal camera, however these images were found to be corrupted after hot testing. The thermal camera itself has an operating range of -40 to 160^{o}C, with an absolute error of $\pm$5^{o}C. This camera would not be suitable for measuring the temperature up to 1000K, as expected from the research goals. However, since the ABLESTIK glue is being used for the thruster inlet, it is expected that the thruster will fail around 150^{o}C. The camera can be found in its package, located in the rear cabinet, in the cleanroom.

4.1.5. Feed tube Adapters

To connect the MINSTAC feed tubes to the dispensing tip, a makeshift adapter was created at the workshop, and can be seen in Figure 4.5. The adapter was made in the workshop by cutting off the end of a syringe and glueing a minstac needle into the end of the syringe backwards, while using a bit off rubber sealant. This was used for all the cold tests, but a better built version would be needed for hot testing. The makeshift adapter would most likely fail when heated up.

It was attempted to manufacture an improved version at DASML using a block of Macor which was provided by Barry Zandbergen. Macor is glass ceramic based substance which has a high temperature tolerance, up to 1000^{o}C, and low thermal conductivity, which makes it an attractive choice for the thesis. However, the cost for manufacturing these adapters, according to the lab supervisors would be at least 400 euros and could be much higher. The lab technicians at 3ME would not allow machining this material, out of fear of breaking the drills on their machines. So for this reason, ordering the adapters was the only option and with an additional budget supplied by Angelo Cervone, they were purchased.

The improved adapter from the Lee company was needed to attach the Minstac tubes to the female luer lock on the stainless steel dispensing tip, seen in Figure 2.14b. The adapters needed were a PEEK: 125/156 Female MINSTAC – Male Luer Lock Adapter and a PEEK: 062 MINSTAC Adapter – 125/156 MINSTAC. Drawings for both, can be found in Figure 4.6a and Figure 4.6b.[1] These adapters can also be seen in Figure 5.3. The adapters can be found in the thesis box of ”Aris Pappadimitriou”, in the workshop.

4.1.6. 3D printed thruster to pendulum interface

Figure 4.7a and Figure 4.7b show the front and top view of the interface, used to attach the PCB to the thrust pendulum. They are located in the thesis box of ”Aris Pappadimitriou”, in the workshop, outside the cleanroom. The PCB would slide into the cover through the side, where the cover would hold it in place. A hole of 4mm is present at the top to allow an M4 screw to be fitted in. A rough chisel was used to widen the hole after the part was printed. Additionally, two rectangular holes were included on the top to allow the heater wires to be attached to the pins in the thruster PCB.

4.1.7. Soldered heater wires

The PCB has pins attached to it, where jumper cables can be fitted in to provide a current. For the thruster R4C7 and R4C9, they both had 5 heaters, therefore two heater wires made from scratch. This was done by clipping off the ends of 5 jumper wires to expose the metal wiring. Then soldering these 5 jumper wires together carefully. This jumper wires were then slid into a female banana plug, ensuring the heater wires made contact with the metal case of the banana plug. The 5 loose jumper cables at the opposite side can then be connected to the pins on the PCB. This complete heater wires can be seen in Figure 4.10 and a close up of the jumper cables attached to the pins in Figure 4.11. These wires can be found in the thesis box of ”Aris Pappadimitriou”.

4.2. Thrust Stand Software

Labview was used to control, read out and record the data produced from the different actuators and sensors. The main code was based off of the work of Silva et al. [27], which was also used by Makhan [18]. Versteeg [36] however was able to clean up and simplify the code for himself and for future users. Additionally, Versteeg [36] has versions which incorporate both the traditionally pendulum method and the force compensation method. It is recommended to read Versteeg [36] to see what changes were made and his reasoning, to the LabView code of Silva et al. [27].

For the testing however, several changes were incorporated into Huib’s code for the testing. When determining the mass flow, the MFC outputs a certain voltage (0-5V or 1-5V), which corresponds to the amount of mass flow through the MFC, were changed. The minimum voltage corresponds to zero mass flow (closed valve) while the maximum voltage output corresponds to the maximum mass flow the MFC can measure within its range. For the leak and thrust tests which use the smaller range mass flow (1-5V), the mass flow scaling computation was altered.

The Labview files can be found on the cleanroom computer in the folder: Aris/Testing/1_Labview_testing. The log in details and password for the computer are written on a note next to the computer. In this folder

[1] https://www.theleeco.com/products/electro-fluidic-systems/minstac-tubing-components/tube-fittings/adapters/

Figure 4.5: Makeshift adapter used for cold testing.

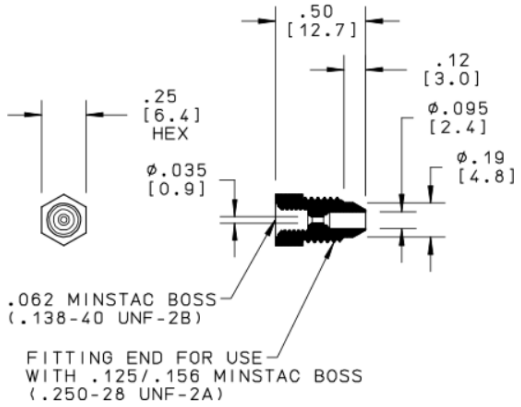

(a) PEEK: 062 MINSTAC Adapter – 125/156 MINSTAC

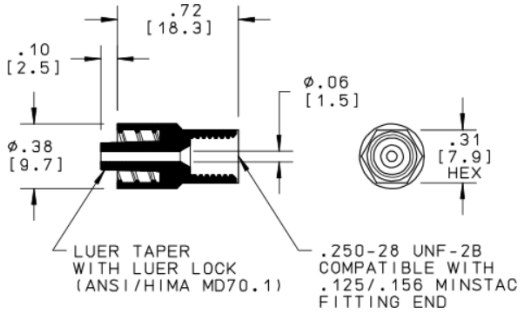

(b) PEEK: 125/156 Female MINSTAC – Male Luer Lock Adapter

Figure 4.6: Design drawings of the adapters used to connect the 062 Minstac tube to the female luer lock of the dispensing tip.

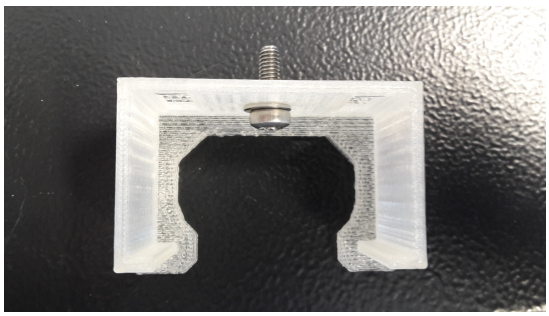

(a) Front cover.

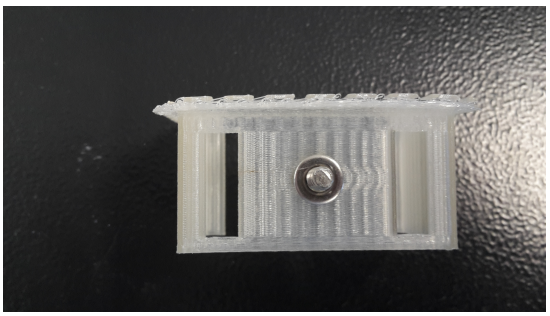

(b) Top view.

Figure 4.7: Top and front view of the 3D printed PCB to pendulum interface.

the following files were used for coil actuator calibration, thrust stand calibration, leak tests and thrust testing respectively: actuator_calibration.vi, calibration.vi, leak_test_144sccm.vi and thrust_test_heated_aris_new.vi. The necessary function blocks used by these vi's are stored in Aris/Testing/1_Labview_testing/functions.

Research IR is the software used for the infrared camera. With Research IR, recordings and pictures can be taken of the thruster during hot testing. Additionally, the temperature of different points on the thruster can be measured and captured by the user. Unfortunately, these pictures were corrupted during the test, but the point temperatures could be recorded. A point cursor measurement was placed near the thruster exit and one was placed near the inlet, where the needle was glued to the chip. Then the temperatures at these points could be captured and saved to a text file, when each thrust measurement is taken.

4.3. Thrust stand set up

Figure 4.9 shows what the thruster test set up looks like. The tube and wire placement here corresponds to HT-R4C7, however for HT-R4C9 the feed tubes and wiring were looped and placed on the top of the pendulum. Then they were thread downwards towards the thruster, to reduce the effects of drift which is explained in subsection 7.1.1, as can be seen in Figure 4.10. Additionally, in Figure 4.1, it can be seen that the thermal camera is placed in front of the nozzle exit at a far enough distance to avoid affecting the propellant exiting the nozzle.

The large black cables, seen in Figure 4.10, and propellant feed tubes can affect the thrust measurements if not mounted properly. Each cable can be thought of as a spring, that can alter the measured thrust force by adding drift or noticeable jumps to the measured displacements. This was very much noticeable in all 3 cold tests with R5C1, as can be seen in Figure 4.8 for example. This was fixed for CT-R4C7 and CT-R4C9 by coiling the tubes and taping them on the very top of the pendulum, which minimizes the effect. Additionally, during hot testing, the cables can heat up meaning that the spring force they exert can also change. However, since the hot thrust testing in chapter 7, is done using the force compensation method, where the pendulum does not move, this eliminates the effect the cables have on the thrust measured.

The heater wires are connected to the thruster pins, through the openings of PCB to pendulum interface seen in Figure 4.11, after the thruster is placed on the interface. Using a pair of tweezers, each wire is attached to the pins on the PCB, like in Figure 4.11. Due to the design of the interface, it was very time consuming to attach all the wires, through the openings on top of the interface. Also, it was very easy to accidentally break the wires connecting the PCB to the thruster, as this was done with both R5C1 and R4C7.

4.4. Thrust measurement methods

There are two different thrust measurements methods that use the pendulum: the displacement method and the force compensation method. The displacement method is a common method that has been used by students before, such as Makhan [18]. The force compensation method is a method that was thought of by Versteeg [36].

The displacement method involves a moving pendulum, where a magnet attached to the end of the pendulum is displaced into a coil. This causes a change in the magnetic field and therefore a change in the measured coil current. This current can then be related to a displacement, which in turn can be related to an estimated thrust force. Equation 5.4 explains how the coil current is related to the pendulum distance, which is in turn related to the estimated thrust force.

The force compensation method uses the same apparatus as the displacement method, however the pendulum is kept at a constant distance set point (determined by the user) through magnetic force that counters the thrust force of the thruster. The amount of magnetic force can be related to the thrust force using Equation 4.1 where F_T is the thrust force, F_{mag} is the magnetic force of the coil, FCF is the force correction factor and S is the magnetic force per unit current relation. The advantage of this method, compared to the displacement method, is the fact that it requires one less preliminary test.

$$F_T = F_{Mag} \cdot S \cdot FCF \tag{4.1}$$

A comparison of the data for each method is given in chapter 6, using thruster R5C1.

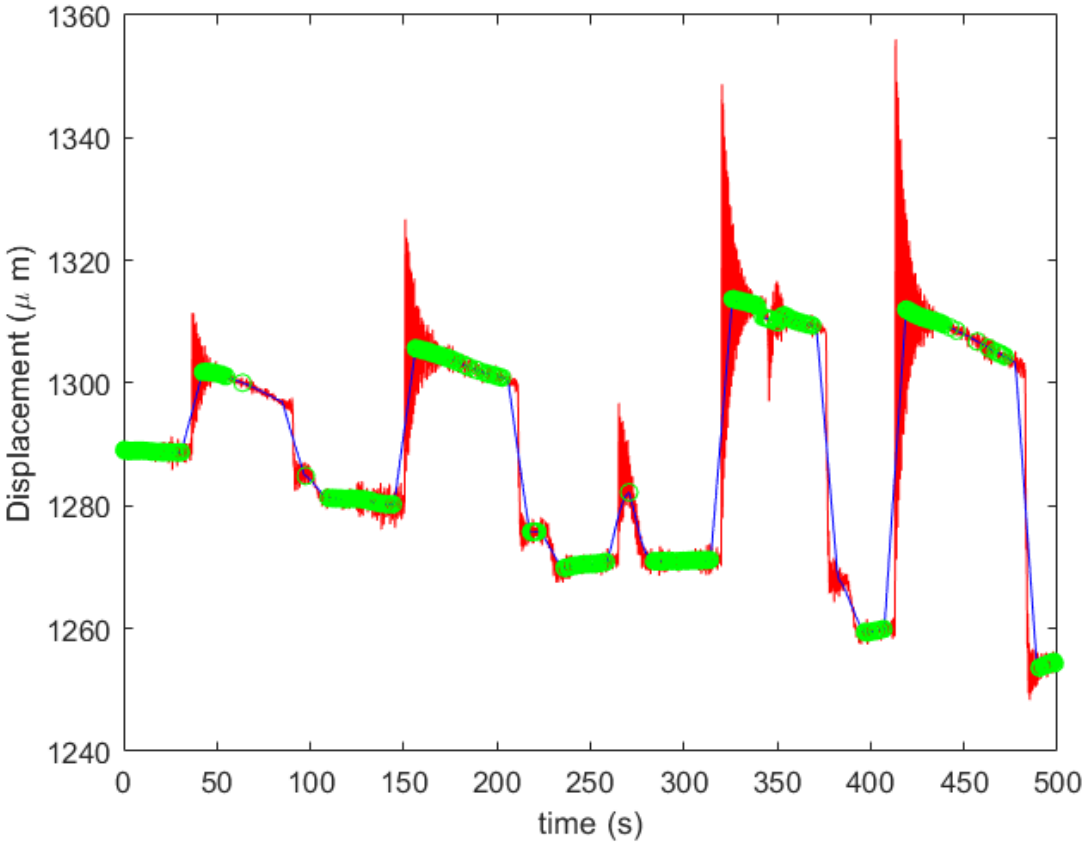

Figure 4.8: Pendulum displacement versus time for CT-R5C1.

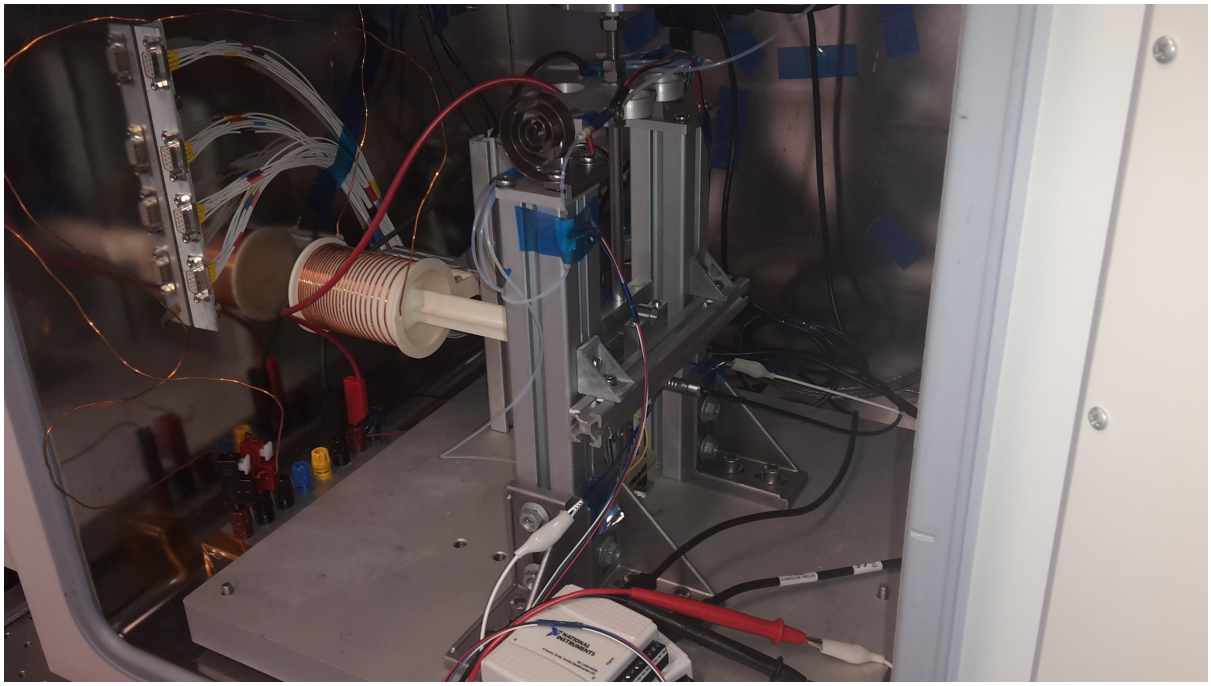

Figure 4.9: Test set up for performing hot thruster tests.

4.5. Conclusions

To conclude this chapter, the 5AE thrust pendulum will be used during thrust testing. The reason is due to its maximum measurable thrust level of 5mN, which is sufficient enough to measure the expected thrusts for the specified thrusters, which was calculated in section 3.8. Additionally, the hardware and software needed for the thrust testing are readily available and are listed, along with their functions in Table 4.1.

Using the thrust pendulum discussed and the listed hardware the following parameters can be measured during thrust testing: chamber pressure, chamber temperature, input power to the heaters, mass flow and thrust. The chamber pressure is approximated since the pressure sensor is placed in a pressure block interface located upstream from the inlet. Finding a method to connect the nitrogen feed tubes to the thruster inlet took longer than expected. A makeshift solution, made from a plastic syringe and spare Minstac parts, would be suitable for cold testing, but not for hot testing. The initial plan of manufacturing an adapter, using a block of Macor, proved to be too costly. The only alternative was to order a PEEK: 125/156 Female MINSTAC – Male Luer Lock Adapter and a PEEK: 062 MINSTAC Adapter – 125/156 MINSTAC to interface the nitrogen feed system to the thruster. Although this took longer and exceeded the provided budget of the thesis, it should help future researchers who wish to use the purchased components for their own work.

With the necessary equipment thrust testing can now be performed, but will not be sufficient to reach chamber temperatures up to 600K. This was already expected once the thruster was fabricated in chapter 2. Therefore, the use of the thermal camera, which can measure up to 150^{o}C, will be used instead.

The given test set up can be used to test with nitrogen propellant, but the necessary additional components for testing with water were not set-up. Therefore, the key requirement **PROP-FUN-1** was only partially achieved.

For future work, it is recommended to:

- Use a thermocouple or pressure-temperature sensor in future tests, to measure temperatures greater than 150^{o}C.
- Determine a way to use the thermal camera, while the vacuum chamber is operational. This would allow users to see the distribution of heat on the thruster chip and take temperature readings.
- Redesign the thruster to pendulum interface from Figure 4.7a, to make it easier to attach the heater wires to the pins on the PCB. It is easy to accidentally dislodge the thruster when threading the

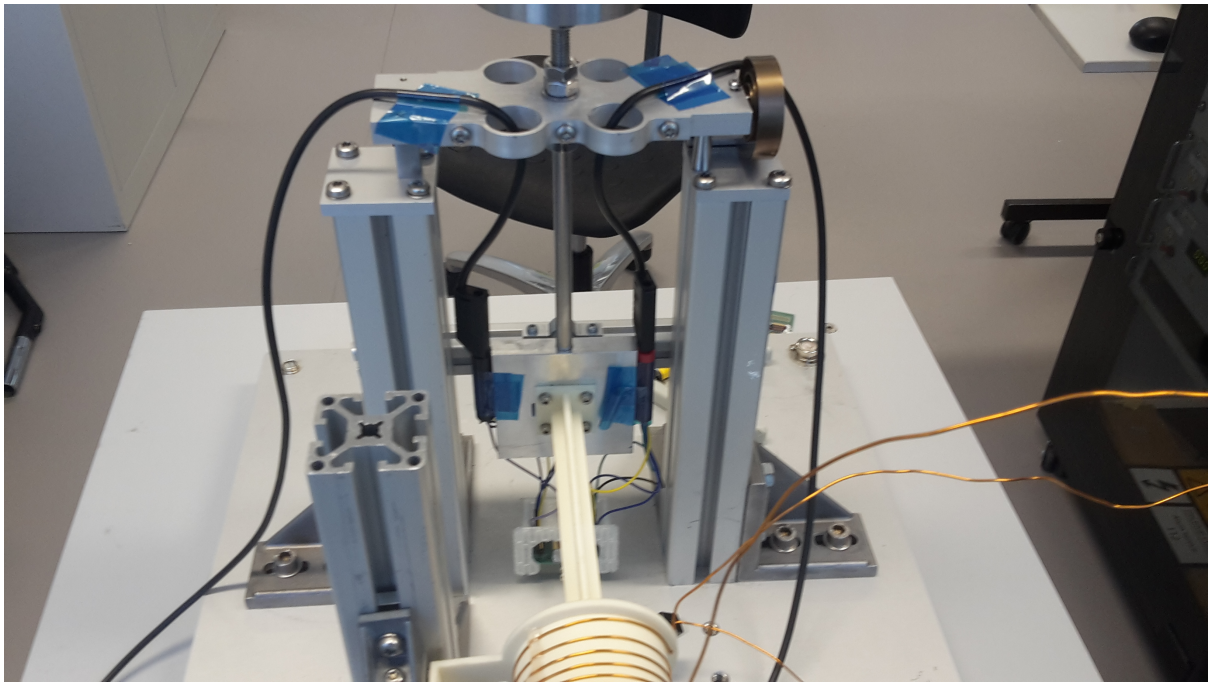

Figure 4.10: Test set up used for the thruster R4C9.

heater wires through the two windows at the top of the cover and connecting them to the pins. This was how two thrusters were broken (R5C1 and R4C7).

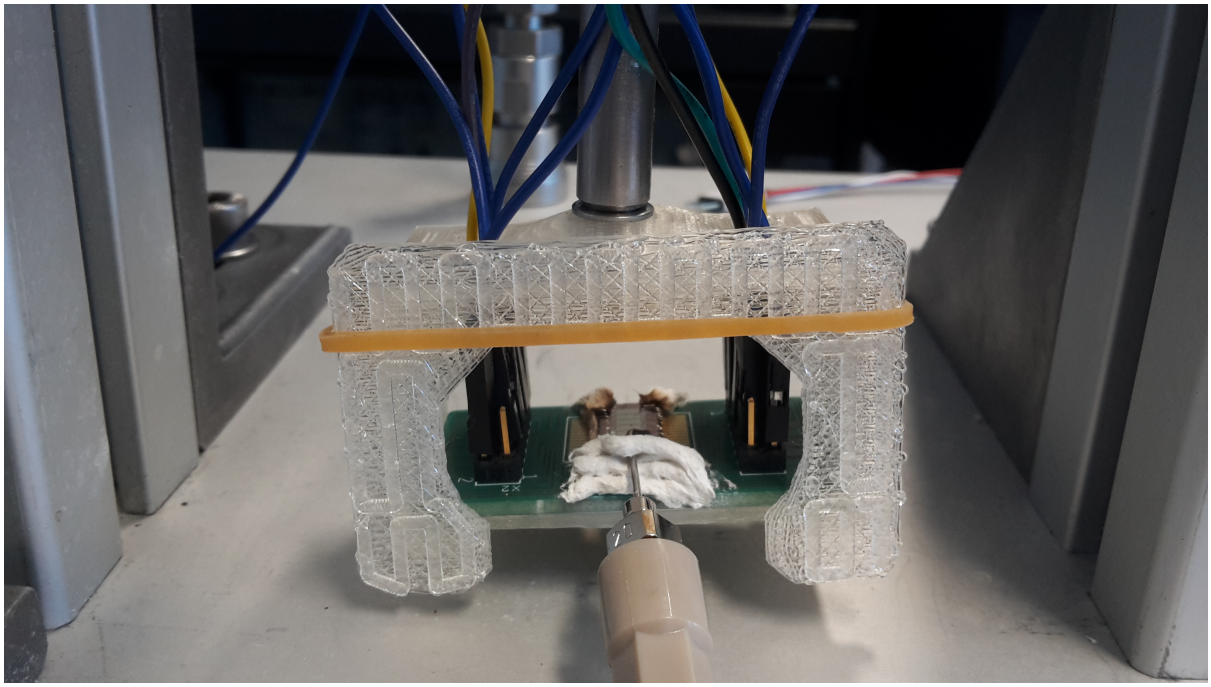

Figure 4.11: Close up showing how the jumper cables attached to the pins of the PCB, through the 3D printed interface.

5

Prepatory Tests

Before the thrust testing is done, several prepatory tests need to be performed beforehand, to ensure that the thrust testing gives reliable data. The goal of this chapter is to determine:

- if the propellant feed system and thruster is sufficiently leak tight for the operating pressure of 2-5 bars.
- a relation between the bench displacement or the current needed to hold the bench in position, to the force exerted on the bench by the thruster.

For determining the leakage, a leak test will be performed by connecting each thruster to the propellant feed system and blocking the nozzle exit so that no flow escapes. The leak test is explained in section 5.1 and is important in ensuring that the mass flow measured by the MFC is indeed the true mass flow. Several prepatory tests need to be performed to determine the relation for calculating the thrust from the thrust pendulum. Thrust pendulum does not measure the thrust directly. It measures the induced current of the coil when a magnetic block, which is attached to the pendulum arm, is displaced into the coil actuator. The coil actuator is calibrated to find the relation between the magnetic force produced and the relative input current or relative displacement of the thrust pendulum. This depends on whether the pendulum is allowed to move during testing or is kept static with a magnetic force that opposes the thrust force. This is seen in section 5.2. Additionally, a correction factor is applied to the measured force, based on the location of the thruster relative to the magnetic coil. This can be seen in section 5.4.

5.1. Leak Testing

The purpose of leak testing is to determine how much, if any, of the propellant is being lost due to leakage. The goal is to ensure that the thruster leakage remains small enough to not affect the results dramatically. No leakage at all is preferable. A leakage would result in some of the mass flow escaping from the interface and feed system, giving a higher mass flow than expected. For example, if the mass flow at a specific operating condition during the thrust test shows 1 mg/s, but a leak test before the test shows a leakage rate of 0.1 mg/s, then the real mass flow would be 0.9 mg/s. The leakage rate was checked for chamber pressures between 2-5 bars.

5.1.1. Exploratory testing

For the first exploratory test, it was attempted to block the thruster exit with a piece of tape, similar to what many students had done previously like Makhan [18], Kurmanbay [15] and Van Wees [35]. However, the design of the interface and the way the thruster was glued to the PCB made it difficult to block the nozzle completely without removing the glued thruster from the PCB. Also, the tape did not stick well enough to prevent leakage.

Additionally, it was found that the thrusters which used the BISON thermal glue had large leakages at pressures of 2 bars and higher, even without attempting to block the nozzles, that could be heard and felt by touch. The flexibility and softness of the glue makes it very easy for gas to escape. Therefore R4C5 and R4C6 can not be tested and the BISON thermal glue is not a suitable glue for the inlet.

Figure 5.1: The metal needle is blocked by the rubber test tube cap, to perform a leak test. The tubing leads to the pressure/temperature block which in turn leads to a solenoid valve which allows/disallows propellant to pass through.

5.1.2. Final Test Results and Analysis

Based on findings from the exploratory testing, the leak test was performed with an inlet needle which was not attached to thruster, as can be seen in Figure 5.1. The inlet needle was then blocked using a rubber test tube cap also seen in Figure 5.1, provided by Barry Zandbergen, which are normally used in the medical field. This means that, the connection of the inlet needle to the thruster inlet was not taken into account into leak testing for the tested thrusters and it was assumed that the inlet connection, where the dispensing tip is glued to the thruster inlet hole, was leak free. It would be better to find a way to include the thruster nozzle during leak tests, by finding a way to block the nozzle before assembly. Kurmanbay [15] found there was no leakage at the inlet during testing, so it will be assumed for now that the inlet is leak tight.

The leak tests were done using two different types of feed tube adapters, which were explained in subsection 4.1.5. Initially, there was a very obvious leakage that could be heard. To resolve this, a clamp was used to force the minstac tube into the syringe end, which deformed the plastic syringe around the minstac, closing any gaps between the minstac and syringe. This fix proved to be successful during leak tests up until 6 bars, according to Figure 5.2, because the leak rate from 2-5 bars was close to zero. The mass flow was measured using the 0-144sccm MFC. At 6 bars, the chamber pressure was enough to slowly push the minstac tube out of the syringe and cause leakage again. Needle interface A was used for all cold tests.

The second needle interface (needle interface B), involved using a specially made adapter from the Lee company, that allowed the 62 minstac tubing to connect to the needle. This needle interface is a lot better in terms of quality and can handle higher pressures compared to needle interface A. This interface showed no sign of leakages, so long as the needle and adapter are screwed together tightly enough. Initially, small leakages around 0.5 mg/s could be noticed, but as the needle was screwed more tightly with pliers, the leakage noticeably decreased. This can be seen in Figure 5.3. Note that the huge spike in mass flow in Figure 5.3 is caused by the act of opening the valve, which leads to a sudden rush of pressure that fills the feed system tubes.

For future work, it is recommended for future testing to use interface B and C, since it will most likely be the case that after continuous use, interface A will eventually become unreliably if the clamping fix is applied repetitively.

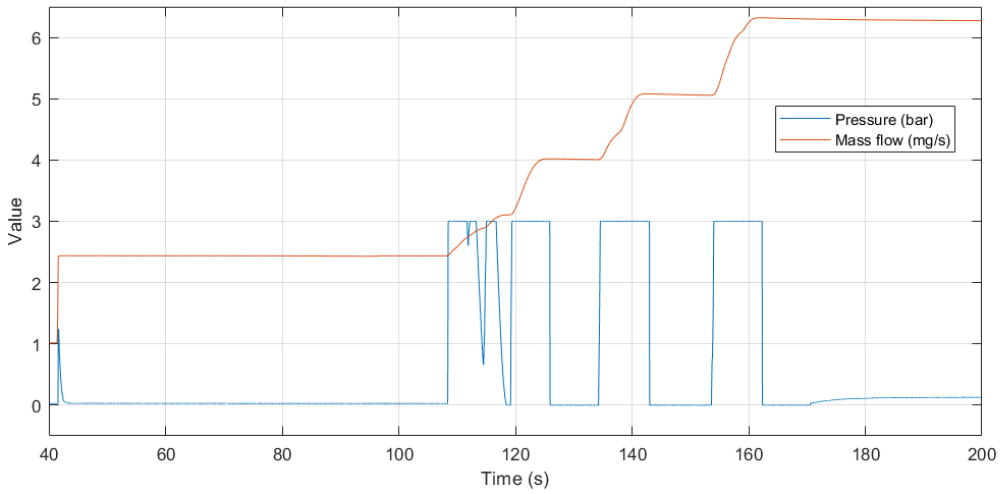

Figure 5.2: Leak test of needle interface A, after the minstac needle was clamped.

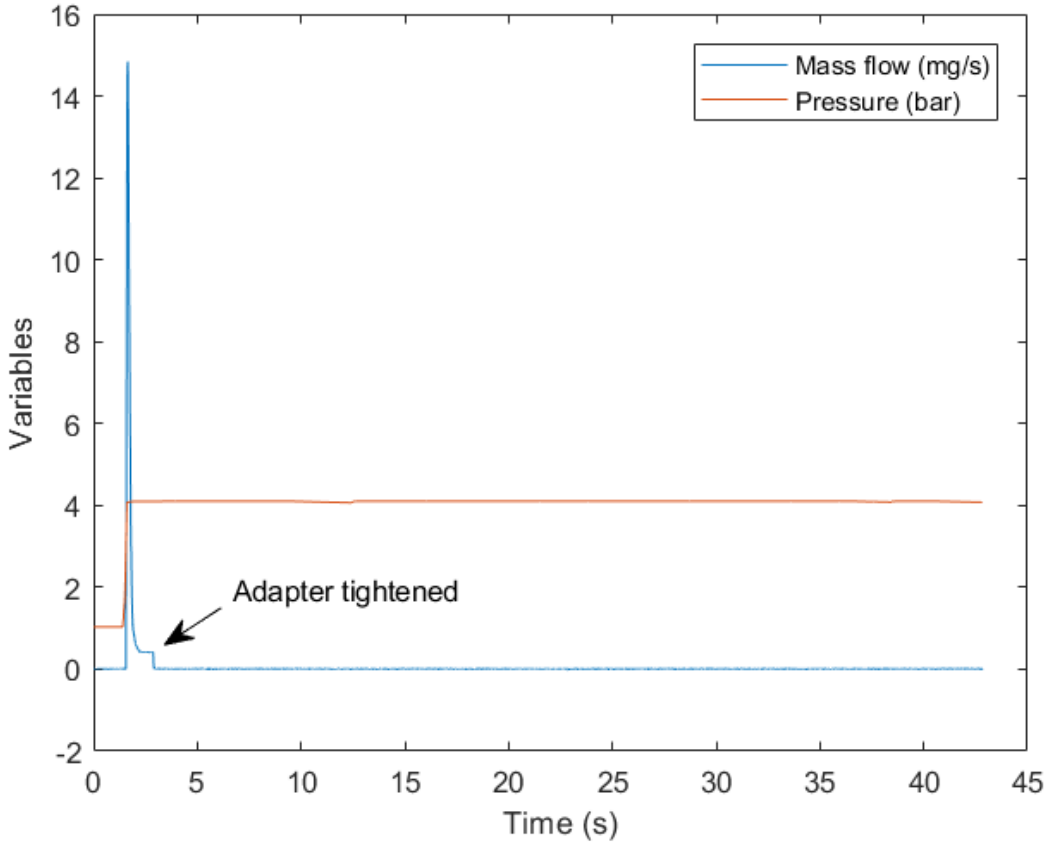

Figure 5.3: Leak test using needle interface B. The arrow shows where the adapter was tightened to reduce the leakage.

5.2. Actuator coil calibration

5.2.1. Purpose and relevant parameters

The purpose of this test is to determine the relationship between the magnetic force created by the VTDC actuator coil and the input current to the coil. The work of Jansen Jansen [12] details how this was done and the results of it showed that the relationship between the input current and the magnetic force from the coil was on average 0.827 mN/A. However, it was decided to redo this experiment since this calibration is from 3 years ago. It would be helpful, for future researchers, to create a document that keeps track of when the actuator has been calibrated. This would make it easier to determine calibration history, without having to scour through multiple past thesis reports.

The only relevant parameters for this experiment is the input current to the coil and magnetic force produced by the coil due to the input current. To consider this test successful, the sensitivity of the coil and its uncertainty must be measured and calculated.

5.2.2. Test Set-up

This test was performed in the work of Jansen [12], however Versteeg [36] made some minor changes to improve the test procedure. So the procedure of Versteeg [36] is used, but the step time was increased from 10s to 15s, to make it easier to write everything down and give a little more time for the measured mass values to settle. The necessary equipment can be seen below:

1. The VTDC coil,detached from the thrust stand.
2. A high-precision Mettler Toledo AG245.
3. A computer, with the labview file.
4. Delta Elektronica SM-7020-D power supply
5. Pen and paper

The Mettler Toledo is the mass balance used for force measurements. The coil, detached from the thrust stand, is placed vertically onto the mass balance as can be seen in Figure 5.4, with the magnet arm placed flat on the scale.

The power supply is then used to supply a current, up to 9.75 A, in 0.25 Amp steps, for 15 seconds at each point. This done by using the Labview file ”Aris/Testing/1_Labview_testing/actuator_calibration.vi”. It was decided to go up to 9.75 amps, as this was done previously by Jansen [12]. So the entire test takes about 10 minutes long and produces 40 points of data once the the Labview program is run. A higher target current can be chosen, but Takken [30] determined that currents larger than 16A would distort the magnetic field, due to heating of the coil. The current and mass measured are then manually written down. The mass is converted to a magnetic force by multiplying the mass by 9.80665 m/s^2.

5.2.3. Test Results and Analysis

This subsection will discuss and analyze the results of the VTDC calibration. The test was done three times to ensure scientific accuracy. The results of each of the three tests are shown in Table 5.1. From the results it can be seen that as the current is increased, the magnetic force created increases linearly as well. The increase in magnetic force causes a pull on the sensor target which in turn reduces the measured mass on the scale. The magnetic force is calculated by multiplying the measured mass of the coil by the gravitational acceleration constant 9.80665 m/s^2. The sensitivity (S) of the data can be found by plotting the data on a graph and finding the slope of the linear trend line.

Additionally, similar to Makhan [18] and Jansen [12], a consistent offset of -0.04A is seen in the I_{coil} measured compared to the $I_{simulated}$, in Table 5.1. However, this should not pose any issues, since the actual coil current is known.

The standard error of estimates (SSE) for each test is found by using Equation 5.1, where Y is the measured value, Y' is value using the best fit line and N is the number of samples. The uncertainty of the final results is based off of the sample standard deviation of the sensitivities for each test. The sample standard deviation (Equation 5.2) of the calculated sensitivities were found to be equal to 2.3 μN/A. Then by taking 3 confidence intervals (3σ), which covers 99.7 % of possible values, the final uncertainty of 6.9 μN/A is achieved. $\bar{Y}$ represents in this case the average sensitivity of 0.827mN/A. The SSE for each test were not used, since they were smaller compared to 3σ of the calculated sensitivities of all the tests.

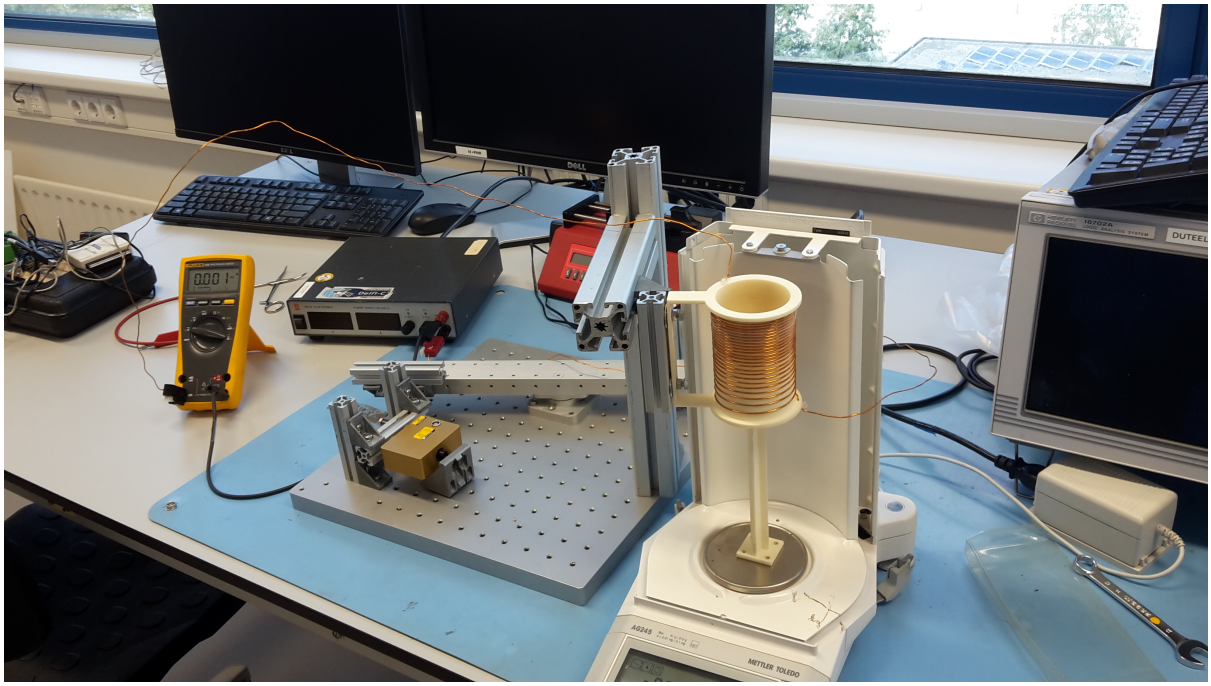

Figure 5.4: Test set up used for coil calibration. Please note that in the figure, the coil is connected to a different power source, but in reality the SM-7020-D power supply was used instead. Also, the multimeter was removed from the test set up, since the Labview file recorded the current measured.

$$SSE = \sqrt{\frac{\sum(Y - Y')^2}{N - 1}} \tag{5.1}$$

$$\sigma = \sqrt{\frac{\sum(Y_n - \bar{Y}_n)^2}{N - 1}} \tag{5.2}$$

The average sensitivity of of all three tests is 0.827 mN/A, which is similar to the value found by Jansen [12]. So it can be concluded that, since the last time the coil calibration was done, the sensitivity of the coil has not changed significantly, but considering how straightforward the test is, future students could still carry out this test to check for themselves. Versteeg [36] did perform the test as well but found a value much higher. This could be attributed to how the coils were positioned during testing and could be avoided by ensuring that the coil wires do no intersect with the magnetic field lines. The coil wires should be perpendicular to the coil axis and as far away as possible, even during thrust testing.

Additionally, Versteeg [36] used my test results for his thesis to calculate an average along with his single calibration test, but those values used a best fit line where the y-intercept was forced to the origin. In this thesis, the best fit line did not force the best fit line to the origin. When the values from Table 5.1 is used instead, the average sensitivity calculated for Versteeg [36] becomes $S = 0.827mN/A$ instead of $S = 0.826mN/A$, as initially calculated by him. This will only cause a slight increase in the thrust values of Versteeg [36] by 0.12%, so a recalculation of his values is not needed. The final equation can be seen in Equation 5.3, with its uncertainty.

$$S = 0.827[mN/A](\pm 6.9[\mu N/A]) \cdot \Delta I[A] \tag{5.3}$$

5.3. Thrust Stand Calibration

The purpose of the thrust stand calibration is to determine the relationship for the magnetic force experienced by the VTDC actuator based on the input current, which in turn is affected by the pendulum displacement. By doing so the thrust of the chip can be determined based off of the magnetic force

Table 5.1: The magnetic force measured of the coil for each input current step. One value is undetermined due to illegible handwriting. CC stands for Coil Calibration.

$I_{simulated}$ (A)	I_{coil} (A)	F_{mag} (mN)		
		CC-1	CC-2	CC-3
0.00	0.00	0.0000	0.0000	0.0000
0.25	0.21	0.1814	0.1765	0.1873
0.50	0.46	0.3883	0.3815	0.3923
0.75	0.71	0.5982	0.5913	0.5962
1.00	0.96	0.8051	0.7953	0.8041
1.25	1.21	1.0081	0.9993	1.0120
1.50	1.46	1.2199	1.2052	1.2160
1.75	1.71	1.4239	1.4151	1.4269
2.00	1.96	1.6308	1.6201	1.6318
2.25	2.21	1.8387	1.8260	1.8338
2.50	2.46	2.0525	2.0329	2.0496
2.75	2.71	2.2565	2.2389	2.2555
3.00	2.96	2.4654	2.4458	2.4566
3.25	3.21	2.6733	2.6537	2.6674
3.50	3.46	2.8783	2.8577	2.8743
3.75	3.71	3.0871	3.0626	3.0803
4.00	3.96	3.2950	3.2705	3.2901
4.25	4.21	3.5029	3.4765	3.4921
4.50	4.46	3.7108	3.6844	3.6971
4.75	4.71	3.9168	3.8952	3.9080
5.00	4.96	4.1217	4.0953	4.1119
5.25	5.21	4.3326	4.3022	4.3247
5.50	5.46	4.5385	4.5071	4.5356
5.75	5.71	4.7484	4.7170	4.7356
6.00	5.96	4.9543	4.9200	4.9426
6.25	6.21	5.1612	5.1269	5.1534
6.50	6.46	5.3672	5.3338	5.3554
6.75	6.71	5.5780	5.5398	5.5692
7.00	6.96	5.7849	5.7457	5.7712
7.25	7.21	5.9870	5.9536	5.9752
7.50	7.46	6.1968	6.1566	6.1831
7.75	7.71	6.4047	6.3626	6.3881
8.00	7.96	6.6116	6.5705	6.5960
8.25	8.21	6.8186	6.7764	undetermined
8.50	8.46	7.0216	6.9804	7.0118
8.75	8.71	7.2295	7.1853	7.2167
9.00	8.96	7.4383	7.3923	7.4227
9.25	9.21	7.6433	7.5972	7.6257
9.50	9.46	7.8532	7.8032	7.8355
9.75	9.71	8.0552	8.0071	8.0365
	S_{test} (mN/A)	0.8294	0.8248	0.8274
	SSE (μN)	2.96	2.20	3.52

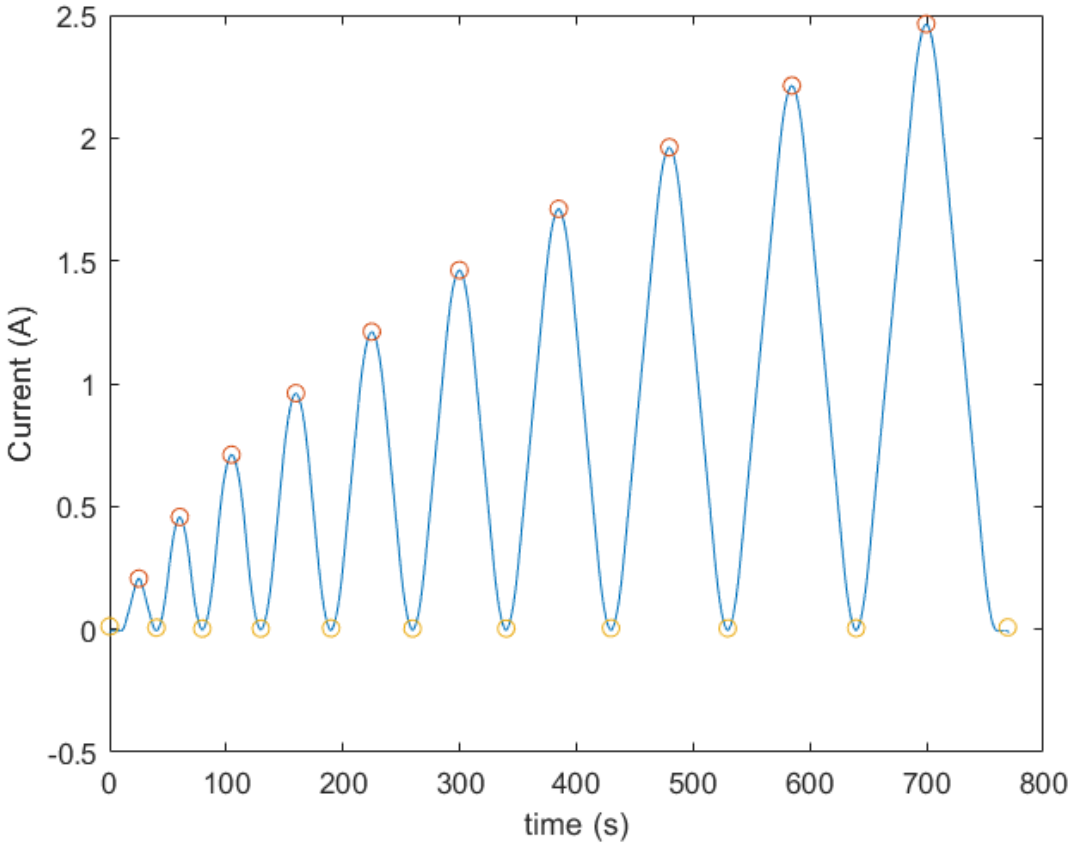

Figure 5.5: The displacement of the pendulum for PC-1 corrected for noise using the smooth function in MATLAB.

experienced by the coils. This test is needed if the displacement method is used for determining thrust. This test is not needed if the force compensation method is used instead. subsection 6.3.1 compares the thrust measurements using both measurements and a comparison will be made for the two methods. The force compensation method, implemented first by Versteeg [36], already has an advantage being that the thrust stand calibration can be removed from the experimental methodology. However, it still needs to be determined if the two methods give similar results. A description for both of these methods can be found in section 4.4. It was determined that both methods were sufficiently similar and is explained in section 4.5.

5.3.1. Test Set-Up

To perform the test, the Variable-Turn Density Coil (VTDC), thrust pendulum, and power devices are needed. The necessary Labview code can be found in the folder Aris, named 'Pendulum calibration.vi', on the computer in the cleanroom, next to the vacuum oven. The procedure made by Makhan [18] was used to carry out the test. Three pendulum calibrations were performed before the cold testing for R4C7. From the outputted data, the displacement and the current at different time steps were recorded, as can be seen in Figure 5.5 and Figure 5.6.

The displacement-current equations can be found by looking for the gradient and y-intercept on the graph and are given in Table 5.3. It can be seen that the slopes found are on average around 0.0241 A/μm, with an uncertainty of 0.00142, referring to 3 sample standard deviations. Equation 5.4 is the final equation for determining the magnetic force, when using the displacement method, which is found by multiplying the slope with magnetic coil current relation, S, which was determined in section 5.2. The following relation was found:

$$F_{mag,disp} = S \cdot (slope_{ave}) \cdot \Delta d = 0.02 mN/\mu m \pm 0.001345 mN/\mu m \Delta d \tag{5.4}$$

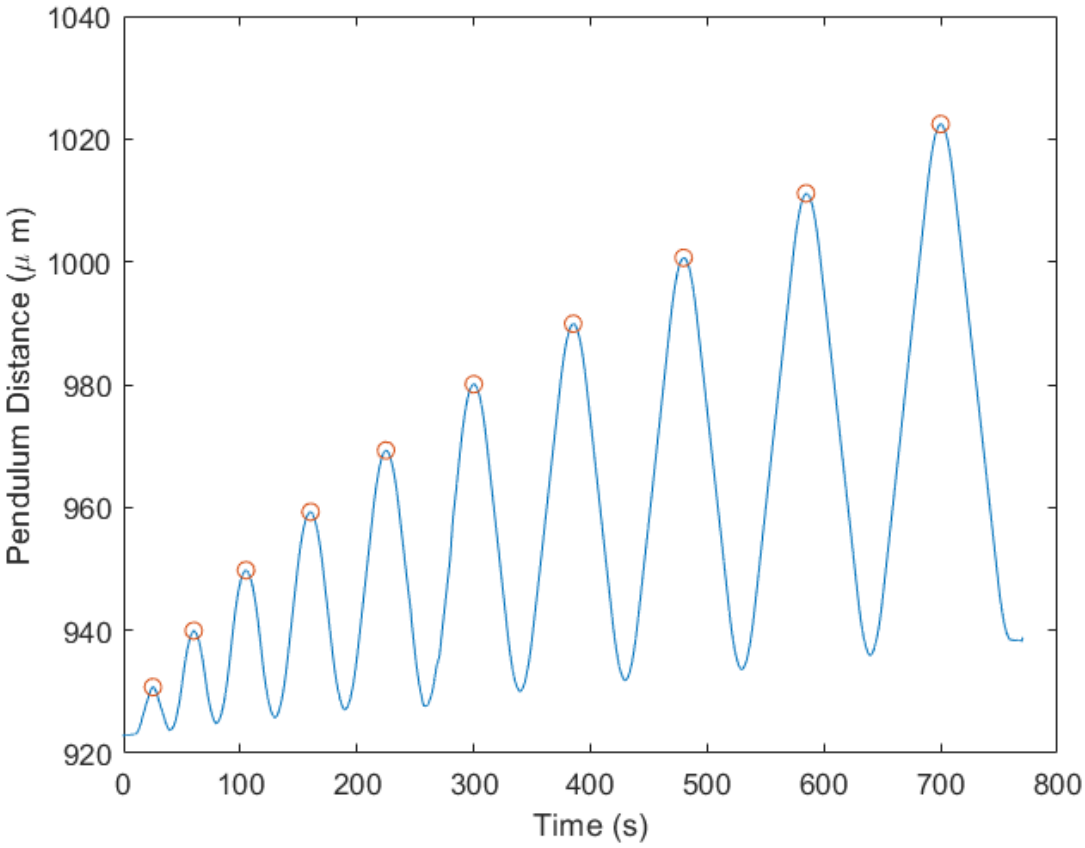

Figure 5.6: The current measured for PC-1 corrected for noise using the smooth function in MATLAB.

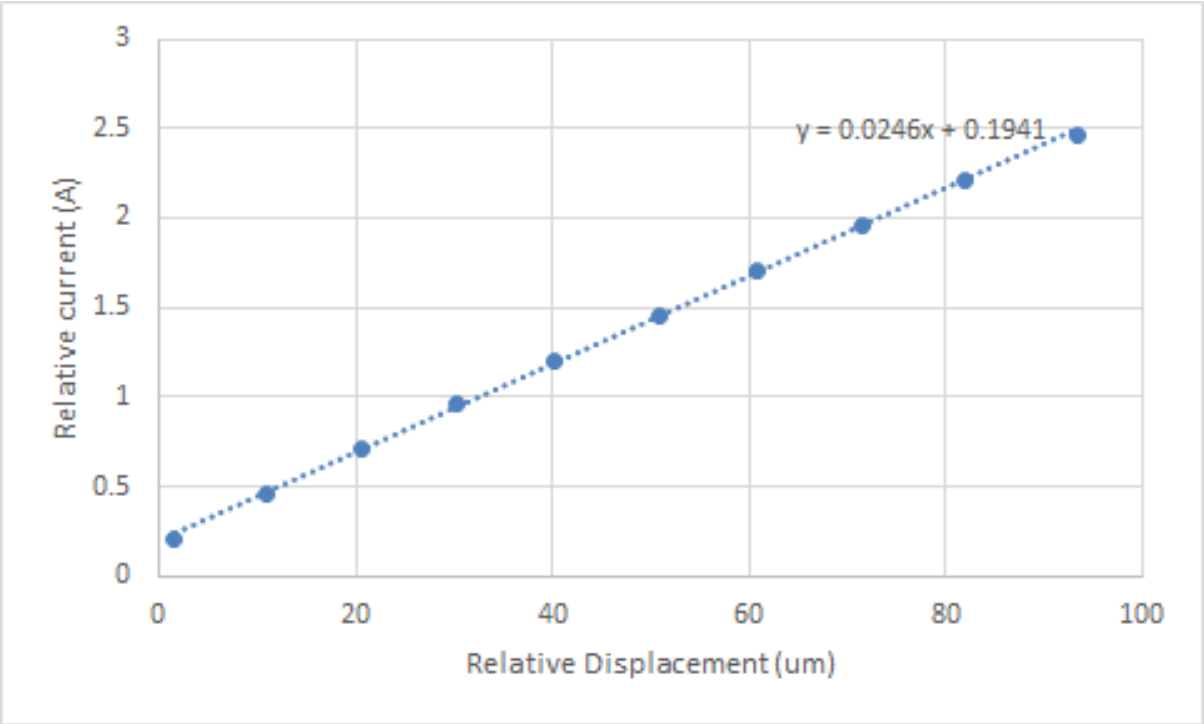

Figure 5.7: The relative current found versus the relative pendulum displacement, with an equation describing the line of best fit.

Table 5.2: The relative current and relative displacement measurements for the pendulum calibration tests, along with their calculated current-displacement relation (slope).

Relative displacement (μm)			Relative Current (A)		
PC-1	PC-2	PC-3	PC-1	PC-2	PC-3
1.661014	0	0	0.201939	0	0
10.83774	12.3	24.9	0.452703	0.3251	0.6135
20.69559	37.3	34.9	0.706224	0.9155	0.8466
30.19313	62.3	44.9	0.956546	1.505	1.079
40.20157	87.3	54.9	1.206625	2.091	1.313
50.97867		64.9	1.457248		1.556
60.82228		74.9	1.707045		1.795
71.56792		84.9	1.957665		2.033
82.05952		94.9	2.208667		2.277
93.34344		104.9	2.459342		2.526
		114.9			2.765
		124.9			3.014

Table 5.3: Results for the pendulum calibrations done for a test pendulum that can move (displacement method).

Test	PC-1	PC-2	PC-3
slope (A/μm)	0.0246	0.0238	0.024
y (μm)	0.1941	0.0178	0.0016
$3\sigma_{slope}$ (A/μm)	0.00142		
$3\sigma_y$ (μm)	0.32		

5.4. Thrust Correction Factor

In this section, the test and results for determining the thrust correction factor will be presented.

The vertical distance between the pendulum pivot and the nozzle outlet of the thruster will be measured, along with the distance between the pendulum pivot and the actuator, which in this case is the centre of the magnet. The reason is that the magnetic force produced by the VTDC actuator is applied at a different height compared to the thrust force of the nozzle. As a result, the actual thrust measured at the nozzle outlet will be lower compared to the measured magnetic force. A correction factor, that takes into account the difference in height, needs to be incorporated to find the real thrust force based on the magnetic force.

The only apparatus needed for the test is the AE-TB-5m thrust bench, the thruster nozzle attached to the thrust bench using the PCB interface and a ruler. Equation 5.5 is the equation that was used to measure the FCF. An uncertainty of $\pm$2 mm was applied to all measured values. It was determined that:

- The vertical distance between the pivot and the nozzle exit of the VLM thruster was $L_{thruster} = L_{PP-C2S} + L_{C2S-nozzle} = 276.44 \pm 4mm$. These dimensions can be seen in Figure 5.8, however the sketch is not to scale. The thruster used in this thesis hangs lower compared to Makhan [18] and Versteeg [36]. The total length was measured using two different lengths added together, because using a tape measure to measure the entire distance directly was too cumbersome to measure accurately.

- The vertical distance between the pivot of the pendulum arm and the centre of the magnet was $L_{act} = L_{PP-C2S} - L_{C2S-M} = 165.67 \pm 6mm$. The dimensions can be seen in Figure 5.8. Makhan [18] measured $L_{act} = 179.66mm$, but he considered the C2S sensor to be the actuator, when in fact it should be the centre of the magnet. This means that his thrust values should be around 8% lower ($1 - \frac{165.67}{179.66}$) than stated in his report, assuming his measurement between the pendulum pivot and the thruster nozzle exit was done correctly. This mistake was also done during this thesis, but was corrected after consultation with Versteeg [36]. This is also the reason why L_{act} was calculated using two length measurements. This correction was therefore made to his $F_{T,exp}$ values, when they are needed in the thesis. The corrected and original thrust values of Makhan [18] can be seen in Table 3.2.

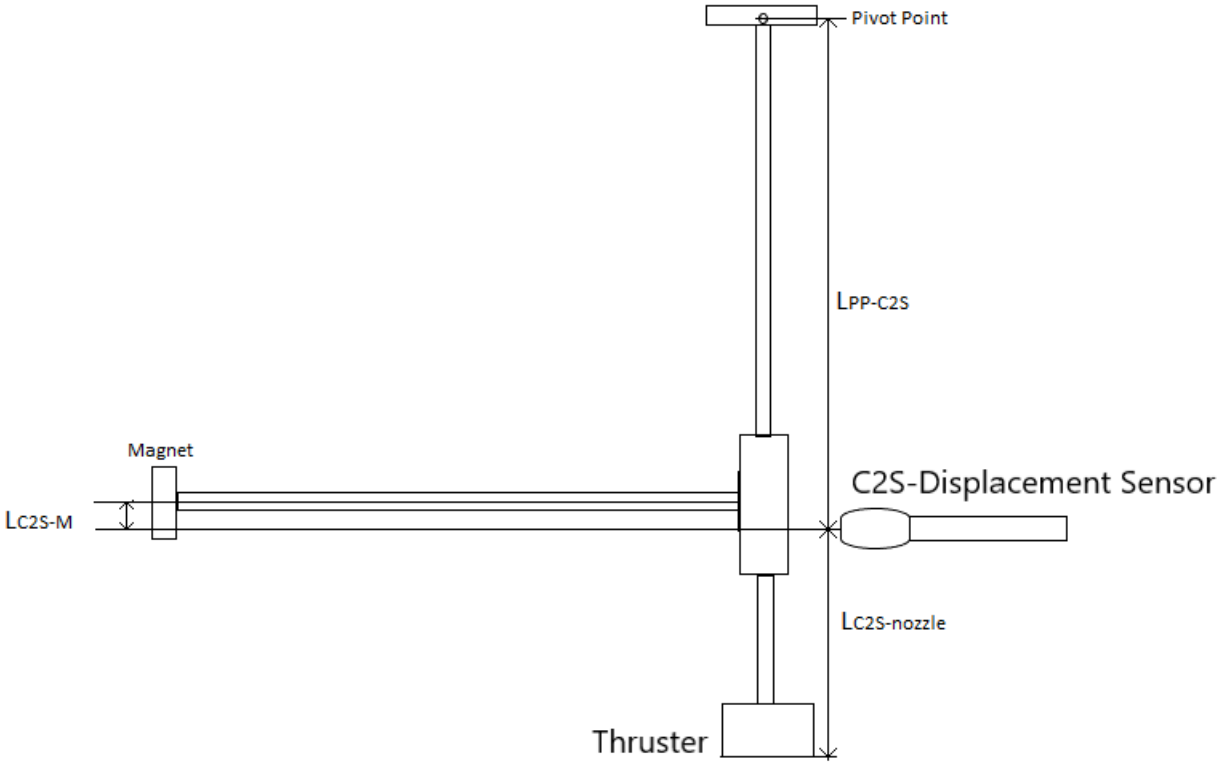

Figure 5.8: Sketch of the assembled AE-TB-5m thrust bench showing the dimensions measured for determining the force correction factor, viewed from the side.

- $FCF = 0.599 \pm 0.0304$ was found using Equation 5.5.

$$FCF = \frac{L_{actuator}}{L_{thruster}} = \frac{165.67 \pm 6}{276.44 \pm 4} \tag{5.5}$$

5.5. Conclusions

Overall the prepatory tests for the thesis have been introduced, explained and discussed. The leakage tests show that there is no leakages anywhere between the nitrogen feed system up to the dispensing tip, for pressures between 2-5bars, when ABLESTIK is used for the thruster inlet. This satisfies the **PROP-INT-2** requirement. Additionally, the BISON glue used for the thruster inlet for R4C5 and R4C6 immediately shows leakages at 2 bars, causing them to become inoperable for thrust testing. Therefore, BISON thermal glue is not suitable to glue the metal dispensing tips to the thruster inlets.

Additionally, the necessary thrust relation needed to determine the nozzle thrust from the current change and displacement of the pendulum has been explained and provided. The relation between the pendulum displacement and the actual thrust is: $F_{T,exp} = 0.599 \cdot 0.02 mN/\mu m \cdot \Delta d\mu$. That is the relation used if the pendulum can freely move. If the force compensation method is used, then Equation 4.1 is: $F_{T,exp} = 0.599 \cdot 0.827 mN/A \cdot \Delta I$.

Since the test set up has been proven to have no leakage from 2-5bars, and the thrust relation has been determined, it is now possible to move towards setting up the thrust test bench and performing the thrust testing.

For future work, it is recommended to determine a way to block thrusters during leak testing, so that the dispensing tip and thruster inlet can be checked for leakages. Otherwise, using liquid soap to check for bubbles, during leak tests, at the thruster inlet, could be a feasible alternative.

Additionally, creating a document that keeps tracks of the calibration history of the actuator coil and thrust stand would be recommended. This will keep things organized and make it easier for future users

to know when the actuator was calibrated last, instead of searching through multiple thesis reports.

Future researchers should use the corrected experimental values of Makhan [18], found in Table 3.2, instead of the values he recorded, when using his data for any purpose. The corrected values take into account the correct actuator distance, which is from the pendulum pivot to the centre of the magnet arm, not the displacement sensor. This meant the actual thrust values were 8% smaller than initially recorded and calculated by Makhan [18].

6

Cold Testing

This section will cover the results and the analysis of the results for the cold thrust tests. Several of the tests were done using the displacement method, while a few were done using the force compensation method. The purpose of this chapter is to:

- Present and discuss the raw data obtained for the cold tests of each thruster.
- Determine and analyze the resulting mass flow, thrust and quality factors for each of these thrusters, versus their throat Reynolds number.
- Compare the data of these thrusters to the tests from Versteeg [36] and Makhan [18].
- Compare the performance model to the measured thrust data and conclude whether the model is valid.

section 6.1 will give an overview of the tests performed during thrust tests. Mainly at which pressure and temperature each thrust measurement was taken. Afterwards, section 6.2 will describe the raw data provided by the tests and how their uncertainties were determined. From the raw data, the measured values are extracted, presented and analyzed in section 6.3, with respect to literature and the predictive model. Lastly, conclusions and recommendations are summarized in section 6.4.

6.1. Test overview

The thrust tests performed are summarized in Table 6.1, showing which thrusters have undergone testing and under what conditions. The temperature and pressures stated are rounded to each 25^{o}C for temperature and to each 0.5bars for pressure, because not every point of data recorded was done at exactly the stated pressure and temperature in the table. From the table it can be seen that for thruster R5C1, 3 tests were done at 25^{o}C, for 4 different pressures, and none were done at any higher temperatures. For the case of R4C9, one thrust test was done at 6 different pressures, for chamber temperatures between 25^{o}C to 125^{o}C.

Additionally, the tests are labelled using CT and HT to refer to cold and hot thrust testing, respectively.

6.2. Experimental Cold Thrust Testing Results

This section will discuss how the experimental results were determined from the raw data providing from the thrust testing. It will also discuss the uncertainty analysis of the different inputs and outputs.

The raw data is located in the thesis folder of Aris Pappadimitriou. The specific name of the subfolder is called ”Experimental Data”, which can be found in the following folder location, as example: Test Data - Aris Pappadimitriou\Cold-Tests\CT-R4C7\Experimental Data\20200225 CT-R4C7-1\Raw Data. Depending on the thruster test one is interested in, the thruster name will be different in folder path stated before.

The test labelling is written as CT-R4C7-1.1 as an example, where CT means Cold Test, R4C7 is the thruster name, and 1.1 represents the first test run and first pressure point.

Table 6.1: Test matrix showing the number of tests performed at each operating point for different thrusters, for cold and hot testing

Temperature (C)	Thruster	Pressure (bar)						
		2	2.5	3	3.5	4	4.5	5
25	R5C1	3	-	3	-	3	-	3
	R4C7	4	-	4	-	4	-	4
	R4C9	-	1	1	1	1	1	1
50	R5C1	-	-	-	-	-	-	-
	R4C7	1	-	-	-	-	-	-
	R4C9	-	1	1	1	1	1	1
75	R5C1	-	-	-	-	-	-	-
	R4C7	1	-	-	-	-	-	-
	R4C9	-	1	1	1	1	1	1
100	R5C1	-	-	-	-	-	-	-
	R4C7	1	-	-	-	-	-	-
	R4C9	-	1	1	1	1	1	1
125	R5C1	-	-	-	-	-	-	-
	R4C7	1	-	-	-	-	-	-
	R4C9	-	1	1	1	1	1	1
150	R5C1	-	-	-	-	-	-	-
	R4C7	1	-	-	-	-	-	-
	R4C9	-	-	-	-	-	-	-

6.2.1. Inputs and Outputs

During testing, certain variables were outputted to excel files. These variables could then be extracted and sorted using a matlab script.

The first variables outputted are the chamber pressure, chamber temperature and the mass flow. These can be read straight off from the graphs in Figure 6.1, Figure 6.2 and Figure 6.3. The temperature variance was very small compared to the absolute uncertainty of the temperature sensor of 1.5 K, so the mean of the entire testing range was taken and applied to each operating pressure. The pressure was taken at the peaks of each point and an uncertainty of ± 0.05 bars was applied to each point. For the mass flow, it was discovered at certain pressure points, the mass flow did not return to 0 mg/s, as can be seen in Figure 6.3. Therefore, the actual mass flow was found by subtracting zeroing error from the measured mass flow. In future tests, the best way to deal with this issue is press the re-zeroing button, located underneath the mass flow sensor block. This was discovered after testing. Additionally, whenever the valve is opened, there is initially a spike in the mass flow before it reduces and stabilizes to the true mass flow. This can be seen in Figure 6.3, at 200s, where the mass flow peaks at 3.02mg/s, which also happens to be the cap of the mass flow controller. The mass flow peak, is a result of a voltage spike which occurs when the valve is suddenly opened and has also occurred in the work of Makhan [18]. It takes around 15-20 seconds for the mass flow to stabilize. This is also the reason why an increase in pendulum distance, and therefore thrust, in Figure 6.4, does not occur when the spike in mass flow is measured. It should be noted that the thick yellow line, on Figure 6.4, represents the the smoothed out data, from the oscillating blue line. This makes it easier to determine the average, maximum pendulum displacement. The smoothed yellow line was created by using the smoothing function in MATLAB, followed the ”pks” function.

There are two methods for determining the thrust of the nozzle: the displacement method and force compensation method. If the displacement method is used, then the pendulum distance changes as the propellant passes through the nozzle. This change in pendulum distance can be related to a magnetic force using Equation 5.4. Then applying a force correction factor, the real thrust force can be achieved in Equation 6.2. For the force compensation method, the pendulum distance remains constant and instead the actuator current varies. So the total thrust for the force compensation method is found using Equation 6.3. ΔI is estimated by using Equation 6.1.

$$\Delta I = \frac{I_{peak}}{I_{trough,mean}} \tag{6.1}$$

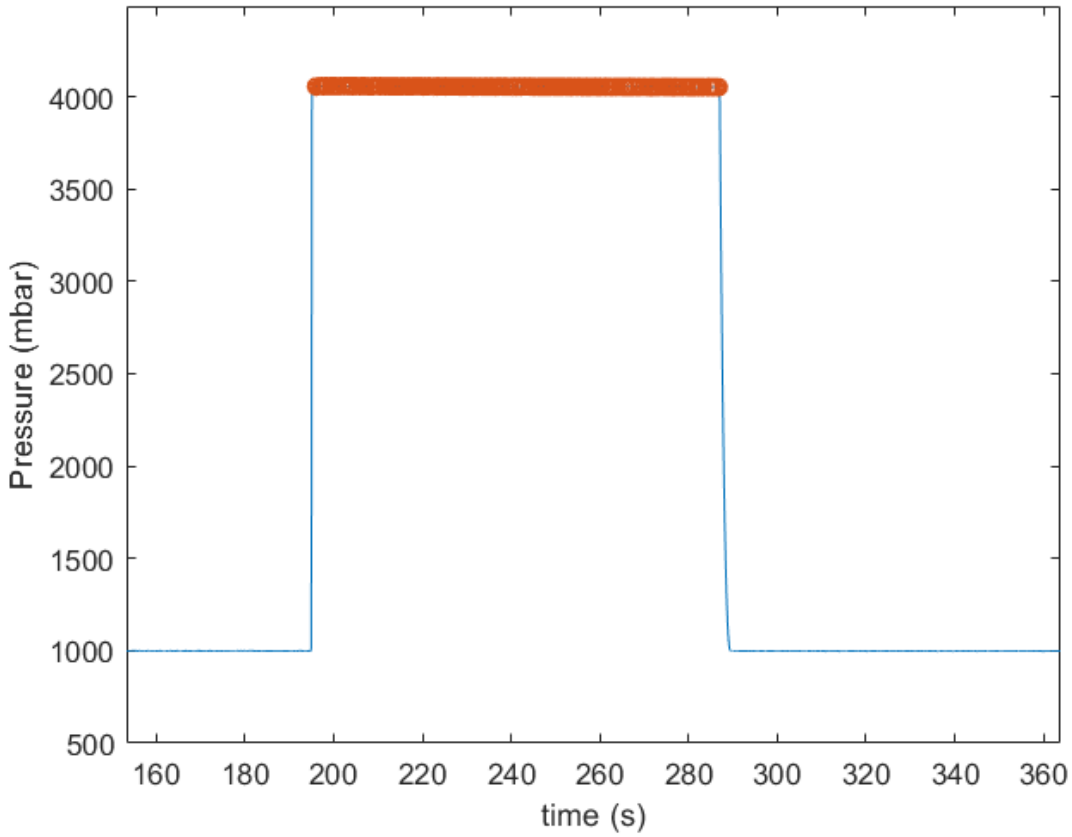

Figure 6.1: Measurement results for the chamber pressure for CT-R4C7-1

$$F_{T,exp} = FCF \cdot F_{mag} \tag{6.2}$$

$$F_{T,exp} = FCF \cdot S \cdot \Delta I \tag{6.3}$$

The Isp_{exp} is found using Equation 6.4, where it is assumed that $g_0 = 9.80665\text{m/s}^2$. The discharge coefficient and Isp efficiency for the experiments can then be found using Equation 6.5 and Equation 6.6. The ϵ_c, from Equation 6.7, is the heating quality, which for cold testing is normally assumed to be equal to one. The nozzle quality is defined by Equation 6.8.

$$Isp_{exp} = \frac{F_{T,exp}}{g_0 \dot{m}_{exp}} \tag{6.4}$$

$$C_{D,exp} = \frac{\dot{m}_{exp}}{\dot{m}_{ideal}} \tag{6.5}$$

$$\eta_{isp,exp} = \frac{Isp_{exp}}{Isp_{ideal}} \tag{6.6}$$

$$\eta_c = \frac{c*_{exp}}{c*_{ideal}} \tag{6.7}$$

$$\eta_n = \frac{CF_{exp}}{CF_{ideal}} \tag{6.8}$$

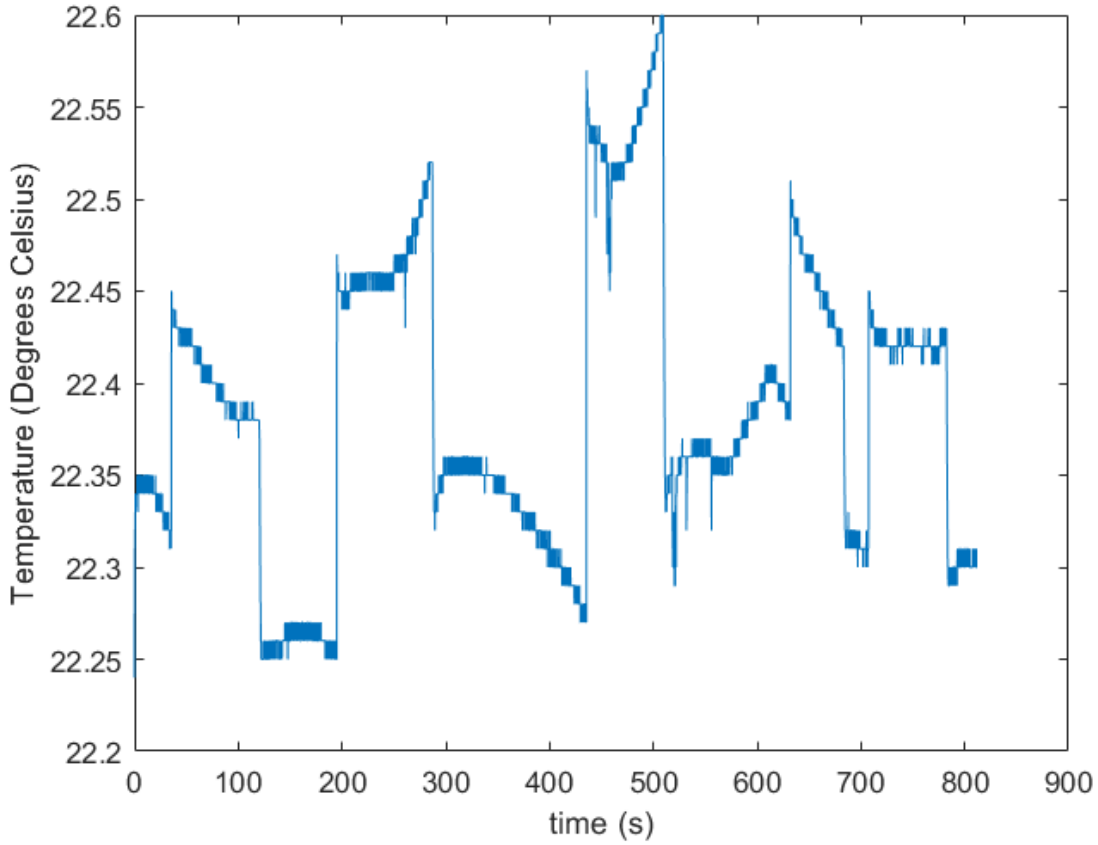

Figure 6.2: Measurement results for the chamber temperature for CT-R4C7-1

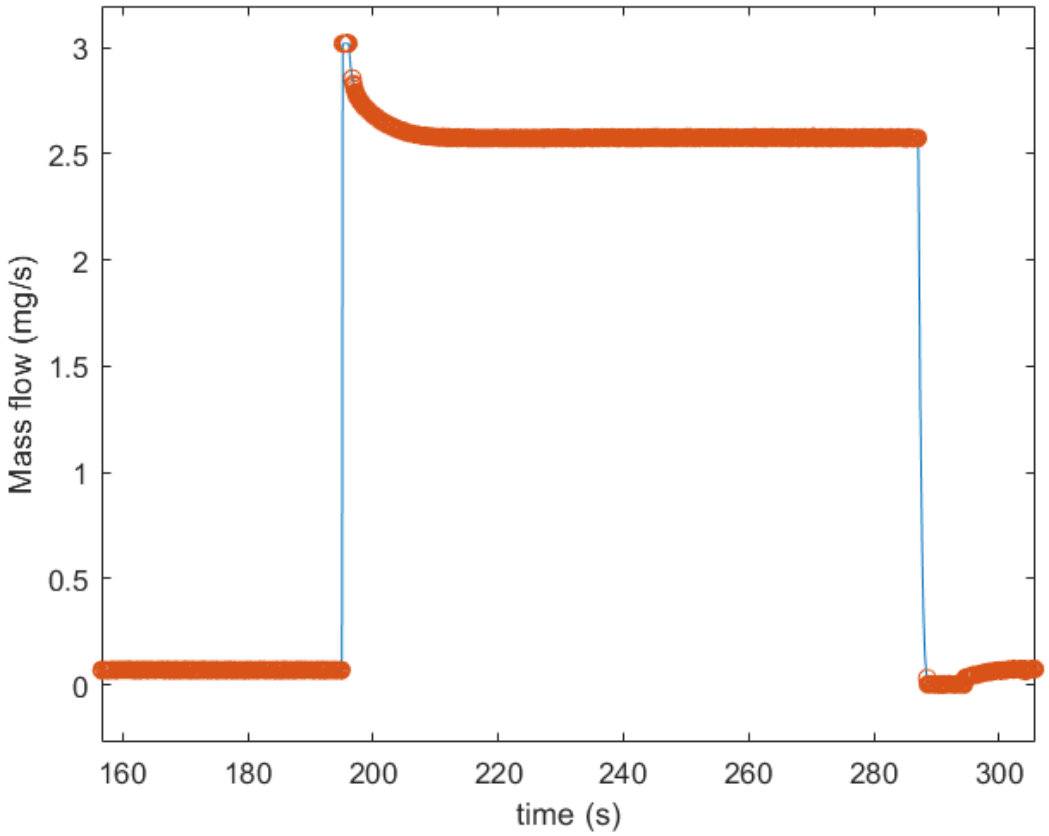

Figure 6.3: Measurement results for the mass flow for CT-R4C7-1

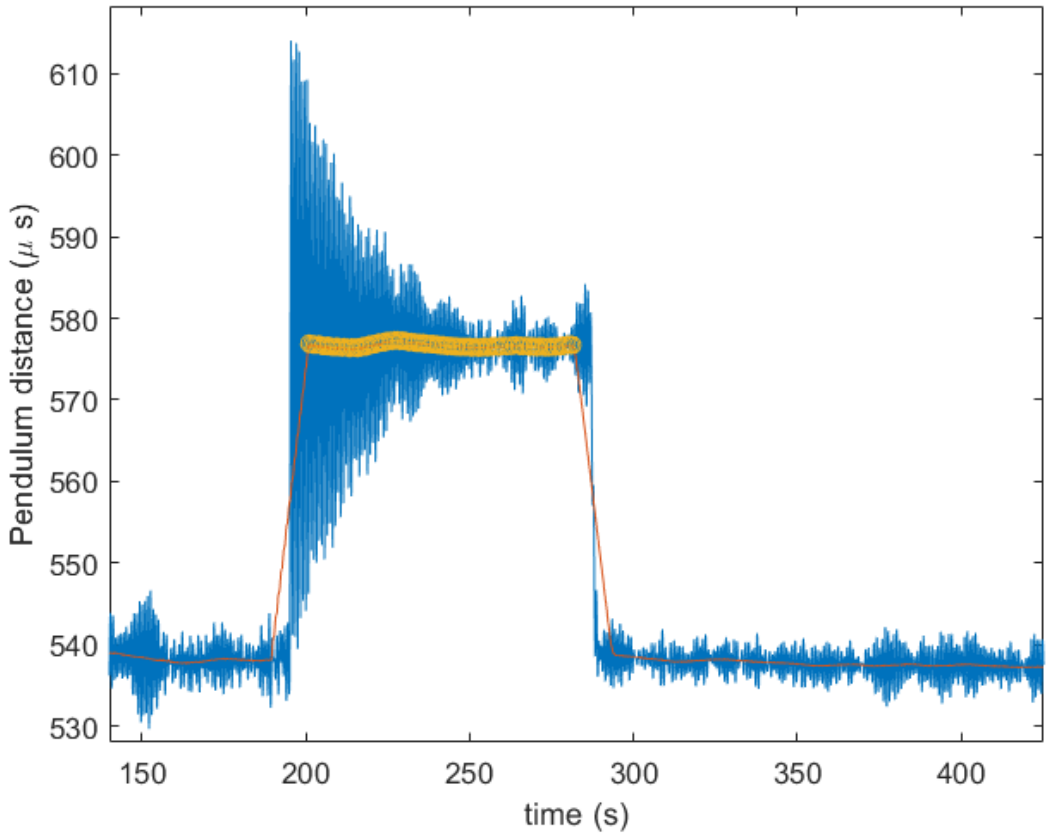

Figure 6.4: Measurement results for the pendulum displacement for CT-R4C7-1.

Table 6.2: Cold test experimental values and their uncertainties.

Test Name	P_c (Bar)	T_c (K)	P_a (Bar)	$\dot{m}$ (mg/s)	F_T (mN)	I_{sp} (s)
CT-R5C1-1.1	2.00±0.05	294.7±1.5	1.03±0.05	1.24±0.009	0.16	12.9
CT-R5C1-1.2	2.99±0.05	294.8±1.5	1.03±0.05	1.99±0.014	0.31	15.6
CT-R5C1-1.3	4.14±0.05	295.0±1.5	1.03±0.05	2.85±0.020	0.51	18.3
CT-R5C1-1.4	5.23±0.05	295.0±1.5	1.03±0.05	3.02±0.021	0.62	21.0
CT-R5C1-2.1	1.83±0.05	294.9±1.5	1.03±0.05	1.12±0.008	0.08	7.6
CT-R5C1-2.2	3.04±0.05	295.0±1.5	1.03±0.05	2.06±0.014	0.29	14.3
CT-R5C1-2.3	3.91±0.05	295.1±1.5	1.03±0.05	2.73±0.019	0.43	16.1
CT-R5C1-2.4	5.22±0.05	295.3±1.5	1.03±0.05	3.02±0.021	0.56	19.0
CT-R5C1-3.1	1.83±0.05	294.9±1.5	1.03±0.05	1.09±0.008	0.16	14.5
CT-R5C1-3.2	3.04±0.05	295.0±1.5	1.03±0.05	2.07±0.014	0.31	15.4
CT-R5C1-3.3	3.91±0.05	295.1±1.5	1.03±0.05	2.86±0.020	0.54	19.3
CT-R5C1-3.4	5.22±0.05	295.3±1.5	1.03±0.05	3.02±0.021	0.67	22.7
CT-R4C7-1.1	2.91±0.05	295.5±1.5	1.00±0.05	1.80±0.013	0.30±	17.2±
CT-R4C7-1.2	4.05±0.05	295.5±1.5	1.00±0.05	2.51±0.018	0.46±	18.7±
CT-R4C7-1.3	5.12±0.05	295.5±1.5	1.00±0.05	3.02±0.021	0.48	16.3
CT-R4C7-1.4	3.04±0.05	295.5±1.5	1.00±0.05	1.88±0.013	0.31	17.1
CT-R4C7-2.1	1.90±0.05	294.9±1.5	1.00±0.05	1.10±0.008	0.12	11.5
CT-R4C7-2.2	2.95±0.05	294.9±1.5	1.00±0.05	1.90±0.013	0.30	16.1
CT-R4C7-2.3	3.93±0.05	294.9±1.5	1.00±0.05	2.49±0.017	0.44	17.8
CT-R4C7-2.4	4.98±0.05	294.9±1.5	1.00±0.05	3.02±0.021	0.44	15.0
CT-R4C7-3.1	1.98±0.05	295±1.5	1.01±0.05	1.14±0.008	0.14	12.6
CT-R4C7-3.2	2.94±0.05	295±1.5	1.01±0.05	1.81±0.013	0.30	16.7
CT-R4C7-3.3	4.08±0.05	295±1.5	1.01±0.05	2.59±0.018	0.46	18.5
CT-R4C7-3.4	5.14±0.05	295±1.5	1.01±0.05	3.02±0.021	0.49	16.58
CT-R4C7-4.1	1.87±0.05	295.1±1.5	1.01±0.05	1.06±0.007	0.12±0.009	11.2±0.9
CT-R4C7-4.2	3.06±0.05	295.2±1.5	1.01±0.05	1.89±0.013	0.32±0.020	17.1±1.2
CT-R4C7-4.3	4.07±0.05	295.3±1.5	1.01±0.05	2.58±0.018	0.45±0.029	18.3±1.3
CT-R4C7-4.4	5.19±0.05	295.4±1.5	1.01±0.05	3.02±0.021	0.49±0.030	16.6±1.1
HT-R4C9-1.1	2.50±0.05	295±1.5	1.00±0.05	1.41±0.010	0.19±0.015	13.5±1.17
HT-R4C9-1.2	3.03±0.05	295±1.5	1.00±0.05	1.93±0.013	0.24±0.010	12.6±0.62
HT-R4C9-1.3	3.59±0.05	295±1.5	1.00±0.05	2.28±0.016	0.29±0.010	12.8±0.55
HT-R4C9-1.4	3.97±0.05	295±1.5	1.00±0.05	2.59±0.018	0.38±0.011	15.1±0.52
HT-R4C9-1.5	4.46±0.05	295±1.5	1.00±0.05	3.01±0.021	0.48±0.012	16.1±0.54
HT-R4C9-1.6	5.08±0.05	295±1.5	1.00±0.05	3.57±0.025	0.52±0.023	14.9±0.76

Table 6.3: Quality factors for the cold tests of R5C1, R4C7 and R4C9. The red color means the test failed due to mass flow capping.

Test Name	$Re_{t,exp}$	CD_{exp}	$\frac{Isp_{exp}}{Isp_{ideal,vacuum}}$
CT-R4C7-1.1	1743±106	0.95	0.23
CT-R4C7-1.2	2438±148	0.95	0.25
CT-R4C7-1.3	2935±178	0.91	0.22
CT-R4C7-1.4	1822±110	0.95	0.23
CT-R4C7-2.1	1067±138	0.89	0.16
CT-R4C7-2.2	1845±197	0.95	0.22
CT-R4C7-2.3	2417±252	0.95	0.24
CT-R4C7-2.4	2932±311	0.90	0.20
CT-R4C7-3.1	1111±143	0.89	0.17
CT-R4C7-3.2	1762±196	0.95	0.23
CT-R4C7-3.3	2450±260	0.95	0.25
CT-R4C7-3.4	2935±319	0.90	0.22
CT-R4C7-4.1	1031±138	0.87	0.15
CT-R4C7-4.2	1834±206	0.95	0.23
CT-R4C7-4.3	2459±263	0.96	0.25
CT-R4C7-4.4	2934±327	0.89	0.22
CT-R5C1-1.1	1186	0.90	0.17
CT-R5C1-1.2	1898	0.96	0.21
CT-R5C1-1.3	2712	0.99	0.25
CT-R5C1-1.4	2880	0.84	0.28
CT-R5C1-2.1	1067	0.89	0.10
CT-R5C1-2.2	1957	0.98	0.19
CT-R5C1-2.3	2601	1.01	0.22
CT-R5C1-2.4	2875	0.84	0.26
CT-R5C1-3.1	1042	0.87	0.20
CT-R5C1-3.2	1970	0.99	0.21
CT-R5C1-3.3	2719	1.06	0.26
CT-R5C1-3.4	2877	0.84	0.31
HT-R4C9-1.1	1306	0.81	0.18
HT-R4C9-1.2	1789	0.92	0.17
HT-R4C9-1.3	2116	0.92	0.17
HT-R4C9-1.4	2404	0.95	0.20
HT-R4C9-1.5	2792	0.98	0.22
HT-R4C9-1.6	3314	1.02	0.20

6.2.2. Uncertainty Analysis

Here, the uncertainties for all of the measured experimental values are determined. This will not include the uncertainties measured for nozzle dimensions and the force conversion relations, which were explained in chapter 2 and chapter 5. Additionally, the quantization error, for converting analogue data to digital, will be considered negligible, compared to the sensor uncertainties.

For measuring the chamber pressure and ambient pressure, the TE Connectivity MS5837 30BA pressure sensor is used. The sensor is located in a pressure sensor block, created by Melaika [20], and is placed upstream of the chamber. The pressure drop to the chamber will be considered negligible. According to the data sheet *TE Connectivity Sensor Solutions. MS5837-30BA Ultra Small Gel Filled Pressure Sensor. Tech. Data Sheet* [32], the maximum accuracy for the pressure range is ± 0.05 bars, in the specified range of 0-6 bars and in within a temperature range of -20 to 85^{o}C. The pressure and temperature sensors take samples at a frequency of 10Hz, as set by the Labview coding.

The same sensor is used for estimating the chamber temperature, for cold testing. According to the same data sheet *TE Connectivity Sensor Solutions. MS5837-30BA Ultra Small Gel Filled Pressure Sensor. Tech. Data Sheet* [32], the maximum accuracy is ± 1.5 K, within the specified range of 0-10 bars and roughly at room temperature, 25^{o}C.

The Brooks MS5850S 0-144 sccm mass flow sensor has an accuracy of 0.7%, assuming the MFC is given at least 45 minutes to warm up and has been recently calibrated, which is the case according to Ganani [9]. The uncertainty from reading out the mass flow from the analogue 0-5 V signal, is considered negligible compared to the sensor accuracy. Additionally, for situations when the mass flow does not return to zero, after closing the solenoid valve, that zero error is subtracted directly from the measured mass flow sensor. So the zero error is not included in the total measured mass flow uncertainty. The mass flow is measured at a sample rate of 100Hz.

When using the force compensation method, to determine the accuracy of ΔI, the error is equivalent to 3σ of the measured change in current. So the uncertainty is equivalent to the standard deviation of the peak current, multiplied by three. For the current troughs (current at zero mass flow), the mean value is taken of the troughs just before and after the current peak. Additionally, half the difference between the current troughs is added to the total error of the change in current, to take into account the zero error. The current is measured at a sample rate of 100Hz.

$$3\sigma_{\Delta I} = 3 * \sigma_{I,peak} + 0.5 \cdot (I_{trough,before} - I_{trough,after}) \tag{6.9}$$

6.3. Result Analysis

The results for the cold test using R4C7, R5C1 and R4C9 will now be presented and discussed.

6.3.1. Overview

Mass flow and Discharge coefficient

Looking at the mass flows of the cold thrust tests, they seem to fall in line with expectations, as seen in subsection 3.8.1. As the pressure increases,the mass flow increases as can be seen in Table 6.2. Additionally, all of the $C_{D,exp}$ values converge to 1 as the Reynolds number increases and are below 1, as can be seen from Table 6.3, except for HT-R4C9-1.6. This has to do with the fact that the HT-R4C9-1.1 to HT-R4C9-1.6 were measured using the 0-2000sccm mass flow sensor, which had to be corrected to give better values. More is explained in subsection 7.1.3. Furthermore, the mass flows and discharge coefficients of each thruster do overlap with each other, when taking into account their uncertainties. However, the discharge coefficient for HT-R4C9-1 seem to give much lower values compared to CT-R5C1 and CT-R4C7. Again this is most likely attributed to using the 0-2000sccm mass flow sensor with corrected values, since the 0-144sccm mass flow sensor broke after performing cold tests with R5c1 and R4C7.

Additionally, the calculated $C_{D,exp}$ at 5 bars for CT-R5C1 and CT-R4C7 shows a decreased value compared to their measurement of 4 bars. This shouldn't be possible since theory is clear that as the pressure increases the C_D should converge to one, not decrease. It was discovered that the reason for this is mass flow capping, where the actual mass flow at 5 bars could not be measured because the maximum measurable mass flow of the 0-144sccm had been reached. The tests that show this have been coloured red in Table 6.2. Therefore, the cold tests for R5C1 and R4C7 have partially failed since data could not be collected for the entire pressure range of 2-5 bars. However, mass flow data for 2-

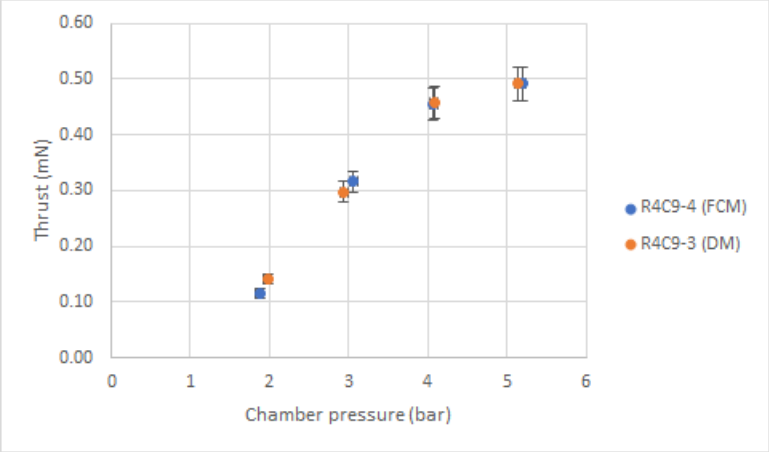

Figure 6.5: Thrust results comparing the force compensation method (CT-R4C7-4) and the displacement method (CT-R4C7-3).

4bars has been collected, which still provides good insights into the performance of the thrusters and can be used to check the validity of the performance model.

Also, the C_D for CT-R5C1-2.3 and CT-R5C1-3.3 are larger than 1, despite giving mass flows that are not limited by mass flow capping. The only reasonable explanation is that a leakage must have occurred at those points. Most likely from the use of the homemade feed tube adapter from Figure 4.5. After repeated testing and reusing, the high chamber pressure pushed out the glued in MINSTAC component from the adapter, causing a leakage.

The absolute errors for the $C_{D,exp}$ is quite large for each operating point. This is mainly due to the large uncertainty in A_t caused by the large uncertainty in w_t (see Table 2.2). The fact that C_D is highly dependent on m_{ideal}, which is in turn reliant on A_t, means that the uncertainty in $C_{D,exp}$ will be large as well.

Thrust and Isp efficiency

Initially, the results of the cold tests seem to fall in line with expectations, as seen in subsection 3.8.1. The force measurements all increase as the chamber pressure rises, as expected. Additionally, all the efficiencies lie below 1. Performance results at each operating point have near identical results, which in turn verifies its repeatability.

It is important to note that due to the fact that the tests were carried out in ambient conditions, the flow did not remain completely supersonic in the nozzle. This can be seen when looking at the low Isp values for all the cold tests in Table 6.2. The range of Isp for the tests was 7.6-18.5s which results in exit velocities between 75-183m/s. These exit velocities are much lower than the speed of sound, 343m/s, therefore it can be concluded that there is subsonic flow in parts of the nozzle. This is undesirable, as subsonic flow and shocks reduces the performance of the thruster. Therefore, the thrusters used are not designed for use in ambient conditions and should be tested in a vacuum.

Lastly, the difference between using the displacement method and force compensation method proved to be minimal. Looking at the force measurements in Table 6.2 and Figure 6.5, they seem to be mostly in line with each other. The largest thrust difference between the calculated values was about 0.02mN when looking at the thrust at each operating pressure. This confirms that the force compensation method can be used as a suitable thrust measurement method. For future work, it is recommended that future students use this method, considering that it is a simpler and more accurate method.

6.3.2. Comparison between model and experiments

Discharge Coefficient

With the measured and calculated cold gas results, the performances between the experiments and model predictions can be compared. Figure 6.6 shows the discharge coefficients for the experiments and models versus the throat Reynolds number, using the hydraulic diameter as the characteristic length. It can be seen that the model of Tang and Fenn [31] overestimates the values of the cold tests, for the throat Reynolds number range of 1000-2750. When compared to CT-R4C7, this overestimation is about

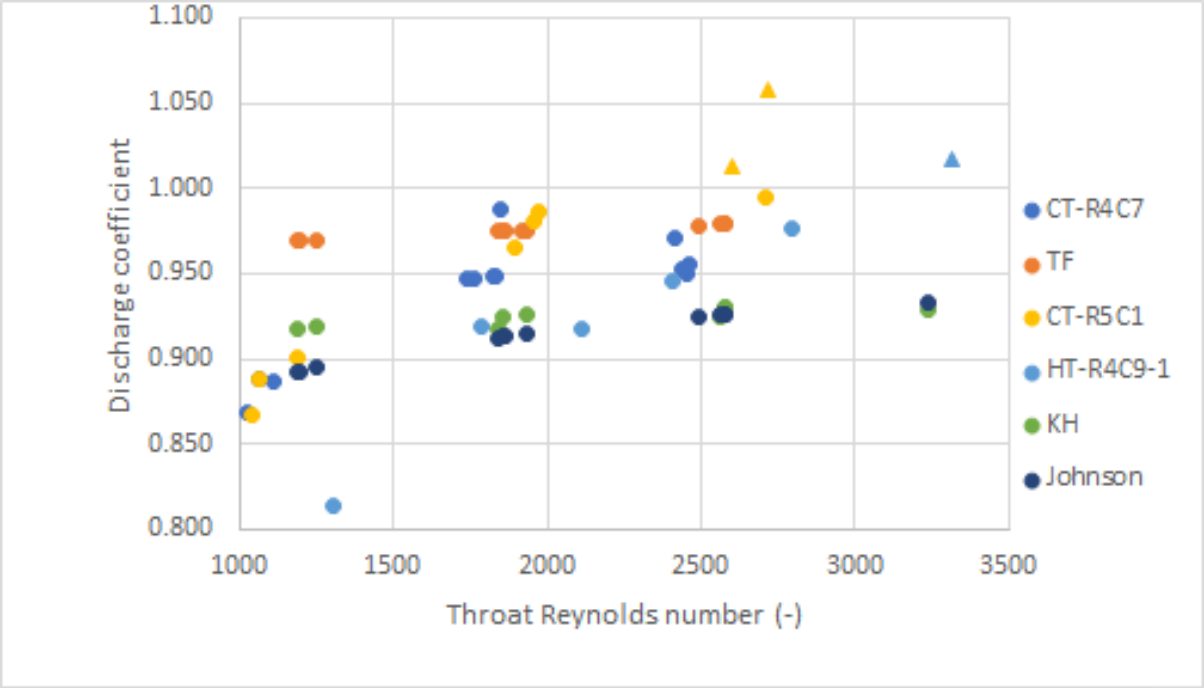

Figure 6.6: Discharge coefficient of CT-R5C1, CT-R4C7 and HT-R4C7-1 versus the throat Reynolds number, for $d = D_{H,t}$. The triangle markers are not to be trusted, since the discharge coefficient is greater than 1.

2-11%, which is just outside of the accuracy needed for validity, However the uncertainty certainly causes some ambiguity on how accurate the results really are.

When using $D_{H,t}$ for the characteristic length, the model of KH ($d = D_{H,t}$) model and J ($d = D_{H,t}$) models predicted the $C_{D,exp}$ of CT-R4C7 with at most 6.6% and 7.9% inaccuracy, respectively. It can therefore be concluded that both of these models are valid and satisfy the 10% inaccuracy requirement. Also, that Kuluva and Hosack [14] provides the most accurate results for the case of these thrusters.

Figure 6.7 shows the effect of using w_t instead of using $D_{H,t}$ for the characteristic length. When using w_t for the characteristic length instead, the TF ($d = w_t$) model is able to predict the experimental discharge coefficients at higher Reynolds numbers more accurately. However, at lower Reynolds numbers the model overestimates the experimental data of CT-R4C7 by 10.3%. The KH ($d = w_t$) ad J ($d = w_t$) models have better accuracies at lower Reynolds numbers and remain within 10% of the experimental data.

Isp Efficiency

Unfortunately, the model is unable to predict the η_{isp} for the thrusters. This is due to incomplete expansion in the nozzle where there is no complete supersonic flow. This made it difficult to predict the C_f, as the model provided by Spisz, Brinich, and Jack [29] assumes complete flow expansion. As a result, tests need to be performed in a vacuum to be able to compare the model to experimental results. Despite this setback, the experimental values from Makhan [18] can be used to validate the model prediction on Isp efficiency. This was done in section 3.7, where it was shown the predicted Isp efficiency was not within 10% of the experimental vales of Makhan [18], unless the fitting constant was altered from 17.6 to 22.75.

6.3.3. Comparison with literature

In this section, the results obtained will be compared to the cold test result of Makhan [18] TT-04 and the cold tests of Versteeg [36].

The $C_{D,exp}$ from Makhan [18] and the experiments are within acceptable ranges, for both $D_{H,t}$ and the h_t models. It can be seen in Figure 6.8, the discharge coefficients between Makhan [18] and the CT-R5C1 and CT-R4C7, show a similar trend. They are both within reasonable agreement with each other, as there is 3-9% difference between them. This difference may be a result of measurement uncertainties,

Table 6.4: Ideal values for the thrusters R5C1, R4C7 and R4C9.

Thruster Test	$\dot{m}_{ideal}$ (mg/s)	$F_{T,ideal,vacuum}$ (mN)	$Isp_{ideal,vacuum}$ (s)
CT-R4C7-1.1	1.89	1.38	74.2
CT-R4C7-1.2	2.64	1.92	74.1
CT-R4C7-1.3	3.33	2.42	74.0
CT-R4C7-1.4	1.98	1.44	74.2
CT-R4C7-2.1	1.24	0.90	74.2
CT-R4C7-2.2	1.92	1.40	74.1
CT-R4C7-2.3	2.56	1.86	74.0
CT-R4C7-2.4	3.24	2.35	74.0
CT-R4C7-3.1	1.29	0.94	74.2
CT-R4C7-3.2	1.91	1.39	74.1
CT-R4C7-3.3	2.65	1.93	74.1
CT-R4C7-3.4	3.35	2.43	74.0
CT-R4C7-4.1	1.22	0.89	74.2
CT-R4C7-4.2	1.99	1.45	74.1
CT-R4C7-4.3	2.65	1.92	74.1
CT-R4C7-4.4	3.38	2.45	74.0
CT-R5C1-1.1	1.38	1.00	74.1
CT-R5C1-1.2	2.06	1.50	74.0
CT-R5C1-1.3	2.86	2.08	73.9
CT-R5C1-1.4	3.62	2.62	73.9
CT-R5C1-2.1	1.26	0.92	74.1
CT-R5C1-2.2	2.10	1.52	74.0
CT-R5C1-2.3	2.70	1.96	74.0
CT-R5C1-2.4	3.60	2.61	73.9
CT-R5C1-3.1	1.26	0.92	74.1
CT-R5C1-3.2	2.10	1.52	74.0
CT-R5C1-3.3	2.70	1.96	74.0
CT-R5C1-3.4	3.60	2.61	73.9
HT-R4C9-1.1	1.73	1.26	74.2
HT-R4C9-1.2	2.09	1.52	74.1
HT-R4C9-1.3	2.48	1.80	74.1
HT-R4C9-1.4	2.74	1.99	74.1
HT-R4C9-1.5	3.08	2.24	74.1
HT-R4C9-1.6	3.51	2.55	74.0

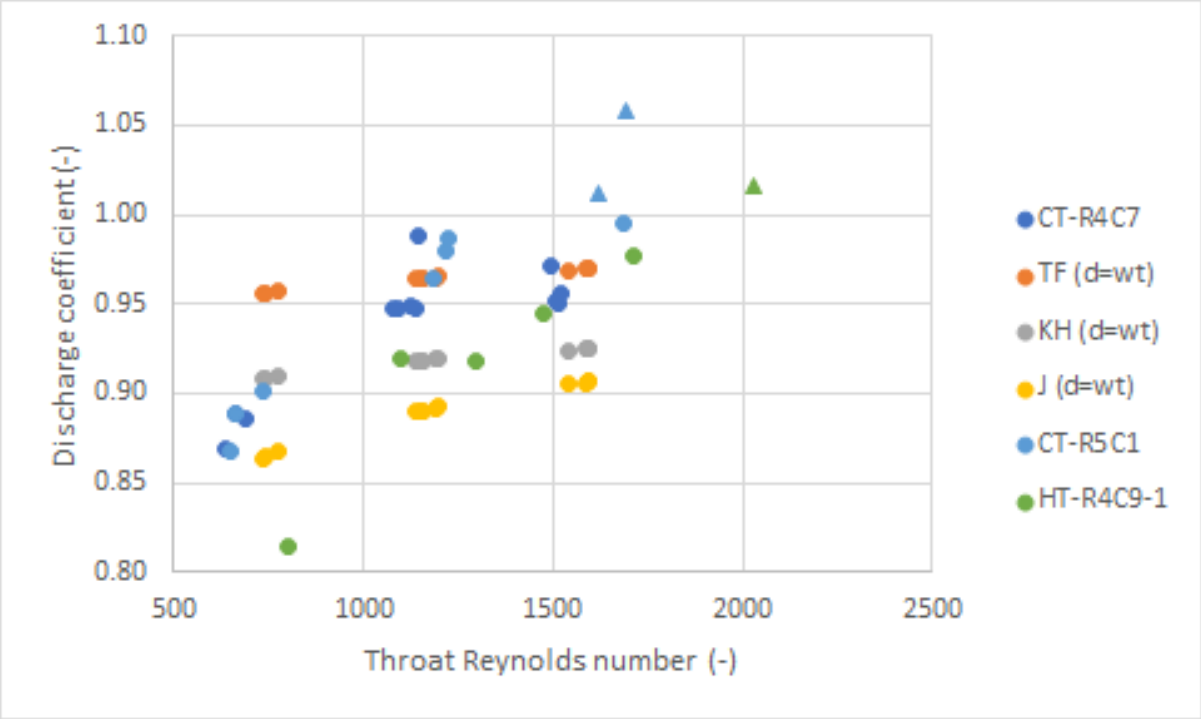

Figure 6.7: Discharge coefficient of CT-R5C1, CT-R4C7 and HT-R4C7-1 versus the throat Reynolds number, for $d = w_t$.

which if added to the graph, show they overlap.

The tests of CT-R5C1, CT-R4C7 and HT-R4C9-1 are all greater than the measured C_D of Versteeg [36], by between 6-15%. This means that the C_D from the tests is much more improved compared to the thruster of Versteeg [36]. The reasoning for this difference is most likely due to the larger throat longitudinal radius of the thruster by Versteeg [36] and the different aspect ratios of the thrusters used in this thesis, compared to Versteeg [36].

It is important to note that the Isp efficiency of the thrust tests is determined by comparing the Isp measured in ambient conditions, to the ideal, vacuum Isp of the same thruster in similar pressure and temperature conditions. When looking at the Isp efficiencies of CT-R5C1, CT-R4C7 and HT-R4C9-1, they are much worse compared to Makhan [18] and Versteeg [36]. The main reason for this is the fact that the thrust tests performed in this thesis, were not done in a vacuum, like the thrust tests done by Makhan [18] and Versteeg [36]. Therefore, the Isp efficiency for the thrust test are around 50% lower compared to Makhan [18]. Until the thrusters are tested in vacuum conditions, it can not really be determined if the thrusters have improved Isp efficiencies compared to the previous thruster of Makhan [18].

Also, looking at Figure 6.9 shows that Versteeg [36] has the best Isp efficiencies near 90%, which is much higher than the smaller thruster of Makhan [18] and the thrusters tested in this thesis. Therefore, currently at the faculty, the thruster of Versteeg [36] is the best performing thruster.

6.4. Conclusions

In conclusion, the cold thrust testing, based on the research goals in chapter 1, was only partially successful. The reason is that mass flow data could not be performed through the complete operating pressure range (2-5bars), because mass flow capping occurred at 5 bars, with the exception of HT-R4C9-1. The selected mass flow sensor could not measure mass flows at 5 bars pressure for thruster R5C1 and R4C7, as this was noticed when looking at how the C_D started decreasing when going from 4 to 5 bars. Literature is clear that C_D converges to 1 when chamber pressure increases. Therefore, the larger mass flow sensor will be used for hot testing. This also means that Isp data can not be determined at 5 bars for R4C7 and R5C1. Despite this, useful data could still be collected for the performances of each of the thrusters.

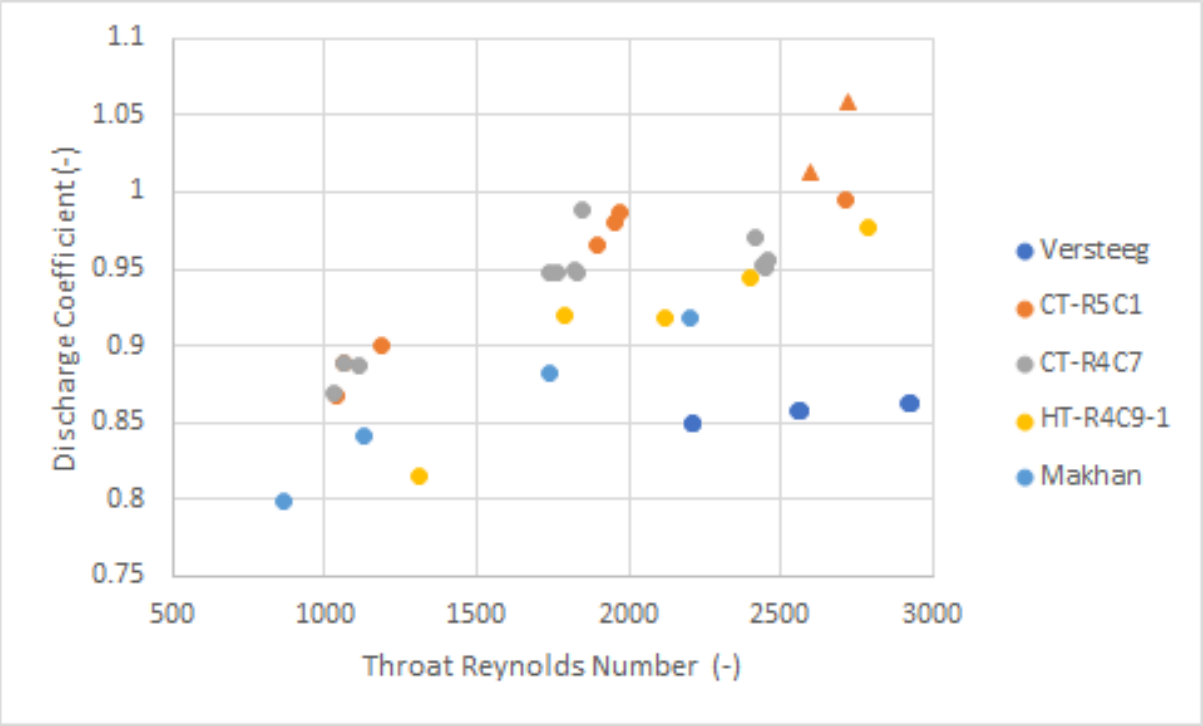

Figure 6.8: Discharge coefficient of thruster CT-R5C1, CT-R4C7 and HT-R4C9-1 versus the experimental data of Makhan [18] and Versteeg [36]. The triangle markers are not to be trusted, since the discharge coefficient is greater than 1.

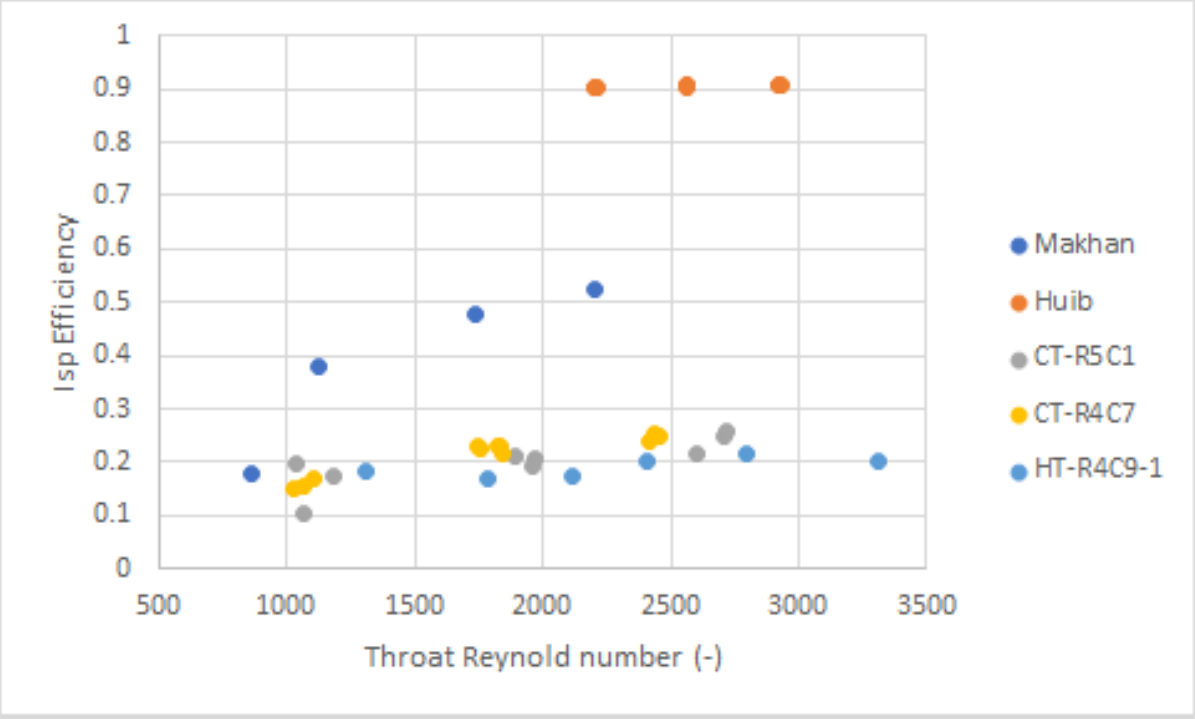

Figure 6.9: Isp efficiencies of CT-R5C1, CT-R4C7 and HT-R4C9-1 versus the experimental data of Makhan [18] and Versteeg [36].

Overall, the $C_{D,exp}$ for each thruster followed expected trends, where as the Reynolds number increased from around 1000 to 3300, the $C_{D,exp}$ converged to 1. Comparisons to the models of Tang and Fenn [31] showed an overestimation of 2-11%. The model of Kuluva and Hosack [14] actually showed a better prediction of CT-R4C7 and CT-R5C1 with an maximum value deviation of 6.6% and 7.9%. The cold test HT-R4C9-1, could not be estimated with a 10% inaccuracy using any of the models. This is due to the use of a different mass flow sensor described in subsection 7.1.3. Overall, it is concluded that the model KH model, from Kuluva and Hosack [14], provided the best prediction for the given Reynolds number range.

When comparing the cold tests performed in this thesis, to the tests done by Makhan [18], the measured values overlap with a 3-9% difference in values. The C_D values of Versteeg [36] were much lower compared to the thrusters tested, by 6-15%. This is most likely due to the difference in design, as the thruster of Versteeg [36] has a larger throat longitudinal radius and lower aspect ratio.

It was clear, looking at the low measured Isp values of 7.6-18.7s, that the thrusters are not designed to be tested in ambient conditions. These low Isp values show very low exit velocities, meaning that the flow is subsonic at the nozzle exit and that shocks may be present. For this reason, the Isp efficiencies for these thrusters are low compared literature. For future work, it is recommended that these thrusters are retested with vacuum conditions. This way the thruster can be compared to previous designs and to see if improvements to performance can be noticed.

From the cold tests, it can be concluded that the force compensation method provides the same thrust values compared to the displacement method, as expected. This method should be used from now on, as it reduces the effects cables and propellant tubes have on the measured thrust and it eliminates the requirement to perform a thrust stand calibration, saving time.

From these cold tests, some guidelines will be presented, considering that only some of the goals of this chapter could be achieved. These guidelines can also be considered as recommendations for future students to learn from and conduct their experimental thesis' more thoroughly.

- Before doing any complete thrust test, perform a single exploratory test using nitrogen and fully evaluate the results of that test. This allows the user to spot any errors and possible improvements before carrying out a more complete test. If this was done first, the issue with ambient pressure would have been discovered and a quick vacuum test could have been performed.

- The calibration of mass flow sensors, at least once a year, should be considered. Makhan [18] and Ganani [9] have shown that over time the mass flow sensors tend to deviate from their true measurement values. Additionally, calibration records should be kept in the cleanroom, for the mass flow sensors.

- Alter the pressure range from 2-5bars to 2.5-4.5 bars. It was already determined that mass flow capping occurred at 5 bars of pressure, when using the smaller mass flow sensor.

- Try to limit the number of tests performed to a single thruster, to three tests maximum. For cold testing, a total of 8 cold tests were done for three different thrusters. This produced far too much data for each operating that can be difficult to handle and compare to the performance model. This extended the time needed to evaluate the data and the performance model, which meant less time could be spent on performing hot tests and vaporized water tests. Future students may also benefit from performing the cold test with the heating cables installed and going straight into hot testing directly after the cold test has been done.

7

Hot testing

This chapter will discuss the hot thrust tests performed for thruster R4C7 ad R4C9. The test matrix from Table 6.1 can be used to understand at which pressure and temperature data was recorded for each hot test. The purpose of this chapter is to:

- Present and discuss the raw data obtained for the hot tests of each thruster.
- Determine and analyze the resulting mass flow, thrust and quality factors for each of these thrusters, versus their throat Reynolds number.
- Determine up to what temperature the design holds up and where any failures occur.
- Compare the data of these thrusters to the tests from Versteeg [36] and Makhan [18].
- Compare the performance model to the measured thrust data and conclude whether the model is valid.

To begin with, an exploratory test was done with thruster R4C7 in section 7.1. From the exploratory test, conclusions could be drawn on the thermal design of the interface and any serious issues could be resolved before proceeding to the real testing. section 7.2 then discusses and analyzes the experimental data from HT-R4C7 and HT-R4C9. That data is also compared to both literature and the predictive to validate the experimental results and the model. section 7.3 then summarizes the main findings of the heated thruster testing and provides recommendations for improvements.

7.1. Exploratory testing

Before a complete hot test was done, an exploratory test was performed first to see how well the interface handled the heat, get a rough idea on any issues that may occur and see how well the VLM design handles the heating. This section describes and provides plausible explanations to the issues and observations found during this test. This test was done using the thruster R4C7, for which cold tests were done for (see chapter 6). It was decided to do this test at one pressure point, 2 bars, because the main focus was to observe the set-up when being heated to high temperatures. The issues and observations encountered can be separated into two categories: issues caused by heating and issues caused by test set up. The test results for the exploratory test will be discussed in section 7.2, along with the real hot test using R4C9.

7.1.1. Drift and inconsistent displacements

During the first hot test, it could be seen that the coil current suffered from a lot of drift. Figure 7.2 illustrates how the coil current continuously decreased over time. A clear drift in the coil can be seen that is slowly decreasing the zero flow set coil current. Additionally, there were points throughout the measurements where small and big jumps in the coil current could be noticed. These current jumps only seemed to happen when the valve was closed. The gradient of this drift was estimated to be around -0.0015 A/s by using the current points just before the valve was opened, but this drift only applies to

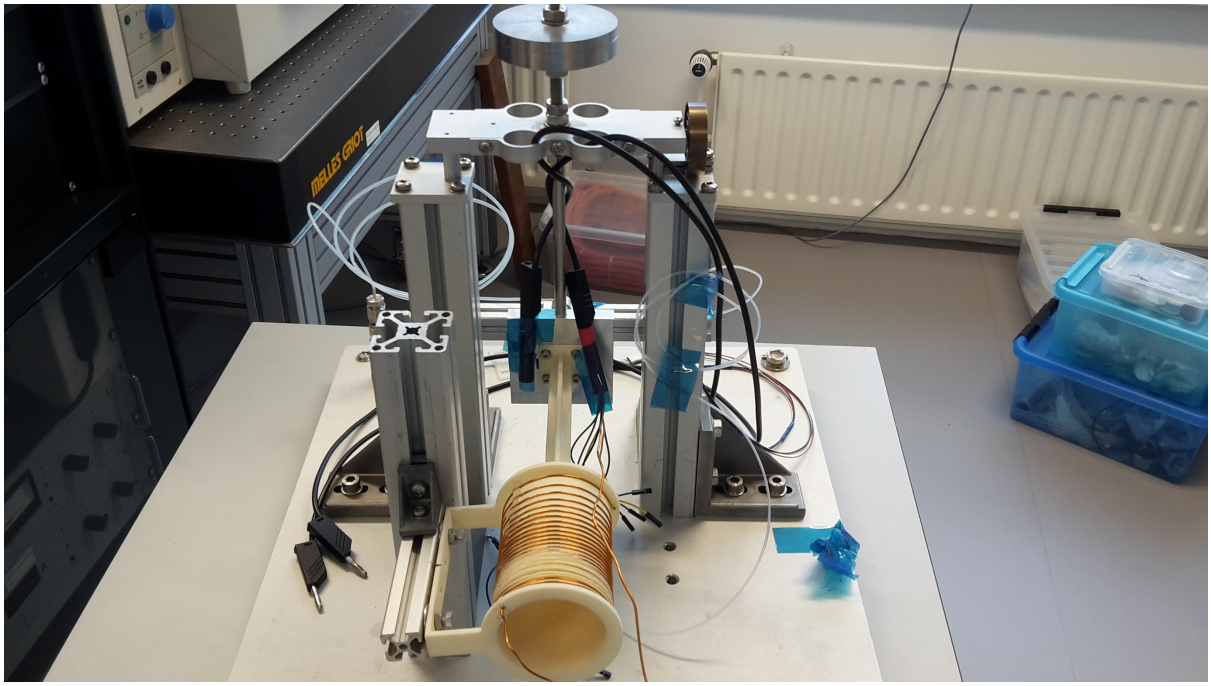

Figure 7.1: Positioning of the heater wires and the propellant feed tubes.

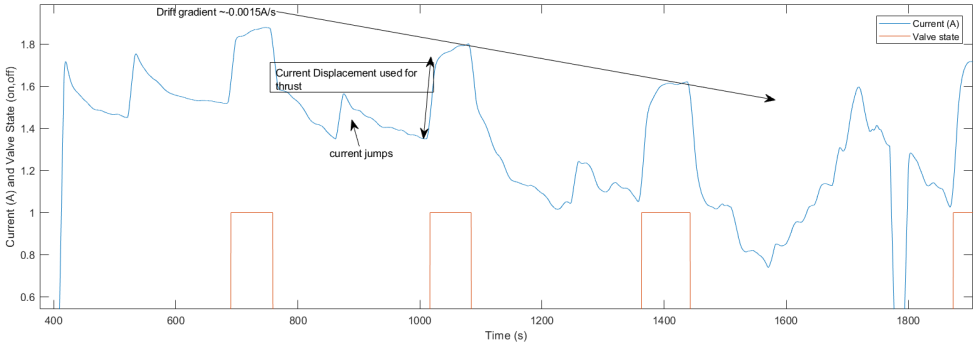

Figure 7.2: Coil current measured and valve state versus time.

these 3 data points of HT-R4C7. It could not be discerned if the other data points for R4C7 had drift. It was suspected, before doing the real hot test with R4C9, that the wire and feed tube positions on the test stand were the cause of this. Initially, the electrical wires were fed through the top of the pendulum and wrapped around the pendulum arm, as can be seen in Figure 7.1. These cables were then connected to the heater wires, which were taped to the sides of the steel cube where the coil is screwed on. So for future hot tests, the position of the heater wires, cables and feed tubes were moved to be as close to the rotational axis of the pendulum as possible. So these wiring and tubes were placed on the top of the pendulum and taped there. According to Salit and Turk [26], the quickest way to avoid the effects of drift is to reduce the time for each sample, so the effects of drift are minimized. For that reason, the sample times for the real hot test with R4C9 will be kept small (around 15-20 seconds).

7.1.2. Heating and thermal discussion

The issues encountered due to heating are described and explained in the following points. Additionally, solutions for these problems are provided as well.

- As can be seen in Figure 7.3, the 3D printed PCB platform melted near the exit of the thruster and directly beneath the thruster chip. The melting point for the material used for 3D printing is at most 180^{o}C, since this is the temperature of the printer extruder during 3D printing. For this reason, the

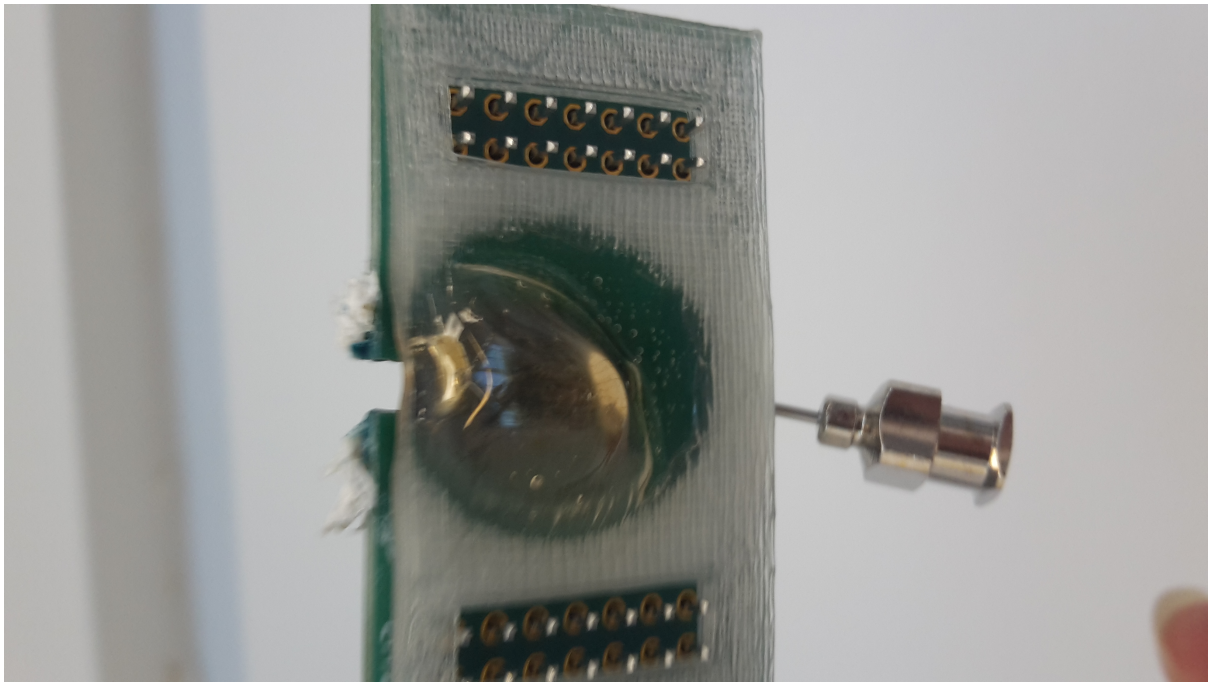

Figure 7.3: PCB platform which melted near the thruster outlet.

platform was discarded for future heat tests. Its only purpose was to act as platform to hold the PCB to the interface, however the interface was able to hold the PCB fine without it.

- Additionally, the 3D printed PCB to pendulum interface showed signs of warping near the screw, as can be seen in Figure 7.4. Most likely the screw absorbed enough heat to cause the interface to warp around the screw. The warping caused the entire interface to misalign and tilt upwards. This warping issue did not occur at temperatures below 150^{o}C, so the thrust values from room temperature up to 125^{o}C should not be affected, including the hot test with R4C9. For future work, it is recommended to replace the interface with a material that has a higher melting point, such as copper or stainless steel.

- The glue used to hold the metallic needle to the thruster inlet melted and separated completely at around 150^{o}C. This can be seen in Figure 7.5. So the current design has a maximum operating temperature of 150^{o}C. The next iteration of the design has to address this issue, to reach higher temperatures.

From these observations, it was clear that the temperature goal from the thesis objectives could not be reached within the time-frame of this thesis. The issues with the 3D printed interface parts can be solved by using a different material such as aluminum or steel. However, the crux of the design is glue used for the inlet, which needs to be replaced with a more adhesive glue, that can still handle the high temperature. Otherwise, a study may have to be done to find a suitable method to redesign the thruster chip or isolate the inlet from the heaters.

7.1.3. Correction for using the 0-2000sccm mass flow controller

It was intended to use the 0-144 MFC for hot thrust testing, however just before the first hot test with R4C7, the MFC failed. Due to time constraints, it was decided to continue the hot testing using the 0-2000 sccm MFC. The defective 0-144 sccm MFC was sent to Brooks for repairs and they determined that the PCB failed and had to be replaced and recalibrated, costing 765 euros to fix. It was not fixed in time to use for the hot testing, unfortunately.

Additionally, when performing the hot tests, several corrections had to be made to the measured mass flow values. After the first hot test with thruster R4C7, it was discovered that all the experimental values gave discharge coefficients greater than 1, which is not possible. The nozzle dimensions

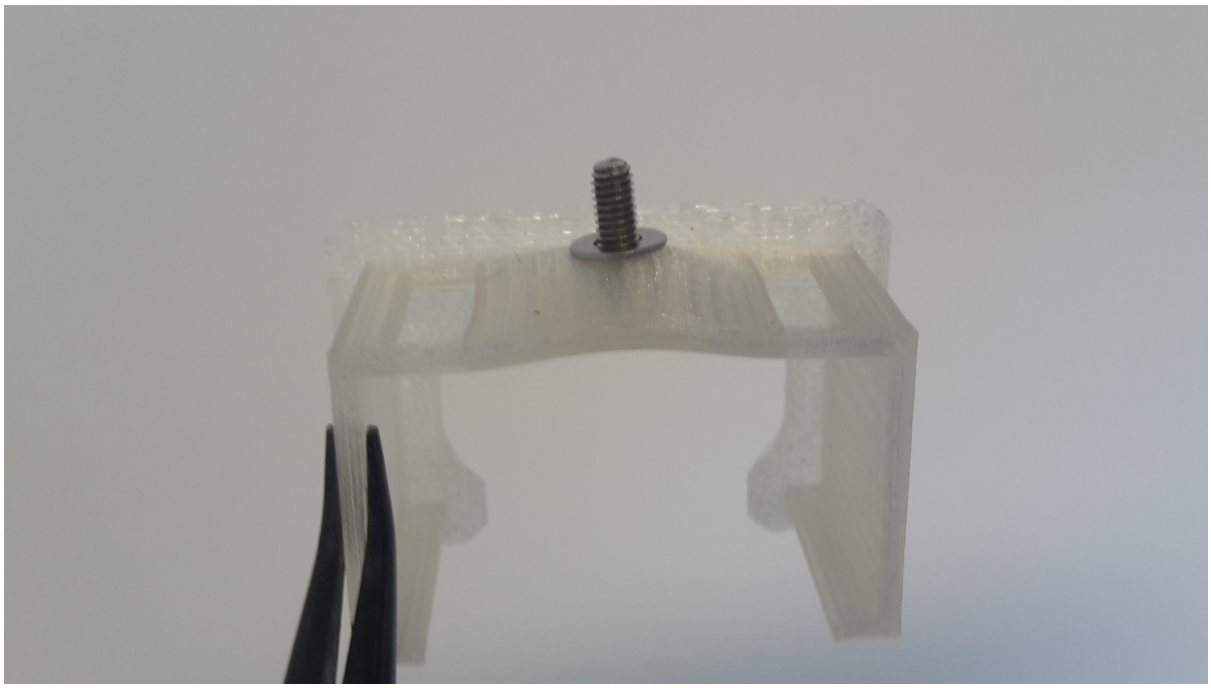

Figure 7.4: Aftermath of the 3D printed interface, during HT-R4C7, where clear warping can be seen near the M4 screw.

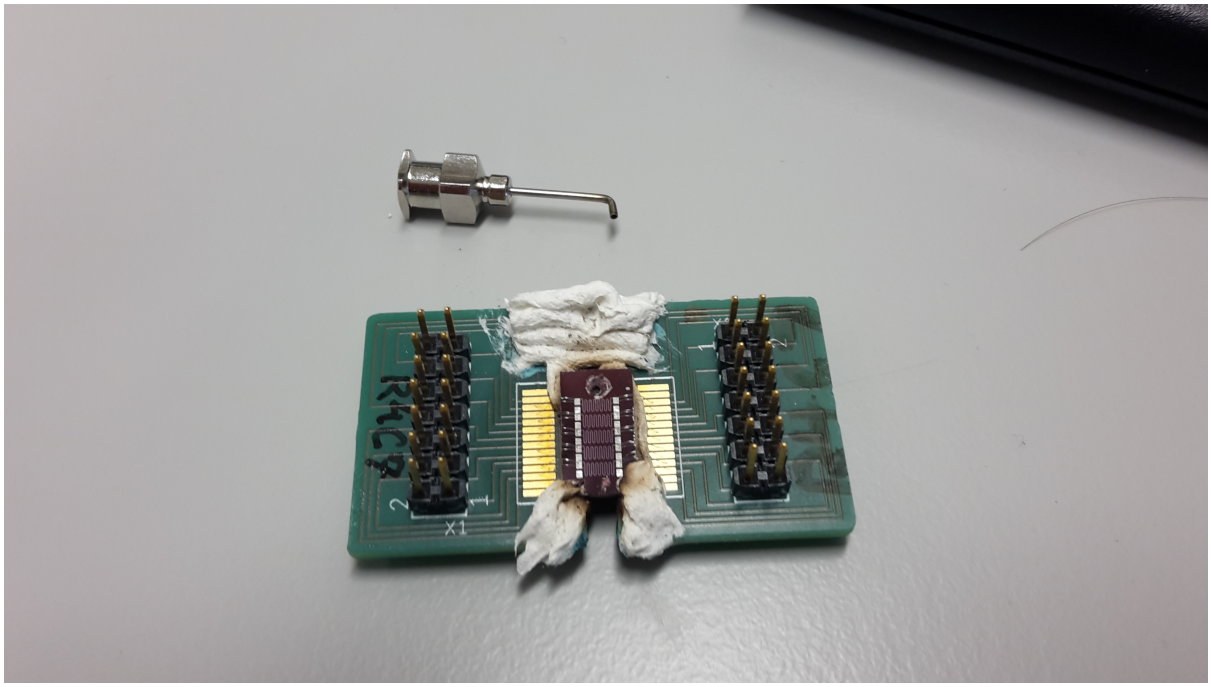

Figure 7.5: Failure of the thruster inlet after HT-R4C7.

were remeasured to see if that would make a difference, but it was determined that incorrect nozzle dimensions were not the cause. A leak test was also performed, but no leakage was found. Later, it was discovered, in the reports of Makhan [18] and Ganani [9], that there was a misalignment difference between the reported mass flows of both the 0-144 sccm MFC and 0-2000 MFC, when operating at the same pressure.

Ganani [9] reported two different misalignment errors of 0.15 mg/s and 0.2419 mg/s, respectively. Figure 7.6 shows the figure from which the value of 0.2419 mg/s was estimated from. These two values conflicted each other, so after contacting Chaggai Ganani it was found before calibrating both mass flow sensors, a difference of 0.15mg/s was found by both Makhan [18] and Ganani [9]. Makhan [18] made the recommendation of recalibrating both mass flow sensors, which Ganani [9] did, but did not have time to redo his experiments with the recalibrated sensors. After calibrating both mass flow sensors, Ganani [9] still determined a difference of 0.2419mg/s, therefore his value is the most recent and will be used.

Additionally, a voltage calibration correction will be added to these values. The mass flow sensor LabView code used a voltage range of 0-5 Volts for the mass flow range. However, after checking this with a multimeter, it was found that the maximum voltage was 5.224 V. This small change would not really affect larger thrusters, but considering the lower mass flow ranges of the thrusters used in this thesis,it is expected to make a noticeable difference. So the real mass flow is determined by Equation 7.1.

$$\dot{m}_{exp,corrected} = \frac{5}{5.244} * (\dot{m}_{exp} - 0.2419) \tag{7.1}$$

Ganani [9] is a best guess and the actual mass flow might be different, considering that his value is from 2 years ago. The misalignment between the MFC's was also checked up to chamber pressure of 2 bars, instead of the intended maximum operating pressure of 5 bars. Therefore, the experimental mass flow and Isp may not be reliable for higher pressures. Despite this, it was decided to continue with the experiment instead of waiting to repair the broken 0-144sccm mass flow sensor, which is now fixed and available for use.

Considering the accuracy of the calibration, it would recommended for future researchers to consider performing in-house calibration. According to the manual for the Mass flow sensors Brooks [5], Brooks recommends having the mass flow sensors calibrated at one of their locations, since calibration requires traceable and accurate calibration equipment. However, if we have this equipment, it would be possible to purchase the Brooks service Suite Calibration software, along with training. An email should be sent to inquire about the cost and equipment needed with their contact centre (`BrooksEU@brooksinstrument.com`). This way time and cost can be saved, in the long term, by avoiding shipping the sensors to the service centres every few years fo recalibration.

7.2. Hot Test Results

After the changes of the exploratory test were incorporated, a complete hot test was done with thruster R4C9. This section will present the results of the hot tests. The thruster tests are labelled as for example HT-R4C9-1.1 where HT means Hot Test, R4C9 is the thruster name and 1.1 represents the first temperature and first pressure point.

7.2.1. New uncertainty analysis

All the uncertainty analysis used for hot testing are similar to the cold tests in subsection 6.2.2, unless stated otherwise in this subsection.

For the temperature values, the temperatures were determined using the A35sc thermal camera, which has an absolute error of 5K. The room temperature value was determined using the pressure/temperature sensor interface, so the absolute error of 1.5K is used for cold measurements. Any errors due to the conversion of analogue to digital data was ignored. The temperatures for HT-R4C9-1.1 to HT-R4C9-R4C9-1.6 were measured using the same pressure/temperature sensor from the cold tests.

7.2.2. Experimental Output and initial analysis

This section will discuss and present the results of the hot testing done for the thesis. Hot testing was only done for the R4C7 and R4C9 thrusters. Initially, a more exploratory type of hot test was planned using the R5C1 thruster, however, the chip was accidentally knocked off the PCB when the heater wires were attached. Due to a lack of time and restrictions on lab accessibility during the COVID pandemic,

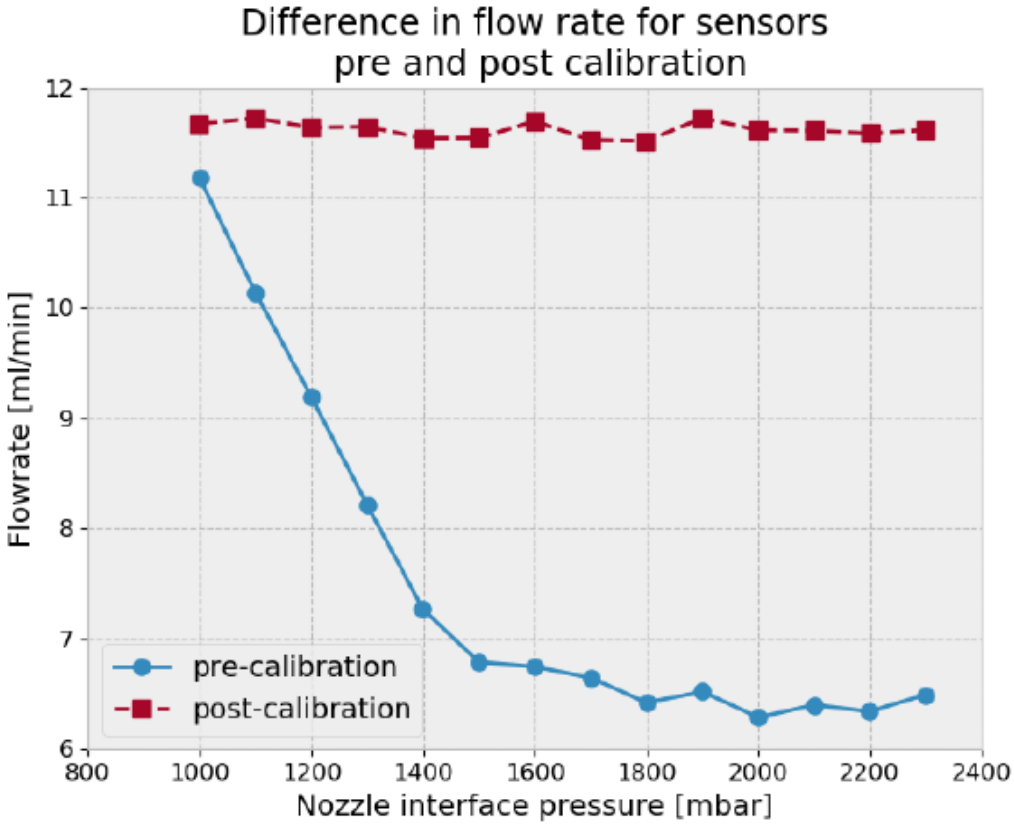

Figure 7.6: The difference in measured mass flows between both mass flow sensors, measured by Ganani [9]. Figure courtesy of Ganani [9].

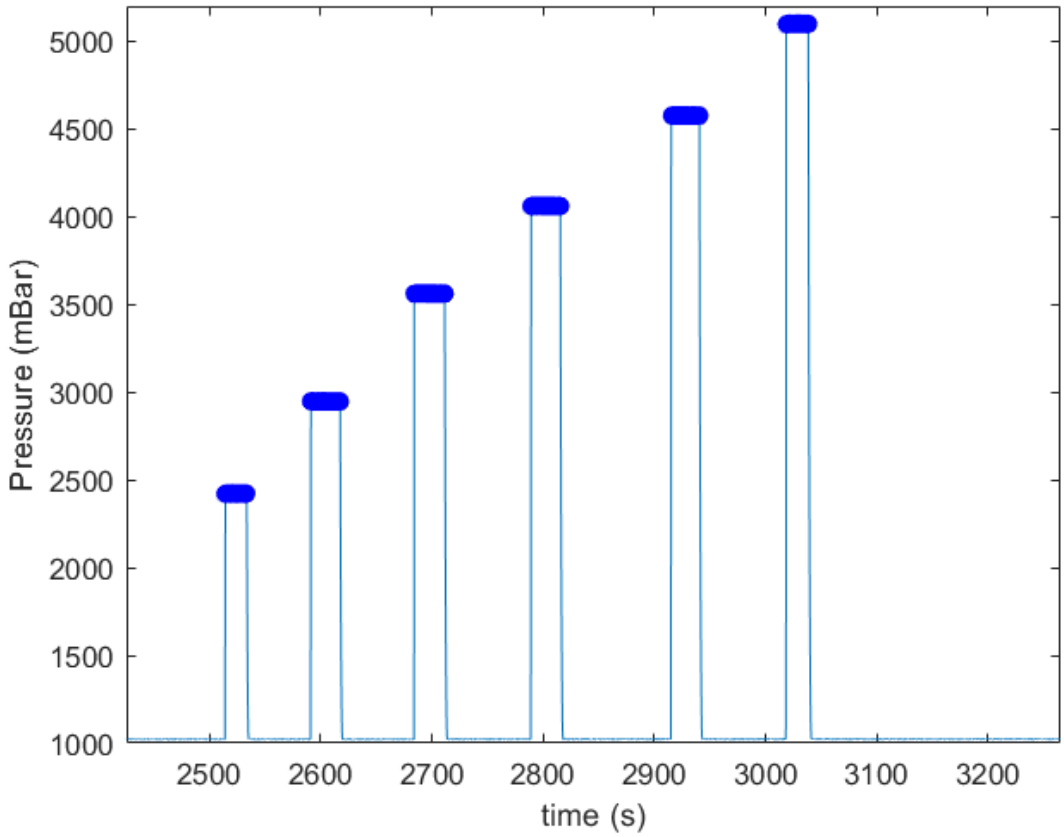

Figure 7.7: Pressure versus time for HT-R4C9-2.

it was decided to perform the exploratory test with the R4C7 thruster instead of requesting the broken thruster to be reattached. The results for this test can be found in Table 7.1. Afterwards, the real hot test was done using R4C9 thruster, where the results can be seen in Table 7.2. The real hot test still suffered from jagged current jumps and a small amount drift which is noticeable when looking at the entire current graph, but to a smaller extent compared to HT-R4C7.

The raw data is located in the thesis folder of Aris Pappadimitriou. The specific name of the subfolder is called ”Experimental Data”, which can be found in the following folder location, as example: Test Data - Aris Pappadimitriou\Hot-Tests\HT-R4C9\Raw Data. For thruster R4C7, HT-R4C9 is replaced by HT-R4C7,in the above route.

To obtain a more complete set of data, measurements were taken from 2.5-5bars in 0.5bar increments. The pressure measurement was using the pressure/temperature sensor block, similar to the cold tests, which was placed upstream from the thruster inlet.Figure 7.7 shows the pressure measured versus time for HT-R4C9-2. The measured pressure stayed relatively constant when the valve was opened.

The temperature was measured using the A35sc thermal camera which would provide a live video which could be seen on Research IR. On Research Ir, a point cursor was placed as close to the exit possible to read out the temperature. The valve was then opened and the temperature was recorded when the temperature was stabilized. This took about 15-20 seconds. Visual shots were also captured from research Ir, but unfortunately these images were corrupted. These visuals showed that the thruster inlet, where the ABLESTIK glue was used, had a much higher temperature compared to the surrounding thruster chip. This was especially noticeable at very high power inputs. Additionally, the entire silicon chip was almost uniform in temperature. This is important, as it indicates that along the thruster, the measured temperature does not vary much from the inlet to the exit of the thruster. Therefore, the variance in temperature across the entire thruster chamber length should not be a factor in the calculation

Table 7.1: The performance of R4C7 hot testing. Data applies to P_a=1.015±0.05 bars and P_c=2.124±0.05 for each temperature.

Thruster	T_c (K)	$\dot{m}$ (mg/s)	F_T (mN)	Isp (s)	$Re_{t,Dh}$ (-)	Cd (-)	η_{isp} (-)	η_s (-)
HT-R4C7-1.1	294.35±1.5	1.17±0.008	0.17	14.47	1136	0.84	0.20	-
HT-R4C7-1.2	317.05±5	1.15±0.008	0.20	19.11	1003	0.82	0.25	
HT-R4C7-1.3	338.35±5	1.08±0.007	0.28	27.42	902	0.80	0.34	
HT-R4C7-1.4	365.95±5	1.01±0.007	0.34	35.98	791	0.78	0.43	
HT-R4C7-1.5	396.45±5	0.93±0.006	0.45	51.67	686	0.75	0.60	

Table 7.2: The results for hot testing using R4C9. The 0-2000 sccm MFC was used.

Thruster	P_c (bar)	P_a (bar)	T_c (K)	$\dot{m}_{exp}$ (mg/s)	$F_{T,exp}$ (mN)	Isp_{exp} (s)
HT-R4C9-2.1	2.42±0.05	1.00±0.05	319±5	1.23±0.009	0.16±0.003	13.0±0.36
HT-R4C9-2.2	2.95±0.05	1.00±0.05	318±5	1.64±0.011	0.18±0.013	11.5±0.93
HT-R4C9-2.3	3.56±0.05	1.00±0.05	317±5	2.11±0.015	0.27±0.009	13.3±0.51
HT-R4C9-2.4	4.06±0.05	1.00±0.05	317±5	2.50±0.017	0.41±0.005	16.9±0.31
HT-R4C9-2.5	4.58±0.05	1.00±0.05	316±5	2.91±0.020	0.50±0.016	17.5±0.69
HT-R4C9-2.6	5.10±0.05	1.00±0.05	317±5	3.35±0.023	0.71±0.021	21.6±0.79
HT-R4C9-3.1	2.45±0.05	1.00±0.05	342±5	1.17±0.008	0.15±0.004	12.7±0.46
HT-R4C9-3.2	2.97±0.05	1.00±0.05	341±5	1.54±0.011	0.19±0.003	12.5±0.27
HT-R4C9-3.3	3.50±0.05	1.00±0.05	339±5	1.93±0.014	0.26±0.010	13.7±0.63
HT-R4C9-3.4	4.01±0.05	1.00±0.05	339±5	2.30±0.016	0.44±0.022	19.7±1.10
HT-R4C9-3.5	4.60±0.05	1.00±0.05	338±5	2.75±0.019	0.56±0.016	20.8±0.73
HT-R4C9-3.6	5.13±0.05	1.00±0.05	337±5	3.19±0.022	0.63±0.013	20.1±0.56
HT-R4C9-4.1	2.44±0.05	1.00±0.05	363±5	1.10±0.008	0.17±0.002	15.7±0.31
HT-R4C9-4.2	2.95±0.05	1.00±0.05	361±5	1.44±0.010	0.19±0.007	13.6±0.60
HT-R4C9-4.3	3.48±0.05	1.00±0.05	359±5	1.81±0.013	0.28±0.005	15.7±0.39
HT-R4C9-4.4	4.06±0.05	1.00±0.05	360±5	2.21±0.015	0.50±0.015	22.8±0.83
HT-R4C9-4.5	4.62±0.05	1.00±0.05	365±5	2.63±0.018	0.60±0.021	23.1±0.99
HT-R4C9-4.6	5.08±0.05	1.00±0.05	356±5	2.99±0.021	0.63±0.010	21.6±0.48
HT-R4C9-5.1	2.45±0.05	1.00±0.05	385±5	1.05±0.007	0.18±0.011	17.6±1.16
HT-R4C9-5.2	3.00±0.05	1.00±0.05	382±5	1.40±0.010	0.20±0.014	14.5±1.11
HT-R4C9-5.3	3.52±0.05	1.00±0.05	382±5	1.73±0.012	0.31±0.005	18.1±0.40
HT-R4C9-5.4	4.04±0.05	1.00±0.05	380±5	2.10±0.015	1.01±0.016	48.9±1.14
HT-R4C9-5.5	4.56±0.05	1.00±0.05	378±5	2.47±0.017	1.10±0.022	45.5±1.21
HT-R4C9-5.6	5.10±0.05	1.00±0.05	377±5	2.86±0.020	1.26±0.023	44.9±1.13

of thrust and mass flow.

Mass flow and thrust

Looking at the mass flow and thrust values measured, they fall in line with what is expected. At similar pressures, the mass flow of the thruster decreases and the thrust increases, as the temperature rises. This can be seen clearly in Figure 7.8b and Figure 7.8a. The thrust lines started with an increase in slope and at around the 4 bar pressure mark these thrust values began to form more of a plateau. The last three thrust measurements of HT-R4C9-5, were much higher than expected, as can be seen in Figure 7.8b. It is not certain what the main cause of this is, but the measured coil current was unexpectedly very high for these values. For those values, the current change was much higher than expected in the raw data. This large current change may have been caused by the feed tubes shifting position without the user's knowledge or the coil itself, but it can not be determined for sure what is the issue.

Discharge Coefficient

Despite using the mass flow correction, explained in subsection 7.1.3, HT-R4C9-1.6 provides a $C_{D,exp}$ greater than unity. After the hot tests, a quick leak test was performed, but it proved to be inconclusive. The reason for this efficiency might be caused by the mass flow estimation used to correct for the values by 0-2000sccm MFC. The estimation used is the best available correction, but considering the small

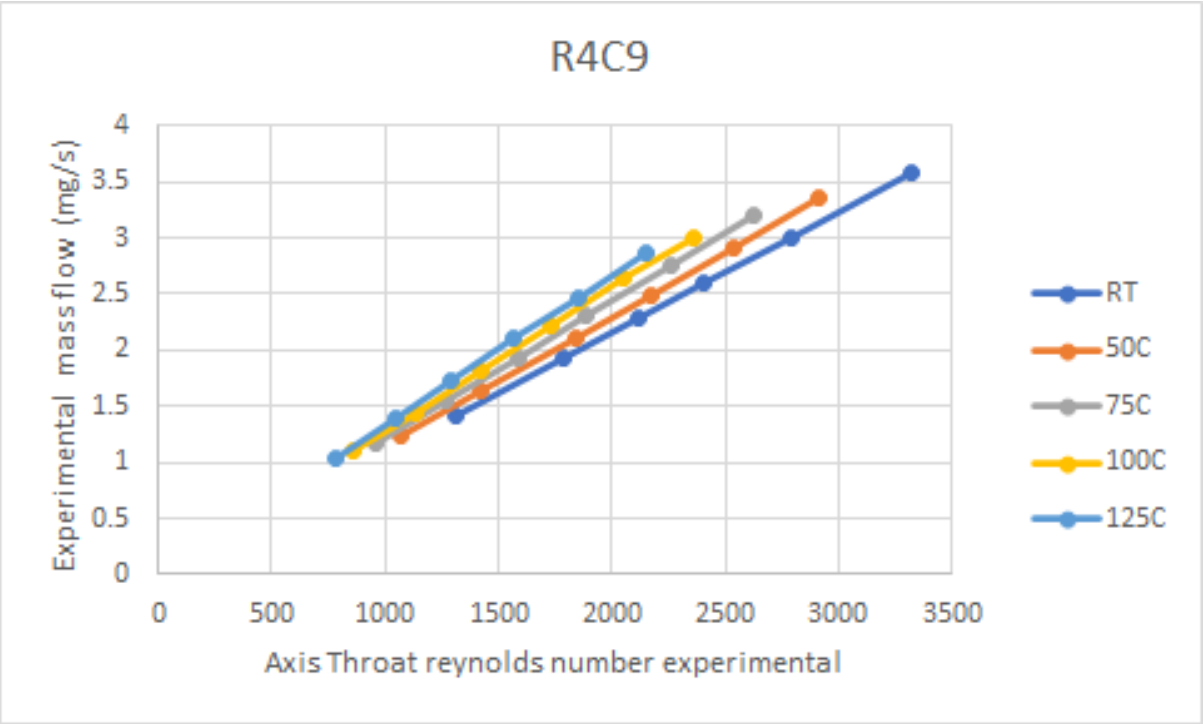

(a) Measured mass flows for HT-R4C9.

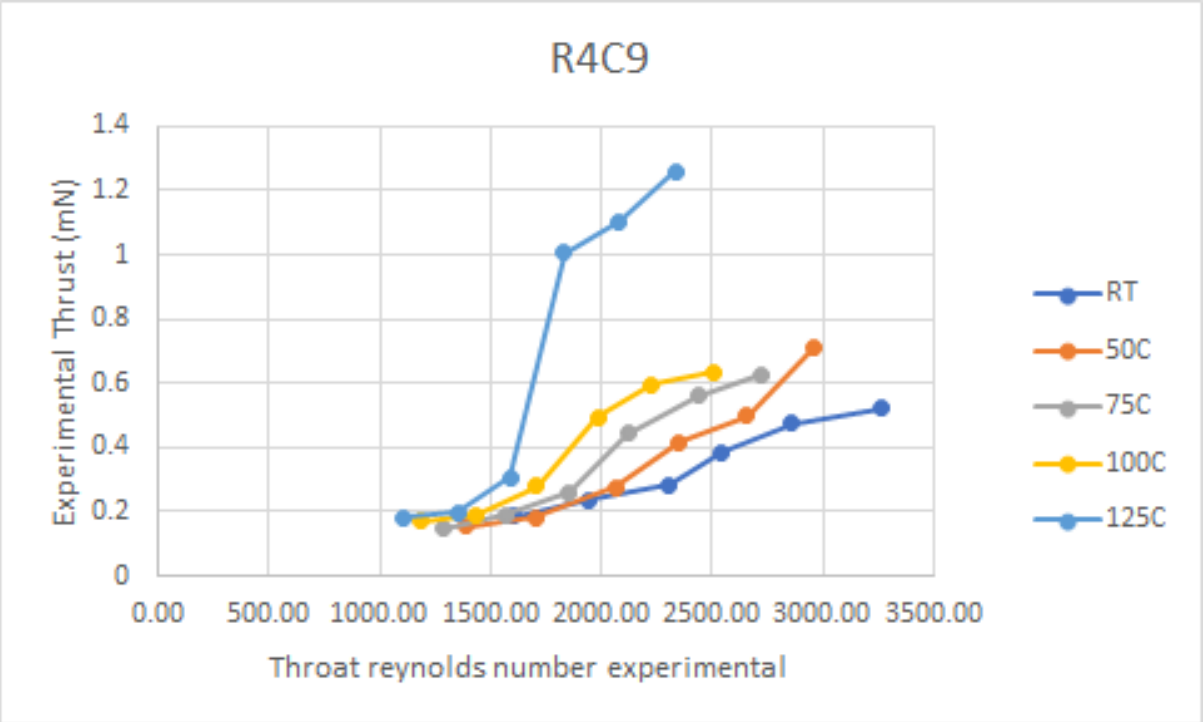

(b) Calculated thrusts for HT-R4C9.

Figure 7.8: Measured performance parameters for HT-R4C9.

Table 7.3: Power input for HT-R4C9.

V_i (V)	I_{input} (I)	P_{input} (W)	$T_{c,average}$ (°C)
4	0.0782	0.3128	49.6±5
6	0.113	0.678	76.1±5
7.5	0.135	1.0125	99.8±5
9	0.153	1.377	124.6±5

mass flow range of the tests, even being 0.01 mg/s magnitude off can make a noticeable effect on the $C_{D,exp}$. When comparing the $C_{D,exp}$ of HT-R4C9-1.1 to that of HT-R4C7-1.1, HT-R4C9-1.1 has a lower $C_{D,exp}$ despite being performed at a higher chamber pressure and both thrusters being nearly identical. This may point to the fact that the correction may be off. Despite the corrections, the only way to be certain of the $C_{D,exp}$ would be to redo the mass flow measurements with the repaired 0-144sccm MFC. For now these discharge coefficients will have to be considered acceptable. Overall, as the chamber temperature increased and/or the pressure increased, the lower the calculated $C_{D,exp}$.This means as the throat Reynolds number increases the $C_{D,exp}$ increases, which agrees with theory.

Isp and Isp efficiency

The Isp values, similar to cold testing, were between 11.5-48.9s. The majority of the values are well below the expected speed of sound, which is around 343m/s for room temperature. This leads to the conclusion that complete expansion has not occurred in the nozzle The nozzle is not suited for testing at an ambient pressure and should be tested in a vacuum. Additionally, a general trend can be seen where as the the pressure and/or temperature increases, the measured Isp increases as well, which is expected when looking at the expected values from subsection 3.8.2.

However, several points show Isp values that suggest supersonic flow was reached: HT-R4C7-1.4, HT-R4C7-1.5, HT-R4C9-5.4, HT-R4C9-5.5 and HT-R4C9-5.6. The Isp values suggest exit velocities greater than the speed of sound for their respective operating points, which would mean hat supersonic flows have been reached at the nozzle exits. When the performance model is used, using ambient pressures instead of vacuum, a thrust value could not be computed as shocks are still expected in the nozzle. The model can not take into account the presence of shocks in the thruster. So it unlikely the presence of supersonic flow at the nozzle exit is the reason for these high jumps in Isp. It may be possible that either the magnetic field of the coil was disrupted by the heater wires being operational, or an external force was acting upon the pendulum.

The η_{isp} generally increased as the throat Reynolds number increases, but not every point agreed with this. Again, the reliability of these values need to be questioned due to the reliance these variables have on the mass flow. Additionally, looking at the Isp of the values, there were some values that did not make sense (HT-R4C9-1.6,3.6, 4.6 for example), which means the Isp efficiency will not make sense. These values were too low and did not give values from which the Isp should increase. This could only be attributed to bad current peaks caused by drift and current jumping.

Heat Efficiency

The heat efficiency was determined by using Equation 3.28. Using the recorded temperatures for the thruster, the enthalpies of nitrogen at the target temperature and at room temperature could be found using Lemmon et al. [17]. Then, knowing the mass flow and the input power, the experimental heating efficiency of thruster chips can be calculated. The heat efficiencies for HT-R4C9 are given in Table 7.5. HT-R4C9-1 and HT-R4C7-1 are not heated, so no values are given.

As the chamber temperature increased, the heater efficiency decreased, showing that as the power input is increased, more of it is wasted. The data on the power input for each target temperature can be seen in Table 7.3. Additionally, as the chamber pressure increases, this led to higher heater efficiencies, due to an increase in mass flow. Silva et al. [27] found a similar trend with his heater efficiencies. The greatest heater efficiency was 0.27 from HT-R4C9-2.6 and the lowest measured heater efficiency was 0.08 from HT-R4C9-5.1. If this were to be improved, a good idea would be to find a way to limit the wasted power. A thermal shield surrounding the thruster would be a suitable way to do this, similar to what Versteeg [36] has done. The voltage to temperature relation, when using a linear trendline, is $T_c = 11.436 \cdot V + 13.61$ and can be seen in Figure 7.9.

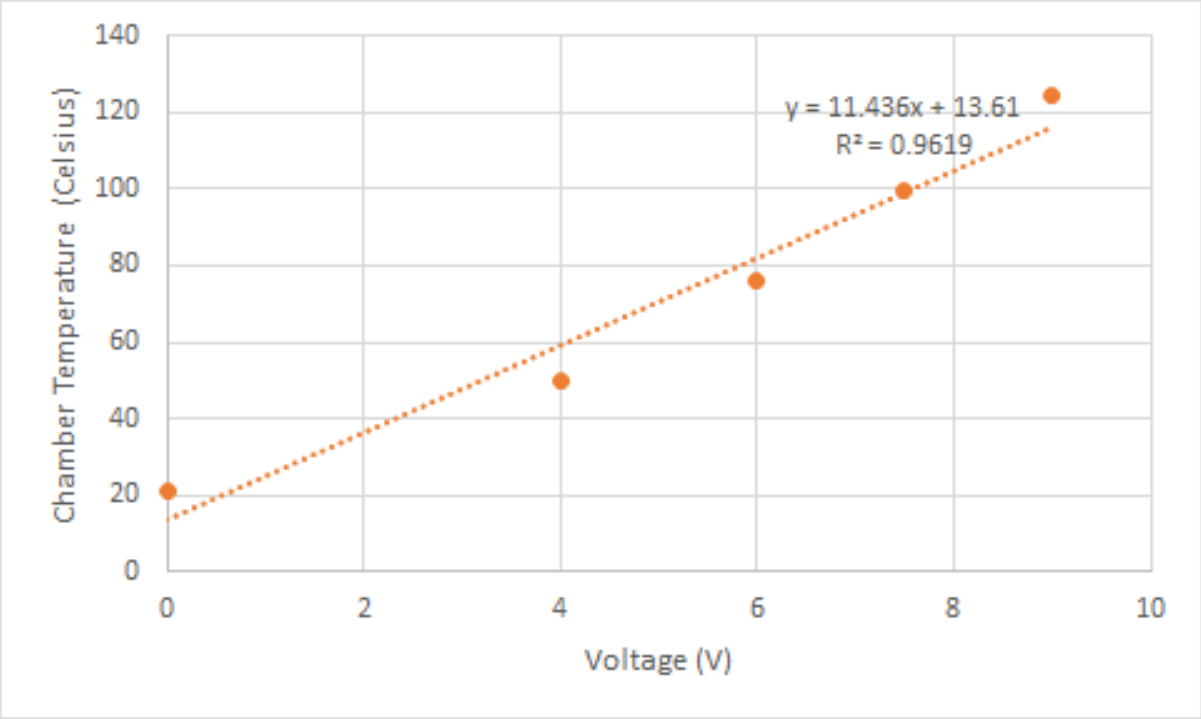

Figure 7.9: Relation between the measured chamber temperature of HT-R4C9 and the measured input voltage.

7.2.3. Comparison to model

Discharge Coefficient

Figure 7.10 provides the experimental discharge coefficients for HT-R4C7 and HT-R4C9, compared to the predicted values of Tang and Fenn [31], Kuluva and Hosack [14] and Johnson et al. [13]. None of the three models were able to predict the hot test results with an inaccuracy of at most 10%. The major deviation can be seen at the lower Reynolds numbers where, all three models overestimate the discharge coefficients. The model of Tang and Fenn [31] was off by 31.1%, the model of Kuluva and Hosack [14] by 25.7% and the model of Johnson et al. [13] by 22.6%, for when $d = D_{H,t}$. However, these large overestimations could be due to the lower than expected measured mass flows for HT-R4C7 and HT-R4C9. When comparing the cold $C_{D,exp}$ values of HT-R4C9 to CT-R4C7 and CT-R5C1, which is seen in Figure 6.6, the values of HT-R4C9-1 are clearly much lower, even though the discharge coefficient for all three thrusters were expected to be similar, as explained in section 3.8. This means that the correction discussed in subsection 7.1.3, may be giving a larger mass flow than it really is. So the validity of the models, based on hot thrust testing, remains inconclusive. The use of $d = w_t$ improves the predictions, however considering the calibration of mass flow sensors and the lower than expected mass flow values, it can not be concluded whether the hot test can validate the performance model. The TF ($d = w_t$), KH ($d = w_t$) and J ($d = w_t$) models had a maximum inaccuracy of 34%, 29% and 22%, which occurred at the lowest recorded Reynolds numbers, when comparing to HT-R4C9. As a result, the hot test data from Versteeg [36] will be used instead, even though the thruster of Versteeg is much larger than the thrusters used in this thesis. This was already done in section 3.7, where the performance models predicted the discharge coefficients of Versteeg [36] within 10%.

Isp Efficiency

Similar to cold testing, the model of Spisz, Brinich, and Jack [29] could not be used to estimate the Isp efficiency. This is due to incomplete expansion in the nozzle where there is no complete supersonic flow. This made it difficult to predict the C_f. As a result, tests need to be performed in a vacuum to be able to compare the model to experimental results.

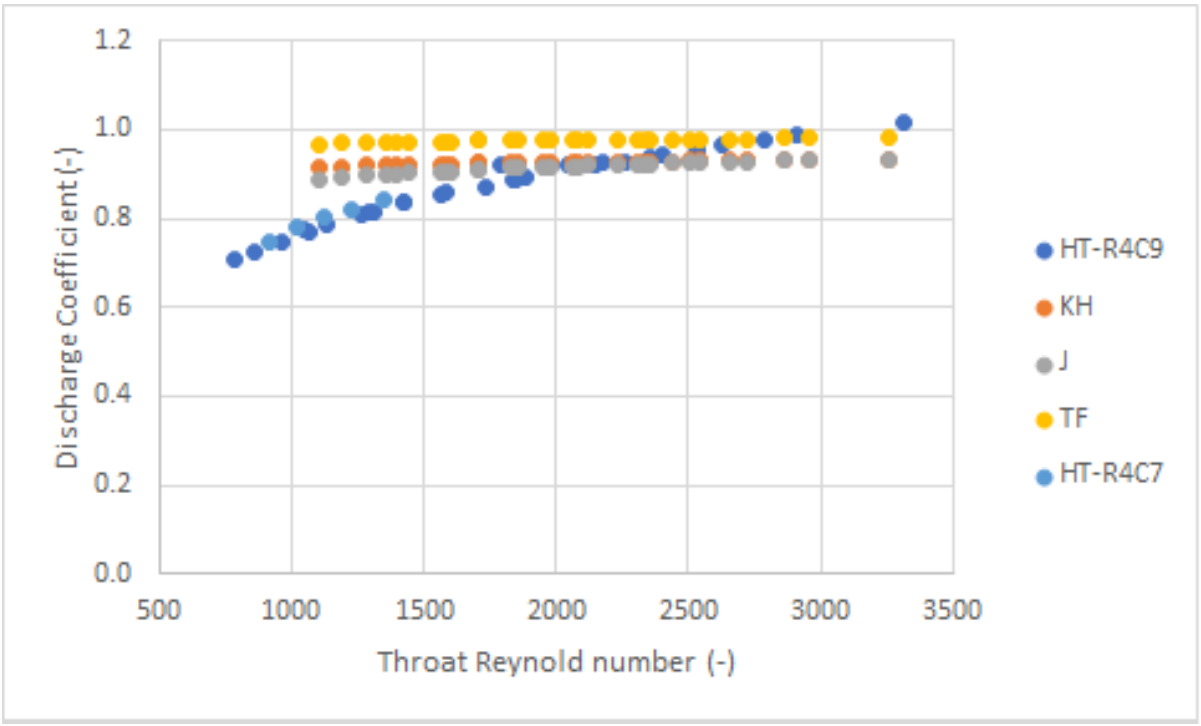

Figure 7.10: Discharge coefficients of the predictive models versus the thrust tests, with $d = D_{H,t}$.

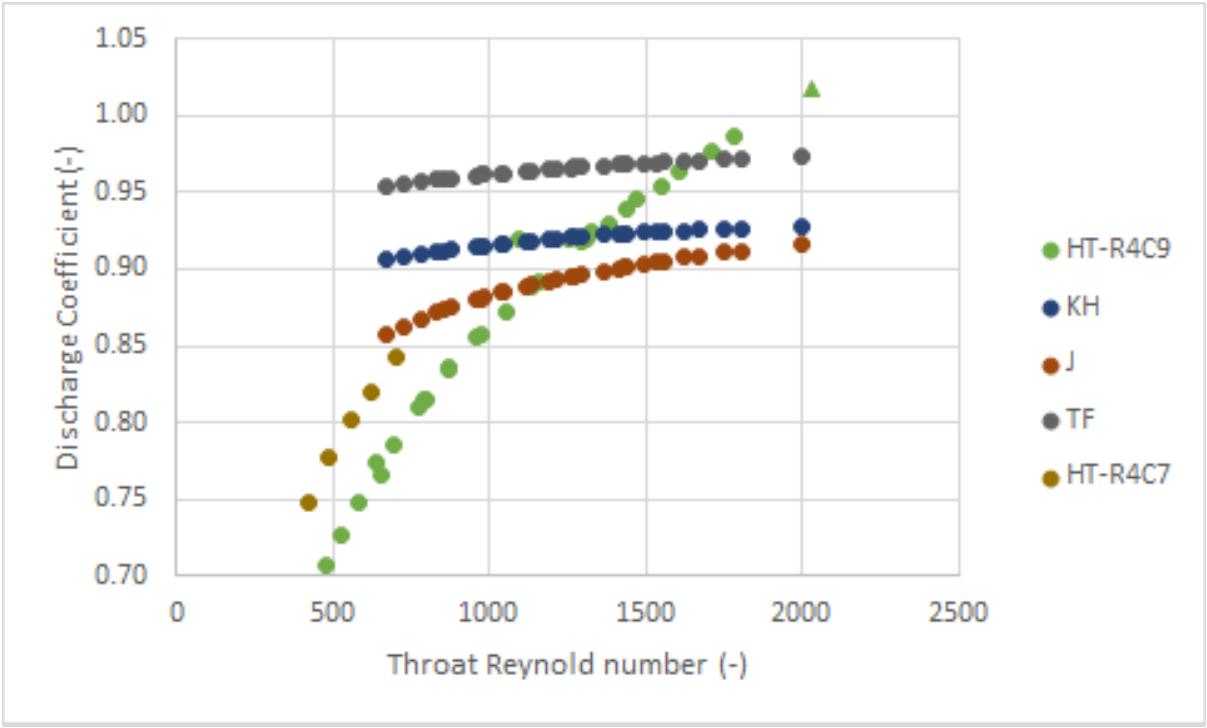

Figure 7.11: Discharge coefficients of the predictive models versus the thrust tests, with $d = w_t$.

Table 7.4: Ideal values for HT-R4C7 and HT-R4C9

Thruster Test	m_{ideal} (mg/s)	$F_{T,ideal}$ (mN)	Isp_{ideal} (s)
HT-R4C7-1	1.38	1.01	74.10
HT-R4C7-2	1.33	1.01	76.94
HT-R4C7-3	1.29	1.01	79.51
HT-R4C7-4	1.24	1.01	82.74
HT-R4C7-5	1.19	1.01	86.19
HTR4C9-1.1	1.73	1.26	74.18
HTR4C9-1.2	2.09	1.52	74.15
HTR4C9-1.3	2.48	1.80	74.12
HTR4C9-1.4	2.74	1.99	74.10
HTR4C9-1.5	3.08	2.24	74.07
HTR4C9-1.6	3.51	2.55	74.04
HT-R4C9-2.1	1.61	1.22	77.26
HT-R4C9-2.2	1.96	1.48	77.06
HT-R4C9-2.3	2.37	1.79	76.91
HT-R4C9-2.4	2.70	2.04	76.92
HT-R4C9-2.5	3.05	2.30	76.79
HT-R4C9-2.6	3.40	2.56	76.81
HT-R4C9-3.1	1.57	1.23	80.03
HT-R4C9-3.2	1.91	1.49	79.84
HT-R4C9-3.3	2.25	1.76	79.58
HT-R4C9-3.4	2.58	2.01	79.60
HT-R4C9-3.5	2.96	2.31	79.43
HT-R4C9-3.6	3.31	2.57	79.31
HT-R4C9-4.1	1.52	1.23	82.47
HT-R4C9-4.2	1.84	1.48	82.27
HT-R4C9-4.3	2.17	1.75	81.92
HT-R4C9-4.4	2.54	2.04	82.04
HT-R4C9-4.5	2.86	2.32	82.63
HT-R4C9-4.6	3.19	2.55	81.53
HT-R4C9-5.1	1.48	1.23	85.01
HT-R4C9-5.2	1.81	1.51	84.68
HT-R4C9-5.3	2.13	1.77	84.66
HT-R4C9-5.4	2.45	2.03	84.39
HT-R4C9-5.5	2.78	2.29	84.12
HT-R4C9-5.6	3.11	2.56	83.94

Table 7.5: Thruster efficiencies for HT-R4C9

Thruster	$Re_{t,exp,Dh}$	$Re_{t,exp,wt}$	$C_{D,exp}$	$\eta_{isp,exp}$	$\eta_{heat,exp}$
HT-R4C9-1.1	1306	800	0.81	0.18	-
HT-R4C9-1.2	1789	1096	0.92	0.17	-
HT-R4C9-1.3	2116	1296	0.92	0.17	-
HT-R4C9-1.4	2404	1473	0.95	0.20	-
HT-R4C9-1.5	2792	1710	0.98	0.22	-
HT-R4C9-1.6	3314	2030	1.02	0.20	-
HT-R4C9-2.1	1068	655	0.77	0.17	0.12
HT-R4C9-2.2	1423	872	0.84	0.15	0.15
HT-R4C9-2.3	1835	1124	0.89	0.17	0.17
HT-R4C9-2.4	2172	1331	0.92	0.22	0.20
HT-R4C9-2.5	2534	1552	0.95	0.23	0.22
HT-R4C9-2.6	2915	1786	0.99	0.28	0.27
HT-R4C9-3.1	958	587	0.75	0.16	0.10
HT-R4C9-3.2	1267	776	0.81	0.16	0.14
HT-R4C9-3.3	1587	972	0.86	0.17	0.16
HT-R4C9-3.4	1888	1157	0.89	0.25	0.18
HT-R4C9-3.5	2263	1386	0.93	0.26	0.21
HT-R4C9-3.6	2627	1610	0.96	0.25	0.24
HT-R4C9-4.1	860	527	0.73	0.19	0.09
HT-R4C9-4.2	1129	692	0.79	0.16	0.11
HT-R4C9-4.3	1422	871	0.83	0.19	0.14
HT-R4C9-4.4	1729	1059	0.87	0.28	0.17
HT-R4C9-4.5	2048	1255	0.92	0.28	0.19
HT-R4C9-4.6	2355	1442	0.94	0.27	0.21
HT-R4C9-5.1	779	477	0.71	0.21	0.08
HT-R4C9-5.2	1048	642	0.77	0.17	0.10
HT-R4C9-5.3	1293	792	0.82	0.21	0.13
HT-R4C9-5.4	1568	960	0.86	0.58	0.15
HT-R4C9-5.5	1849	1133	0.89	0.54	0.18
HT-R4C9-5.6	2145	1314	0.92	0.53	0.20

Table 7.6: Predicted Discharge Coefficients for HT-R4C7 and HT-R4C9.

Thruster Test	$Re_{t,Dh}$	$C_{D,TF,Dh}$	$C_{D,KH,Dh}$	$C_{D,J,Dh}$	$Re_{t,wt}$	$C_{D,TF,wt}$	$C_{D,KH,wt}$	$C_{D,J,wt}$
HT-R4C7-1	1136	0.97	0.90	0.920	834	0.95	0.91	0.87
HT-R4C7-2	1003	0.97	0.89	0.918	757	0.96	0.91	0.87
HT-R4C7-3	902	0.968	0.90	0.92	696	0.95	0.91	0.86
HT-R4C7-4	791	0.966	0.88	0.91	629	0.95	0.90	0.85
HT-R4C7-5	686	0.965	0.88	0.91	568	0.95	0.90	0.85
HT-R4C9-1.1	1604	0.973	0.923	0.907	983	0.96	0.92	0.88
HT-R4C9-1.2	1946	0.976	0.926	0.915	1192	0.97	0.92	0.89
HT-R4C9-1.3	2304	0.978	0.928	0.922	1412	0.97	0.92	0.90
HT-R4C9-1.4	2543	0.979	0.930	0.925	1558	0.97	0.92	0.91
HT-R4C9-1.5	2859	0.980	0.931	0.929	1752	0.97	0.93	0.91
HT-R4C9-1.6	3259	0.981	0.933	0.934	1997	0.97	0.93	0.92
HT-R4C9-2.1	1394	0.971	0.920	0.900	854	0.96	0.91	0.87
HT-R4C9-2.2	1703	0.974	0.924	0.909	1043	0.96	0.92	0.88
HT-R4C9-2.3	2064	0.976	0.927	0.917	1264	0.97	0.92	0.90
HT-R4C9-2.4	2352	0.978	0.929	0.922	1441	0.97	0.92	0.90
HT-R4C9-2.5	2655	0.979	0.930	0.927	1626	0.97	0.93	0.91
HT-R4C9-2.6	2955	0.980	0.932	0.930	1810	0.97	0.93	0.91
HT-R4C9-3.1	1282	0.970	0.919	0.896	785	0.96	0.91	0.87
HT-R4C9-3.2	1566	0.973	0.922	0.906	959	0.96	0.91	0.88
HT-R4C9-3.3	1853	0.975	0.925	0.913	1135	0.96	0.92	0.89
HT-R4C9-3.4	2118	0.977	0.927	0.918	1297	0.97	0.92	0.90
HT-R4C9-3.5	2437	0.978	0.929	0.924	1493	0.97	0.92	0.90
HT-R4C9-3.6	2727	0.980	0.931	0.928	1670	0.97	0.93	0.91
HT-R4C9-4.1	1184	0.969	0.917	0.892	725	0.96	0.91	0.86
HT-R4C9-4.2	1438	0.972	0.921	0.902	881	0.96	0.91	0.88
HT-R4C9-4.3	1705	0.974	0.924	0.909	1044	0.96	0.92	0.89
HT-R4C9-4.4	1983	0.976	0.926	0.916	1215	0.97	0.92	0.89
HT-R4C9-4.5	2228	0.977	0.928	0.920	1365	0.97	0.92	0.90
HT-R4C9-4.6	2509	0.979	0.929	0.925	1537	0.97	0.92	0.90
HT-R4C9-5.1	1101	0.968	0.916	0.888	674	0.95	0.91	0.86
HT-R4C9-5.2	1354	0.971	0.920	0.899	930	0.96	0.91	0.87
HT-R4C9-5.3	1587	0.973	0.923	0.906	972	0.96	0.92	0.88
HT-R4C9-5.4	1832	0.975	0.925	0.912	1122	0.96	0.92	0.89
HT-R4C9-5.5	2082	0.977	0.927	0.918	1275	0.97	0.92	0.90
HT-R4C9-5.6	2334	0.978	0.929	0.922	1430	0.97	0.92	0.90

Table 7.7: Hot performance data from Bayt [1], assuming a pressure of 2.69 bars (39 psia). This table was copied from Versteeg [36].

Re_{t,W_t} [-]	Re_{t,D_h} [-]	T_c [K]	C_D [%]	ξ_F [%]	F_{exp} [N]	$I_{sp,exp}$ [s]
966	1706	677	87.8 ± 5.2		9.43	81.58
1032	1823	⋮	88.7 ± 5.0	75.1 ± 4.7	9.60	79.80
1178	2081	⋮	90.0 ± 4.6	75.3 ± 4.7	9.75	75.51
1322	2335	⋮	91.9 ± 4.2	75.9 ± 4.8	10.00	72.58
1413	2495	⋮	92.7 ± 4.0	76.4 ± 4.8	10.15	71.12
1675	2959	⋮	94.5 ± 3.4	77.4 ± 4.8	10.40	67.12
1864	3292	⋮	94.9 ± 3.0	79.0 ± 4.8	10.64	65.64
2251	3975	⋮	95.9 ± 2.4	79.2 ± 4.8	10.80	61.05
2421	4275	⋮	96.4 ± 2.2	79.8 ± 4.8	10.87	59.75
2564	4528	⋮	96.8 ± 2.0	79.9 ± 4.8	10.89	58.47
2618	4624	300	97.0 ± 1.9	80.2 ± 4.8	10.95	58.22

Table 7.8: Hot performance data from Bayt [1], assuming a pressure of 3.03 bars (44psia). This table was copied from Versteeg [36].

Re_{t,W_t} [-]	Re_{t,D_h} [-]	T_c [K]	C_D [%]	ξ_F [%]	F_{exp} [N]	$I_{sp,exp}$ [s]
1057	1867	692	89.9 ± 5.0	75.7 ± 4.7	10.90	83.77
1139	2012	⋮	90.8 ± 4.8	76.7 ± 4.7	11.15	82.01
1260	2226	⋮	92.2 ± 4.4	77.3 ± 4.7	11.40	79.22
1334	2357	⋮	93.3 ± 4.3	77.3 ± 4.8	11.55	77.50
1438	2539	⋮	94.4 ± 4.0	78.1 ± 4.8	11.80	75.91
1575	2782	⋮	95.4 ± 3.7	78.0 ± 4.8	11.90	72.79
1718	3034	⋮	95.9 ± 3.4	78.4 ± 4.8	12.05	70.65
1908	3369	⋮	96.1 ± 3.0	79.2 ± 4.8	12.19	68.55
2065	3647	⋮	96.2 ± 2.8	79.6 ± 4.8	12.27	66.77
2433	4297	⋮	96.4 ± 2.3	80.6 ± 4.8	12.44	63.26
2968	5241	300	96.3 ± 2.0	79.8 ± 4.8	12.29	57.88

7.2.4. Comparison of the experimental data to literature

The experimental data from HT-R4C7 and HT-R4C9, will now be compared to the thrusters tested by Bayt [1] and Versteeg [36].

Discharge Coefficient

When comparing both tested thrusters to the results of Versteeg [36] and Bayt [1], it can be seen that the $C_{D,exp}$ from both thrusters seem to match well. At Reynolds numbers of 500-1500, the C_D for HT-R4C7 and HT-R4C9, seem to overlap when taking into account their uncertainties. This could also be due to using two different mass flow sensors. The largest difference between HT-R4C7 and HT-R4C9 is 5.6%, for similar Reynolds numbers. The results are much more comparable at lower Reynolds numbers, however at higher Reynolds numbers the two sets of data deviate away from each other. The maximum deviation occurs at a Reynolds number around 2900, where the C_D of thruster R4C9 overestimates the value of Versteeg [36] by 12.5%. This can all be seen in Figure 7.12. This was only done using $Re_{t,Dh}$, since the Reynolds number scales with h_t, so no new information would have been provided.

The tables for Bayt [1] can be seen in Table 7.7 and Table 7.8. When comparing the $C_{D,exp}$ to the values of Bayt [1], it was noticed from Figure 7.12, that a clear pattern and trend can be seen. The $C_{D,exp}$ of R4C9 at 2.5 bars and varying temperatures, leads into the values of Bayt [1], which is for a much larger thruster and therefore has much larger $Re_{t,Dh}$. It is like a single line can be drawn using all the data points from Figure 7.12.

Considering that the Cd for experiments overlap well with each other, it could be verified that the mass flows measured are valid. However, for the case for HT-R4C9, at larger Reynolds numbers this large deviation from the literature data may need to be investigated more thoroughly, with the newly repaired 0-144sccm, to ensure the mass flows measured can be trusted.

Isp efficiency

When comparing the η_{isp} from the hot test in Table 7.5 to the η_{isp} from Figure 7.13, it can be seen that the hot test is nowhere near the efficiency of the Bayt [1] and Versteeg [36] thruster. The difference in

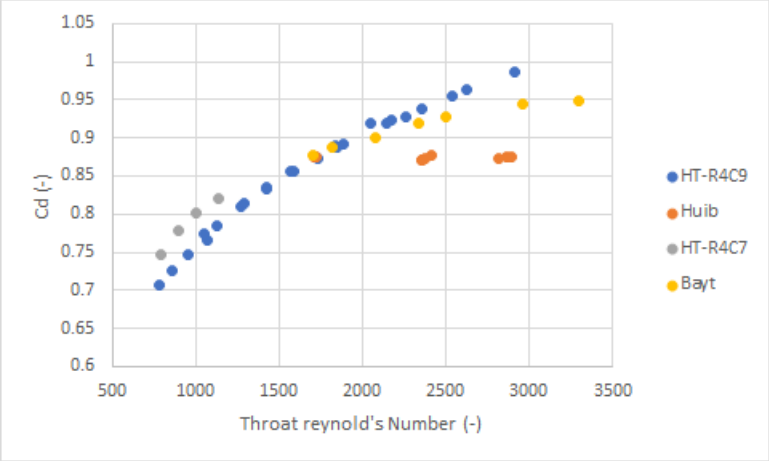

Figure 7.12: $C_{D,exp}$ of HT-R4C7, HT-R4C9, Bayt [1] and Versteeg [36].

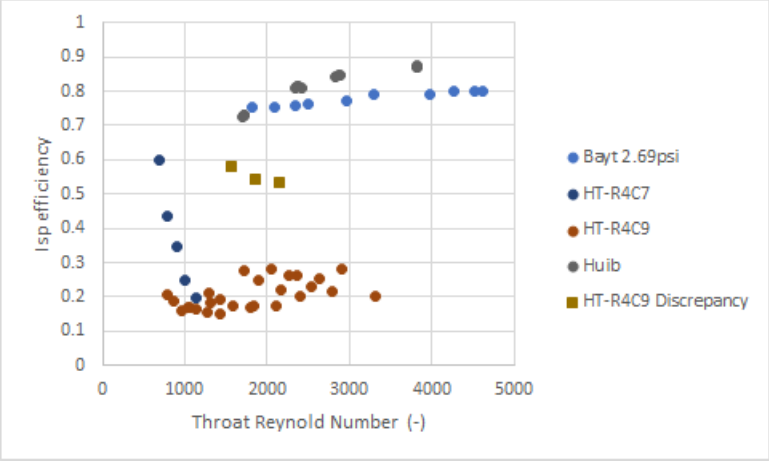

Figure 7.13: $\eta_{isp,exp}$ of HT-R4C7, HT-R4C9, Bayt [1] and Versteeg [36].

efficiency between HT-R4C9 and literature is around 50-80% worse, depending on the Reynolds number. The main reason is that the thrust tests for R4C7 and R4C9 were not done in a vacuum, meaning that complete nozzle expansion did not occur and the efficiency therefore is much lower compared to literature. Unfortunately, the comparison of the hot tests with Versteeg [36] and Bayt [1] are not comparable, and therefore the hot tests can not be validated.

The Isp efficiencies of R4C7 seem to behave differently to R4C9. the isp efficiencies for HT-R4C7 are much higher than that of HT-R4C9 for low Reynolds numbers. Looking at Table 7.1 and Table 7.2, the reason is the force values are larger than expected, despite having a lower operating pressure of 2 bars. This could be a by product of the drift and current jumps in the data, causing the true thrust values of HT-R4C7 to be lost. HT-R4C7 was meant to be an exploratory test, so its thrust and Isp data may not be reliable.

Heater efficiency

The heater efficiency for Ht-R4C9 can be read from Table 7.5. Compared to the heat efficiency of Versteeg [36], it did not perform as well. Versteeg [36] achieved heater efficiencies of 33-48% for mass flows increasing from 15.5mg/s to 17.7mg/s. The reason for these higher efficiencies is due to a radiation shield used by Versteeg [36], which retained heat during testing. Despite having a larger design, which means losing more heat through radiation, it can be learned that by incorporating a method to shield the thruster from the environment, a better heat efficiency can be achieved.

7.3. Conclusions

From the exploratory test, it could be concluded that the thruster was able to reach a temperature of 150^{o}C before failing, and thrust measurements were made up to a target temperature of 125^{o}C. As a result, the requirement **PROP-INT-1** could not be met, since the interface design could not reach a temperature of at least 600K. This performed roughly the same as the interface from Silva et al. [27] who reached around 150^{o}C. However, the recent design from Versteeg [36] was able to reach 450^{o}C, which is a vast improvement compared to the silicon MEMS thrusters used at the department. It was determined that the main issue of the design was the glue used to connect the dispensing tip to the thruster inlet, which had melted at 150^{o}C. An attempt was made to find a suitable replacement glue, but nothing was found within the time-frame of the thesis. For this packaging design to be able to compete with the design of Versteeg [36], a suitable replacement glue, with a high melting temperature must be found to connect the dispensing tip to the thruster inlet. Otherwise, a more thorough investigation will need to be carried out to isolate the glued dispensing tip from the heaters.

For temperatures up to 150^{o}C, measurements were taken for pressures between 2-5 bars. For Reynolds numbers between 686-2915 the $C_{D,exp}$ varied between 0.75 to 0.99. However, the $C_{D,exp}$ measured for hot testing seemed to be lower than expected. The three models for predicting C_D over-estimated the experimental values at low Reynolds number by 22.6% for Kuluva and Hosack [14] and 31.1% using Tang and Fenn [31]. So none of the models could validate the hot tests. However, the approximate correction for the 0-2000sccm mass flow sensor is most likely the reason why. This will require further testing to see if the models can indeed predict the hot thrust tests accurately, but this time using the repaired 0-144sccm mass flow sensor. This means that the main goal of the research, of validating a chosen model with experimental data, could not be achieved.

Similar to the cold tests, the model by Spisz, Brinich, and Jack [29], could not be used to predict the thruster Isp efficiency, which were very low compared to the experimental values of Makhan [18] and Versteeg [36], due to the presence of an ambient pressure.

When comparing the hot tests to the experiments of Versteeg [36] and Bayt [1], the C_D values seem to be verifiable, as it seems to follow the same trend as the thruster of Bayt [1], as seen in Figure 7.12. The Isp efficiency for the hot tests is very low compared to Bayt [1] and Versteeg [36]. This is expected due to the presence of ambient pressure.

Additionally, the heat efficiency was rather low for the thrusters (8%-27%) most likely due to rather large radiative losses of the thruster chips. To improve these efficiencies, a heat shield design should be considered for the thruster and its interface.

Based on the hot thrust tests, the following recommendations could be made:

- Replace the 3D printed interface with a material that has a higher melting point, such as copper or stainless steel. This way the interface does not warp at higher temperatures
- Find a more heat resistant glue, with good adhesive qualities, for the thruster inlet. This is key design failure that must be addressed for future research to continue with this design. The use of epoxy glues hat can bond to various materials and at high temperatures, should be considered.
- Compare the measured mass flows for both mass flow sensors for a large pressure range (1-5bars), to determine the misalignment. It may be necessary to send the 0-2000sccm mass flow sensor for re-calibration if this misalignment is large.
- Perform heated thrust tests with the same thrusters in a vacuum and using the repaired 0-144sccm mass flow sensor. Similar to cold testing, ambient conditions caused flow separation in the nozzle. The thrusters are not designed to perform at ambient conditions.
- Provide heat shielding or thermal insulation to help improve the heating efficiency of the design. Currently, a lot of the power is radiated to the environment.

8

Conclusions and Recommendations

8.1. Conclusions

As stated before, the main purpose of this thesis was as follows: " The objective is to verify and validate a model presented in the work of Zandbergen [37] and improved by Makhan [18], that can predict the thrust performance of a Vaporizing Liquid microthruster across the entire operating range by comparing predicted data with experimental data." Overall, this goal partially achieved, but insights could still be drawn from this thesis. To achieve this objective, the main goal was divided into sub-objectives. An for these sub-objectives, the research questions could be formulated to obtain these sub-objectives. The end of each chapter already provides some detailed conclusions and recommendations in hopes of answering these sub-objectives. The most important points will be reiterated here.

1.*Obtain experimental performance data, using both nitrogen and water through an operating range of 2-5 bars chamber pressure and to at least 600K in chamber temperature, that is reproducible and accurate.*

Overall, testing has been done up to a temperature of 150^{o}C for the throat Reynolds numbers of 2935 down to 779, for three different thrusters. For these large Reynolds numbers, the $C_{D,exp}$ for the thrusters, were between 0.75-1 and the Isp efficiencies were between 0.16-0.60, for the three different thrusters. Unfortunately, the Isp values were very low due to the presence of an ambient pressure, which worsened the performance of the thrusters.

When comparing the experimental data to literature, the discharge coefficient was between 3-9% larger than the values of Makhan [18], which shows reasonable agreeableness with his values, for pressures between 2-5bars at room temperature.

For hot testing, the heater efficiency increased as the mass flow of the test increased and the chamber temperature increased. The largest heater efficiency measured for HT-R4C9 was 27%. These values could be improved by preventing heat wastage, through implementing and using a thermal shield for the thruster. The thruster of Versteeg [36] managed heater efficiencies up to 48%, due to higher mass flows and the thermal radiation shield which helps retain more heat.

The displacement method and force compensation method, for calculating the thrust, gave similar results for the same thruster. IT was expected to be the case, considering the only difference between the two methods is that the displacement allows the pendulum to move and the force compensation method keeps the pendulum static. However, it is good that it has been verified to be true. Therefore, the force compensation method, which reduces the effects that tubes and wiring have on the pendulum and does not require the thrust stand calibration to be performed before testing, should be used in future experiments. This will save time and reduce the effects of wiring on the pendulum displacement.

2.*Design and/or improve the thruster interface to allow thrust tests to take place at high temperatures, above 600 K, without damaging the set up, by investigating different insulative/protective solutions.*

The packaging method for the VLM involved the use of certain high temperature glues to attach the thruster chip to its PCB. It was determined during fabrication by Henk van Zeijl, that the low adhesivity of the chosen glue, Thermeez 7020, would mean that the dispensing tip for the thruster inlet could not be attached. Therefore, ABLESTIK glue, which was readily available at the faculty, and used by Kurmanbay [15] and Van Wees [35], had to be used despite its lower maximum operating temperature.

The VLM packaging used for the thrust testing was able to function up until a chamber temperature of 150°C with a minimum pressure of 2 bars. At that point the ABLESTIK glue used to attach the metal dispensing tip to the thruster inlet melted and failed, as predicted. Additionally, the interface used to attach the VLM to the thruster pendulum, began warping at that operating temperature as well.

Compared to previous designs, the current design did not fair well. The interface used by Silva et al. [27] was able to reach a wet run temperature of 150°C, while Versteeg [36] reached 450°C with his wire electric discharge machining fabricated thruster.

Despite this, there is reason to believe that the current design can perform well if a more adhesive glue can be found with a a high operating temperature for the inlet or if the inlet can be isolated from the heaters. The current package shows promise, but if no suitable glue replacements can be found, then a thorough investigation is needed to solve this issue.

3.*Determine the accuracy of the model at different operating conditions by comparing the predicted performance values and efficiencies with the real experimental values, including their measurement uncertainties, for each propellant.*

Additionally, several improvements have been made on the performance model created by **makhan**. An important discovery is the fact that the KH model and J model, improved the prediction of the C_D and η_f compared to the TF model. Additionally, the use of the throat width for the characteristic length provided better accuracy of the C_D and η_f, compared to the hydraulic diameter.

When comparing the predicted discharge coefficient to the cold experimental data in chapter 6, the KH and J models were able to estimate the $C_{D,exp}$ up to within 6.6% and 7.9% of the true value, when using the hydraulic diameter as the characteristic length. The TF model provided a minimal correction on the mass flow of the thruster, with a a maximum deviation of 11%. When using w_t for the characteristic length, the accuracy improved for lower Reynold's numbers for all three models. It was difficult to validate the model using the hot test data, since the calibration of the larger mass flow sensor was not very trustworthy. However, when comparing to the hot data of Versteeg [36], the percentage difference between the predictive model and the experimental data varied between 2-9% as Reynolds number increases. Which means that the performance model is valid for hot testing.

Unfortunately, since the thrust tests were not performed in a vacuum, the model was unable to predict the η_f of the thrusters. However, using the experimental data from Makhan [18] and Versteeg [36], the improved models were unable to predict the experimental data within 10%, meaning that the model is not strictly valid for the given percentage goal. The percentage difference with Makhan [18] was 14-189% and -10% to -21% for the case of Versteeg [36], depending on the Reynolds number and which characteristic length is used. When changing the fitting constant in Equation 3.25, from 17.6 to 22.75, the estimation of η_f falls within 10% of the experimental values of Makhan [18], when using the KH ($d = w_t$) model). Considering that the thruster of Makhan [18] is most similar the thrusters used in this thesis, it would be interesting to see if this new fitting constant can give accurate predictions of the η_f, for the thrusters tested in this thesis, in a vacuum and also at higher operating temperatures.

Therefore, the validity of the models could be determined for predicting the discharge coefficients using the expeeriemtnal data from this thesis, the data from Makhan [18] and Versteeg [36]. However, for determining the Isp efficiency,

4.*Investigate the difference in performance between using nitrogen and vaporized water as a propellant, by comparing the acquired experimental data between them.*

It was intended to perform hot testing using vaporized water as well, however this could not be done due to a lack of time during the thesis. Currently, only the work of Silva et al. [27] and Kurmanbay [15] has data concerning vaporized water testing. However, neither of these papers have directly measured thrust data using this propellant.

8.2. Recommendations

5.*Provide recommendations to improve the chip design, chip interface, test-up and the models used, by providing solutions to any limitations and/or deficiencies in the work.*

For the thruster packaging, it is recommended to look into finding a more adhesive glue for the thruster inlet, that still has good thermal properties similar to Thermeez 7020. If nothing can be found, then a more thorough investigation will be needed to isolate the thruster inlet from the heaters.

Additionally, it is recommended to replace the 3D printed pendulum-thruster interface with a re-designed machined steel or aluminium part, that also provides more room for attaching the heater wires

to the PCB. This way, higher chamber temperatures can be reached, without misaligning the thruster through warping and the thrusters are not accidentally torn off the PCB when heater wires are being applied to the PCB.

Furthermore, building a heat shield along with the improvements to the package design, will improve the overall heater efficiency.

A major issue in thrust determination was the presence of data drift and random current jumps. The cause for these phenomena was the placement of the wires and nitrogen feed tubes. It would be recommended for future researchers to use smaller, thinner wires and/or tubes.

As stated in the report, ambient pressure does not allow for full flow expansion within the nozzle. This meant that the performance model was unable to predict the Isp efficiency of the thrusters used, meaning that the performance model could not be validated using the thrusters in this thesis. It is recommended to perform the thrust tests in a vacuum for all future tests.

For future experimentation, it is recommended to repeat a hot nitrogen thrust test using thruster R4C9, which is still functional, to help verify the experimental results found in this thesis through repeatability. One downfall of the thrust testing is that only one hot test could be done with R4C9 and that another test could not be done in time. Repeating this test may help in determining whether the performance values are true or not for this thruster. Additionally, the mass flow values can be remeasured using the repaired 0-144sccm, to give much better mass flow values.

It is recommended to determine thruster performances using vaporized water and comparing these values against nitrogen. Looking at Equation 3.10, based on ideal rocket theory, it is expected to see the exit velocity increase compared to using nitrogen, due to the lower molar mass of water. This would lead to higher thrusts and Isp values, when using water compared to nitrogen. It would have been great if the thrusters could have been tested with water, to see the difference in performance compared to nitrogen and also to have a liquid propellant to of which the data can be used to validate the proposed performance model. However, due to a lack of time this could not be done and therefore objective 4 could not be achieved.

Lastly, it is recommended that future users use the corrected experimental data in Table 3.2, when referring to his work as reference. This correction takes into account the incorrect actuator distance used for determining the force correction factor. This correction factor reduces the measured thrust values of TT-04 and TT-05 (see Makhan [18]) by 8%.[1] This should be helpful for future researchers who wish to use his thrust data for validation or comparison.

[1] TT-04 and TT-05 are the labels for cold thrust tests done by Makhan [18] using nitrogen as a propellant.

Bibliography

[1] Robert L Bayt. *Analysis, fabrication and testing of a MEMS-based micropropulsion system*. Tech. rep. Aerospace Computational Design Laboratory, Dept. of Aeronautics, 1999.

[2] RJF Bijster. “Design, Verification and Validation of a Micropropulsion Thrust Stand”. MA thesis. the Netherlands: TU Delft, 2014.

[3] *Bison Siliconenkit High Temp Zwart Tube 60 ml NL /FR*. Rev. 1. Bison International BV. 2021.

[4] J Bouwmeester et al. “Preliminary Results of the Delfi-n3Xt Mission”. English. In: *Proceedings of the 4S symposium 2014*. Ed. by s.n. The 4 S Sypmosium ; Conference date: 26-05-2014 Through 30-05-2014. ESA, CNES, 2014, pp. 1–15.

[5] Brooks. *Installation and Operation Manual*. Brooks. Apr. 2013. URL: https://www.brooksinstrument.com/~/media/brooks/documentation/products/mass-flow-controllers/elastomer%5C%20sealed/sla5800/revision%5C%20a/mass-flow-controller-installation-manual-sla5850-sla5851-sla5853-sla5860-sla5861-sla5863-en.pdf?la=en.

[6] *Ceramic Adhesives and Putty*. Rev. 1. Cotronics Corporation. 2008.

[7] A. Cervone et al. “Green micro-resistojet research at Delft University of Technology: new options for Cubesat propulsion”. In: *CEAS Space Journal* 9.1 (Mar. 2017), pp. 111–125. ISSN: 1868-2510. DOI: 10.1007/s12567-016-0135-3. URL: https://doi.org/10.1007/s12567-016-0135-3.

[8] Saeed Farokhi. *Aircraft propulsion*. John Wiley & Sons, 2014.

[9] Chaggai Ganani. “Micronozzle Performance: A Numerical and Experimental Study”. MA thesis. the Netherlands: TU Delft, 2019.

[10] M.G. De Giorgi and D. Fontanarosa. “A novel quasi-one-dimensional model for performance estimation of a Vaporizing Liquid Microthruster”. In: *Aerospace Science and Technology* 84 (2019), pp. 1020–1034. ISSN: 1270-9638. DOI: https://doi.org/10.1016/j.ast.2018.11.039. URL: http://www.sciencedirect.com/science/article/pii/S1270963818320881.

[11] J Guo, J Bouwmeester, and EKA Gill. “In-orbit results of Delfi-n3Xt: Lessons learned and move forward”. English. In: *Acta Astronautica* 121.April-May (2016). harvest, pp. 39–50. ISSN: 0094-5765. DOI: 10.1016/j.actaastro.2015.12.003.

[12] EHW Jansen. “Improvement and validation of test stand performance for novel micropropulsion systems”. MA thesis. the Netherlands: TU Delft, 2016.

[13] Aaron N Johnson et al. “Numerical Characterization of the Discharge Coefficient of Critical Nozzles”. PhD thesis. Pennsylvania State University, 2000.

[14] NM Kuluva and GA Hosack. “Supersonic nozzle discharge coefficients at low Reynolds numbers”. In: *AIAA journal* 9.9 (1971), pp. 1876–1879.

[15] Alisher Kurmanbay. “Design, Fabrication and Characterization of MEMS bassed Micro Heater for Vaporizing Liquid Microthruster”. MA thesis. the Netherlands: TU Delft, 2019.

[16] Federico La Torre. “Gas flow in miniaturized nozzles for micro-thrusters”. MA thesis. the Netherlands: Delft university of Technology, 2011.

[17] EW Lemmon et al. “NIST chemistry WebBook, Nist standard reference database number 69”. In: *National Institute of Standards and Technology, Gaithersburg* (2011).

[18] Rajeev Makhan. “Performance of the MEMS Vaporizing Liquid Microthruster using cold nitrogen gas as propellant”. MA thesis. the Netherlands: TU Delft, 2018.

[19] TV Mathew. “Design of a MEMS micro-resistojet”. MA thesis. TU Delft, 2011.

[20] Antanas Melaika. “Design and Verification of Delfi-PQ Satellite Propulsion Sub-system: Experimental Analysis and Design Improvements of the Technology Demonstration Payload for Micro-Thrusters”. MA thesis. the Netherlands: TU Delft, 2019.

[21] L. Mele et al. “A molybdenum MEMS microhotplate for high-temperature operation”. In: *Sensors and Actuators A: Physical* 188 (2012). Selected papers from The 16th International Conference on Solid-State Sensors, Actuators and Microsystems, pp. 173–180. ISSN: 0924-4247. DOI: https://doi.org/10.1016/j.sna.2011.11.023. URL: http://www.sciencedirect.com/science/article/pii/S0924424711006820.

[22] Aris Pappadimitriou. “Literature Report: Testing a MEMS-VLM microresistojet in hot conditions”. MA thesis. the Netherlands: TU Delft, 2019.

[23] RMA Poyck. “Design, manufacturing and characterisation of a water fed CubeSat micro-resistojet (Dondersteen)”. MA thesis. the Netherlands: TU Delft, 2014.

[24] *Pressure Sensors: Absolute pressure sensor die for wet media*. TJA1043. Rev. 1. EPCOS. Jan. 2013.

[25] *ResearchIR 4 User’s Guide*. 3. FLIR. 2015. URL: https://assets.tequipment.net/assets/1/26/FLIR_ResearchIR_User_Manual.pdf.

[26] Marc L. Salit and Gregory C. Turk. “A Drift Correction Procedure”. In: *Analytical Chemistry* 70.15 (1998). PMID: 21644656, pp. 3184–3190. DOI: 10.1021/ac980095b. eprint: https://doi.org/10.1021/ac980095b. URL: https://doi.org/10.1021/ac980095b.

[27] Marsil AC Silva et al. “Vaporizing Liquid Microthrusters with integrated heaters and temperature measurement”. In: *Sensors and Actuators A: Physical* 265 (2017), pp. 261–274.

[28] Stefano Speretta et al. “Cubesats to pocketqubes: Opportunities and challenges”. English. In: *Proceedings of the 67th International Astronautical Congress (IAC)*. 67th International Astronautical Congress, 67th IAC ; Conference date: 26-09-2016 Through 30-09-2016. IAF, 2016. URL: https://www.iac2016.org/.

[29] Ernie W Spisz, Paul F Brinich, and John R Jack. *Thrust coefficients of low-thrust nozzles*. Tech. rep. NATIONAL AERONAUTICS and SPACE ADMINISTRATION CLEVELAND OH LEWIS RESEARCH CENTER, 1965.

[30] Aeilt-Jan Takken. “Development of a high-temperature Solar Thermal Propulsion engine”. MA thesis. the Netherlands: TU Delft, 2021.

[31] SP Tang and JB Fenn. “Experimental determination of the discharge coefficients for critical flow through an axisymmetric nozzle”. In: *AIAA Journal* 16.1 (1978), pp. 41–46.

[32] *TE Connectivity Sensor Solutions. MS5837-30BA Ultra Small Gel Filled Pressure Sensor. Tech. Data Sheet*. Rev. C2. TE connectivity. 2019. URL: https://www.te.com/usa-en/product-CAT-BLPS0017.html#mdp-tabs-content.

[33] *Technical Data Sheet LOCTITE ABLESTIK 84-1LMI*. Rev. 1. Loctite. 2014.

[34] Leon Turmaine. “A technology demonstration payload for micro-resistojet thrusters on Delfi-PQ”. MA thesis. the Netherlands: TU Delft, 2018.

[35] TX Van Wees. “Characterization and Testing of a MEMS-Vaporizing Liquid Microthruster for Small Satellite Propulsion”. MA thesis. the Netherlands: TU Delft, 2017.

[36] Huib Versteeg. “Novel fabrication method for a hot gas supersonic micro-thruster”. MA thesis. the Netherlands: TU Delft, 2020.

[37] Barry Zandbergen. “Thermal rocket propulsion”. In: *Delft University of Technology* 2 (2003).

A

Example Calculations

These example calculations will be done using the input values of HT-R4C9-1.1, where $d = D_{H,t}$. This only shows discharge coefficients for each model and Reynolds number.

$$Re_{t,exp,Dh} = \frac{\dot{m} \cdot Dh}{\mu_t \cdot A_t} = \frac{1.41 \cdot 4.23e-5}{1.53e-5 \cdot 2.98e-9} = 1604 \tag{A.1}$$

$$Re_{mod} = Re_t \cdot \sqrt{\frac{Dh \cdot 0.5}{r_{t,c}}} = 1604 \cdot \sqrt{\frac{0.5 \cdot 4.23e-5}{0.5e-6}} = 10429 \tag{A.2}$$

$$\begin{aligned} C_{d,TF} &= 1 - \left(\frac{\gamma+1}{2}\right)^{0.75}\left(\frac{72-32\sqrt{6}}{3(\gamma+1)} + \frac{4\sqrt{6}}{3}\right)\left(\frac{1}{\sqrt{Re_{mod}}}\right) + \left(\frac{2\sqrt{2}(\gamma-1)(\gamma+2)}{3\sqrt{\gamma+1}}\right)\left(\frac{1}{R_{mod}}\right) \\ &= 1 - \left(\frac{1.404+1}{2}\right)^{0.75}\left(\frac{72-32\sqrt{6}}{3(1.404+1)} + \frac{4\sqrt{6}}{3}\right)\left(\frac{1}{\sqrt{10429}}\right) + \left(\frac{2\sqrt{2}(1.404-1)(1.404+2)}{3\sqrt{1.404+1}}\right)\left(\frac{1}{10429}\right) \\ &= 0.973 \end{aligned} \tag{A.3}$$

$$C_{d,J} = \alpha - \frac{\beta}{\sqrt{Re_t}} = 1 - \frac{3.62}{\sqrt{1604}} = 0.907 \tag{A.4}$$

$$\begin{aligned} C_{D,KH} &= \left(\frac{r_{t,c} + 0.05 \cdot 0.5d}{r_{t,c} + 0.75 \cdot 0.5d}\right)^{0.019} \cdot \left[1 - \left(\frac{r_{t,c} + 0.10 \cdot 0.5d}{0.5d}\right)^{0.21} \cdot \frac{1}{\sqrt{Re_{t,ideal}}}(0.97 + 0.86\gamma_c)\right] \\ &= \left(\frac{0.5 + 0.05 \cdot 0.5 \cdot 4.23e-5}{0.5 + 0.75 \cdot 0.5 \cdot 4.23e-5}\right)^{0.019} \cdot \left[1 - \left(\frac{0.5e-6 + 0.10 \cdot 0.5 \cdot 4.23e-6}{0.5 \cdot 4.23e-6}\right)^{0.21}\right. \\ &\left. \cdot \frac{1}{\sqrt{1604}}(0.97 + 0.86 \cdot 1.404)\right] = 0.923 \end{aligned} \tag{A.5}$$

B

Computer Aided Design Drawings

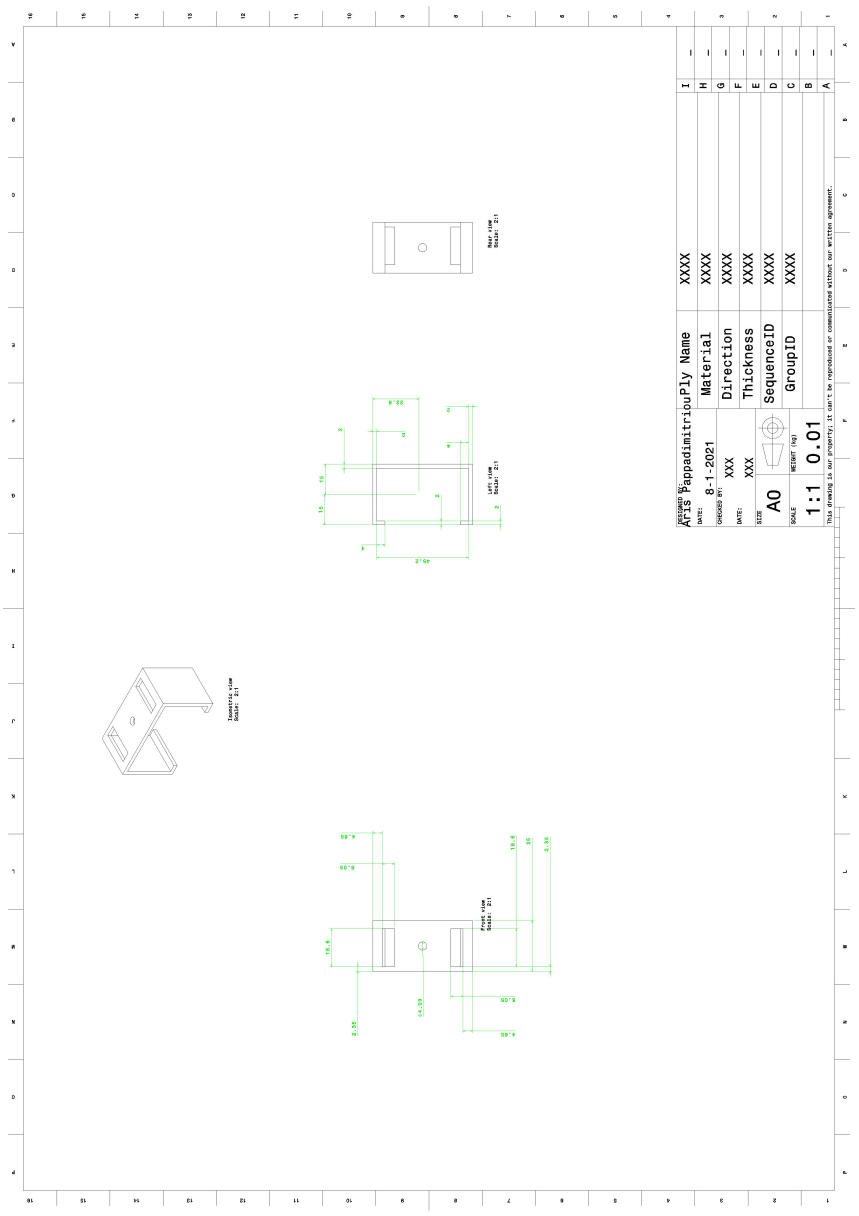

Figure B.1: CAD drawing for the interface cover.

C

Experimental Cold and Thrust Test Outputs

The purpose of this appendix is to provide examples of what the experimental outputs of the cold and hot thrust testing looks like. The example of CT-R4C7 and HT-R4C7 is used in this appendix. The graphs and excel data for CT-R5C1, CT-R4C7, HT-R4C7 and HT-R4C9 can be found in the student folder of Aris Pappadimitriou. Additionally, the files for the prepatory tests can also be found in the folder, however some of those graphs can already found in chapter 5. All output files are separated and categorized into prepatory test folders, cold testing folders and hot testing folders, within the main student folder.

C.1. CT-R4C7-1

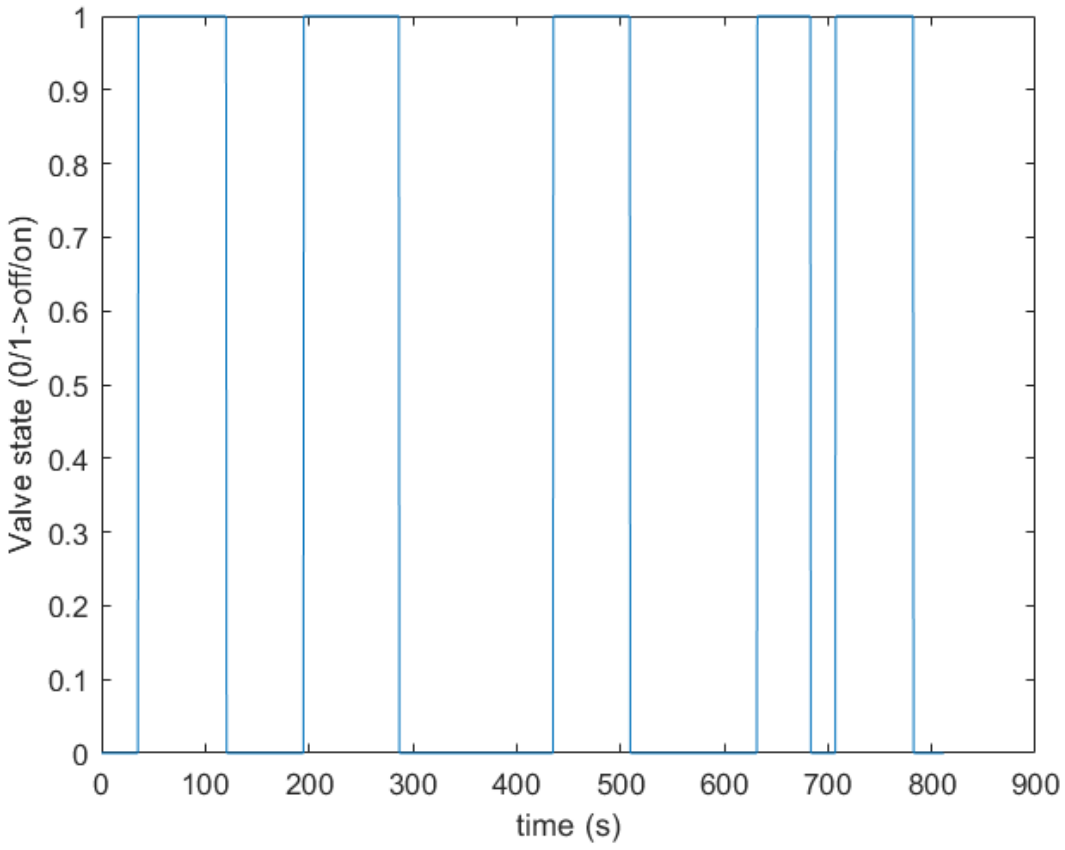

Figure C.1: Valve state versus time.

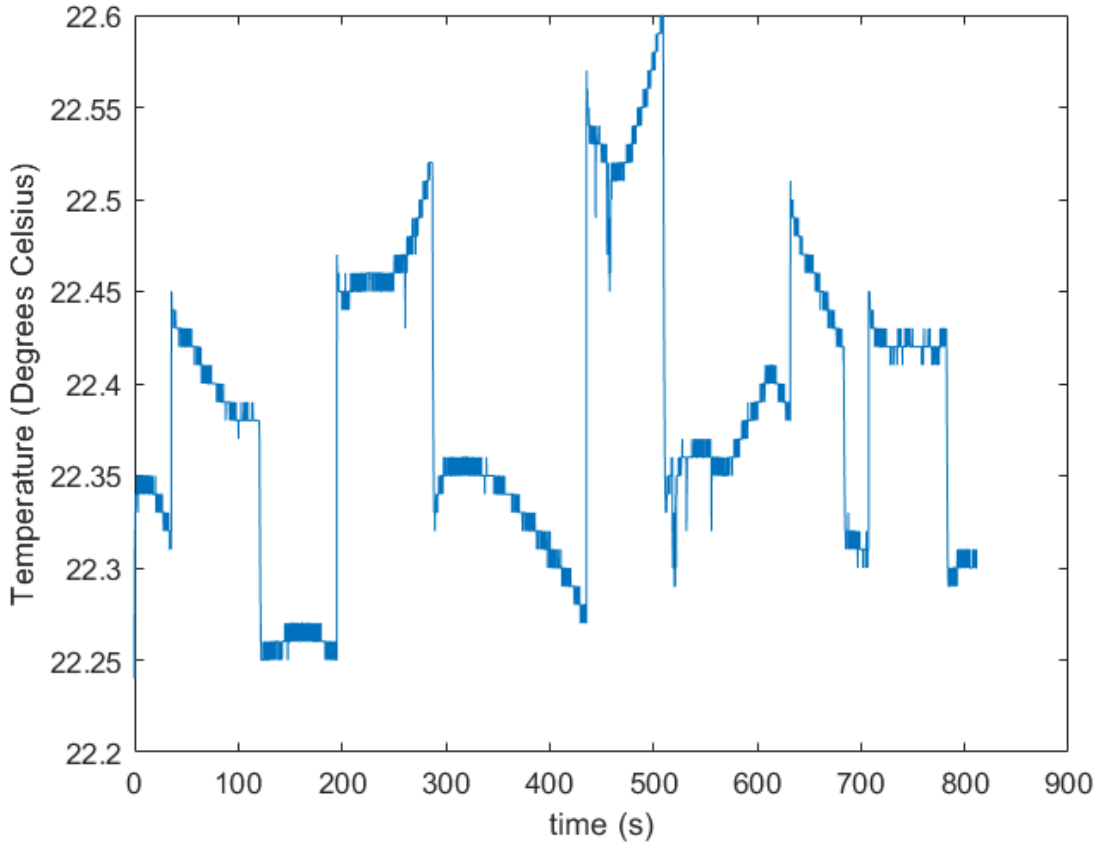

Figure C.2: Temperature versus time.

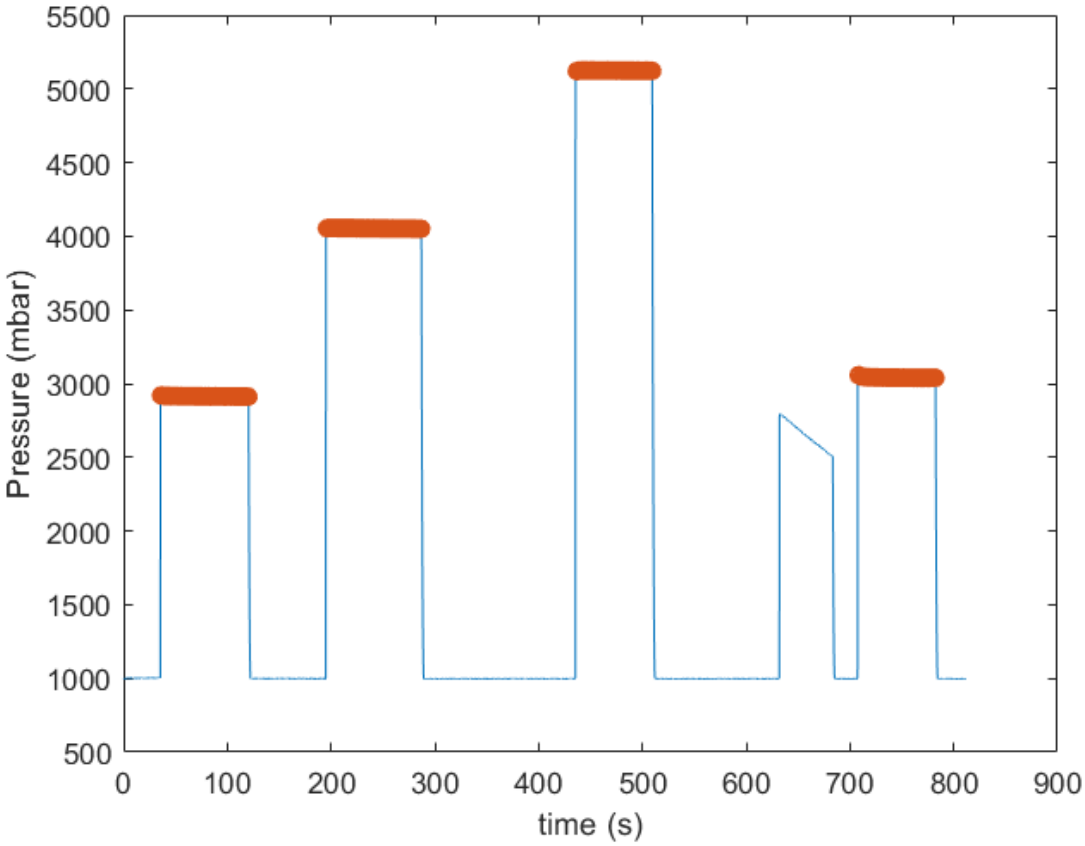

Figure C.3: Inlet pressure versus time.

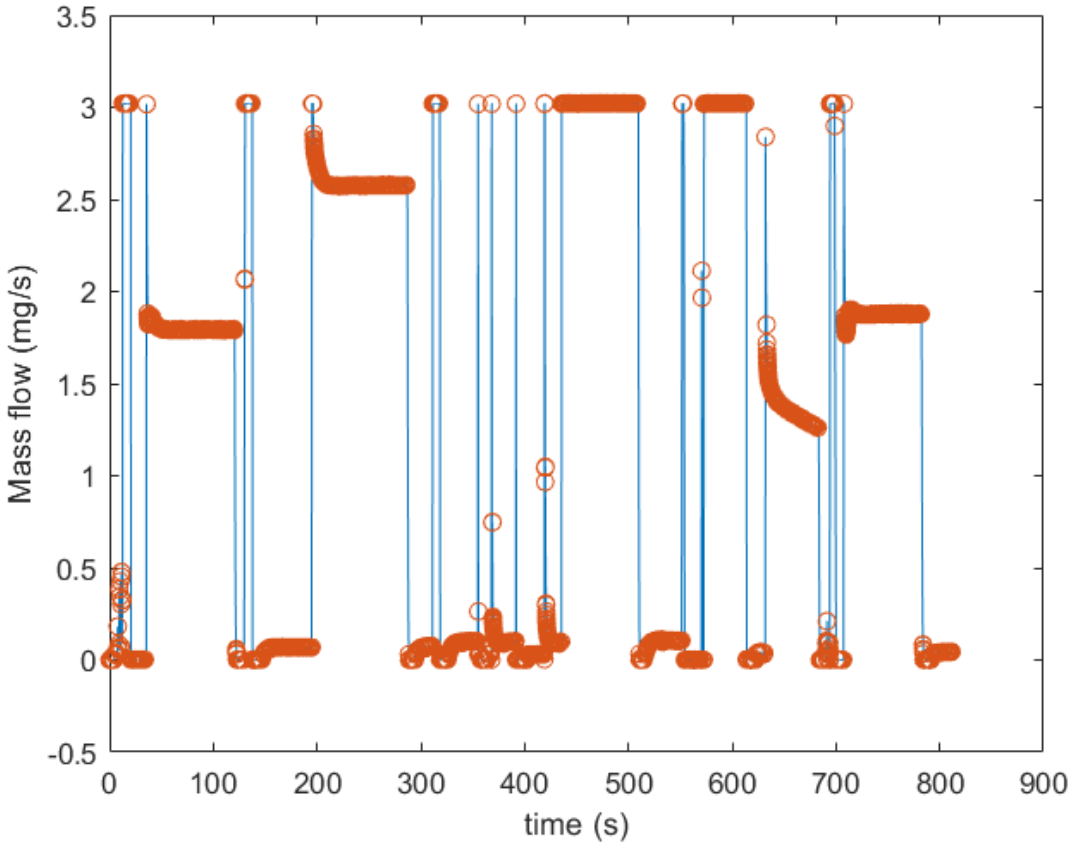

Figure C.4: Mass flow versus time.

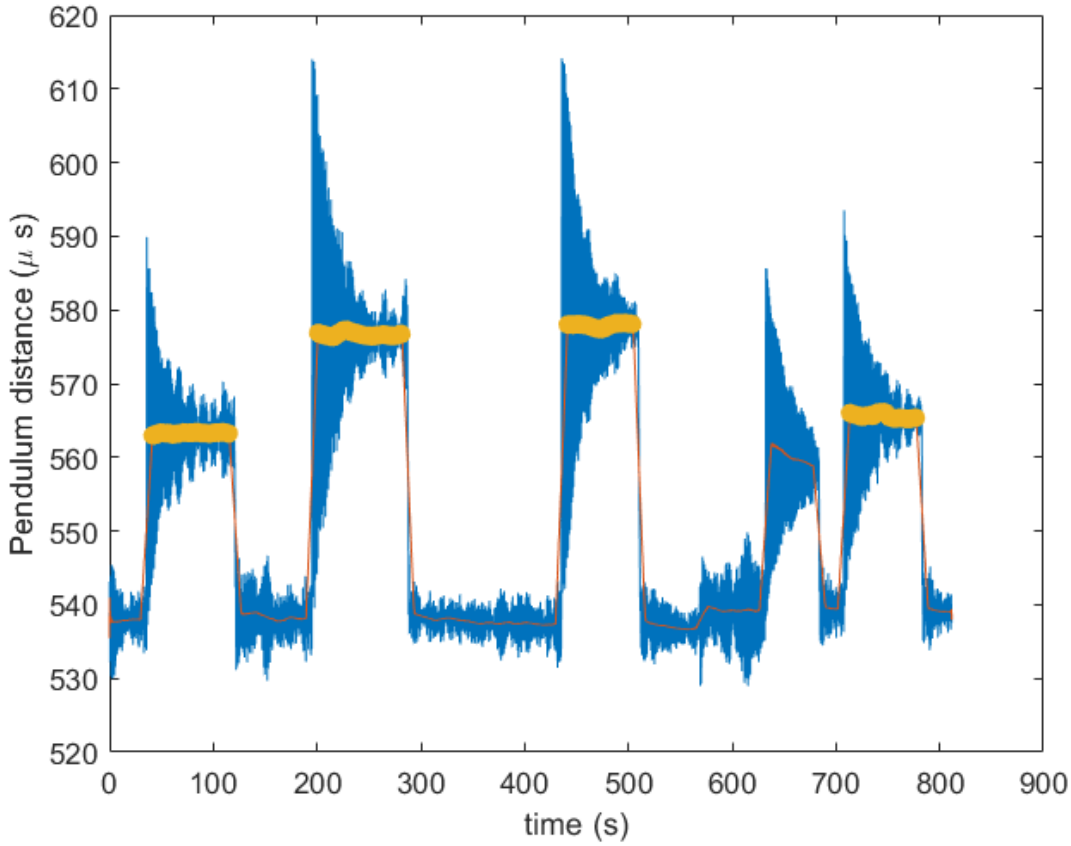

Figure C.5: Pendulum displacement versus time.

C.2. CT-R4C7-2

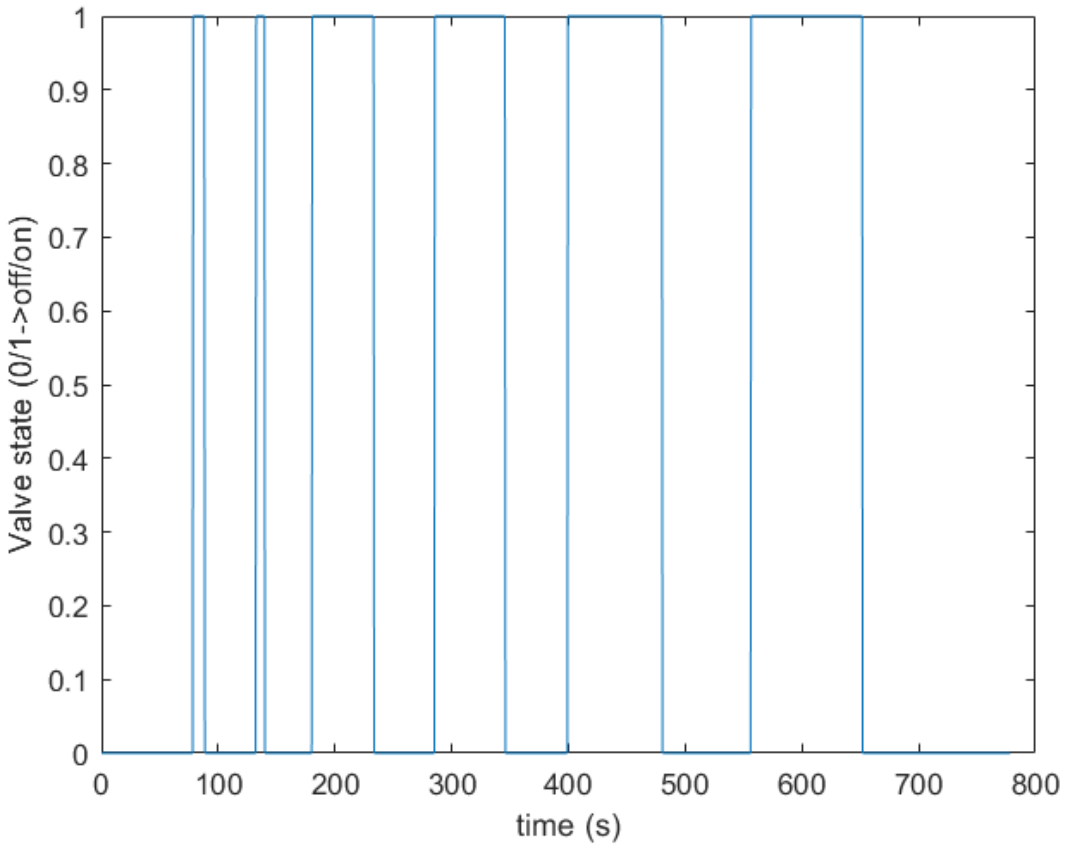

Figure C.6: Valve state versus time.

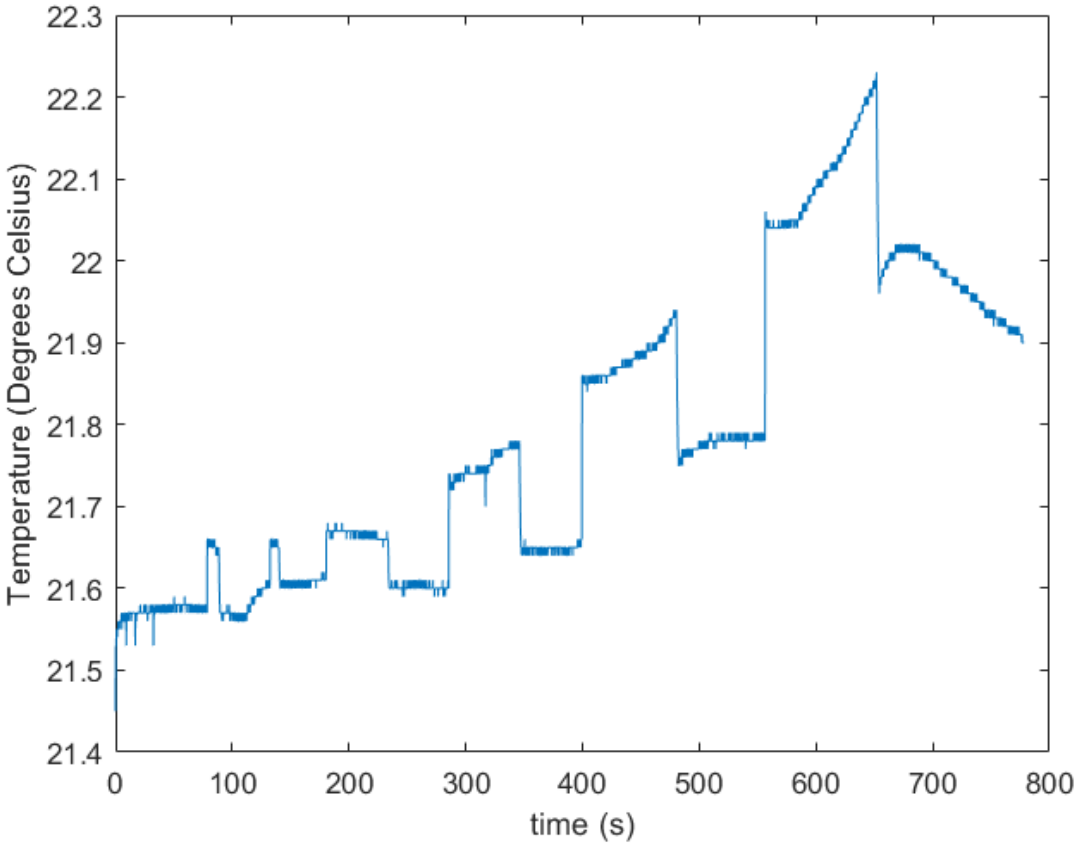

Figure C.7: Temperature versus time.

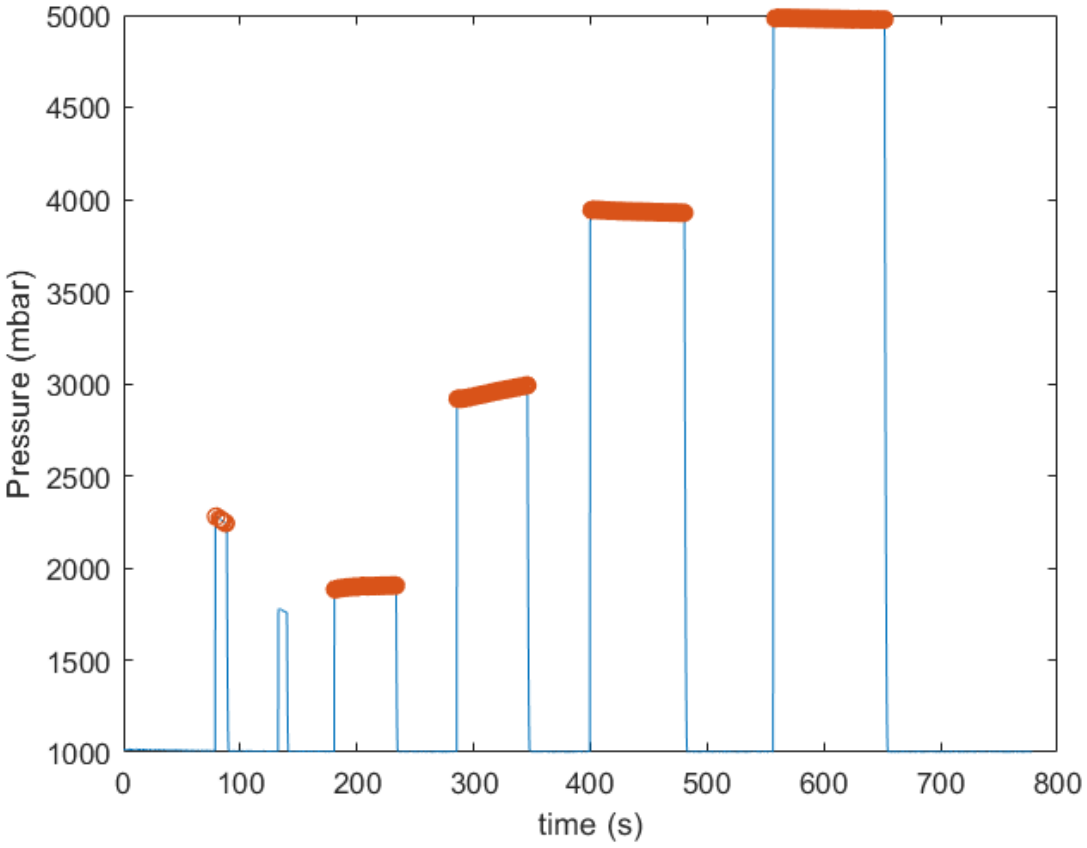

Figure C.8: Inlet pressure versus time.

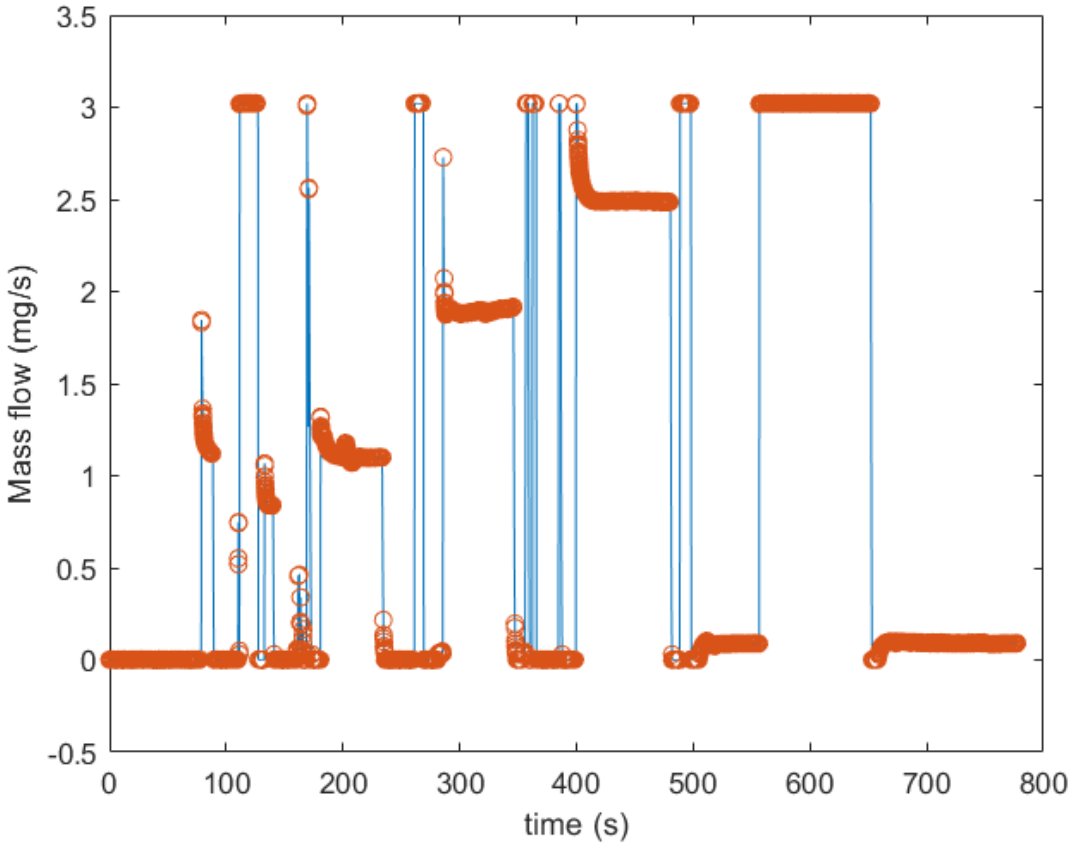

Figure C.9: Mass flow versus time.

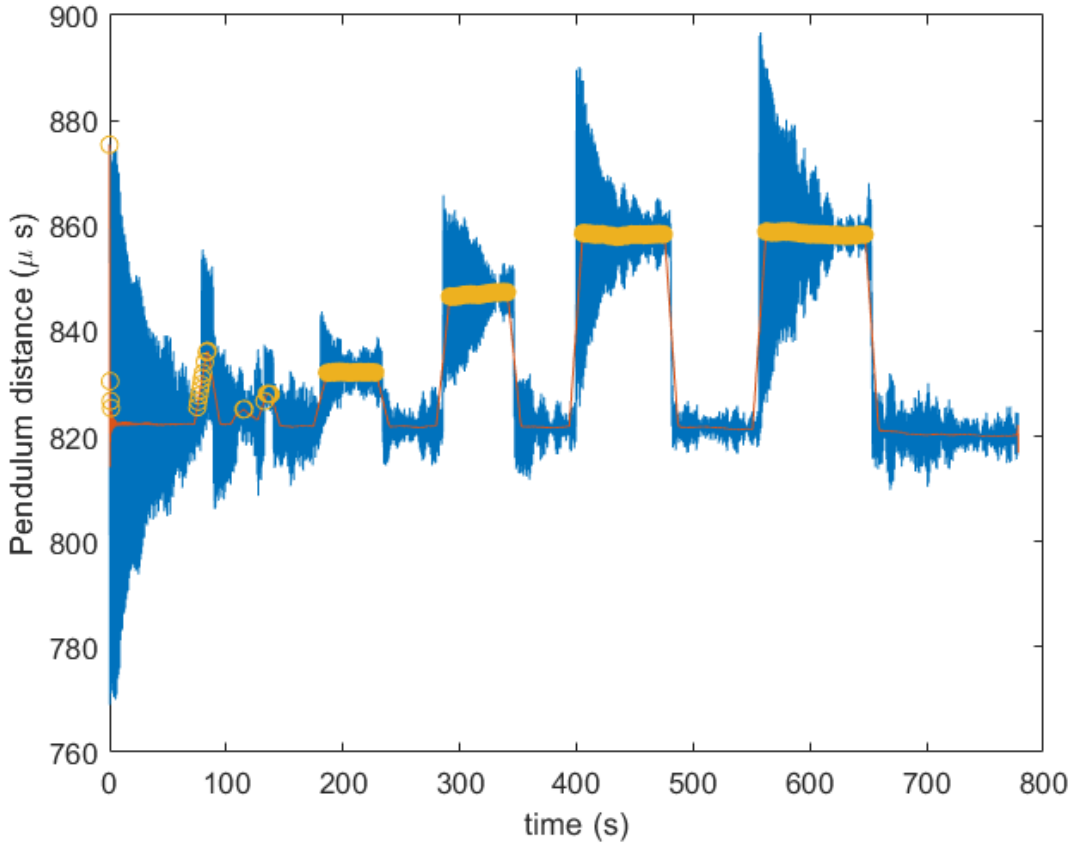

Figure C.10: Pendulum displacement versus time.

C.3. CT-R4C7-3

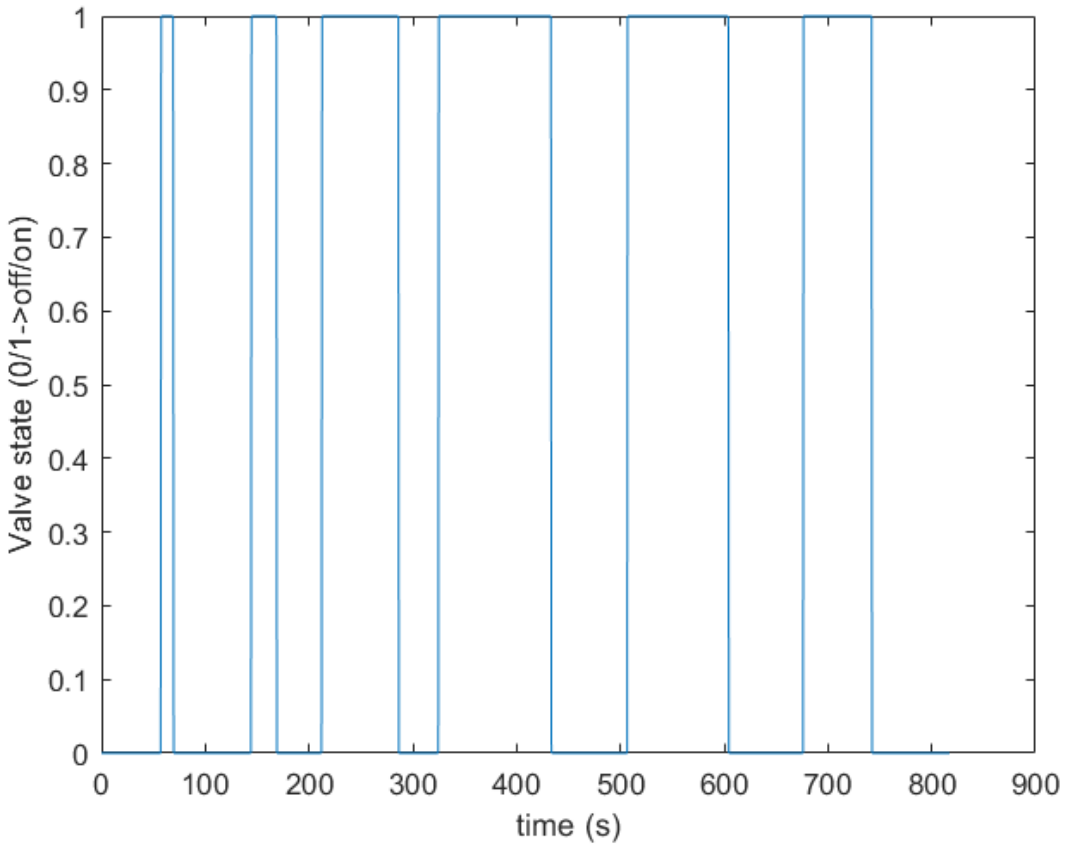

Figure C.11: Valve state versus time.

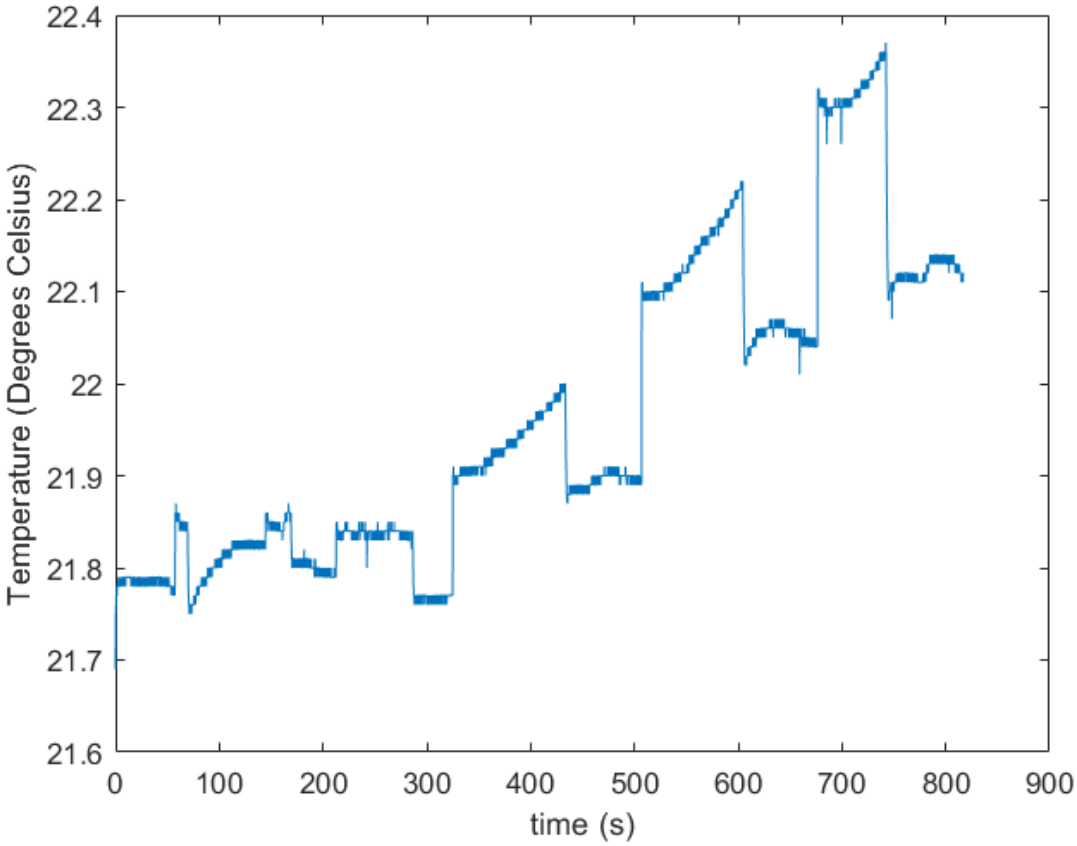

Figure C.12: Temperature versus time.

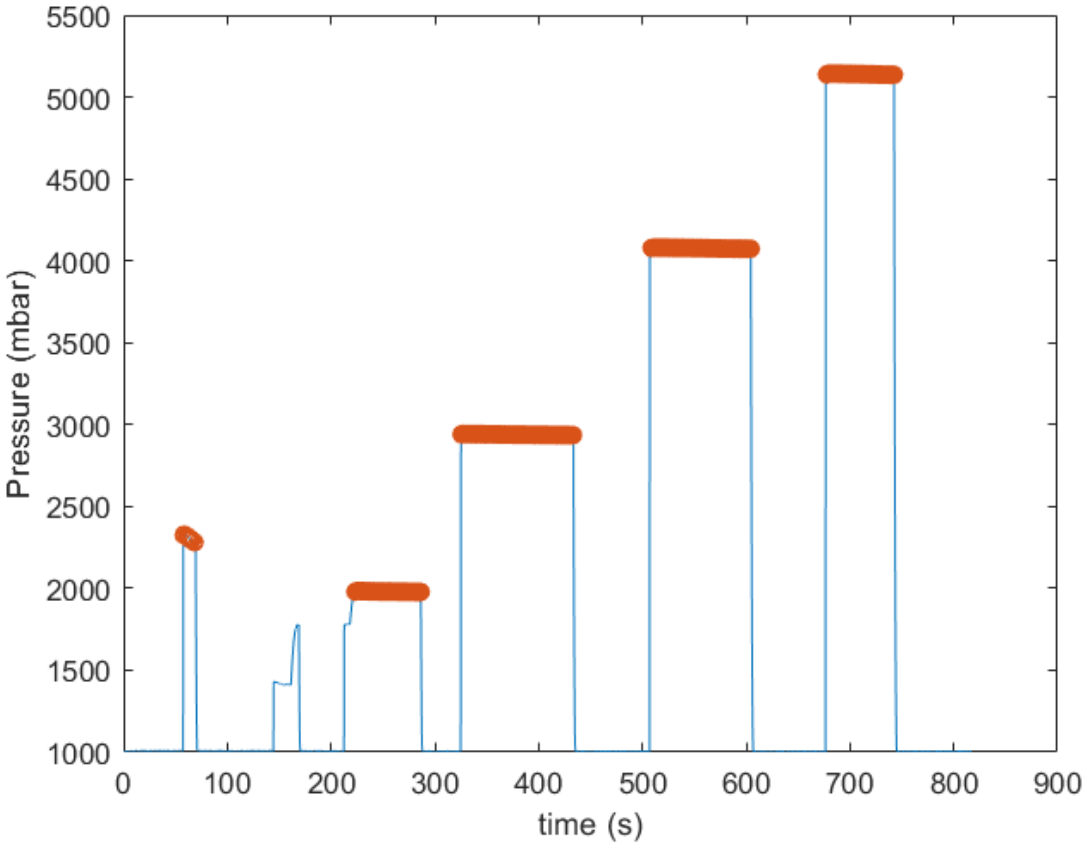

Figure C.13: Inlet pressure versus time.

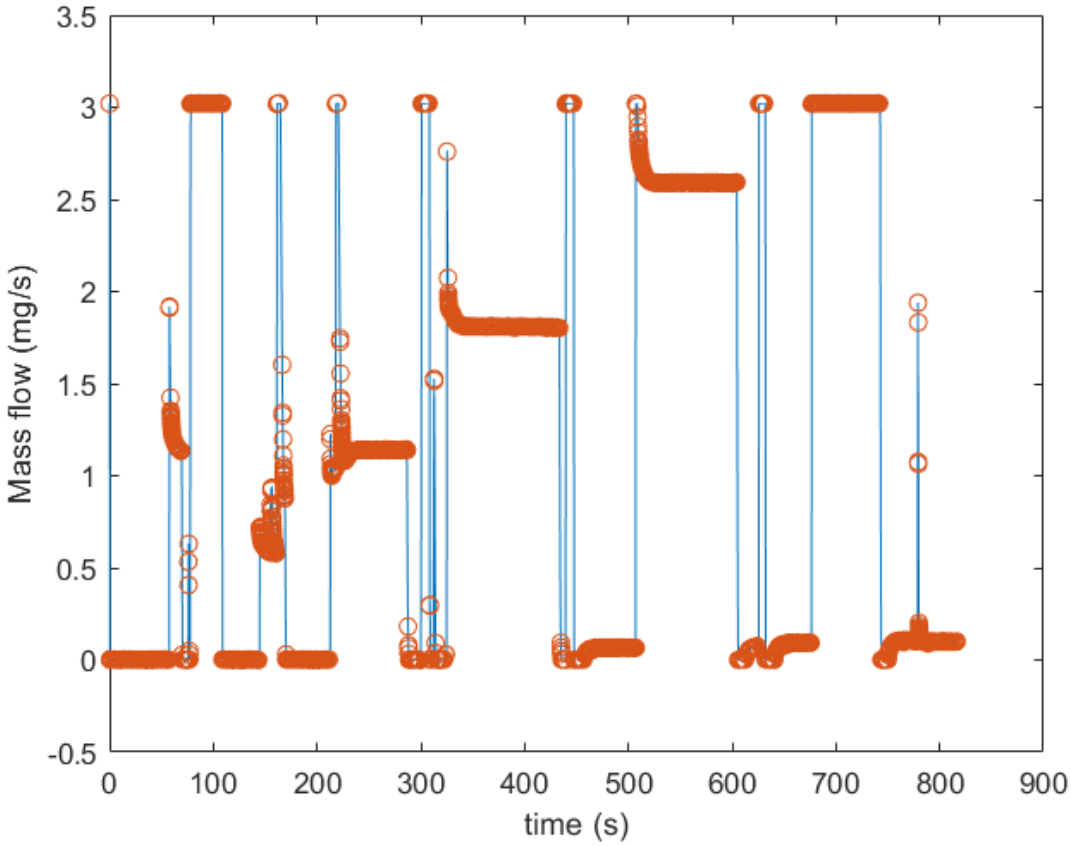

Figure C.14: Mass flow versus time.

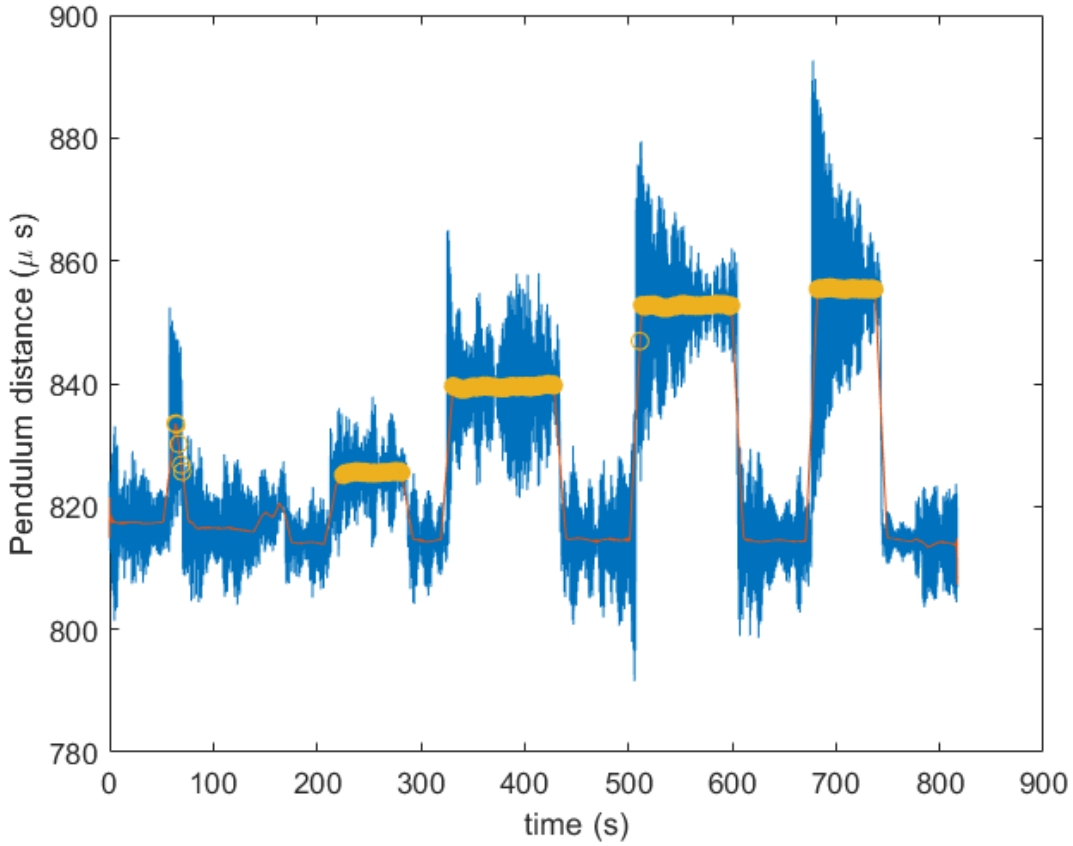

Figure C.15: Pendulum displacement versus time.

C.4. CT-R4C7-4

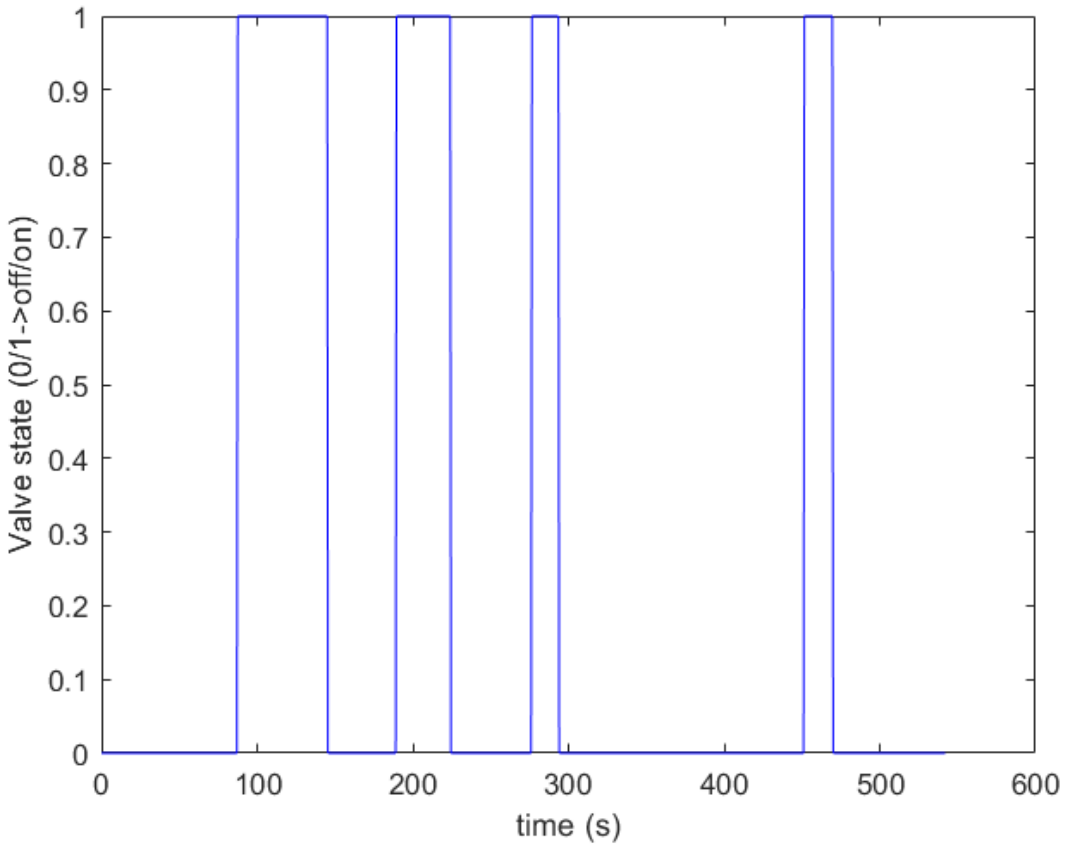

Figure C.16: Valve state versus time.

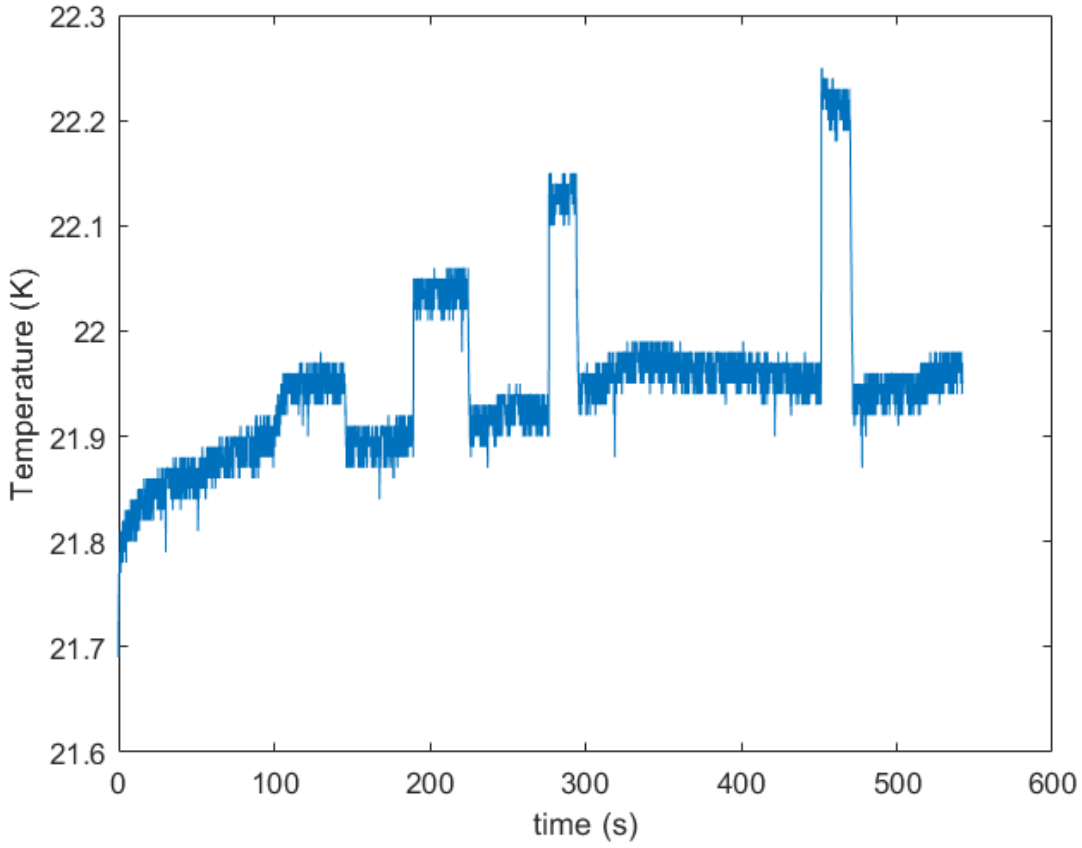

Figure C.17: Temperature versus time.

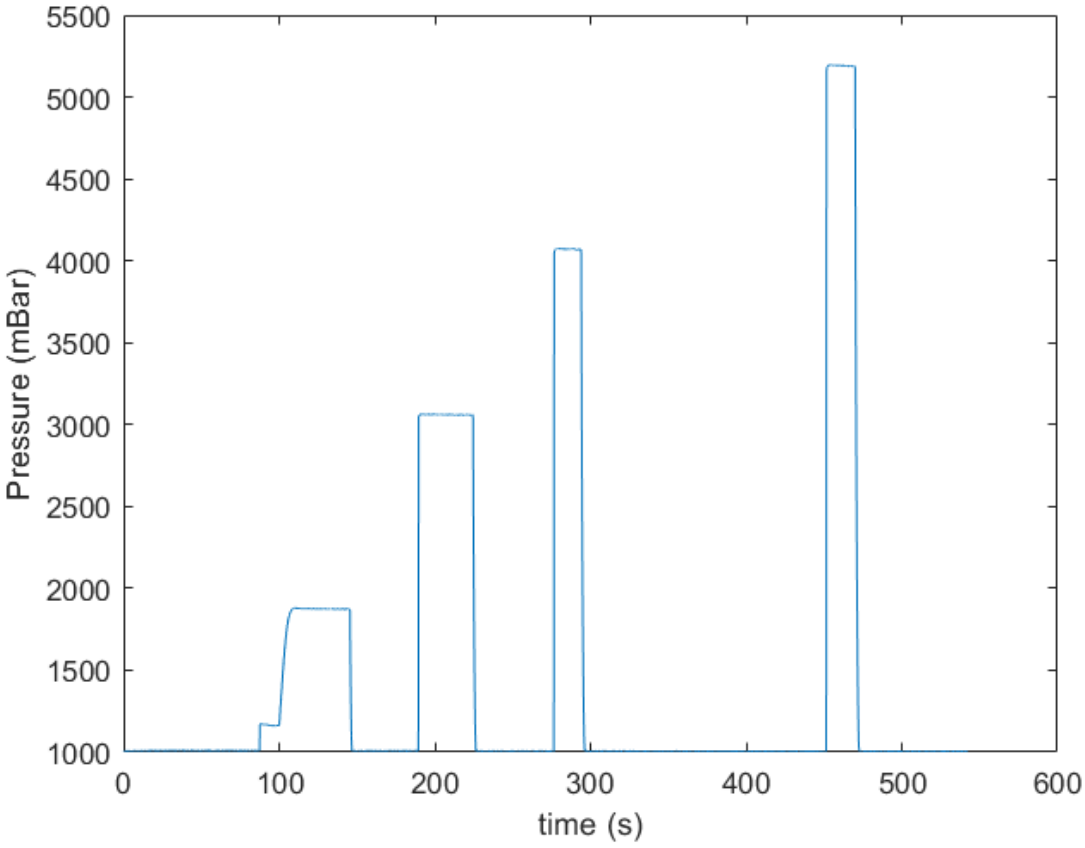

Figure C.18: Inlet pressure versus time.

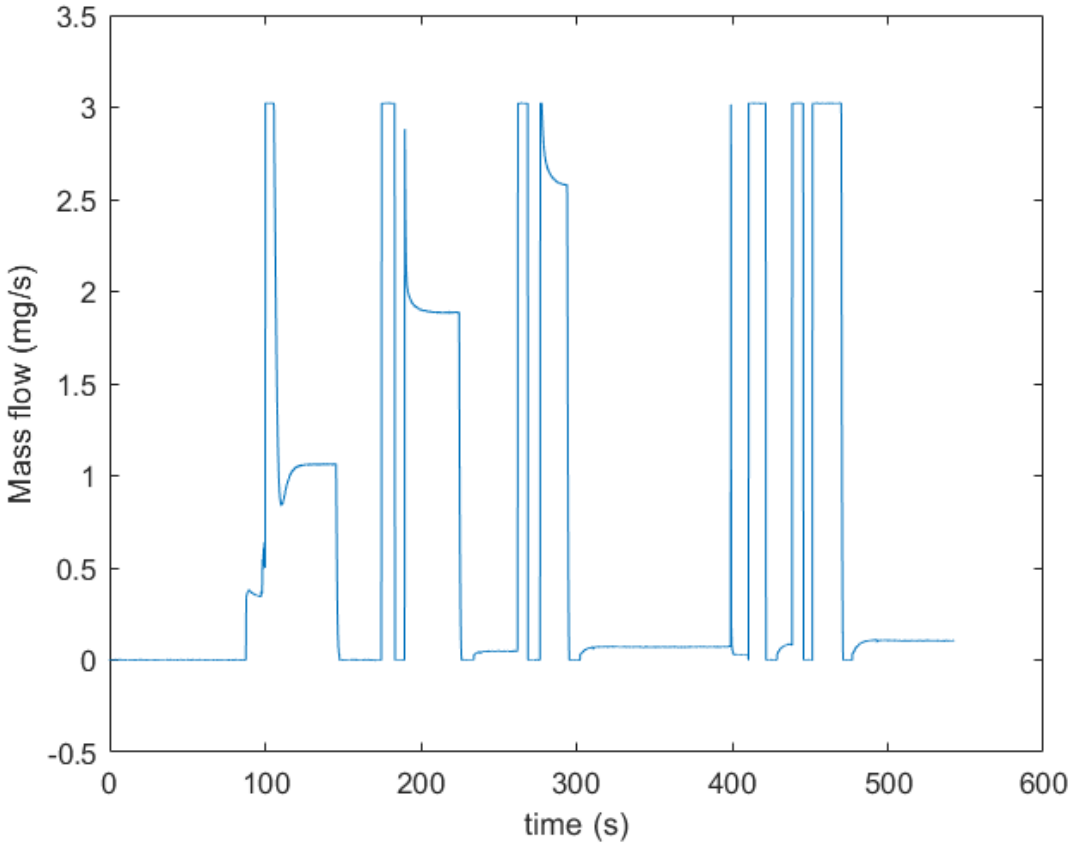

Figure C.19: Mass flow versus time.

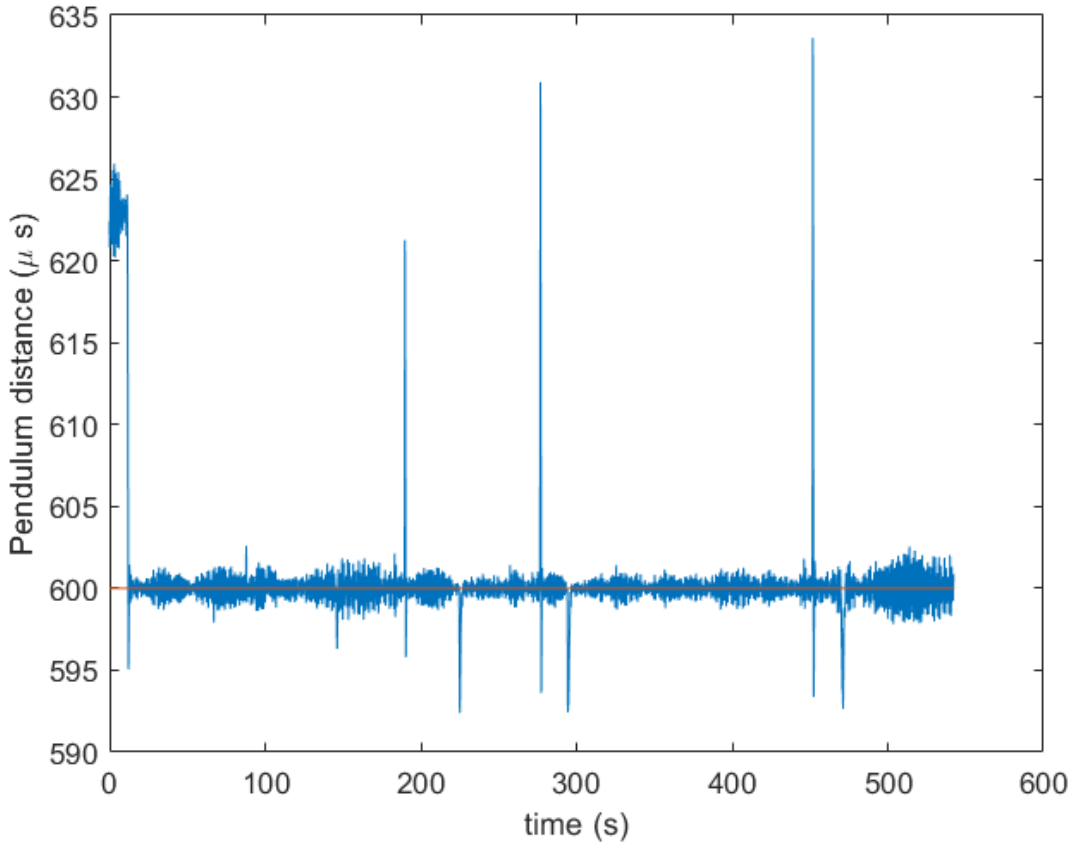

Figure C.20: Pendulum displacement versus time.

C.5. HT-R4C7

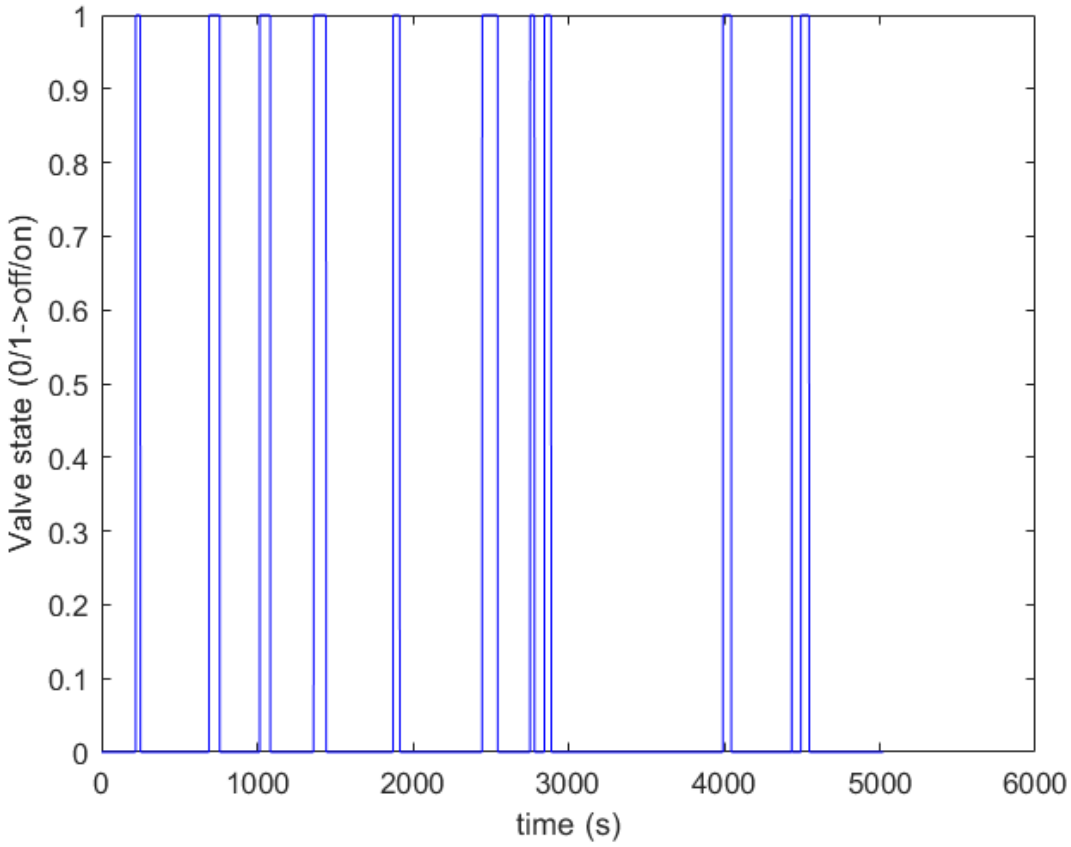

Figure C.21: Valve state versus time.

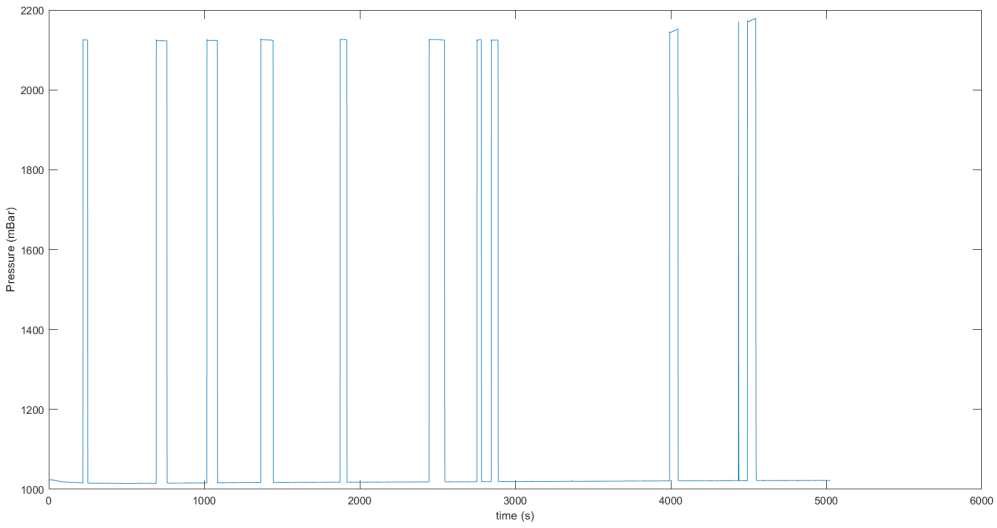

Figure C.22: Inlet pressure versus time.

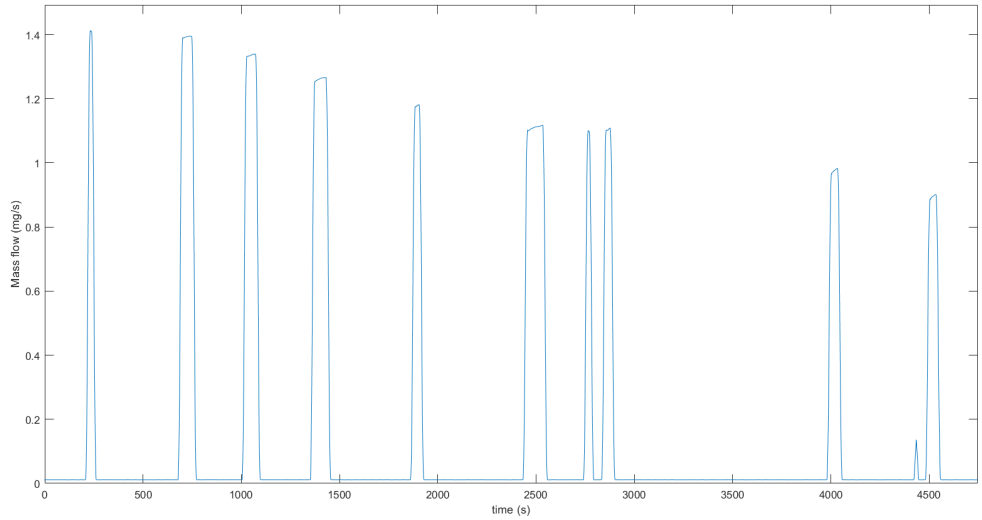

Figure C.23: Mass flow versus time.

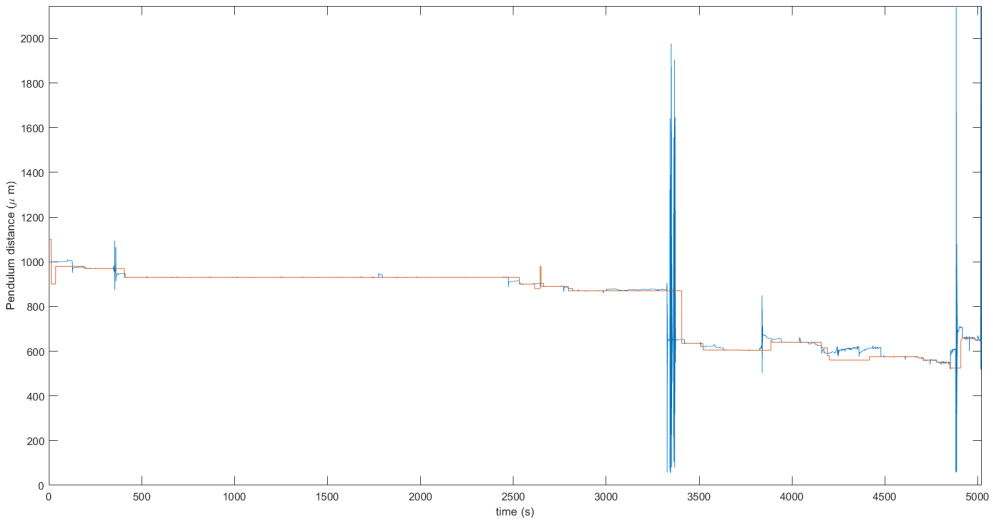

Figure C.24: Pendulum displacement versus time.

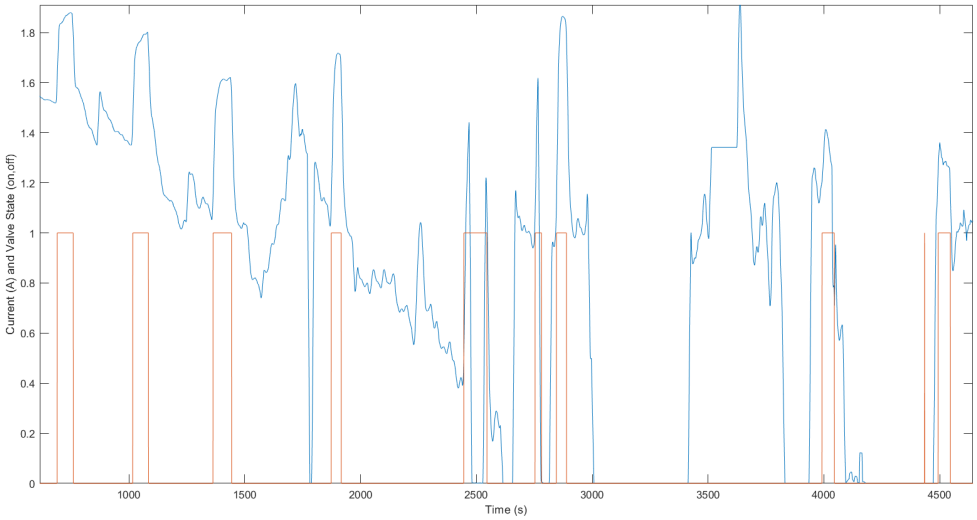

Figure C.25: Actuator current versus time.

D

Project Plan

Project Proposal and Plan: Performance modelling and testing of a heated MEMS-VLM microresistojet

Aris Pappadimitriou, 4340884
Profile - MSc Space Engineering
Supervisor - Barry Zandbergen
Department of Space Systems Engineering, Delft University of Technology
Version 2.0

October 22, 2020

Abstract

The purpose of this paper is to outline and plan the main steps involved in performing a thesis assignment about a Vaporizing Liquid Microthruster (VLM), which are designed to be used on CubeSats and PocketCubes.The main objective of the thesis is about creating a model that can accurately predict the performance parameters of the microthruster, while also addressing deficiencies in experimental knowledge in the performance of microthrusters at very high temperatures. To achieve this goal, the thermal design of the current test set-up needs to be redesigned to allow for thrust tests at higher chamber temperatures. This will be done in corporation with Henk van Zeijl from the Microelectronics department, by elevating the chip above the interface and using ceramic adhesives to reduce conductive heat transfer. Doing so will allow future students and researchers to have a design to experiment with heated VLM's for their research. The completion of this thesis could provide needed experimental data and thruster interface improvements for high chamber temperature tests, which is lacking from literature, while also providing a reliable performance model that can predict the thrust to within 10% of the experimental thrust.

1 Introduction

The Delft University of Technology is currently interested in the implementation and development of new designs for micropropulsion, to be used on future nano- and pico- satellites. Examples of implementations they have done in the past include the nano-satellites Delfi-C3 and Delfi-n3Xt, and the pico-satellite Delfi-PQ. The micropropulsion designs for these satellites were implemented using cold gas thrusters. Cold gas thrusters have lower propulsion performances compared to when the propellant is heated. The use of microresistojets, which heat the propellant, is of particular interest, because these resistojets would be able to reach higher specific impulses (Isp) and therefore better propulsion performances than cold gas thrusters. Microresistojets usually reach thrust levels between 1-10 mN and specific impulses between 50-200 s [1].

Currently, analytical and numerical models have been developed by researchers and students for predicting the performance of different microresistojets. It would be good to have a model that can predict the thruster performances, which include all the different operational ranges, at a sufficiently good accuracy. Additionally, models are normally able to be used for all different kinds of propellant and do not take into account processes such as the condensation of water in the nozzle right after the vaporization temperature. By understanding how the thruster efficiencies vary over the entire the operational condition and with different performance models, the validity of the models can be tested for experimentally. Creating a a valid model is useful, because this would reduce the number of experiments needed to map the performance of the thruster throughout the entire operating range. Without a model, experiments need to be repeated to improve the confidence in the

performance data. Therefore, the department needs a model that can determine the thruster performance of a VLM thruster accurately, for various propellants, under the entire operating range. The entire operating range takes into account aspects such as whether the propellant is heated or cold, different pressures and different inlet pressures.

The goal of this thesis is to test and analyze the performance of a heated MEMS-VLM thruster, with sufficient accuracy and with different propellants, and be able to validate the analytical models using experimental data. The purpose of this paper is to outline a plan on how the thesis assignment will be approached.

In this thesis proposal a review of the different information from literature sources will be provided in section 2. The research questions and objectives will be described in section 3. The methodology behind the thesis will be presented in section 4. section 5 will describe the experimental set-up expected to be used in the thesis. section 6 will give an overview of the expected results for the thesis assignment. The project planning, including Gantt chart, can be seen in section 7, followed by a conclusion in section 9.

2 State of the art / Literature review

This section will discuss what areas of literature are relevant to the thesis assignment, as well as summarize the current understanding within literature about thruster performance models, experimental data and test set-ups.

Currently, there are many different methods that can be used to predict the performance parameters of the thruster. The thesis to be done is a continuation on the work performed by Makhan [2]. His work focused on trying to determine the relationship between the throat Reynold's number and the performance characteristics of a VLM microthruster with an accuracy of 10% throughout the entire operating range. This included developing an analytical approach, based off of the work of Zandbergen [3], to predict the performance characteristics of the VLM microthruster. The work of Makhan [2] was able to this using cold nitrogen, however there was not enough time for him to investigate the results of using heated nitrogen and heated vaporized water as the propellants. The analytical model used to predict the performance of the thruster is based off of ideal rocket theory with adjustments made to the discharge coefficient and thrust coefficient to incorporate the effects of throat boundary layer losses, viscous losses and divergence losses.

The effect of throat boundary layer loss on the discharge coefficient can be found by using a relation from the work of Tang and Fenn [4], which is what Makhan [2] did in his performance model. However, another method using empirical relations from the work of Johnson [5] may also be used to to predict the effects on the discharge coefficient. The method of Johnson [5] does not require thruster dimensions, such as the longitudinal radius of the throat which is really hard to measure, and uses a relation using constants that are derived from his own experiments. However, these constants correspond to a special rounded nozzle throat, while the microthrusters that will be used in the thesis have sharp nozzles. Additionally, this relation can only be applied to the propellants that Johnson used for his testing which are nitrogen, argon, carbon dioxide and hydrogen gas.

Viscous losses are a direct result of boundary layer formation in the thruster nozzle and directly affects the thrust coefficient, which in turn reduces the thrust. In the work of Spisz [6], a qualitative correlation for the loss in thrust coefficient was created in terms of the nozzle area ratio and the throat Reynold's number, where the temperature dependent properties were taken at nozzle wall temperature. One relation was created for cold flow data and the other for hot flow data.

In ideal rocket theory, it is assumed that the flow is one dimensional, when in reality this is not true. The relations for divergence losses from the work of Zandbergen [3] and Farokhi [7] are able to correct for this assumption. The divergence loss factor is a function of the divergence half angle of the thruster, where a larger divergence factor will result in greater divergence losses. Relations were found for conical designs assuming 2D and 3D thrusters, however relations for bell nozzles still need to be found or developed.

The work of Maurya [8], van Wees [9] and Silva [10] presented analytical methods to model the heat transfer of their microthruster. The thermal model is important to predict the efficiency of the heater attached to the thruster and estimate how much of the input power goes into heating up the propellant. During heating, not all of the energy will go into heating the propellant, as some will be lost to the environment. Addition-

ally, the required heater power will vary depending on which propellant. The models of Maurya [8] and van Wees [9] use heat transfer analysis to determine how much of the energy is transferred through convection, radiation and conduction. The work of Silva [10] used a linear relationship between the molybdenum heater resistance and temperature.

For the thesis, the thruster interface available at the micropropulsion department will be used to perform the thrust tests for the VLM. This thruster interface is described very well in the work of Silva [10] and Makhan [2]. The test set-up to be used is important to achieving the thruster performance data needed to account for knowledge deficiencies in data for literature and also validating the performance and thermal models. If the experimental data matches the predicted model data accurately, then this would satisfy objective 3 from section 3. Silva [10] mentioned that the current thruster interface available within the department is severely limited by the low melting temperature of teflon (600 K), while other researchers do not provide much experimental data above 600 K, with the exception of the work of Bayt [11]. This has created a need to redesign the interface to allow for thruster tests to occur at higher chamber temperatures, as stated in objective 2 in section 3.

In the work of Kurmanbay [12], a different thruster interface was used that attached the thruster to a Printed Circuit Board (PCB). This set-up is available at the department of microelectronics, at the Delft University of Technology. The PCB would act as a an interface that would connect the thruster heater and thruster to the different measuring devices and data gathering instruments. Additionally, he was able to incorporate a pressure and temperature sensor that could directly measure the chamber conditions. The majority of literature [13] [2] [8] assume that the inlet pressure is equivalent to the chamber pressure, which adds uncertainty to the data. In reality there is a pressure drop, which can be estimated using relations from the reader of Zandbergen [3] and the work of van Wees [9]. Another option is to directly attach pressure and temperature sensors to the thrust chamber or, as Silva [10] had done, attach the sensors as close to the chamber inlet as possible where it was found that the pressure drop is negligible. Comparing the measured pressure in the chamber to the inlet pressure will be important to tackle question 1c which has to do with finding the pressure drop between the thruster inlet and the thruster chamber. Additionally, it is important to have a high enough input power to ensure that the water propellant is completely vaporized throughout the nozzle. The pressure drop at the nozzle throat will can cause condensation if the propellant's temperature is not higher than the vaporization temperature at the design pressure, which in turn can reduce the performance and efficiency of the thruster. Therefore,

One main finding within literature is the lack of data for high temperature thruster testing. To name a few examples, Silva [10] was able to perform vaporized water tests, using the same thruster interface and chips that will be used during the thesis. However, he was only able to reach a chamber temperature of 420 K using water as a propellant. This is due to the melting temperature of the thruster interface, which is made of teflon with a melting temperature of 600K. The work of Bayt [11] was able to reach chamber temperatures of 690 K using nitrogen as a propellant, however he performed his test in a bell jar where the thruster chip was attached to a thrust plate. Additionally, the work of Cen [13] reached chip temperatures of 573 K by attaching the thruster to a copper block that would be heated electrically. It can be seen that the field of VLM thrusters would benefit greatly if a test set-up could be designed to be able to carry out and record performance data for for chamber temperatures at 600 K and higher. Therefore, the acquisition of performance data at high chamber temperatures will be included in the main research question and its sub-questions.

3 Research question, aims and objectives

The main objective of the thesis is as follows: " The objective is to create a model that can predict the thrust performance, within 10% accuracy, of a VLM microthruster across the entire operating range by comparing predicted data with experimental data." The sub-objectives to achieve the main goal of thesis can be seen below. Additionally, each sub-objective is linked to a central research question, as can be seen in italics at the end of each objective.

1. Obtain experimental performance data, using both nitrogen and water throughout the entire operating range, that is reproducible and accurate. (*RQ 1a, 1d, 1e*)
2. Design and/or improve the thruster interface to allow thrust tests to take place at high temperatures, above 600 K, without damaging the set up, by investigating different insulative/protective solutions. (*RQ 2a-c*)
3. Determine the accuracy of the model at different operating conditions by comparing the predicted performance values and efficiencies with the real experimental values, including their measurement uncertainties, for each propellant. (*RQ 1b, 1c*)
4. Investigate the difference in performance between using nitrogen and vaporized water as a propellant, by comparing the acquired experimental data between them. (*RQ 3a-d*)
5. Provide recommendations to improve the chip design, chip interface, test-up and the models used, by providing solutions to any limitations and/or deficiencies in the work. (*RQ 4*)

The main research question to be answered is the following: "What are the effects of heating the 3rd gen. VLM microthruster on the thruster performance when thrust experiments are performed throughout the operating range and used to validate a performance predicting model?" The central questions below will be used to help answer the main research question above. Additionally, the central questions are also used to achieve the sub-objectives stated above.

1. What can be learned by investigating the mass flow, thrust, specific impulse, Isp quality, discharge coefficient, the thrust quality, heater power and heater efficiency of the VLM thruster, with respect to its operating conditions (chamber pressure and chamber temperature)?
   (a) To what extent do the relationships found match experimental data from literature?
   (b) To what extent can the performance and thermal model predict the experimental thruster performances stated in the central question?
   (c) Does the accuracy vary throughout the operating range?
   (d) What is the pressure drop between the thruster inlet and the thruster chamber throughout the operating range?
   (e) What is the contribution of the throat sharpness (nozzle throat divergence half angle) to the discharge coefficient?
2. Which thermal protection method is suitable to allow VLM testing to occur at chamber temperatures higher than 600 K?
   (a) What is the maximum achievable chamber temperature and pressure before failure or damage occurs?
   (b) Where on the thruster interface and test set-up does failure occur due to heating with and without the thermal protection?
   (c) Are there any alterations to the design and/or dimensions of the thruster interface and/or thruster test set-up that need to be considered to fit the thermal protection design?
3. What is the influence between using nitrogen and vaporized water as well as propellant for the VLM?
   (a) What is the difference in performance parameters attained?
   (b) What is the influence of the required heater power for each propellant?
   (c) At what operating point can complete vaporization, for liquid water, be noticed in the experimental results?

(d) What changes to the test set-up need to be incorporated to perform thrust tests using vaporized water compared to gaseous nitrogen?

4. What are the recommendations for improving the thruster chip design, thruster interface design, thruster performance model design, thruster thermal model, the test set-ups and procedures?

4 Theoretical Content/Methodology

The theoretical content is the main basis that will make up the thruster model used to predict the performance of a microthruster, given certain input parameters. The steps that build up the methodology of the thesis are derived and related to the objectives mentioned in section 3. In subsection 4.1 the methodology for improving the thermal design of the interface will be discussed. The models and experimentation will be discussed in subsection 4.2.

4.1 Improving the thruster interface's maximum workable temperature

To be able to reach chamber temperatures larger than 600 K. This work will be done with the help Henk van Zeijl, who is a professor at the Department of Microelectronics. Additionally, he was the supervisor for the work of Kurmanbay [12] and has been involved in the MEMS aspect behind the VLM microthrusters. A discussion with Henk, through a meeting, has resulted in a approach that can be followed to improve the thermal capabilities of the design. It involves elevating the thruster chip above the PCB/teflon interface and attaching the thruster to the PCB/teflon interface using a viscous ceramic putty. Additionally, the PCB can be replaced with a ceramic PCB to make the design more thermally robust. A figure of the idea can be seen in Figure 1. The propellant would be fed into the thruster using a microfluidic tip, as can be seen by the pink component in Figure 3b. This tip can be glued into place using the same ceramic putty. Kurmanbay [12] reported in his work that no leakage occurred using a different glue, however it was not specified which pressure ranges and temperatures this was tested for. The approach can be summarized in the following steps:

1. Acquire ceramic adhesives [14] and ceramic PCB. They should both have as low a conduction factor as possible. One adhesive should have a high viscosity to attach the thruster to the elevating columns and one other set should have a low viscosity for glueing the pressure/temperature sensor to the thruster to measure chamber conditions.

2. With the help of Henk, apply the thermal protection design to the PCB and test it. Check to see what temperatures the thruster and PCB can handle before failure occurs. This means the temperature should be recorded and input power should be noted as well, along with the area/point of failure.

3. If 2 works well, redesign the teflon interface to fit the thermal protection design used on the PCB.

4. Apply and test the newly designed interface. Record the temperature and heater input power at failure. Additionally, note down where the failure occurs on the thruster and/or its interface.

5. Attach the pressure sensor and temperature sensor to the design, using the low viscosity ceramic glue. Check at what temperature and input power the sensors fail and/or give off erroneous values.

4.2 Performance Model and Experimentation

The chosen method that will be used to predict the performance parameters of the thruster, will be an analytical model based off of the work of Makhan [2] and the reader of Zandbergen [3]. The performance model uses the concept of ideal rocket theory, which is a well understood concept in propulsion fields and is explained completely in the reader of Zandbergen [3], as a foundation. From this foundation, improvements are applied from literature to the theory to make the predicted parameters more realistic and therefore more

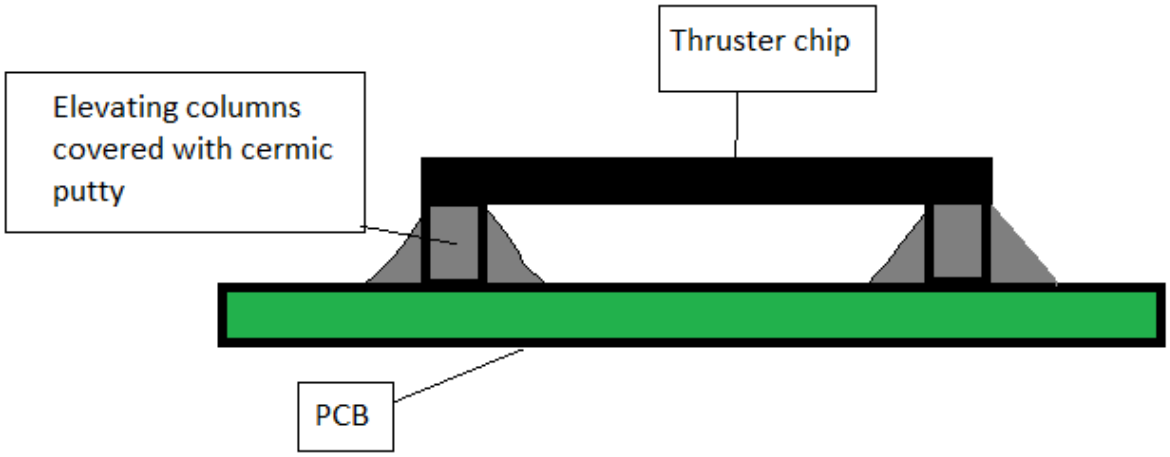

Figure 1: The thermal design proposed by Henk. The thruster chip (black) will be elevated above the PCB (green) using columns covered in low thermal conducting ceramic putty/adhesive (gray).

accurate. Several improvements have already been mentioned in section 2, such as the throat boundary loss predictions using the relations of Tang and Fenn [4] or Johnson [5], viscous losses discussed by Spizs [6] and divergence losses as discussed by Zandbergen [3] and Farokhi [7]. Additionally, the thermal models of Maurya [8] can be used to predict the heater efficiency of the thruster, which will become important for determining performance parameters for heated thrust tests. Then the models can be validated through experimentation.

Furthermore, the thrust stand needs to be calibrated to ensure that the thrust measured is valid and measured correctly. The procedure for calibrating the thrust stand is described, step by step, in the work of Makhan [2]. Through calibration, systematic errors can be reduced from the tests.

Additionally, the accuracy of the model is important in determining the validity of it as stated in objective 3. For this thesis assignment, it is required to try and predict the thrust and heater efficiency with a 10% accuracy. The specific impulse of the thruster is proportional to $\frac{thrust}{masflow}$, so if the thrust is at least within 10 % accuracy then the specific impulse is at most within 10 % accuracy, depending on the accuracy of the mass flow. If the specific impulse of the thruster is within 10 % accuracy, then this can be compensated by adding 10 % more propellant mass to the spacecraft. This in turn would only increase the total weight of spacecraft by 1 % assuming that the propellant mass makes up 10 % of the total spacecraft mass, according to Barry Zandbergen. Additionally, if the heater efficiency is not within 10 % accuracy, then this has to be compensated by increasing the power subsystem mass of the spacecraft, to provide a larger power input for the heater. The number of thrust experiments that will be done in total are 15: 5 cold nitrogen tests, 5 heated nitrogen tests and 5 vaporized/heated water tests. The repetition of the same experiments provides more statistical confidence within the data. The more a test is repeated the greater the precision of the data, which means that the random errors in the testing will be reduced. Doing more than 5 repetitions however would increase the work load and risk falling behind schedule. These performance results can then be averaged and fitted using linear and non linear regression curves. To determine whether the accuracy of the thrust is within 10%, the root sum squared errors of all the variables that the thrust is a function of need to be taken into account. These errors can then be added, subtracted, multiplied or divided depending on the relations for the thrust. For example, if the thrust is a function of $X \cdot Y$, then the errors ϵ_X and ϵ_Y can be added together to find the error of the thrust ϵ_{thrust}. The root mean squared error can be found using Equation 1 where ϵ_x is relative/total uncertainty of the variable x, δ_{SEm-x} is the standard error of mean for the variable x and $\delta_{sensor-x}$ is the absolute error of the measuring device for the variable x [15].

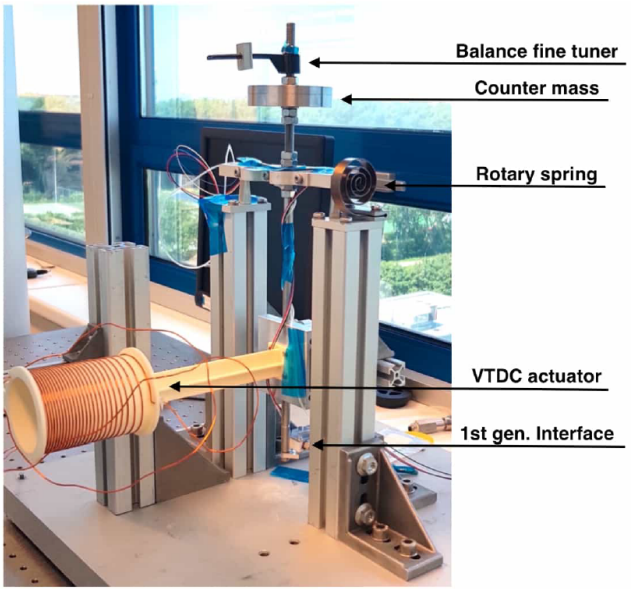

Figure 2: The test set-up used to perform the thrust tests with hardware labelled

$$\epsilon_x = \frac{1}{x}\sqrt{\delta^2_{SEM-x} + \delta^2_{sensor-x}} \cdot 100\% \tag{1}$$

5 Experimental Set-up

The purpose of this section is to provide an overview on the experimental set-up that will be used to determine the real performance parameters of the microthruster. The experimental set-up is vital in achieving the main thesis objective, by providing real performance values to validate the performance model and provide experimental data of the microthruster at operating ranges which are not documented much in literature.

The thrust pendulum that is is readily available and most likely to be used is the AE-TB-5m thrust bench. The thrust pendulum was designed in the work of Bijster [16], while Jansen [17] made some improvements on the design. The thrust bench is made up of a pendulum that measures the displacement of the pendulum arm pivot, when propellant flow is switched on causing thrust. Figure 2 shows an illustration of the test set-up used by Makhan [2]. One important piece of hardware is the VTDC actuator, which is important in calibrating the thrust force during prepatory testing and measuring the thrust caused by the thruster. The VTDC has a constant current running through it that creates a magnetic field. A magnetic holder is placed on an arm attached to the sensor. When the arm pivots the magnetic holder is pushed inside the VTDC, which causes a change in current and magnetic force. The thrust bench, in short, measures the magnetic force caused by magnetic holder being displaced into the VTDC, and then relations from Makhan [2] can be used to convert this magnetic force to a real thrust.

An illustration of the teflon thruster interface can be seen in Figure 3 on the left side. The PCB interface used at the microelectronics department can be seen in Figure 3b. An updated version of the interface may be available in the future, as improvements and design changes may be implemented to it over time. The main limitation of the teflon interface is the low melting point of the teflon, which is 600 K. This means that thrust tests at high temperatures are not possible, as was the case with Silva [10] who could only make it to 420 K. Once the thermal design, suggested by Henk, is tested on the PCB interface, the design will be translated to the teflon interface according to the methodology in subsection 4.1. Additionally, the sensor hole allows the pressure and temperature sensors to determine the inlet conditions of the nozzle.

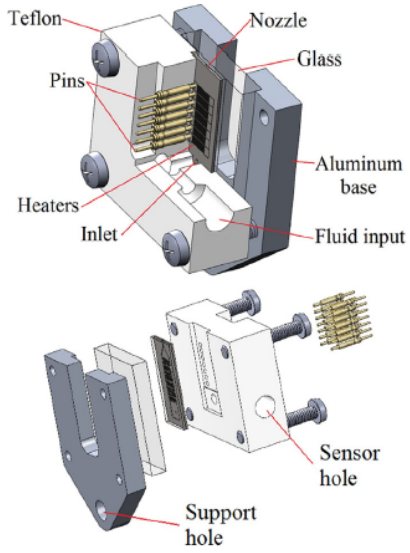

(a) The teflon interface available as the space systems engineering department [10]

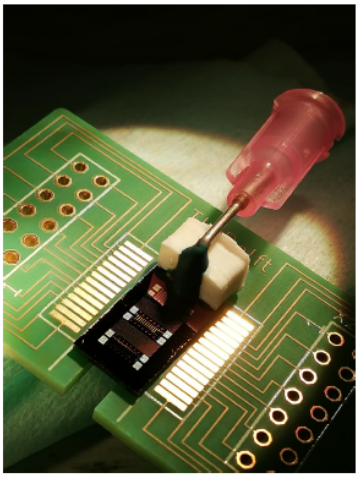

(b) The PCB interface used at the micro-electronics department [12]

Figure 3: The two different thruster interfaces

However, the interface does not allow for the direct measurement of chamber conditions and it is not fully known what the pressure drop is between the inlet and the chamber of the thruster. This is the reason why the pressure and temperature sensors from Kurmanbay [12] shall be incorporated for measuring the direct chamber conditions. This can then be compared to the inlet conditions to see if there is much of a difference in the condition. Therefore, at least one thruster will have the temperature sensor and pressure sensor integrated, while one or more thrusters will not have these sensors. This way if the sensors fail on the thruster, several back-up thrusters without the thruster will be available. The PCB interface, according to Henk as a guess, can handle up to 300 °C, however the PCB can be replaced easily with a ceramic PCB instead which can withstand much higher temperatures, however the temperature limit for the moment is unknown.

Now that the experimental set-ups have been discussed, the computer modelling can be briefly presented as well. The thruster performance and thermal model will be constructed using microsoft excel, due to the fact that the models are analytical in nature. Additionally, a software program called the Chemical Equilibrium with Applications program (CEA) created by NASA will be used [18]. This program allows the user to estimate the percentages of the different output species of the propellant, when the thruster is heated. That means it can also determine how much of the water is gaseous and liquid at different parts of the nozzle, at different temperatures and pressures. Lastly, a Matlab program called XSTEAM [19] is a simple program that can provide steam and water data for different temperatures and pressures between 0-2000 °C and from 0-1000 bar, respectively. This will be important for determining predicting enthalpies for the water at different pressures and temperatures for thermal modelling.

6 Results, Outcome and Relevance

This section will discuss the outcomes of the thesis assignment and ultimately the relevancy of this work. The outcomes of the thesis can be derived from the thesis objectives and the research questions that must

be answered to achieve these objectives. Additionally, predictions for the results of these objectives and research questions will be given.

The first outcome of the thesis are the experimental performance data of the VLM thruster, according to objective 1. The outcomes expected for this objective are detailed tables and/or graphs that show how the performance parameters vary throughout the operating range of the thruster. The defined operating ranges for the thruster are a chamber pressure of 2-5 bars and a chamber temperature from room temperature (300 K) to the chamber temperature to which the test set-up fails. Overall, the results are expected to show an increase in mass flow, thrust, specific impulse and efficiency (discharge coefficient, specific impulse quality and thrust quality) when the chamber pressure increases and/or when the chamber temperature decreases. Additionally, if the performance and thermal model can help predict the experimental results accurately, then a validated model would be available that could be used within the field of micropropulsion.

From the thesis one important outcome is a thruster interface design that allows for thruster testing at high temperatures, as stated in objective 2, and determining the temperature limits of the new design, as stated by objective 3. Having a set-up that can tolerate much higher temperatures will be beneficial for future students and researchers who wish to perform high chamber temperature testing for their work. The most desirable outcome is to improve the thermal design of the thruster interface, so that it can tolerate chamber temperatures up to 1000 K for the run-time of the thruster testing. However, it is expected that reaching chamber temperatures near 1000 K will be a challenge, since no evidence has been found from literature that shows a microthruster reaching such high temperatures. However, attempting to reach as close to this goal as possible is very relevant to this field of research due to the lack of experimental data at these high temperatures. Having heated experimental data can be useful for other researchers who wish to validate their own performance models, without performing the actual thruster tests. Additionally, having a good thermal design will benefit future students and researchers at the space systems engineering department and microelectronics department, who wish to investigate phenomena at high chamber temperatures.

From objective 4, it is expected to obtain experimental data using gaseous nitrogen and vaporized water as propellants. The performance data should give an indication of how the thruster's efficiency (thrust, specific impulse, discharge coefficient), mass flow and thrust are affected by using different propellants. Additionally, another outcome of interest is the heater power needed to increase the chamber temperature to a specific value. Since, the water propellant is in liquid form at room temperature, it is expected that the required heater power to reach a specific chamber temperature will be greater using water compared to gaseous nitrogen. It is predicted that the required heater power will be greater for water due to energy needed to convert the water from liquid to gaseous phase. Additionally, the vaporized water should give better thruster efficiency compared to gaseous nitrogen according to results obtained from literature. At least in this case, if the water is gaseous at the nozzle throat that the propellant is gaseous throughout the entire nozzle. This is why it is important to predict at what temperature the flow is completely vaporized throughout the entire nozzle and validate this prediction with the test results.

At the end of the thesis it is expected to provide recommendations to improve the thruster interface, thruster chip and thruster models. This all depends on the amount of work that can be completed on time, as well as any complications and/or findings discovered during the thesis that may be worth investigating in future research.

7 Project Planning and Gantt Chart

This section will outline the project plan for the thesis, which is then illustrated in a Gantt chart in Figure 5. The work breakdown structures show the detailed tasks needed to complete each of the objectives from section 3, while the Gantt chart shows when the main tasks are expected to start and end. Note that the work breakdown structure and Gantt chart are related by the sub-objectives that need to be achieved to reach the main objective.

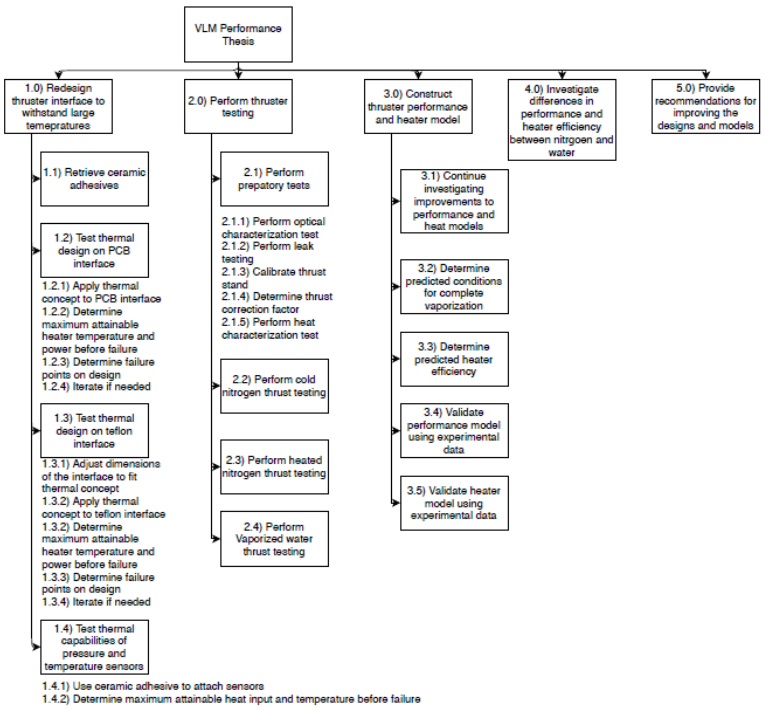

Figure 4: A work breakdown structure showing the tasks needed to complete the thesis

8 Project Management and Risk assessment

This section will discuss the project management and identification of risks within the thesis. By identifying the most critical risks within the thesis, several methods of mitigation can sought after ahead of time, to ensure the thesis runs smoothly.

Meetings will be conducted with Barry Zandbergen after every phase from the Gantt chart and whenever issues arise, to ensure the thesis is on track. Additionally, close contact will be kept with Huib, Aeilt-Jan and Rick who are also investigating the VLM microthrusters. Huib is investigating alternative fabrication methods for developing VLM chips and Aeilt-Jan is investigating the method of heating VLM chips using focused solar radiation. Their findings, especially for thermal protection and thruster testing and modelling, could be valuable. Additionally, we will share our resources with each other in order to save money from our budgets.

One risky element from the proposed work is that the thermal redesign of the interface may not increase the maximum temperature limit high enough for full vaporization to occur in the nozzle. It may be possible that certain parts, such as the propellant tube that connects to the thruster or the PCB/teflon may fail before complete vaporization occurs in the nozzle. To mitigate this risk, a test readiness review will be conducted on the new thruster interface to find any points of failure and determine at what input power the interface fails. Afterwards, these failure points can be addressed. Another risk involves the incorporation of the pressure and temperature sensors which can directly measure the chamber conditions. These sensors need to be attached directly to the thruster using a low viscosity glue and can not handle temperatures above 105 °C. Therefore, several thrusters will have the sensors, while several others will not have any sensors incorporated. This way if the sensors fail, several thrusters will be available without the sensors and the experimentation can continue.

Figure 5: The Gantt chart for the thesis assignment

9 Conclusions

Overall, an outline for a thesis assignment involving a VLM thruster has been presented and discussed. From this outline several conclusions and recommendations can be drawn.

To begin with, it is clear from literature in section 2 where knowledge can be added to the field of VLM thrusters. Literature has shown a lack of experimental data for thruster tests occurring at high chamber temperatures. Therefore, using the experimental set up shown in section 5 the performance data for thruster can be attained for the entire operating range of the thruster. Doing so would add much needed experimental data to this field of research, which can be used for example to validate other analytical, numerical and empirical models.

Additionally, the experimental set-up has shown that the current thruster interface will not be able to handle the high chamber temperatures to carry out heated thruster testing. The method proposed by Henk involves elevating the thruster chip above the interface and using ceramic adhesives with a low conduction quality to minimize the amount of heat transferred to the teflon interface. This can first be tested by using the PCB interface used by Henk van Zeijl of the microelectronics department, and after successful testing can be adapted to fit the teflon interface available at the space systems engineering department at the aerospace faculty. If the interface can be thermally improved this would provide a good basis for future researchers to adapt their thruster designs to perform their own heated thruster experiments. Additionally, this design could have continued use at the microelectronics and space systems engineering departments at the Delft University of Technology for future work.

Furthermore, the thruster testing done will also be used to validate an analytical performance and thermal model for predicting the performance and efficiency of the VLM thruster. The model will be based off of the work of Makhan [2], however certain points of improvement will continue to be investigated and incorporated into the model. Having a model that can predict the thrust of the VLM microthruster within 10% accuracy can be valuable for analyzing and designing future VLM thrusters. Additionally, future researchers can incorporate the model to predict the performances of their own thrusters, especially if the model is accurate throughout the entire operating range (cold flow, heated flow and different chamber pressures).

Overall, the assignment can provide much needed experimental data, models and experimental set-ups to perform high temperature thrust testing.

References

[1] A. Cervone, B. Zandbergen, D. C. Guerrieri, M. De Athayde Costa e Silva, I. Krusharev, and H. van Zeijl. Green micro-resistojet research at delft university of technology: new options for cubesat propulsion. *CEAS Space Journal*, 9(1):111–125, Mar 2017.

[2] Rajeev Makhan. Performance of the mems vaporizing liquid microthruster using cold nitrogen gas as propellant, 2018.

[3] Barry Zandbergen. Thermal rocket propulsion. *Delft University of Technology*, 2, 2003.

[4] SP Tang and JB Fenn. Experimental determination of the discharge coefficients for critical flow through an axisymmetric nozzle. *AIAA Journal*, 16(1):41–46, 1978.

[5] Aaron N Johnson, Pedro I Espina, GE Mattingly, JD Wright, and CL Merkle. *Numerical Characterization of the Discharge Coefficient of Critical Nozzles*. PhD thesis, Pennsylvania State University, 2000.

[6] Ernie W Spisz, Paul F Brinich, and John R Jack. Thrust coefficients of low-thrust nozzles. Technical report, NATIONAL AERONAUTICS AND SPACE ADMINISTRATION CLEVELAND OH LEWIS RESEARCH CENTER, 1965.

[7] Saeed Farokhi. *Aircraft propulsion*. John Wiley & Sons, 2014.

[8] DK Maurya, S Das, and SK Lahiri. An analytical model of a silicon mems vaporizing liquid microthruster and some experimental studies. *Sensors and Actuators A: Physical*, 122(1):159–166, 2005.

[9] TX Van Wees. Characterization and testing of a mems-vaporizing liquid microthruster for small satellite propulsion, 2017.

[10] Marsil AC Silva, Daduí C Guerrieri, Henk van Zeijl, Angelo Cervone, and Eberhard Gill. Vaporizing liquid microthrusters with integrated heaters and temperature measurement. *Sensors and Actuators A: Physical*, 265:261–274, 2017.

[11] Robert L Bayt. Analysis, fabrication and testing of a mems-based micropropulsion system. Technical report, Aerospace Computational Design Laboratory, Dept. of Aeronautics , 1999.

[12] Alisher Kurmanbay. Design, fabrication and characterization of mems based micro heater for vaporizing liquid microthruster, 2019.

[13] JW Cen and JL Xu. Performance evaluation and flow visualization of a mems based vaporizing liquid micro-thruster. *Acta Astronautica*, 67(3-4):468–482, 2010.

[14] Cotronics Corporation. *Ceramic Adhesives and Putty*, 2008. Rev. 1.

[15] Hugh W Coleman and W Glenn Steele. *Experimentation, validation, and uncertainty analysis for engineers*. John Wiley & Sons, 2018.

[16] RJF Bijster. Design, verification and validation of a micropropulsion thrust stand, 2014.

[17] EHW Jansen. Improvement and validation of test stand performance for novel micropropulsion systems, 2016.

[18] CEA NASA. Chemical equilibrium with applications. *Software Package, Ver*, 2, 2010.

[19] Magnus Holmgren. X steam, thermodynamic properties of water and steam. *MathWorks, Natick, MA, accessed Dec*, 2:2014, 2007.

[20] R. Curran and G. Saunders. Ae4010: Template project proposal and plan. Available on Blackboard, 2013.

LaTeX template based on [20].

E

Test Procedures for prepatory tests

E.1. Optical Characterization Test

The procedure list, created by [18], was used for the optical characterization of the thrusters. However, the thrusters were not placed flat on the microscope platform, as stated by item 3 in [18]. The entire thruster, with its PCB, was held by a 3D printed bracket (see Figure 2.5), which was then placed on the platform.

E.2. Leak Testing

The procedure is based off of procedure of [18], however several alterations have been made. The main alteration is the method as to how the dispensing tip is blocked, which can be seen in Figure 5.1.

E.3. Actuator Coil Calibration

The procedure of [36] was used for calibrating the actuator coil. Overall, its a very clear and concisely written procedure list, and it is recommended to use this procedure for future calibrations. However, one change was made where the step time was changed from 10s to 15s. This gives a bit more time to the user to write down the mass measured on the scale, in exchange of increasing the total testing time to 10 minutes. The used labview file can be found on the main computer in the cleanroom lab, in the folder:

E.4. Thrust Stand Calibration

For the thrust stand calibration, the procedure of Makhan [18] was used. It was sufficient enough to understand how to set up the equipment and carry out the calibration. However, two differences should be taken into account:

1. The pendulum calibration was not performed in a vacuum. The presence of a vacuum should not affect how the magnetic current and pendulum displacement relate to each other.
2. The file used to carry out the pendulum calibration is called: ”calibration.vi”, found in the folder of Aris, on the cleanroom computer.